Polymersomes stimulables à base de polypeptoids

Yangwei Deng

PSL UNIVERSITÉ PARIS

THÈSE DE DOCTORAT
DE L'UNIVERSITÉ PSL

Préparée à Chimie ParisTech

Polymersomes stimulables à base de polypeptoids

Stimuli-responsive polymersomes based on polypeptoids

Soutenue par

Yangwei DENG

Le 23 novembre 2018

Ecole doctorale n° 406

Chimie Moléculaire de Paris-Centre

Spécialité

Chimie Moléculaire

Composition du jury :

Patrick, KELLER Directeur de recherche émérite, CNRS Institut Curie	*Président*
Véronique, SCHMITT Directeur de recherche, CNRS Centre de Recherche Paul Pascal	*Rapporteur*
Sébastien, LECOMMANDOUX Professeur des universités Institut Polytechnique de Bordeaux	*Rapporteur*
Yixian, WU Professeur des universités Beijing University of Chemical Technology	*Examinateur*
Min-Hui, LI Directeur de recherche, CNRS Institut de Recherche de Chimie Paris - Chimie ParisTech	*Directeur de thèse*

Chimie Paris ParisTech | PSL

Stimuli-Responsive Polymersomes Based on Polypeptoids

Polymersomes Stimulables à Base de Polypeptoids

Comme un nanoconteneur robuste formé d'une bicouche de polymères amphiphiles, vésicule polymère, aussi appelée polymersome, a été considérée comme un vecteur de médicament potentiel dans le domaine biomédical, grâce à sa structure imitant les cellules, sa grande stabilité et sa capacité à être fonctionnalisée. Pour l'utilisation pratique des polymeromes dans des applications biomédicales, la biocompatibilité des copolymères qui composent les vésicules devient un sujet important. Le polypeptoid est une classe de dérivés polypeptides dont les atomes d'azote des amides sont substitués. En évitant la formation de liaisons hydrogène inter- et intramoléculaires, les polypeptoids ont des solubilités bien meilleures que les polypeptides dans des solvants organiques usuels, tandis que la biocompatibilité est bien maintenue. Des travaux sur l'auto-assemblage de copolymères à blocs contenant polypeptoids émergent dans la littérature. Cependant, les travaux sur les vésicules polypeptoids sont encore rares.

Dans cette thèse, notre objectif est de synthétiser de nouveaux copolymères à blocs amphiphiles contenant polypeptoids, de préparer les vésicules polypeptoids par auto-assemblage contrôlé des copolymères synthétisées, et de développer les polymersomes sensible à base de polypeptoids. Les copolymères à blocs amphiphiles contenant les polypeptoids ont été synthétisées par la polymérisation par ouverture de cycle (ROP) de *N*-thiocarboxyanhydrides d'acides aminés *N*-substitués (NNTA). Différentes techniques telles que la nanoprécipitation, l'hydratation de film mince et la double émulsion ont été utilisées pour réaliser les auto-assemblages dans le but d'obtenir des vésicules polypeptoids. Les auto-assemblages ont été étudiés en détail par DLS, cryo-EM, microscope confocale à balayage laser (CLSM) et ^{1}H-RMN.

Synthèse des copolymères à blocs amphiphiles contenant polypeptoids

Nous avons synthétisé deux familles de copolymères a blocs amphiphiles

contenant polypeptoids. Dans la première famille de copolymères, la ROP de sarcosine NTA (Sar-NTA) a été éiniti ée par le poly(ε-caprolactone) (PCL) à terminaison -oxyamine (PCL-ONH_2 and H_2NO-PCL-ONH_2), pour obtenir le copolymère dibloc PCL-*b*-PSar, et le copolymère tribloc PSar-*b*-PCL-*b*-PSar (Schème 1), avec différents poids moléculaires (MWs) et proportions hydrophiles. Parmi eux, PSar-*b*-PCL-*b*-PSar possède une structure ABA à peine rapportée avec PCL au milieu et les blocs PSar aux deux côtés. Les resultats de RMN et chromatographie sur gel perméable (GPC) révèlent la structure claire des copolymères à blocs (Figure 1 et Figure 2). Cependant, les degrés de polymérisation (DPs) des blocs PSar ne peuvent pas être bien contrôlés avec la proportion du monomère sur l'initiateur, à cause de la faible activité d'initiation des oxyamines.

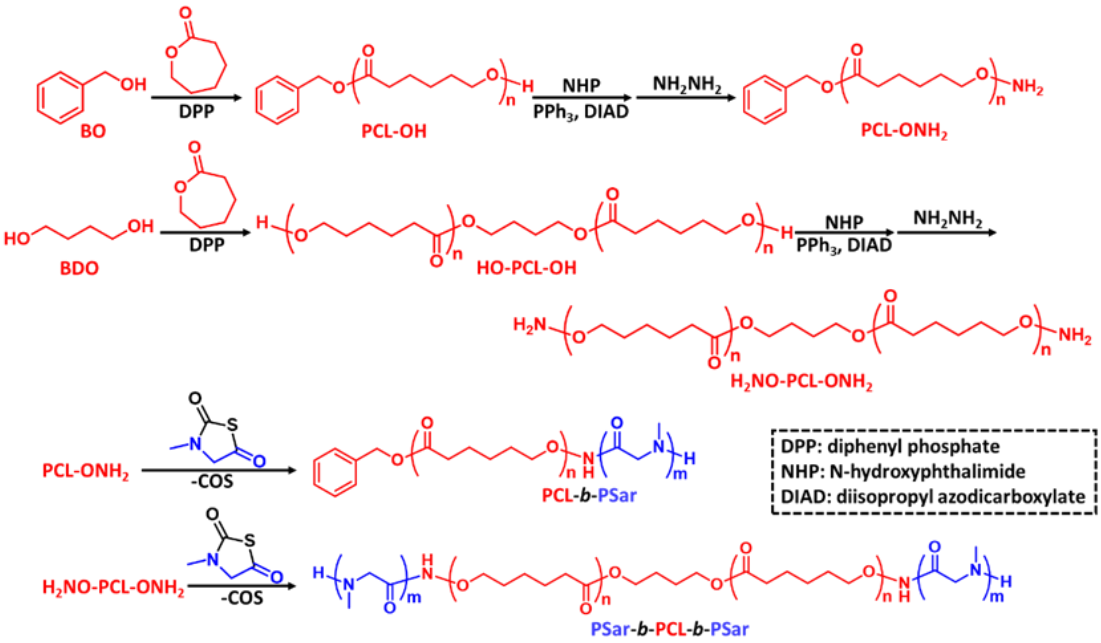

Schème 1. Préparation du copolymère dibloc PCL-*b*-PSar et le copolymère tribloc PSar-*b*-PCL-*b*-PSar.

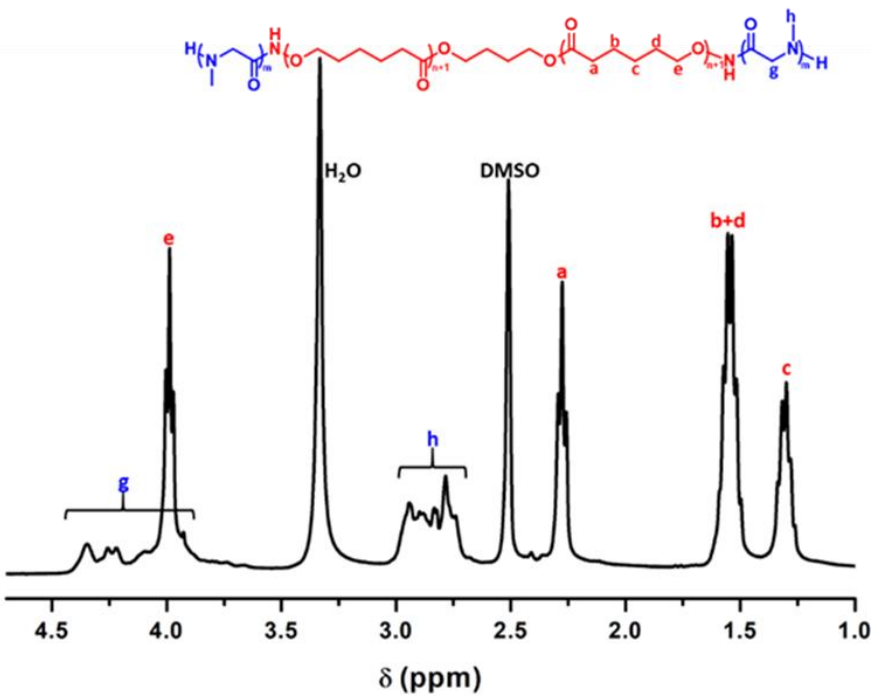

Figure 1. Spectre ^{1}H-RMN de PSar$_{16}$-*b*-PCL$_{40}$-*b*-PSar$_{16}$ (CS10).

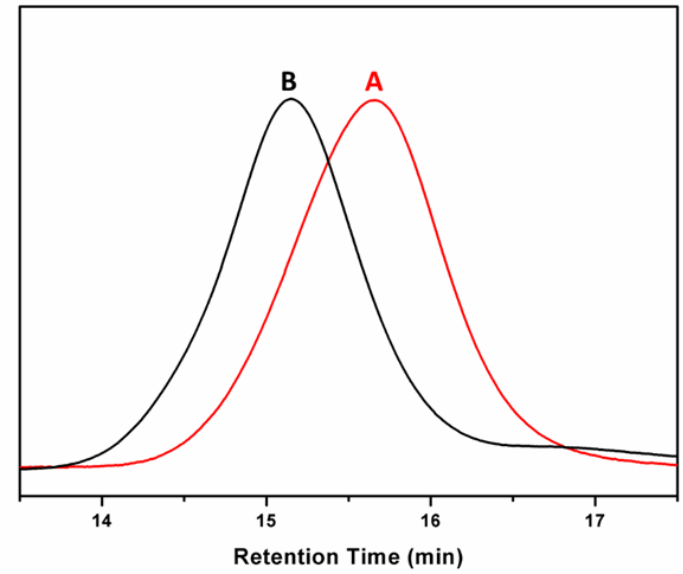

Figure 2. Traces GPC (0.05 M LiBr/DMF comme l'éluant) de PSar$_{16}$-*b*-PCL$_{40}$-*b*-PSar$_{16}$ (CS10, B) et son initiateur H_2NO-PCL$_{40}$-ONH_2 (PCL5, A).

La seconde famille de copolymères est basée sur un polypeptoid portant thioéthers, la poly(*N*-3-(méthylthio)propyl glycine) (PMeSPG). Le nouveau monomère, MeSPG-NTA, a été préparé par une procédure de « décarboxylation–*N*-carboxyméthylation » à

partir de la méthionine, suivie d'une reaction de cyclisation (Schème 2). La ROP de MeSPG-NTA initié par polyéthylène glycol amine de DP = 45 (PEG_{45}-NH_2) donne les copolymères à blocs amphiphiles PEG-*b*-PMeSPG (Schème 3B) avec différents MWs et proportions hydrophiles/hydrophobes, *i. e.*, EM1 (PEG_{45}-*b*-$PMeSPG_{17}$), EM2 (PEG_{45}-*b*-$PMeSPG_{40}$) et EM3 (PEG_{45}-*b*-$PMeSPG_{71}$). Les copolypeptoids à blocs amphiphiles PMeSPG-*b*-PSar est synthétisé par la ROP sequentielle de MeSPG-NTA et Sar-NTA initié par benzylamine (Schème 3C). Les réactions sont bien contrôlées et donnent les copolypeptoids, MS1 ($PMeSPG_{45}$-*b*-$PSar_{65}$), MS2 ($PMeSPG_{60}$-*b*-$PSar_{50}$) et MS3 ($PMeSPG_{75}$-*b*-$PSar_{25}$). Les structures des copolymères sont confirmées par RMN et GPC (Figure 2 et Figure 3).

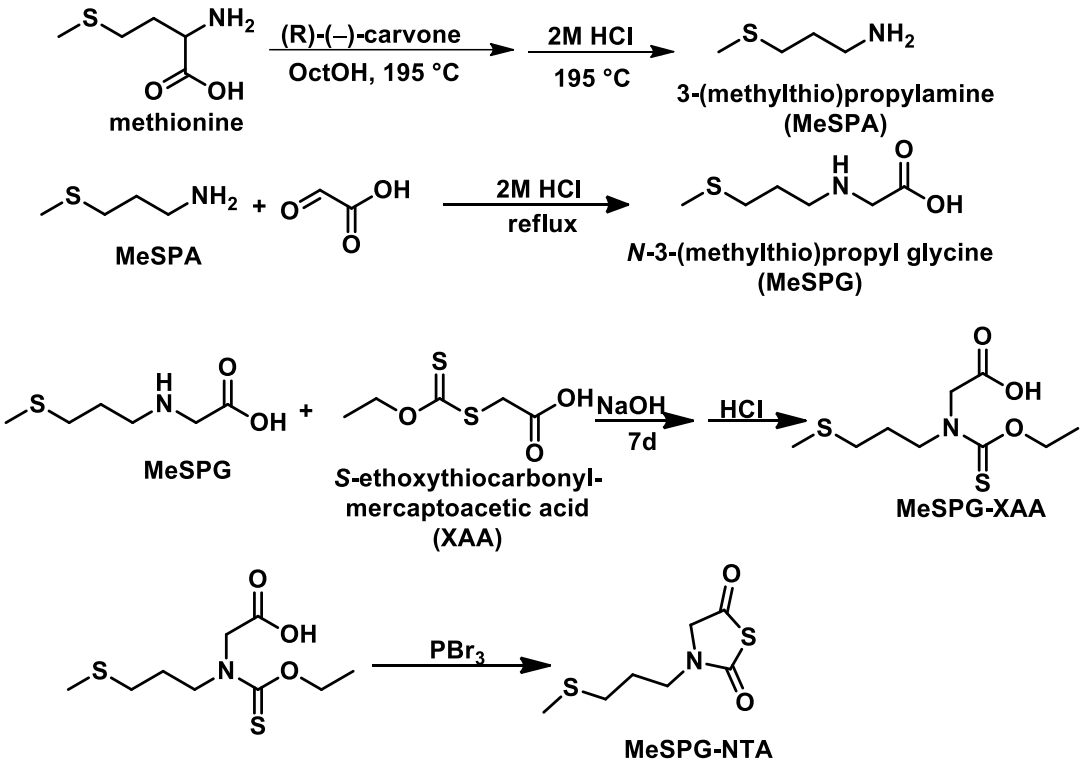

Schème 2. Synthèse du monomère MeSPG-NTA.

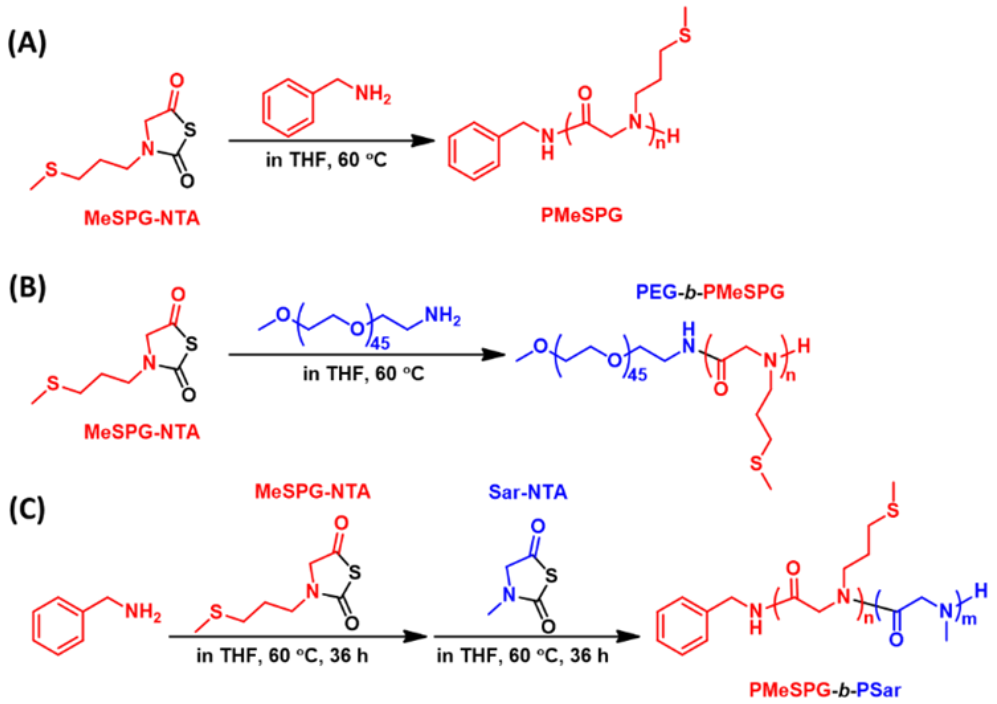

Schème 3. Synthèses du homopolymère PMeSPG (A), le copolymère PEG-*b*-PMeSPG (B), et le copolypeptoid PMeSPG-*b*-PSar (C).

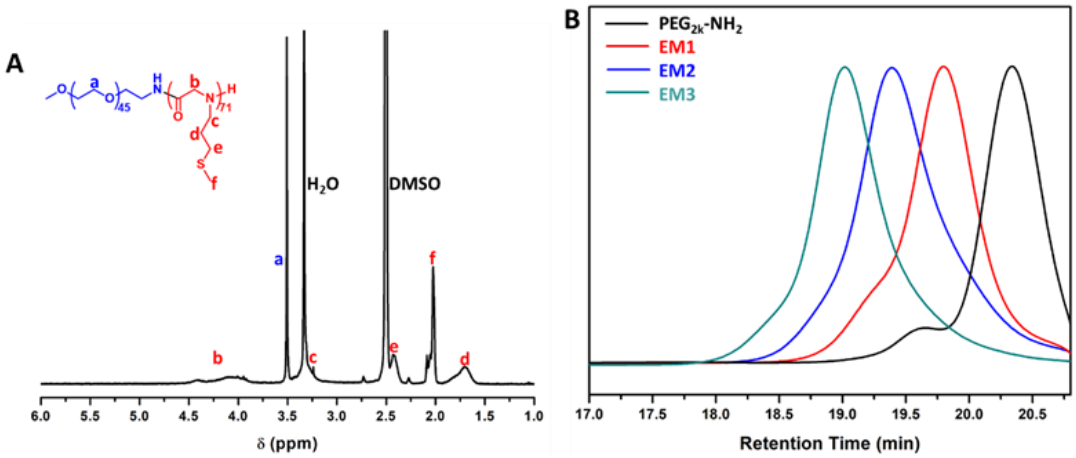

Figure 3. (A) Spectre ^{1}H-RMN de EM3 (PEG_{45}-*b*-$PMeSPG_{71}$); (B) Les traces GPC (0.01 M LiBr/DMF comme l'éluant) des copolymères EM1, EM2, EM3 et leur initiateur PEG_{45}-NH_2.

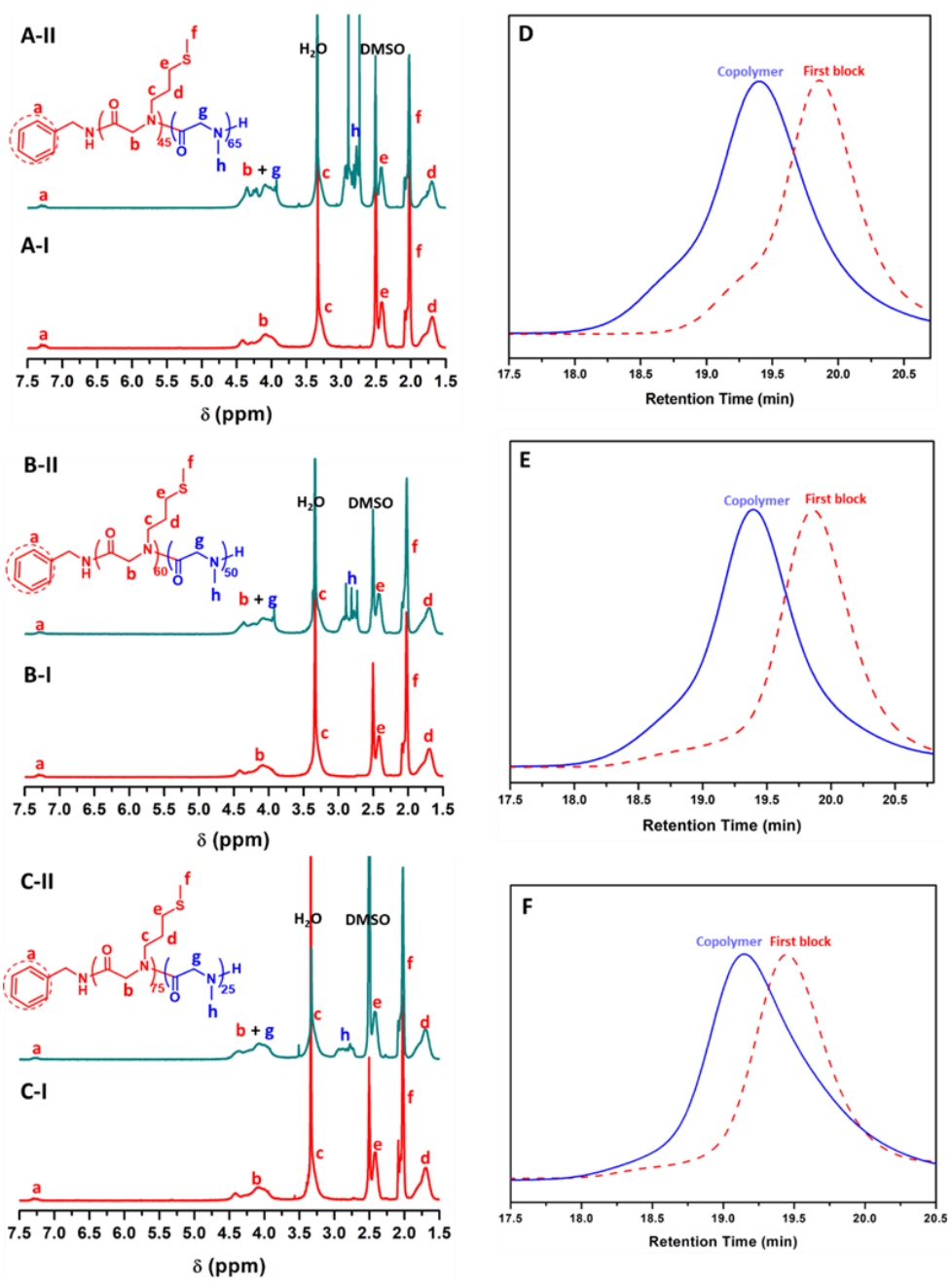

Figure 4. Spectres ^{1}H-RMN de (A) MS1, (B) MS2 et (C) MS3 révélant les structures des premiers blocs (I) et des copolymères (II); Traces GPC de (D) MS1, (E) MS2 et (F) MS3 révélant les MWs des premiers blocs (rouge) et les copolymères (bleu).

Auto-assemblage thermo-sensible de PSar-*b*-PCL-*b*-PSar

L'auto-assemblage de deux copolymères triblocs PCL-PSar, CS7 ($PSar_8$-*b*-PCL_{28}-*b*-$PSar_8$) et CS10 ($PSar_{16}$-*b*-PCL_{40}-*b*-$PSar_{16}$) dans l'eau est étudié en détail à l'aide de méthodes de nanoprécipitation et d'hydratation de film. Des feuilles et nanofibres unilamellaires (8−10 nm d'épaisseur et de diamètre) ont été obtenues par nanoprécipitation des copolymères à température ambiante (Figure 5). Ces lamelles et structures fibreuses peuvent être transformées en particules cylindriques et sphériques (30−100 nm de diamètre) après chauffage à 65 °C (Figure 6A&B), au-dessus de la température de fusion (T_m) du PCL et de la température de transition vitreuse (T_g) du PSar. Le chauffage à 90 °C conduit finalement aux polymeromes multilamellaires pour CS10 (100−500 nm de diamètre and 20−50 nm d'épaisseur), coexistant avec quelques sphères (Figure 6C). Alors que seules des sphères sont obtenues pour CS7 après le chauffage à 90 °C (Figure 6D). La mesure de la turbidité en fonction de la température révèle que la transformation morphologique commence autour du T_m des blocs PCL (50−55 °C, en Figure 7). Il suggère un lien étroit entre l'auto-assemblage et la cristallisation des blocs PCL.

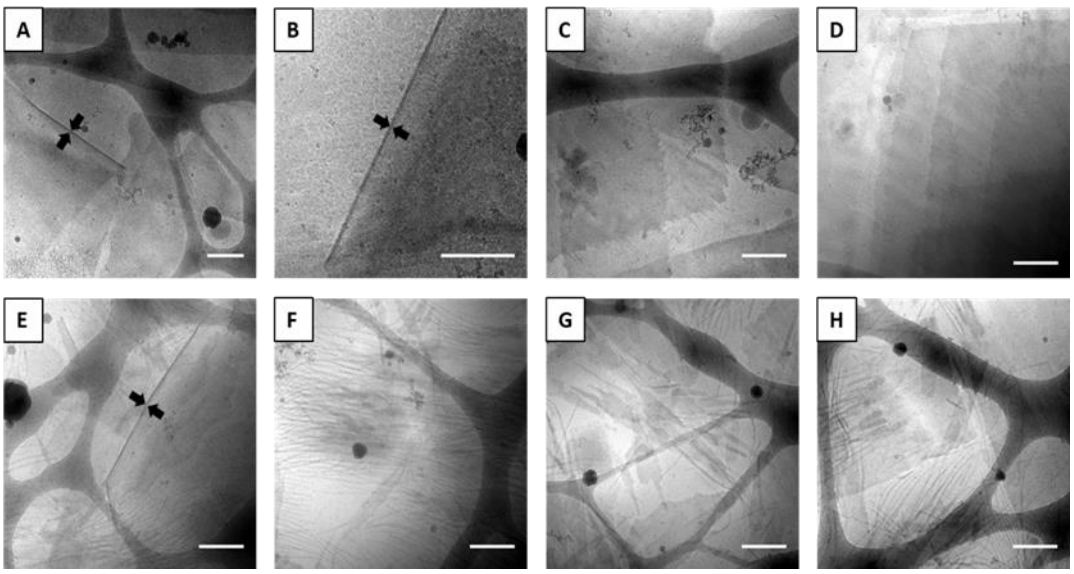

Figure 5. Images cryo-EM d'échantillons nanoprécipités de CS7 (A−D) et CS10 (E−H). Barre d'échelle = 300 nm.

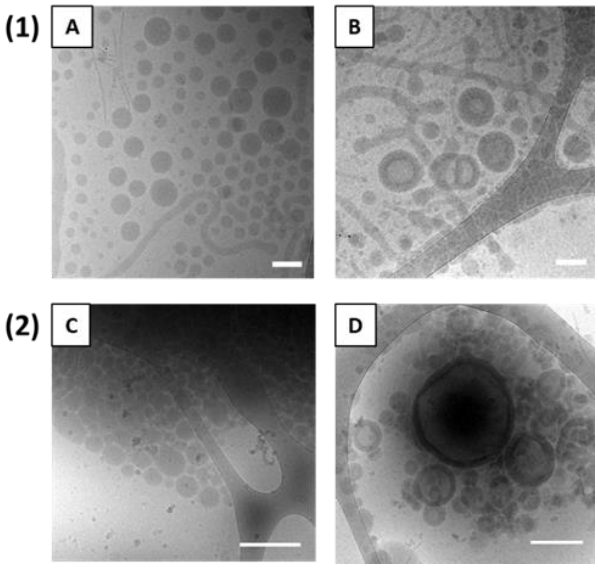

Figure 6. Images cryo-EM d'échantillons nanoprécipités de: (1) CS7 (A) et CS10 (B) après le chauffage de 30 min à 65 °C; (2) CS7 (C) et CS10 (D) après le chauffage de 24 h à 90 °C. Barre d'échelle = 100 nm en A et B. Barre d'échelle = 300 nm en C et D.

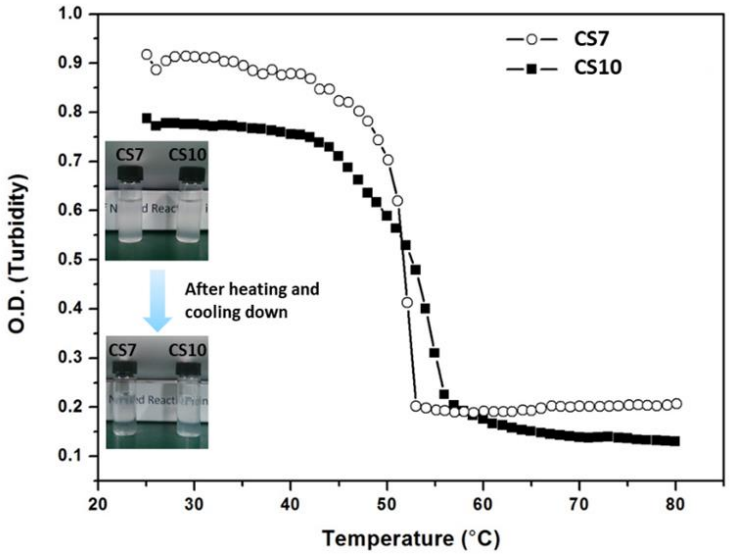

Figure 7. Evolution de la turbidité en fonction de la température pour les dispersions aqueuses d'auto-assemblages de CS7 (○) et de CS10 (■) préparées par nanoprécipitation, mesurées à une longueur d'onde de 600 nm avec un intervalle de température de 1 °C à la vitesse de 1 °C / min de 25 à 80 °C. Les photographies à gauche révèlent directement le changement de turbidité des échantillons nanoprécipités de CS7 et CS10 après le chauffage.

La transformation morphologique commence à partir des lamelles, cependant, la formation de vésicules CS10 semble différente de celle du Mécanisme I, où les lamelles se ferment en vésicules. Une analyse détaillée des polyméromes de CS10 révèle que les vésicules ne sont pas unilamellaires mais multilamellaires. Le scénario de formation des vésicules est proche du Mécanisme II, où les polymeromes multilamellaires sont formés par diffusion d'eau dans des sphères de polymère (c'est-à-dire des micelles plus grosses et complexes) lors du chauffage.

Une autre méthode d'auto-assemblage, l'hydratation du film, qui comprend également un traitement thermique au cours de l'étape d'hydratation, est réalisée sur CS7 et CS10, afin d'obtenir des vésicules de taille micrométrique. Comme indiqué par CLSM, des bâtonnets (Figures 8A&B) et quelques vésicules de taille micrométrique (Figures 8C&D) sont observées pour les deux copolymères.

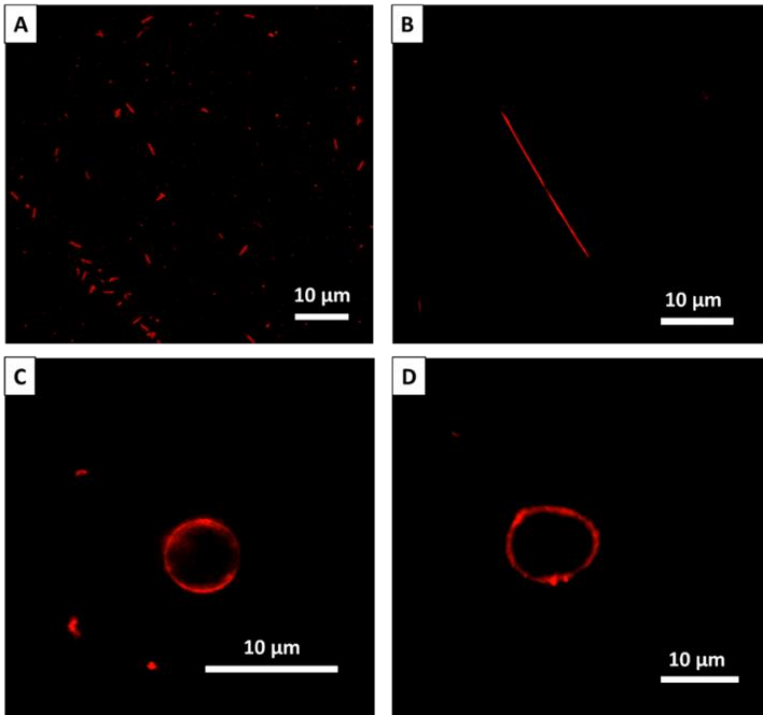

Figure 8. Images CLSM d'auto-assemblages obtenues par l'hydratation du film de CS7 (A, C) et CS10 (B, D). Le rouge de Nil a été ajouté dans la préparation à un rapport pondéral de 1 : 100 (rouge de Nil au copolymère) pour observation. Des bâtonnets (A, B) et des vésicules géantes (C, D) sont observés. Barre d'échelle = 10 µm.

Pour évaluer la biocompatibilité, la solution aqueuse dialysée de CS10 provenant de la nanoprécipitation est utilisée dans le test de viabilité cellulaire avec le MTT comme indicateur. L'histogramme présenté à la Figure 9 indique que la viabilité relative des cellules testées dépasse 80% même avec les auto-assemblages de CS10 à une concentration de 0.69 mg/mL, ce qui confirme la biocompatibilité fiable des copolymères PCL-PSar et leurs échantillons d'auto-assemblage.

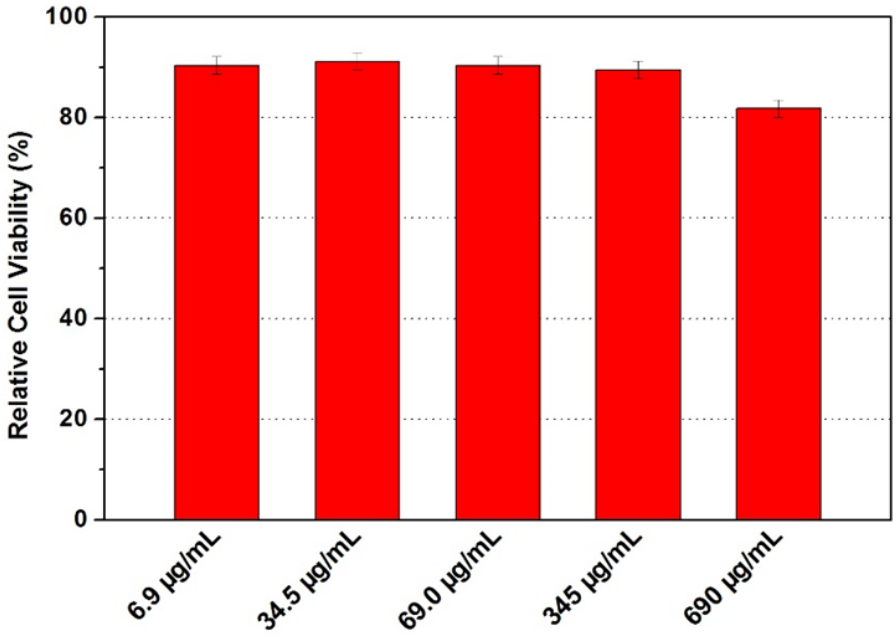

Figure 9. Viabilité cellulaire relative de CS10 pour les cellules L929 après 4 h d'incubation à 37 °C et à une concentration de 6.9, 34.5, 69.0, 345 et 690 µg/mL.

Auto-assemblage de copolymères à blocs amphiphiles contenant PMeSPG

Les études d'auto-assemblage ont été menées sur les copolymères PEG-*b*-PMeSPG et PMeSPG-*b*-PSar, pour la formation de vésicules polypeptoids. Dans l'étude d'auto-assemblage par nanoprécipitation, trois copolymères PEG-*b*-PMeSPG, EM1 (PEG_{45}-*b*-$PMeSPG_{17}$, $f_{PEG,\ wt}$ = 45%), EM2 (PEG_{45}-*b*-$PMeSPG_{40}$, $f_{PEG,\ wt}$ = 26%) et EM3 (PEG_{45}-*b*-$PMeSPG_{71}$, $f_{PEG,\ wt}$ = 16%), avec le MW croissant et le rapport hydrophile décroissant, forment respectivement les nanosphères solides, les micelles sphériques et vermiculaire, ainsi que les lamelles et vésicules, comme les structures dominantes (Figure 10).

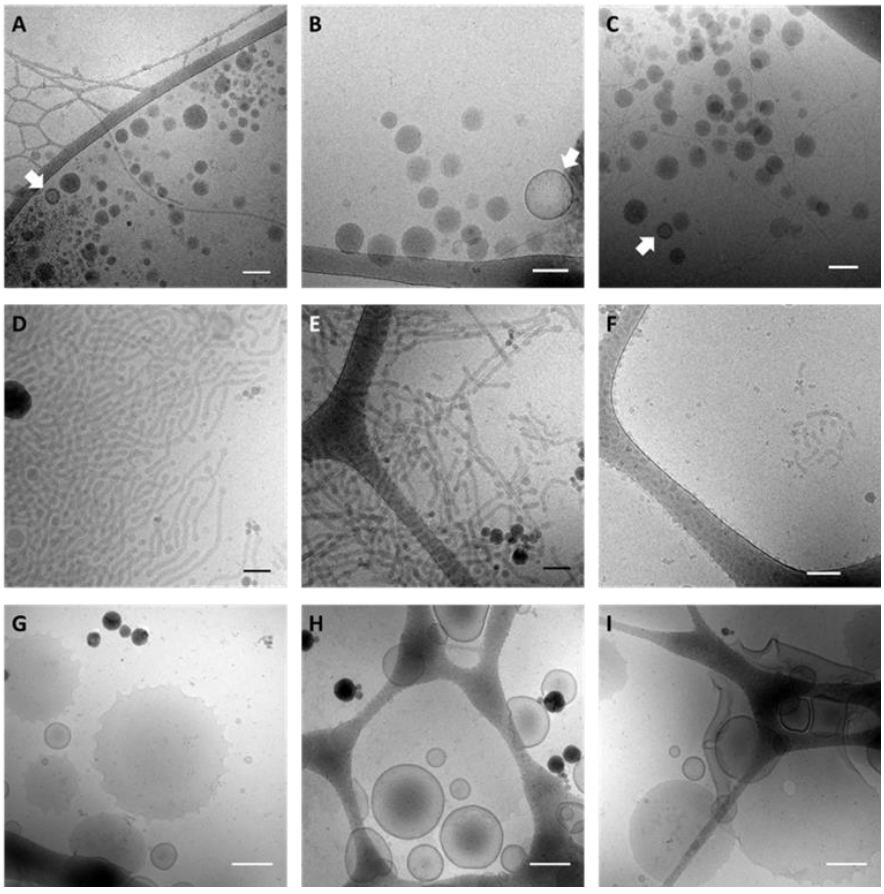

Figure 10. Images cryo-EM des auto-assemblages de EM1 (A−C), EM2 (D−F) et EM3 (G−I) par nanoprécipitation. Barre d'échelle = 100 nm pour A−F; barre d'échelle = 300 nm pour G−I.

Tous les trois copolypeptoids PMeSPG-*b*-PSar, MS1 (PMeSPG$_{45}$-*b*-PSar$_{65}$, $f_{PSar, wt}$ = 41%), MS2 (PMeSPG$_{60}$-*b*-PSar$_{50}$, $f_{PSar, wt}$ = 29%) et MS3 (PMeSPG$_{75}$-*b*-PSar$_{25}$, $f_{PSar, wt}$ = 14%), peuvent former polymérosomes par nanoprécipitation (Figure 11). La structure des vésicules diffère dans les morphologies et les tailles en raison des différents rapports hydrophiles et MWs. Dans le même temps, les auto-assemblages des trois copolypeptoids sont évidemment non ergodique: les structures métastables, y compris micelles sphérique, lamelles, vésicules non fermés et vésicules de forme irrégulière coexistent dans le résultat du même copolypeptoid. Le comportement de PSar dans l'eau est analysé par la diffusion de neutrons à petit angle (SANS) et DLS, qui révèlent que PSar forme des grappes dans l'eau, plutôt que des bobines à chaîne unique comme le PEG. La différence de solubilité dans l'eau entre PSar et PEG est une des principales raisons de la différence d'auto-assemblage entre PEG-*b*-PMeSPG et PMeSPG-*b*-PSar, ainsi que la solubilité insuffisante de PSar dans l'eau est également probablement responsable de la nonergodicité de l'auto-assemblages de PMeSPG-*b*-PSar.

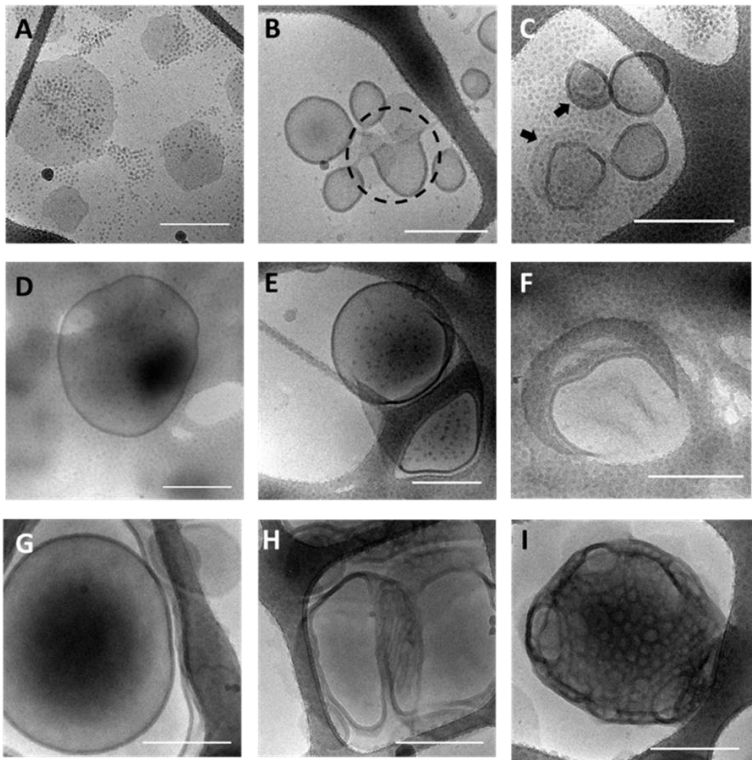

Figure 11. Images cryo-EM des auto-assemblages de MS1 (A−C), MS2 (D−F) et MS3 (G−I) par nanoprécipitation. Barre d'échelle = 300 nm.

En utilisant les propriétés thermodynamiques de PMeSPG, Vésicules sont obtenues de MS1 et MS2 par hydratation de film impliquant un chauffage (Figure 12). La transformation des vésicules MS2 de formes irrégulières à formes sphériques uniformes, parallèlement au temps du chauffage, confirme la possibilité de contrôler la morphologie d'auto-assemblage en fonction des conditions de préparation (Figure 13). Vésicules de taille micrométrique peuvent être obtenues de MS1−MS3 par la méthode de double émulsion, où les vésicules sont formées sous la direction de gouttelettes de double émulsion eau dans huile dans eau (W/O/W), pendant l'évaporation du chloroforme (Figure 14).

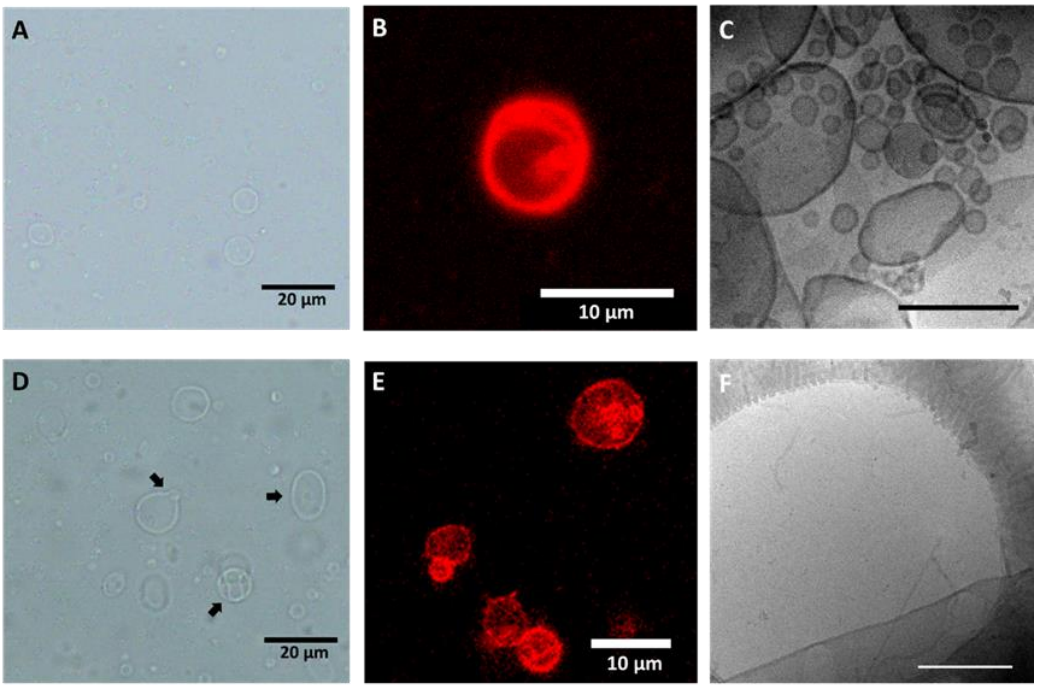

Figure 12. Images par microscopie optique à champ clair (A, D), CLSM (B, E) et cryo-EM (C, F) d'auto-assemblages de MS1 (A−C) et MS2 (D − F), par hydratation de film avec le chauffage de 48 h à 70 °C. Barre d'échelle = 300 nm pour C et F.

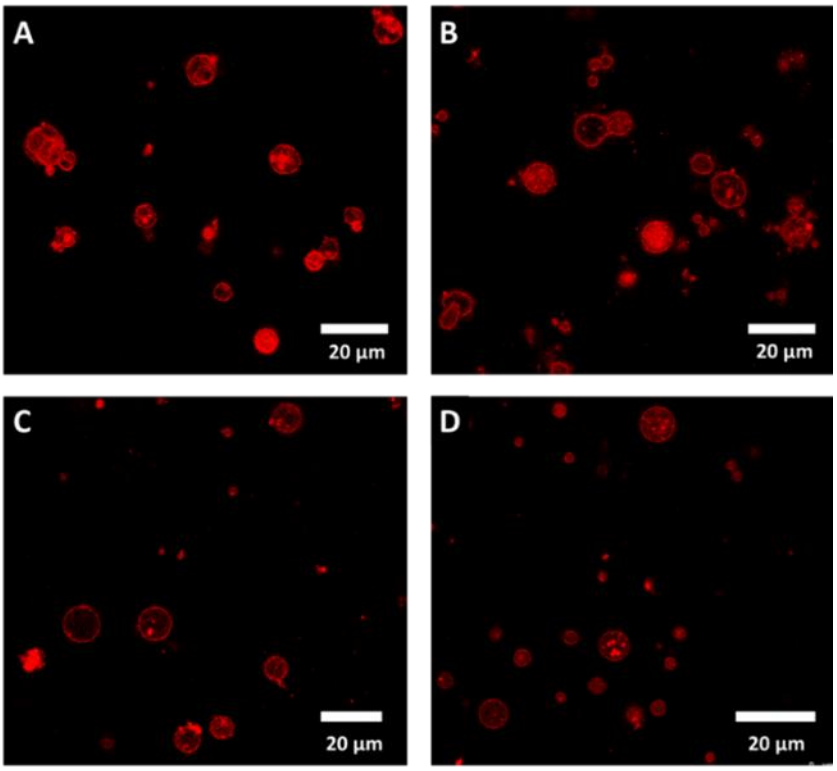

Figure 13. Images CLSM des vésicules MS2 par hydratation de film, après 48 h (A), 72 h (B), 144 h (C) et 168 h (D) du chauffage à 70 °C.

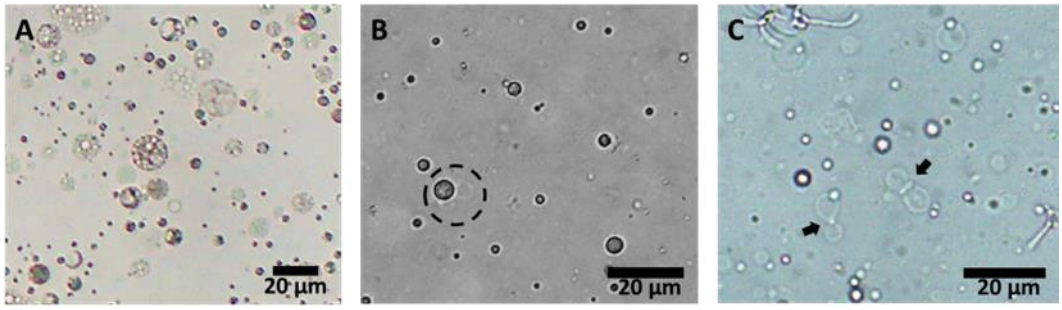

Figure 14. Images microscopiques optiques à champ clair de l'émulsion double W/O/W de MS1 avant l'évaporation du chloroforme (A), après 12 h d'évaporation du chloroforme (B), et après 24 h d'évaporation du chloroforme (C).

MS3 forme les nanoparticules à structure bicontinue à l'intérieur, dans les auto-assemblage par nanoprécipitation et hydratation de film, en raison du rapport hydrophobe dominant (Figure 15). Les intermédiaires métastables sont capturés en tant qu'aspect de la nonergodicité des auto-assemblages de MS3, et l'analyse

morphologique de ces intermédiaires peut prouver le mécanisme de formation de nanoparticules bicontinues par fusion interlamellaire (Schème 4).

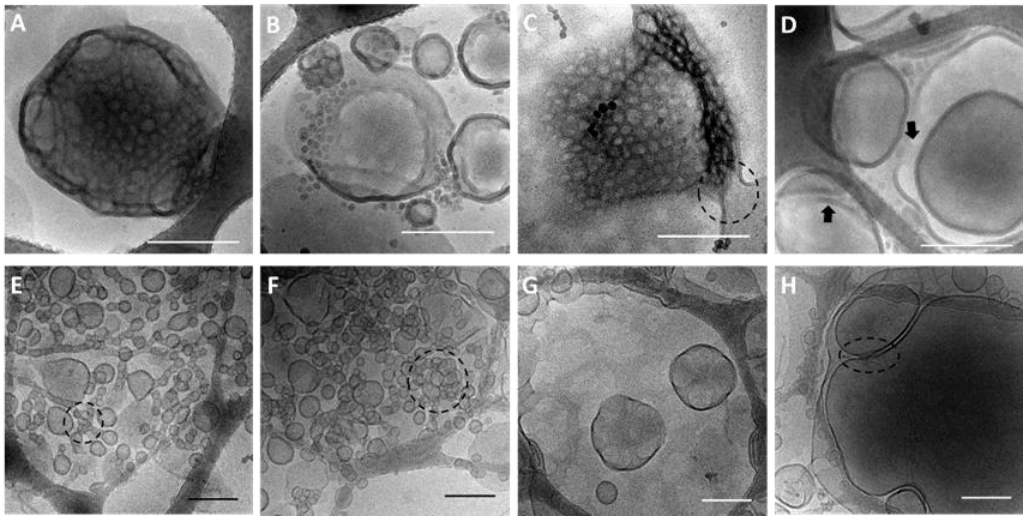

Figure 15. Images cryo-EM des nanoparticules bicontinues et les structures intermédiaires de MS3 par nanoprécipitation (A−D) et double émulsion (E−H). Barre d'échelle = 300 nm.

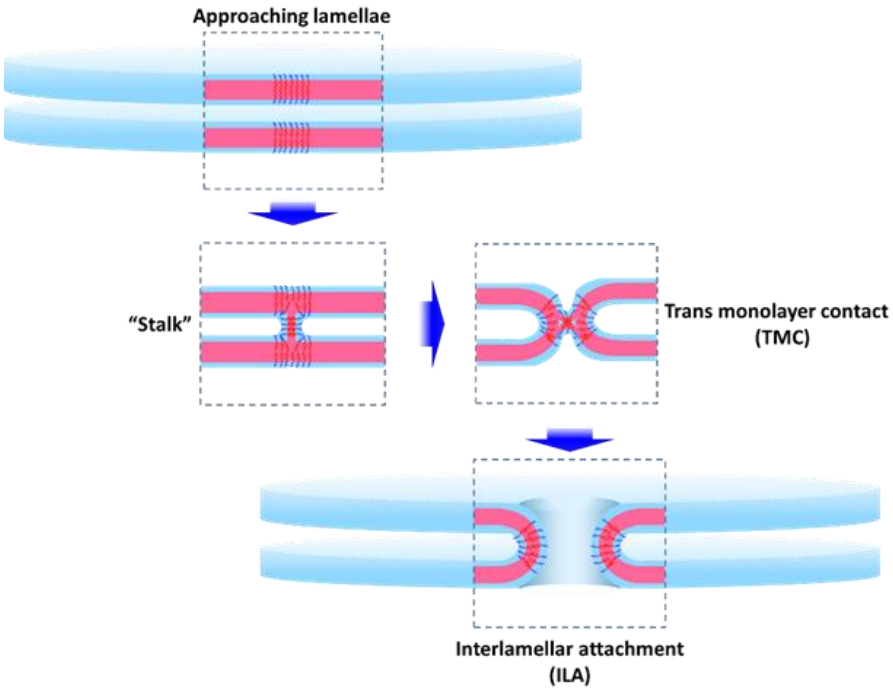

Schème 4. La procédure de formation d'un attachement interlamellaire (ILA) entre deux lamelles approchées, dans le mécanisme de fusion interlamellaire.

Vésicules stimulables à base de PMeSPG-*b*-PSar

Le polypeptoid portant thioéthers est conçu pour ses caractéristiques stiumulables en réponse à l'oxydation. En effet, le desassemblage des vésicules polypeptoids de PMeSPG-*b*-PSar sensible à l'oxydation a été obtenu en raison de la transition « thioéther−sulfoxyde » (Figure 16) stimulée respectivement par le peroxyde d'hydrogène (H_2O_2) et par l'oxygène singulet ($^1O_2$) produit en presence de la lumière. Les polymérosomes et autres structures d'auto-assemblage de MS1 par nanoprécipitation sont désassemblés après le traitement avec 10 wt% (2.94 M) H_2O_2, ne laissant que peu de grappes irrégulières lâches avec certaines cavités en forme de disques, révélés par cryo-EM (Figure 17).

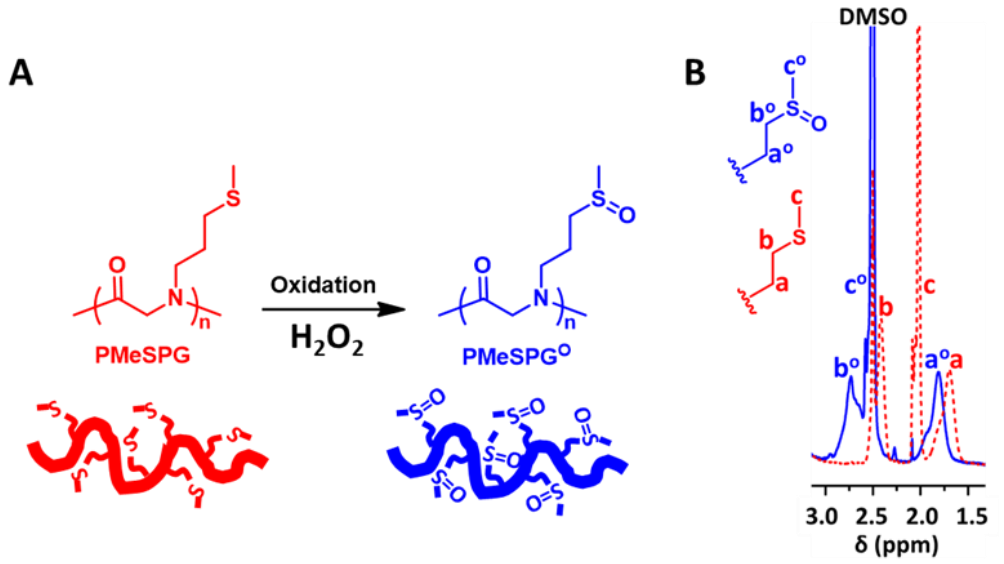

Figure 16. (A) Schéme d'oxydation de PMeSPG avec thioéther à PMeSPG^O avec sulfoxyde. (B) PMeSPG et PMeSPG^O suivis par spectres ^{1}H-RMN (dans DMSO-d_6). Les pics des protons adjacents à l'atome de soufre (a, b, c, tiret rouge) se déplacent vers le bas du champ (a^o, b^o, c^o, solide bleu) et confirment le passage du thioéther au sulfoxyde.

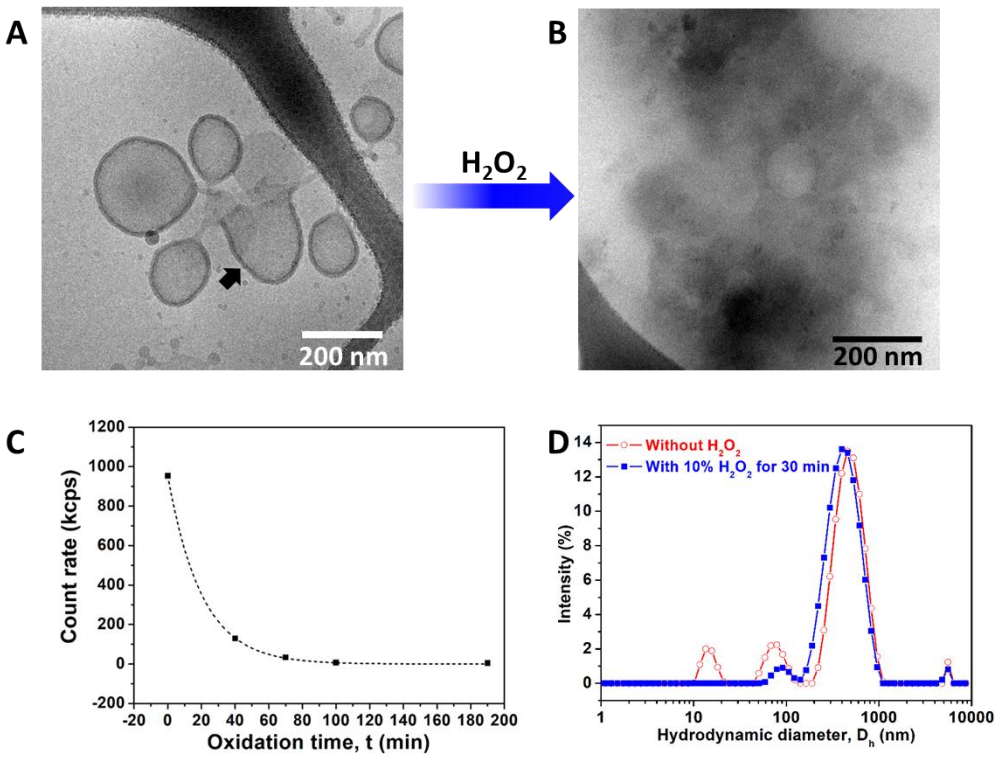

Figure 17. (A) et (B) Images cryo-EM des auto-assemblages MS1 obtenues par nanoprécipitation avant tout traitement (A) et après 90 minutes d'un traitement à 10 wt% H_2O_2 (B). (C) Évolution du diamètre hydrodynamique moyen (D_h) (sphères noires) et des taux de comptage (triangles bleus) des auto-assemblages MS1 mesurés par DLS en fonction du temps du traitement de 10 wt% H_2O_2. (D) La distribution en taille des auto-assemblages MS1 mesurée par DLS avant (rouge) et après (bleu) le traitement de 10 wt% H_2O_2 de 30 min.

La transformation détaillée en réponse à l'oxydation est enregistrée par CLSM des vésicules géantes MS2 par double émulsion, qui ont deux voies à distabliser sous la stimulation de 8.8 mM H_2O_2 (Figure 18). DLS et RMN sont utilisés pour confirmer l'oxydation chimique des copolymères (Figure 19).

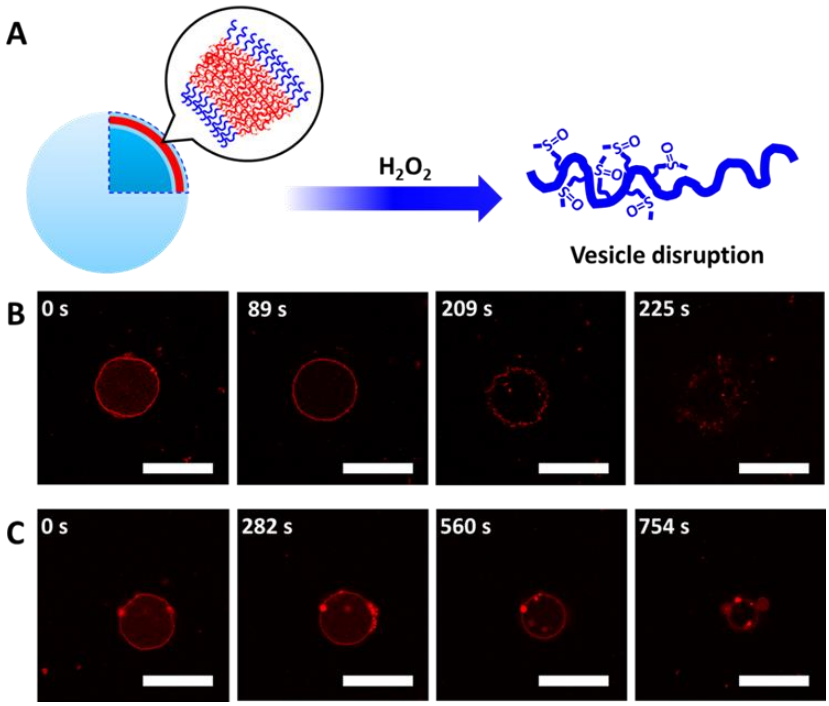

Figure 18. (A) Illustration schématique de la destablization de la vésicule PMeSPG-*b*-PS en raison de la transition « thioéther−sulfoxyde » dans les blocs de PMeSPG sous la stimulation de H_2O_2. Le CLSM enregistre la rupture de la vésicule dans deux voies différentes représentées par (B) et (C), sous la condition de 8.8 mM H_2O_2, avec le rapport molaire de [H_2O_2]: [MeSPG] = 3.62 : 1. (B) voie I^O: la vésicule passe d'abord de vésicule ondulée et disquette à une vésicule bien arrondie dans les 89 premières secondes, puis la membrane commence à fluctuer de plus en plus intensément et de nombreux pores apparaissent autour de la surface de la vésicule (209 s) conduisant finalement à l'éclatement de la vésicule (225 s). (C) Voie II^O: la vésicule change d'abord en passant de vésicule ondulée et disquette à une vésicule bien arrondie au cours des 282 premières secondes; elle rapetisse en taille plus petite (exemple à 560 s) et a un bourgeonnement externe au dernier scène (754 s). Barre d'échelle = 25 µm.

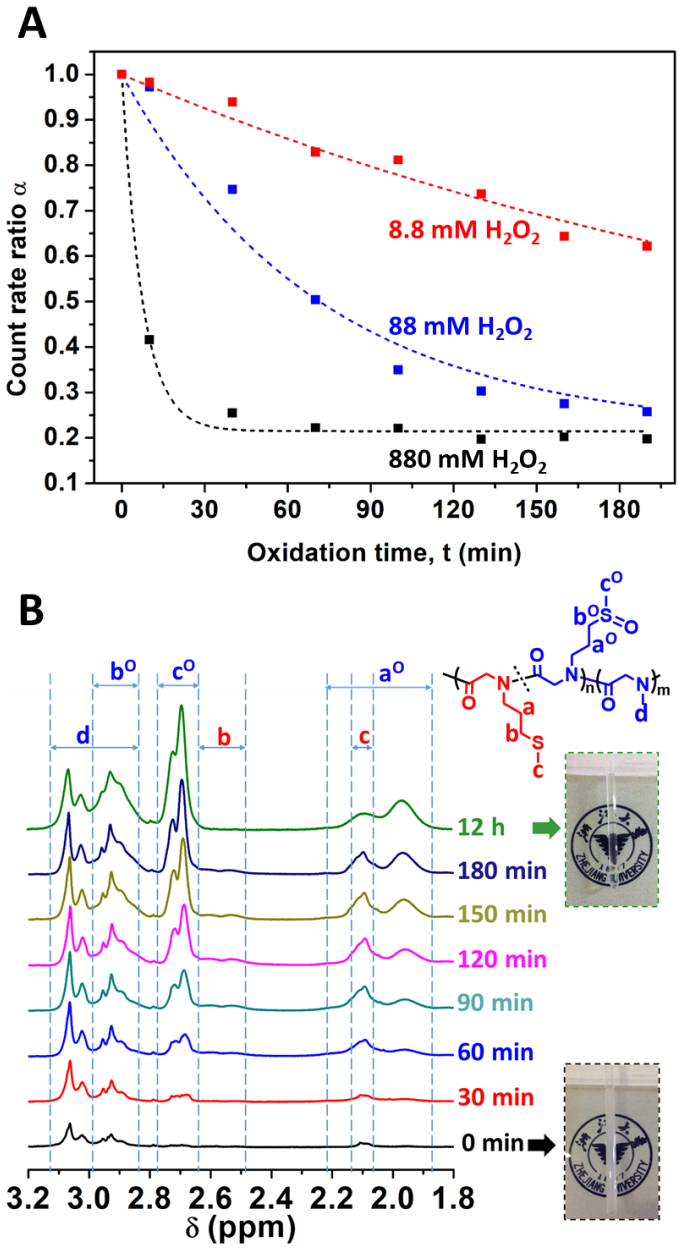

Figure 19. (A) Le rapport des taux de comptage α_t (α_t = taux de comptage à l'instant t) / (taux de comptage à t = 0 avant l'addition de H_2O_2) en fonction du temps d'oxydation t, à différentes concentrations de H_2O_2 (8.8 mM, 88 mM et 880 mM). (B) Spectres ^{1}H-RMN de polymersomes MS2 obtenus par émulsion double dans D_2O en présence de 176 mM H_2O_2 avec le rapport molaire de [H_2O_2] : [MeSPG] = 3.62 : 1. Les photographies d'un tube d'échantillon RMN à côté des spectres ^{1}H-RMN montrent clairement le changement de turbidité (de turpide à transparent) de la dispersion de polymersomes avant et après oxydation.

Afin d'obtenir la vésicule sensible au stimulus distant et contrôlable, les polymersomes MS2 sont chargés avec le photosensibilisateur tétraphénylporphyrine (TPP), qui peut générer du $^1O_2$ par l'activation de la lumière. Dans l'observation en temps réel sous CLSM, la déstabilisation des polymérosomes MS2 chargés en TPP est capturée, ce qui est initiée par le laser confocal localisé (HeNe 543 nm avec une puissance maximale de travail à 1.5 mW) du CLSM (Figure 20 et Figure 21). La déstabilisation photo-stimulable a des voies similaires à celles de la déstabilisation stimulée par H_2O_2, mais peut être obtenue avec une contrôlabilité et une efficacité bien meilleures.

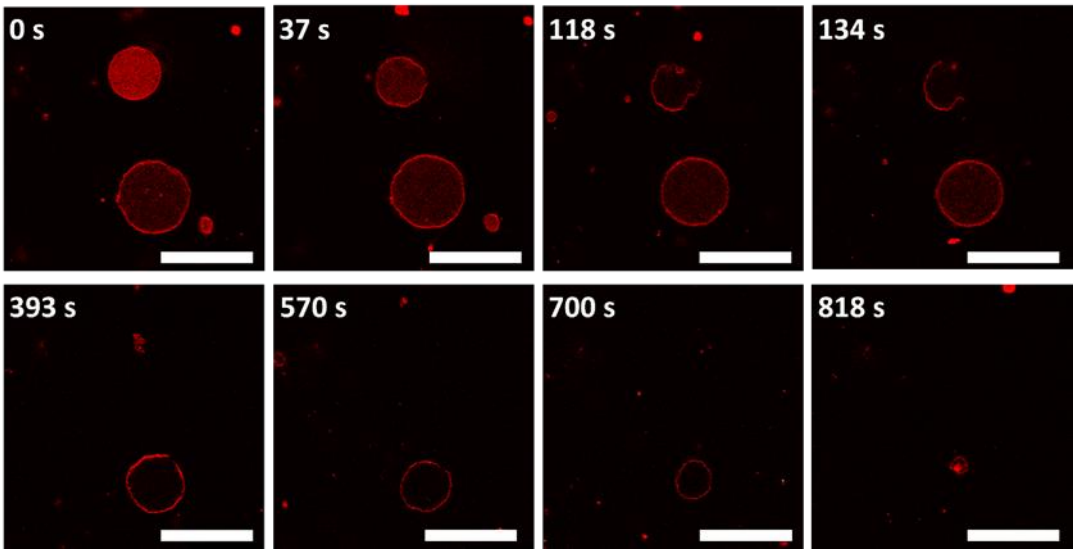

Figure 20. Instantanés de la séquence d'évolution de deux polymersomes MS2 marqués au rouge de Nil et chargés de TPP (rapport molaire de [TPP] : [MeSPG] = 1 : 30) sous l'éclairage du laser confocal (543 nm) de CLSM à la puissance de travail maximale de 1.5 mW. Deux voies sont observées pour la perturbation de polymersome. Barre d'échelle = 25 nm.

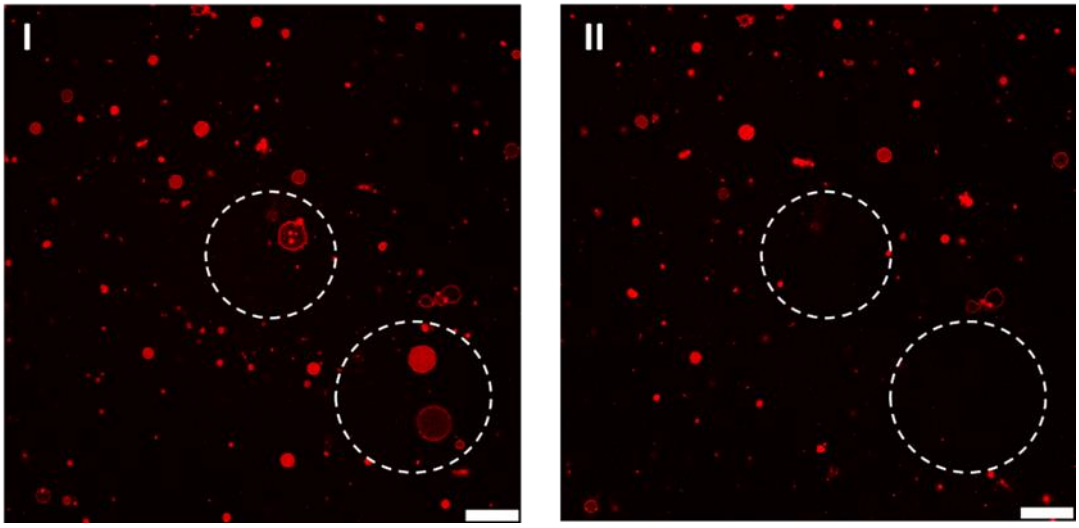

Figure 21. Les images CLSM d'une grande zone avant (I) et après (II) l'observation d'environ 15 minutes, avec deux points focalisés repérés par les cercles décrits en Figure 20. Les vésicules dans la mise au point du laser disparaissent, alors que celles des autres régions demeurent. Barre d'échelle = 25 nm.

Acknowledgements

Firstly, I would like to express my sincere gratitude to my supervisor Dr. Min-Hui Li for the continuous support of my Ph.D. study and related research, for her patience, motivation, and immense knowledge. Her guidance helped me in all the time of research and writing of this thesis. I could not have imagined having a better advisor and mentor for my Ph.D. study.

Besides my supervisor, I would like to thank the rest of my thesis committee: Prof. Sébastien Lecommandoux, Dr. Véronique Schmitt, Prof. Yixian Wu and Dr. Patrick Keller, for their insightful comments and encouragement, but also for the hard question which incented me to widen my research from various perspectives.

I thank my fellow labmates and friends: Yujiao Fan, Dapeng Zhang, Hui Chen, Bin Ni, Liang Zhao, Wei Qiang, Benoît Rhonés… for the stimulating discussions, for the sleepless nights we were working together before deadlines, and for all the fun we have had in the last three years. Also I thank my coworkers and friends in Zhejiang University. In particular, I am very grateful to Prof. Jun Ling and Dr. Xinfeng Tao for enlightening me the first glance of research.

I acknowledge the French National Research Agency (project ANR-16-CE29-0028) and the National Natural Science Foundation of China (project 21528402 and 21674091) for financial support. I also thank the China Scholarship Council for funding my Ph.D. scholarship in France.

Last but not the least, I would like to thank my parents for supporting me unswervingly throughout the accomplishment of the thesis. Their encouragement reinforced me to overcome every challenge coming from the work. My father was a diligent and respectable police officer, his hard work supported the whole family, but also damaged his health. He was diagnosed with cancer, and fought against it for five years. The news that I got an opportunity to persue the Ph.D. degree was his last comfort.

My mother is an incredible woman. She was not defeated by the sorrow and bitterness that life brought to her, but smiled to life, and kept a warm home in my back. Mother has an independent spirit, and persues a new life with considerable bravery and wisdom. She is a role model in my life. I will take my every effort to fulfill my dream, to be a responsible and respectable scientist. It would be the best present I can give back to my loving family and friends.

Outline

Abstract

As a robust nanocontainer with polymeric bilayer structure, polymer vesicle, also called polymersome, has been considered as potential drug carrier in biomedical field, because of its cell-mimicking structure, high stability and capability to be functionalized. For practical use of polymersomes in biomedical applications, the biocompatibility of the copolymers that compose the vesicles become an important issue. Polypeptoid is a class of polypeptide derivatives of which the nitrogen atoms of amides are substituted. By avoiding the formation of inter- and intramolecular hydrogen bonds, polypeptoids have much better solubility than polypeptides in common organic solvent, while the biocompatibility is well maintained. Reports on self-assemblies of polypeptoid-containing block copolymers start to appear in the literature. However, works on polypeptoid vesicles are still scarce. In the present study, two families of polypeptoid-containing amphiphilic block copolymers are synthesized through the ring-opening polymerization (ROP) of *N*-substituted amino acid *N*-thiocarboxyanhydrides (NNTAs). Various techniques like nanoprecipitation, film hydration and double emulsion are used to perform the self-assemblies with the objective to obtain polypeptoid vesicles. The self-assemblies are investigated in detail by DLS, cryo-EM, confocal laser scanning microscope (CLSM) and ^{1}H-NMR.

In the first family of copolymers, ROP of sarcosine NTA (Sar-NTA) is initiated by oxyamino-ended poly(*ε*-caprolactone) (PCL), to obtain diblock copolymer PCL-*b*-PSar and triblock copolymer PSar-*b*-PCL-*b*-PSar. Unilamellar sheets and nanofibers are obtained by nanoprecipitation of PSar-*b*-PCL-*b*-PSar copolymers at room temperature. These lamellae and fibrous structures are transformed into worm-like cylinders and spheres after heating to 65 ℃. Heating at 90 ℃ leads eventually to multilamellar polymersomes.

The second family of copolymers is based on a thioether-bearing polypeptoid, poly(*N*-3-(methylthio)propyl glycine) (PMeSPG). The new monomer, MeSPG-NTA is

obtained from a "decarboxylation−*N*-carboxymethylation" procedure from methionine, followed by cyclization. The amphiphilic block copolymers PEG-*b*-PMeSPG and PMeSPG-*b*-PSar are synthesized with different molecular weights and hydrophilic/hydrophobic ratios. Vesicles have been achieved with different methods, and the mechanism of vesicle formation through diverse nonergodic morphologies are discussed in detail.

The thioether-bearing polypeptoid is designed because of its oxidation-responsive features. Effectively, oxidation-responsive disruption is achieved for the PMeSPG-*b*-PSar polypeptoid vesicles, based on the "thioether−sulfoxide" transition stimulated by hydrogen peroxide (H_2O_2) and light-induced singlet oxygen ($^1O_2$) respectively. The oxidation- responsive and photo-responsive polypeptoid vesicles can be used as promising vehicles for smart drug release applications.

Résumé

Comme un nanoconteneur robuste formé d'une bicouche de polymères amphiphiles, vésicule polymère, aussi appelée polymersome, a été considérée comme un vecteur de médicament potentiel dans le domaine biomédical, grâce à sa structure imitant les cellules, sa grande stabilité et sa capacité à être fonctionnalisée. Pour l'utilisation pratique des polymeromes dans des applications biomédicales, la biocompatibilité des copolymères qui composent les vésicules devient un sujet important. Le polypeptoid est une classe de dérivés polypeptides dont les atomes d'azote des amides sont substitués. En évitant la formation de liaisons hydrogène inter- et intramoléculaires, les polypeptoids ont des solubilités bien meilleures que les polypeptides dans des solvants organiques usuels, tandis que la biocompatibilité est bien maintenue. Des travaux sur l'auto-assemblage de copolymères à blocs contenant polypeptoids émergent dans la littérature. Cependant, les travaux sur les vésicules polypeptoids sont encore rares. Dans cette thèse, deux familles de copolymères à blocs amphiphiles contenant les polypeptoids ont été synthétisées par la polymérisation par ouverture de cycle (ROP) de *N*-thiocarboxyanhydrides d'acides aminés *N*-substitués (NNTA). Différentes techniques telles que la nanoprécipitation, l'hydratation de film mince et la double émulsion ont été utilisées pour réaliser les auto-assemblages dans le but d'obtenir des vésicules polypeptoids. Les auto-assemblages ont été étudiés en détail par DLS, cryo-EM, microscope confocale à balayage laser (CLSM) et ^{1}H-RMN.

Dans la première famille de copolymères, la ROP de la sarcosine NTA (Sar-NTA) a été initiée par le poly(ε-caprolactone) (PCL) à terminaison -oxyamine, pour obtenir le copolymère dibloc PCL-*b*-PSar, et le copolymère tribloc PSar-*b*-PCL-*b*-PSar. Des feuilles et nanofibres unilamellaires ont été obtenues par nanoprécipitation des copolymères PSar-*b*-PCL-*b*-PSar à température ambiante. Ces lamelles et structures fibreuses peuvent être transformées en particules cylindriques et sphériques après

chauffage à 65 °C. Le chauffage à 90 °C conduit finalement à des polymeromes multilamellaires.

La seconde famille de copolymères est basée sur un polypeptoid portant thioéthers, la poly(*N*-3-(méthylthio)propyl glycine) (PMeSPG). Le nouveau monomère, MeSPG-NTA, a été préparé par une procédure de « décarboxylation−*N*-carboxyméthylation » à partir de la méthionine, suivie d'une cyclisation. Les copolymères à blocs amphiphiles PEG-*b*-PMeSPG et PMeSPG-*b*-PSar ont été synthétisés avec de différentes masses moléculaires et de différents rapports de blocs hydrophile/hydrophobe. Les études d'auto-assemblage ont été menées sur ces copolymères pour la formation de vésicules polypeptoids. Des vésicules ont été obtenues avec de différentes méthodes, et le mécanisme de la formation des vésicules à travers diverses morphologies non-ergodiques a été discuté en détail.

Le polypeptoid portant thioéthers est conçu pour ses caractéristiques stiumulables en réponse à l'oxydation. En effet, le desassemblage des vésicules polypeptoids de PMeSPG-*b*-PSar sensible à l'oxydation a été obtenu en raison de la transition « thioéther−sulfoxyde » stimulée respectivement par le peroxyde d'hydrogène (H_2O_2) et par l'oxygène singulet ($^1O_2$) produit en presence de la lumière. Les vésicules polypeptoids oxydation-stimulable et photo-stimulable ainsi réalisés peuvent être des systèmes prometteurs dans des applications de relargages contrôlés des médicaments.

Chapter 1. State of the Arts

1.1 Self-assembly of amphiphilic block copolymers

Amphiphilic molecules can self-assemble in water, and form nano- or micro-structures of which the morphology is determined by the molecular properties and self-assembly conditions.[1] As one kind of macromolecules with amphiphilic structure, amphiphilic block copolymer observes the same principle and can self-assemble into various structures. As a dimensionless geometric parameter of the amphiphile, packing parameter, *p*, can be used to predict the self-assembly structure. Packing parameter is defined in equation: $p = v/a_0 l_c$, where v is the volume of hydrophobic part, a_0 is the optimal area of the hydrophilic part at the interface, and l_c is the length of hydrophobic chain. Generally, amphiphilic block copolymers form spherical micelles when $p \leq 1/3$, cylindrical micelles are favored from copolymers with $1/3 \leq p \leq 1/2$, and for the copolymers with $1/2 \leq p \leq 1$, copolymers tend to form vesicles, with enclosed membrane structure (Figure 1.1).[1-3]

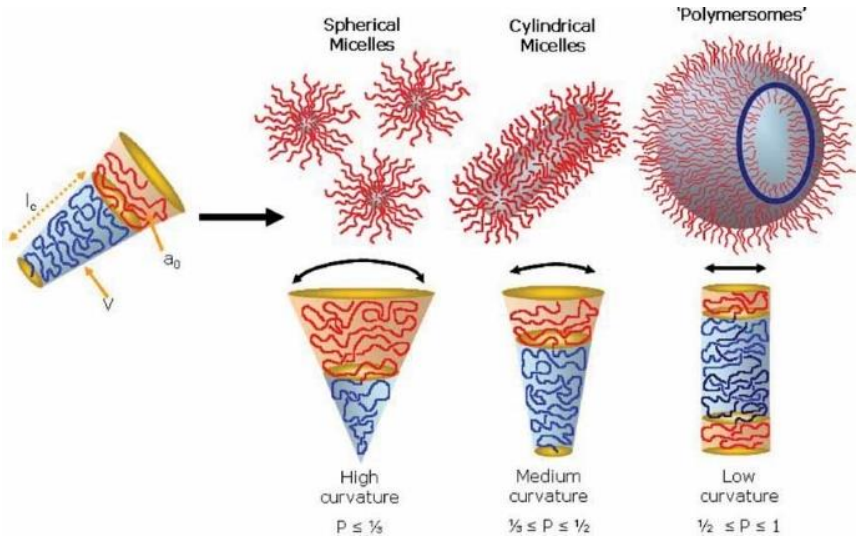

Figure 1.1. Self-assembly structures of amphiphilic block copolymers: spherical micelles, cylindrical micelles and polymer vesicles, with corresponding packing parameters.[3]

Packing parameter reveals the inherent molecular curvature and favorable conformation of a block copolymer in water, which is determined by properties including chain structure, molecular weight, hydrophilic/hydrophobic ratio, chain rigidity and intermolercular interactions, *etc*. In the thermodynamic view, the self-assembly of amphiphilic block copolymers is driven by the minimization of free energy. Nevertheless, the relatively high molecular weight sets barriers for copolymers to adjust conformation and position towards global equilibrium state, which is much more difficult than small molecules. Consequently on the one hand, self-assembly structures of amphiphilic block copolymers have relatively high stability, on the other hand, it is often found that the self-assembled structures of copolymers stop at a metastable stage, which is called "kinetically frozen".[4] As the result, the self-assembly of block copolymers shows nonergodic properties, with the coexistence of multiple morphologies.[5] The nonergodicity endows polymeric self-assemblies the potential of forming a large diversity of morphologies from the same block copolymer, which can be controlled by different preparing conditions. Various controlling or assistant methods come up in the research on block copolymer self-assemblies, including concentration variation,[6] temperature variation,[7] polarity of solvents,[8] crystallization,[9] addition of surfactant,[10] emulsification,[11] applying of electric field,[12] *etc*. By combining the inherent properties of block copolymers with the intervention of external process, structures with higher complexity can be generated, such as janus nanoparticles,[13] cyclic micelles,[14] alternating cylinders,[15] helix structures,[16] networks,[17] lamellae,[9] tubules,[7] onion-like vesicles,[18] faceted vesicles[19] and ellipsoidal vesicles,[20] *etc*.

For example, with the kinetic control, the team of Pochan and Wooley reported the preparation of cylinders and worm-like micelles with an alternating structure, by manipulating solvents in self-assembly.[15] Water is slowly added to the solution of poly(acrylic acid)-*block*-poly(methyl acrylate)-*block*-polystyrene (PAA-*b*-PMA-*b*-PS) and 2,2'-(ethylenedioxy)diethylamine (EDDA) in tetrahydrofuran (THF), forming separate spherical micelles (Figure 1.2A), where PMA and PS accumulate inside the

core, while the corona is composed of PAA, which is ionized by EDDA. THF is pipetted into the suspension quickly, turning the THF : H_2O ratio from 1 : 4 to 2 : 1. The system is forced back to a solvent composition where local lamellar structure is favored. As the result, spherical micelles turn into a disk-like shape, and tend to accumulate since the PAA-diamine pairs in the corona are immiscible in THF. With the anisotropic shape, disk-like micelles pack in a one-dimensional way, forming cylinders with an alternating structure (Figure 1.2B). The cylinders grow as the disks continue to pack, and develop into worm-like micelles (Figure 1.2C). In the late stage of growth, branches are formed when two disks pack to one end of the worm (Figure 1.2D).

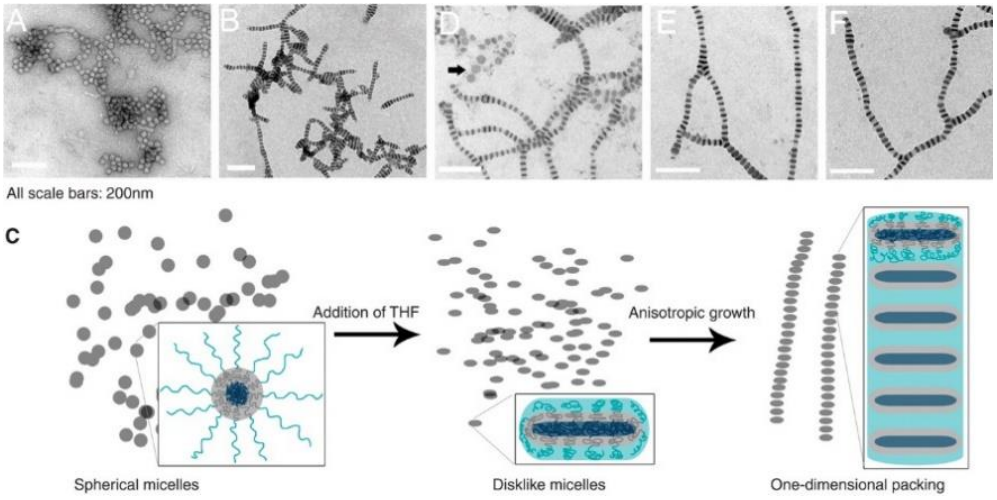

Figure 1.2. (A) The spherical micelles formed by triblock copolymer PAA_{94}-*b*-PMA_{103}-*b*-PS_{44} and EDDA (AA : EDDA = 1 : 1) in the mixture of THF : H_2O = 1 : 4; (B) cylinders resulted from the quick introfuction of THF; (C) the schematic illustration on the growth mechanism of ribbon-like structures; (D) worm-like micelles and separate disk-like micelles marked by black arrows; (E and F) branched structures formed in the late stage of growth. Scale bar = 200 nm.[15]

1.2 Polymersomes

Among the self-assembly structures of amphiphilic block copolymers, polymersome, that is polymer vesicle, has been a very attractive research object since the end of last century.[21] Polymersome has a cell-mimicking membrane structure,

which is a curved bilayer composed of block copolymers, and an aqueous inner cavity. Based on the polymeric composition, polymersome has higher bilayer thickness (10−30 nm) than that of liposome (~5 nm), possessing relatively higher stability.[21-22] Functional polymersomes can be obtained by molecular design on block copolymers. These outstanding capabilities endow polymersomes with high potential in applications such as drug delivery vehicles and nanoreactors, harvesting lots of attentions in the field of new materials and biomedicine.

1.2.1 Self-assembly mechanism of polymersomes

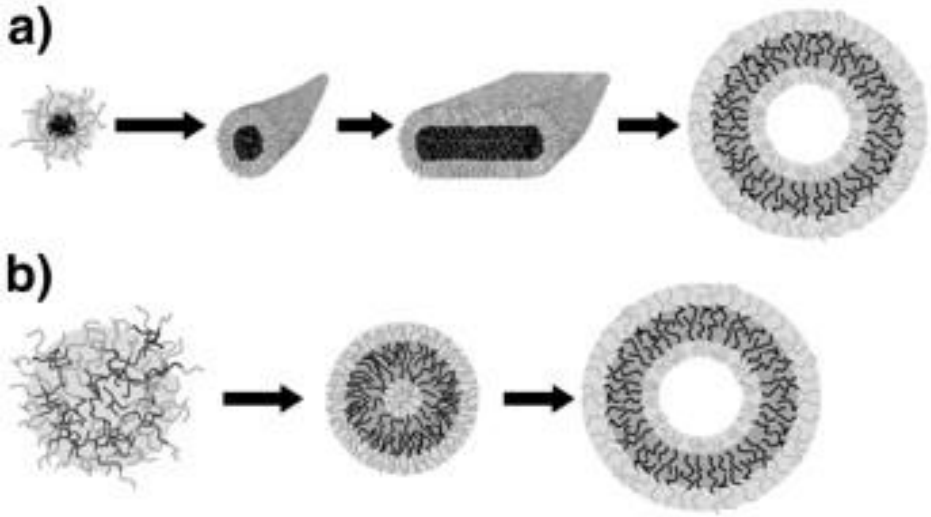

Figure 1.3. Two mechanisms on the formation of polymersome: (a) in Mechanism I, polymersome is formed through the route of "spherical micelle−cylindrical micelle−bilayer−enclosed vesicle"; (b) in Mechanism II, the sperical micelle increases in size, and form a hydrophilic core by the rearrangement of copolymers, and polymersome is formed by water diffusing into the core.[25]

Polymersomes are favored to be formed from the self-assembly of the block copolymers with packing parameter $1/2 \leq p \leq 1$. While the mechanism of polymersome formation which involves both thermodynamic and kinetic aspects, is still not fully understood. Two mechanisms were put forward to illustrate the process (Figure 1.3). In Mechanism I, spherical micelles are firstly formed instantly, then collide with each

other and slowly evolve into cylindrical micelles and in further open lamellae. Driven by minimization of edge energy, the lamellae close up and form vesicles.[23] The Mechanism II also starts from spherical micelle, however, instead of evolving into cylinder and lamella, the sphere grows bigger with the constituting copolymers reorganizing, and forming hydrophilic core inside. Water then diffuses into the core and forms a vesicle.[24]

Early in 1998, Eisenberg *et al.* reported the observation of lamellae with curved or folded structures, from the self-assembly of polystyrene-*block*-poly(ethylene glycol) (PS-*b*-PEG).[26] The copolymers are firstly dissolved in *N*,*N*-dimethylformamide (DMF) blended with some water (H_2O wt% = 4.0−6.5%). Water is added to the system until H_2O wt% = 25%, and dialysis is conducted to remove DMF. According to the results, if the copolymers are dissolved in DMF/water mixture for longer time, the obtained lamellae will have higher curvature, and more vesicles with complete enclosed structure will be found. It suggests that polymersomes are formed via Mechanism I, with the curved lamellae playing the role of intermediate.

In the self-assembly of PEG-*block*-polybutadiene (PEG-*b*-PBD), Discher and coworkers obtained nonergodic results from the blended system of PEG_{66}-*b*-PBD_{170} and PEG_{150}-*b*-PBD_{170}, where multiple structures coexist.[5] As revealed from the cryogenic electronic microscopic (cryo-EM) image (Figure 1.4), besides spherical micelles, worm-like micelles and vesicles, two octopus-like structures are observed. The right “octopus” stretches out 11 “arms” from the central disk, while the left one presents a semispherical shape. Both of them seem to be in the midway of bilayer enclosing to vesicle.

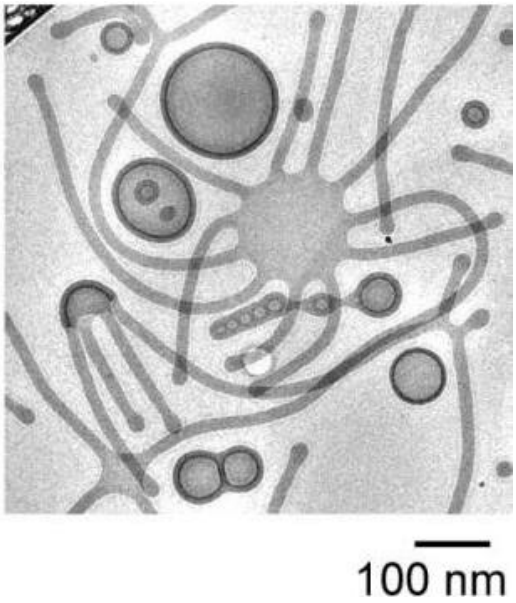

Figure 1.4. The nonergodic self-assembly result from the blended system of PEG_{66}-*b*-PBD_{170} ($f_{PEG,\,wt}$ = 24%) and PEG_{150}-*b*-PBD_{170} ($f_{PEG,\,wt}$ = 42%).[5]

In the study of the polymerization-induced self-assembly (PISA), the mechanism of polymersome formation is further explored. Blanazs and coworkers reported the PISA using poly(glycerol methacrylate) as the macromolecular chain transfer agent (CTA), and initiating the reversible addition−fragmentation chain-transfer (RAFT) polymerization of (2-hydroxyl)propyl methacrylate (HPMA) in water.[27] As HPMA is consumed, a series of self-assembly structures are observed during the reaction, through the characterization under transmission electronic microscope (TEM). The mixture of spherical micelles and worm-like micelles are found from the system with monomer conversion at 55−68%, while for the system with conversion at 72−82%, intermediates with octopus- and jelly-fish-like structures emerge. Enclosed vesicles make up the majority of self-assemblies when the reaction completes with 100% conversion (Figure 1.5). In the procedure of PISA, monomers act as plasticizer, and render the formed copolymers mobile. At the late stage of reaction, most of monomers are consumed, leaving the copolymers with relatively longer chains and poorer mobility. Figure 1.5. shows all intermediates captured that help to describe the whole procedure of vesicle formation.

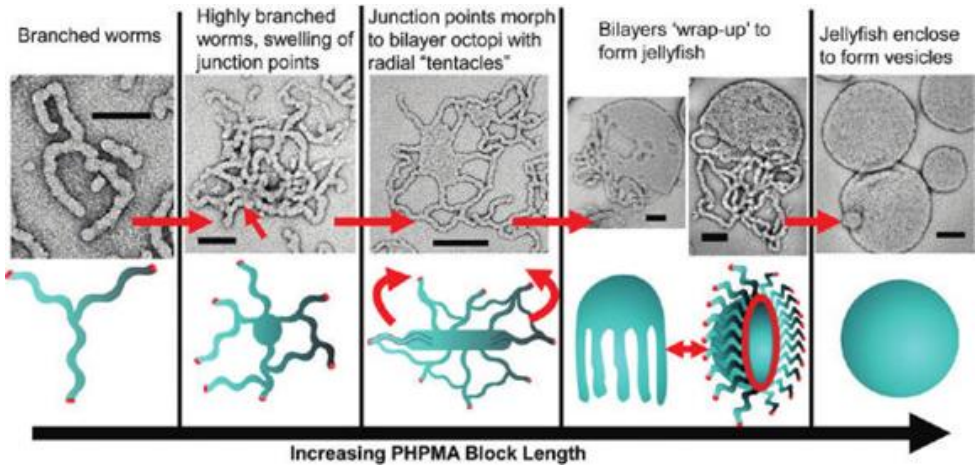

Figure 1.5. A series of self-assembly structures along with the monomer conversion of PISA, for the synthesis of $PGMA_{47}$-*b*-$PHMA_{200}$. Scale bar = 200 nm.[27]

Unlike the work above-discussed, the mechanism of polymersome formation of PEG-*block*-poly((2-*N*,*N*-diethyl)aminoethyl methacrylate) (PEG-*b*-PDEAMA) reported by Adams *et al.*[25] is closer to Mechanism II. PEG_{45}-*b*-$PDEAMA_{81}$ is dissolved in water with pH = 2, where the protonated PDEAMA make the copolymers totally dispersed individually. NaOH is added to deprotonate PDEAMA, driving copolymers to self-assemble. The results of dynamic light scattering (DLS) and cryo-EM reveal that neither cylindrical micelles nor lamella appear during the procedure. Instead spherical micelles, vesicles and spheres with loose cores are observed, which are supposed to be the intermediates in Mechanism II. The obtained vesicles cannot efficiently load hydrophilic fluorescent molecules, because in Mechanism II, the aqueous interior is formed by the diffusion of water molecules from outside to inside across rather thick barriers, and consequently water-soluble fluorescent molecules with rather high MW diffuse difficultly across these barriers.

1.2.2 Preparations of polymersomes

As the block copolymers have high molecular weight and their self-assembly shows nonergodic properties, the block copolymers with appropriate hydrophilic/hydrophobic ratios cannot self-assemble automatically into veiscles by just

adding them into water. Among various techniques to prepare polymersomes, nanoprecipitation, hydration and double emulsion are the three commonly used methods.

1.2.2.1 Nanoprecipitation

Nanoprecipitation is the most frequently employed method to perform the self-assembly of amphiphilic block copolymers. Generally, copolymers are first dissolved in an organic solvent, common for both polymer blocks and miscible with water. Water is then added to the system, driving the hydrophobic blocks to accumulate together. The self-assembling starts and continues upon the water addition. Finally the organic solvent is removed ether by dialysis againt water or by evaporation, leading to aqueous dispersions of polymer self-assemblies. In the procedure of nanoprecipitation, many factors such as the starting concentration, addition rate of water, water/organic solvent ratio, and polarity of the organic solvent, *etc.*, can influence the morphology, the structure and the size of the obtained self-assemblies.

As a pioneer in the research of block copolymer self-assembly, the team of Eisenberg has reported early in 1997 the self-assembly of PS-*b*-PAA, through nanoprecipitation with organic solvents including THF, DMF, 1,4-dioxane (simply written as dioxane) and their mixtures as the starting solvents.[28, 29] For example, in the self-assembly of PS_{200}-*b*-PAA_{18}, spherical micelles are formed with DMF. When DMF/THF mixture is used as solvent, and other conditions keep the same, the finally obtained self-assembly structures vary as a function of THF ratios (Figure 1.6): 5 wt% THF leads to the formation of worm-like micelles; 10 wt% THF leads to a mixture of worm-like micelles, lamellae and vesicles; 25−67 wt% THF allow the formation of polymersomes alone, and as the THF ratio increases further, the sizes of polymersomes get bigger. However, only large compound micelles are formed with pure THF as organic solvent. The difference in self-assembly may be explained by the difference of polarity of the organic solvent: THF has lower polarity than DMF, and comparatively

to DMF the polarity of THF is closer to that of PS. In the solvent with higher content of THF, on the one hand PS is more solvated, has higher degree of chain stretching, and keeps longer time of being solvated during the water addition procedure, which as the result gives the copolymers higher chance to adjust conformation towards the global equilibrium state. On the other hand, PAA blocks interact less with low-polar solvents, thus have less repulsion between corona chains, which is beneficial for the mutual fusion of self-assemblies for morphological evolution.

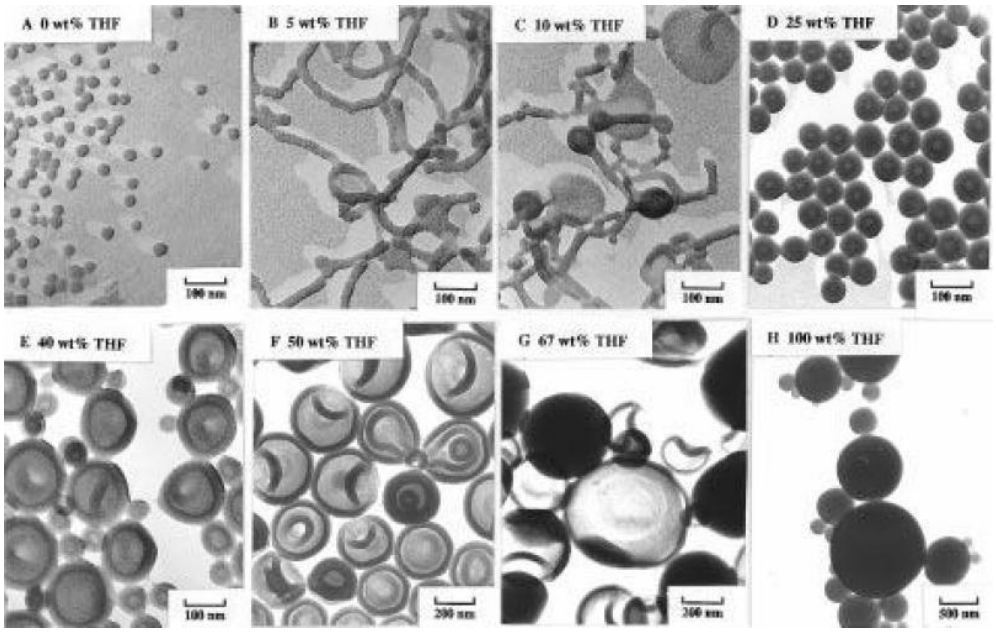

Figure 1.6. TEM images of self-assemblies of PS_{200}-*b*-PAA_{18} from solutions in DMF, THF and their mixtures: (A) pure DMF; DMF-THF mixtures of (B) 5 wt% THF; (C) 10 wt% THF; (D) 25 wt% THF; (E) 40 wt% THF; (F) 50 wt% THF; (G) 67 wt% THF; (H) pure THF.[29]

1.2.2.2 Hydration

In the hydration method, copolymer bulk is swollen by water to generate polymersomes. The copolymers are either dispersed directly in water, or processed first as thin film followed by hydration by water. The latter is referred as "film hydration" method, which origins from the preparation of liposomes, majorly for micrometer-sized giant vesicles.[30] Copolymers are firstly dissolved in volatile organic solvent, and the

solution is deposited to a roughened surface (such as bottle bottom and Teflon plate). As the solvent evaporates, polymeric thin film is formed. The deposited surface is immersed in water. The film detaches from the surface and gets destabilized during the swelling of water, and external forces including heating, stirring, sonication and electric field can be introduced to accelerate the process.

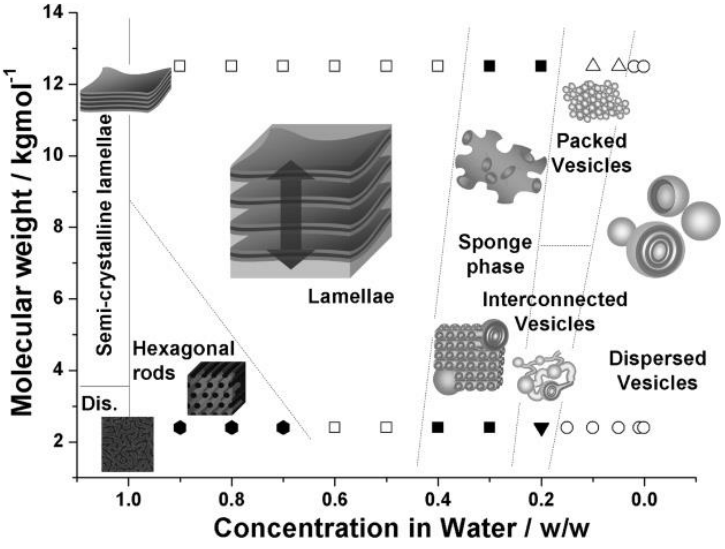

Figure 1.7. A series of structures from the hydration process of PEG-*block*-poly(butylene oxide) (PEG-*b*-PBO).[31]

Battaglia and Ryan made detailed researches and reports on the mechanism of vesicle formation from hydration of copolymers.[31, 32] Starting from the swollen lamellae or hexagonal rods, series of structures are formed as the degree of hydration increases, including sponge phase, packed vesicles and interconnected vesicles. Dispersed vesicles are finally obtained when the system is diluted below a certain concentration (Figure 1.7).

The process of film hydration undergoes similar structural evolution. Through the observation under confocal laser scanning microscope (CLSM), Battaglia and Ryan captured a series of intermediate structures. Among them the multilamellar tubule is the most representative structure.[33] Contacting with the surrounding water, the surface of the polymeric film starts to wrinkle. Along with the mutual diffusion between

copolymer bulk and water, the wrinkling evolves into long tubular structures, which resemble the myelin connecting neuronal cells, and therefore are called “myelins”. As the further development of hydration, “myelins” destabilize into vesicles (Figure 1.8), where the concentration gradient works as a key factor. In the swelling process, more and more intermediates are formed because of the low mobility of copolymers, which lower the concentration gradient. The external driving force like electric field can be used to accelerate the transformation of intermediates, maintaining the concentration gradient, and consequently increase the efficiency of vesicle generation.[12]

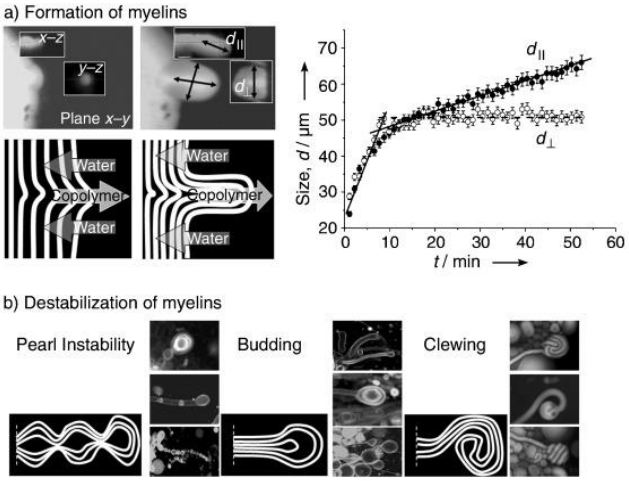

Figure 1.8. (a) The formation of “myelin”, and the variation of size parameters during the transformation from wrinkling to “myelin”; (b) the mechanisms for “myelins” destablizing into vesicles.[33]

Lack of size control in the process, the vesicles obtained from film hydration method present often broad size distribution, and a coexistence of unilamellar and multilamellar vesicles. Further processes like sonication, extrusion and freeze-thaw cycles are needed to obtain mono-disperse and/or small vesicles.[34-35] Based on the work of Battaglia and Ryan, Howse and coworkers employed photolithography to modify a hydrophilic, fluorocarbon-decorated surface, with uniformly distributed hydrophilic domains.[36] Through the spin-coating of copolymer solution, the surface is deposited with mono-distributed polymer islands after dewetting. The hydration of polymer

islands can generate unilamellar vesicles with uniform size in micrometer (Figure 1.9). The size of vesicle can be controlled by the size of hydrophilic domains.

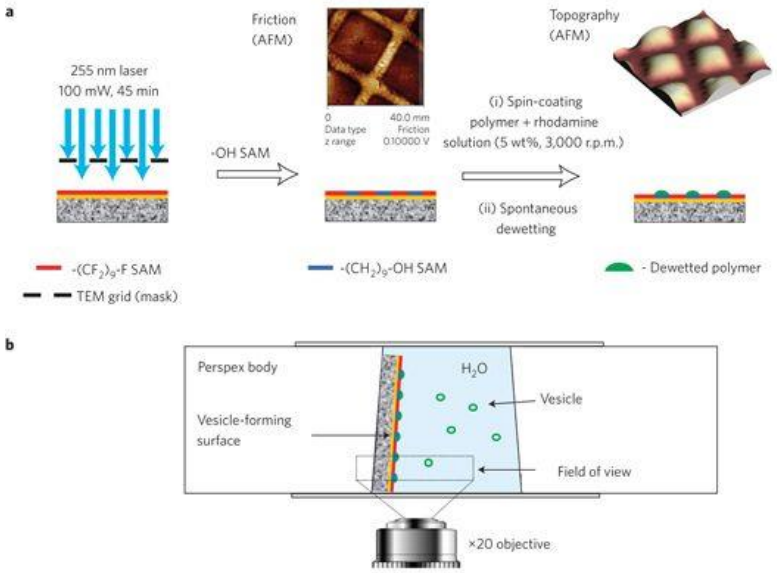

Figure 1.9. (a) The formation of mono-distributed polymer islands through the patterned hydrophilic, fluorocarbon-decorated surface by photolithography, and spin-coating of copolymers; (b) observation of vesicle formation under CLSM.[36]

1.2.2.3 Double emulsion

Microemulsion are often used to form micrometer-sized spheres and capsules from crystallizable homopolymers, with the help of surfactants.[37-39] In recent years the emulsification-induced method, more precisely the method via water-in-oil-in-water (W/O/W) double emulsion, has become a versatile approach to study the self-assembly of amphiphilic block copolymers.[11, 40-42] Copolymers are packaged in the W/O/W emulsion composed of water and water-immiscible volatile organic solvent. With the amphiphilic property, copolymers accumulate in the W/O and O/W interfaces, stabilizing the emulsion as macromolecular surfactants. Upon the removal of organic solvent by evaporation, the monolayers of two interfaces meet with each other, forming the bilayer membrane of vesicles. In the work of Weitz *et al.*, a capillary microfluidic device was employed to prepare double emulsions (Figure 1.10A).[43-44] Three phases

are divided in the device, where the inner and outer phases are aqueous solutions with balanced osmolality, the middle phase is the organic solvent dissolving the copolymers. The inner aqueous droplet is formed in the dripping regime from a small injection tube, in the coaxial flow with the middle phase, while the middle oil droplet containing the inner droplet is formed from the breaking up of oil stream by the focused flow of the outer continuous phase. During the dewetting of emulsion droplets, acron-like structures are formed with oil droplet attached to the bilayer of copolymers (Figure 1.10B, C). Oil droplets shrink as the organic solvent evaporates, leading to vesicles with complete bilayer structure (Figure 1.10 D). With microfluidic control, the obtained polymersomes have a highly uniformed size. By adjusting the flow rates of inner and middle phases, and the number of inner tubes, the number of inner droplets inside an oil droplet can be controlled. In this way, multicompartment polymersomes from the stacking of plural vesicles can be obtained.[45]

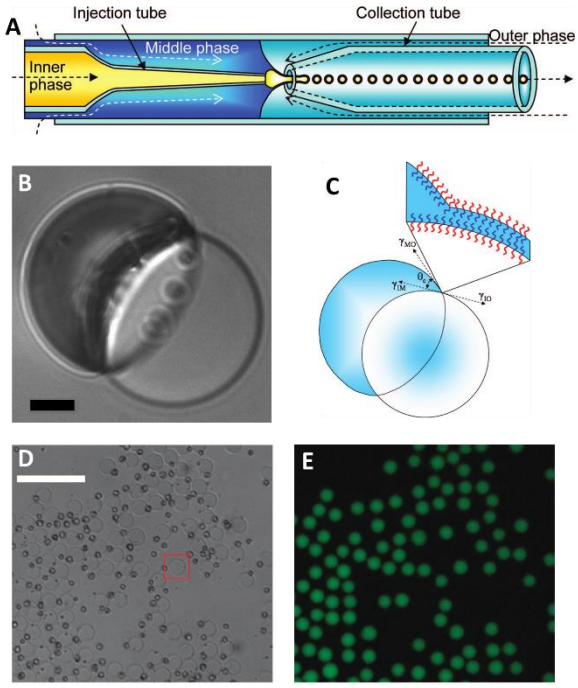

Figure 1.10. (A) Schematic structure of the capillary microfluidic device generating W/O/W double emulsion droplets; (B) bright-filed microscope image of an acron-like structure formed from the partial dewetting of a double emulsion droplet, with the oil droplet on the left side, attched to the copolymer bilayer of an embryonic vesicle on the

right side, scale bar = 10 μm; (C) schematic illustration of the acron-like structue; (D) bright-field image of polymersomes after dewetting and solvent evaporation, with shrunk oil droplets, scale bar = 100 μm; (E) fluorescence microscope image of the same area as in (D), fluorescent HPTS solutes are encasulated inside polymersomes, by dissolution in the inner aqueous droplet in double emulsion preparation.[44]

1.2.3 Properties of polymersomes

In general, the properties of polymersomes depend on the properties of the copolymers that compose the vesiclular membranes. When compared with liposomes, polymersomes are distinguished by their larger membrane thickness, higher stability and lower permeability in most cases. These characteristics are the basis for the design of functional polymersomes, and determine their practical applications, especially as the encapsulating vehicles employed in biomedical fields.

1.2.3.1 Stability of polymersomes

Polymersomes have the high stability to keep their structure from the changes by external environment. The low mobility of block copolymers is a major factor. Polymer chains with higher MWs possess lower mobility, and higher chance for entanglement, which induces the barriers for rearrangement in conformation and position, keeping polymersomes from unwanted fluctuation and defect formation. Polymersomes can maintain its number, shape and encapsulated content basically unchanged over a month, while under the same condition, liposomes are found with the half-life only around 10−20 h.[46] The low mobility also causes the formation and long-term existence of metastable structures with irregular shapes.[2] The shape of a vesicle can be parameterized by a normalized volume-to-area ratio v, and a normalized area-difference ΔA.[47] $v = 6\pi^{1/2}VA^{-3/2}$, where V and A respectively stand for the volume and area of a vesicle, v actually represents the capsulated water content per membrane area; $\Delta A = A_{out} - A_{in}$, representing the difference of layer area between outside and inside parts, which is proportional to the number difference of amphiphiles on the two sides

of the bilayer. For a uniformly spherical vesicle, $v = 1$ as the maximum, other non-spherical vesicle with the same membrane area entrap less water molecules, all with $v < 1$. ΔA is set as 1 for spherical vesicles, when $\Delta A > 1$, the membrane tends to curve outward, causing the formation of vesicle budding and tubular structures; whereas $\Delta A < 1$ leads to an inwardly curved membrane, which leads to stomatocyte-like vesicles.[48, 49] v can be adjusted by a "swelling-deswelling" process, and ΔA can be adjusted by the flip-flop of molecules in the bilayer. Figure 1.11a shows the various morphological structures of vesicles formed with different v and ΔA in theory. In practice, v and ΔA could be adjusted respectively through water permeation and amphiphile exchange between layers and vesicles, leading to the uniformly spherical shape. However, due to the low mobility of copolymers, it is slow for polymersomes to reach the global equilibrium state, resulting in the kinetically trapped structures with metastable shapes. This phenomenon is also part of the nonergodic nature of polymer self-assemblies. Figure 1.11b shows the various forms of vesicles from the film hydration of PEG-*b*-PBO,[2] which can basically correspond to the theoretical structures in Figure 1.11a.

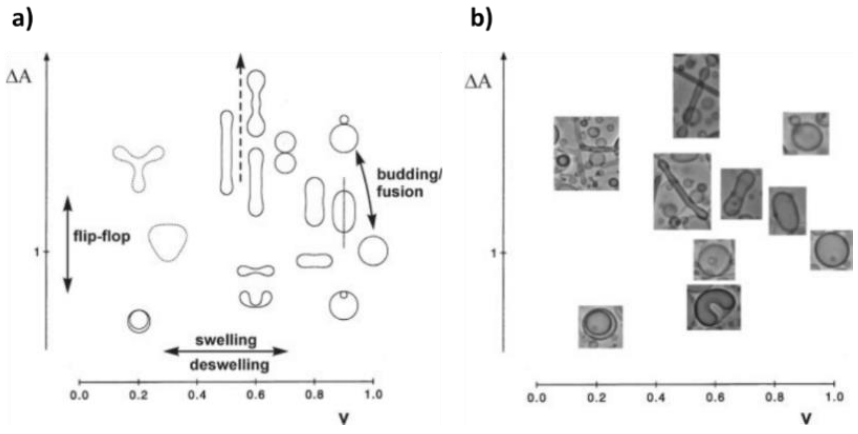

Figure 1.11. Phase diagrams of (a) theoretical vesicle shapes, and (b) vesicles obtained from the film hydration of PEG-*b*-PBO. Ways to adjust the vesicle shapes are indicated in (a).[2]

As reported by the team of van Hest and Wilson, PS-*b*-PEG was found to form inwardly curved structure from nanoprecipitaion.[50-52] The obtained vesicles have a

shape resembling stomatocyte, a kind of erythrocytes with slit-like central sink, thus are referred as “polymersome stomatocyte”. PS-*b*-PEG is dissolved in the mixture of dioxane and THF as the starting solvent, and water is then slowly added to preform self-assembling. After the formation of vesicles in the process of water addition, the exchange of water inside and outside the vesicle becomes difficult, due to the hydrophobicity of the polymer membrane. During the dialysis process, the osmotic pressure drives the organic solvent molecules to unidirectionally release outwards from the vesicle. Without appropriate amount of water entering the vesicle for supplement, the encapsulated content decreases, so does the *v* value, transforming the vesicle to a disk-like shape. The anisotropic arrangement in the membrane of disk-like vesicle is unstable, driving the vesicle to fold up into the stomatocyte-like shape. In this process, the organic solvent acts as plasticizer in the membrane, and gives the membrane certain mobility. As the solvent slowly dissipates, the PS region in the membrane enters glass state, which makes the stomatocyte-like shape fixed as the final form. The stomatocyte-like morphology can be maintained over 4 months.[50] There is a relationship between the vesicle structure and the mixing ratio of the starting solvents: the opening of the polymersome stomatocyte decreases as the increase of THF ratio from 40% to 65% (Fig. 1.12). Because THF swells PS better than dioxane does. In the dialysis procedure, the amount of THF in the initial solvent mixture would influence the shape change, as higher THF ratio can increase the degree of swelling, and lower the rate of vitrification of the PS domain in the membrane. This would consequently results in a difference in the time allowed for the change of shape during dialysis. In the following studies, they adjusted the assembly conditions to precisely control the morphological structure of the obtained polymersomes.[51-53] Platinum nanoparticles (PtNPs) can be loaded inside the one-way opening inner cavity of the polymersome stomatocytes, to prepare nanomotors with active targeting function (Detailed discussion in 1.3.2 H_2O_2 gradient-sensitive targeting nanomotor).[54, 55]

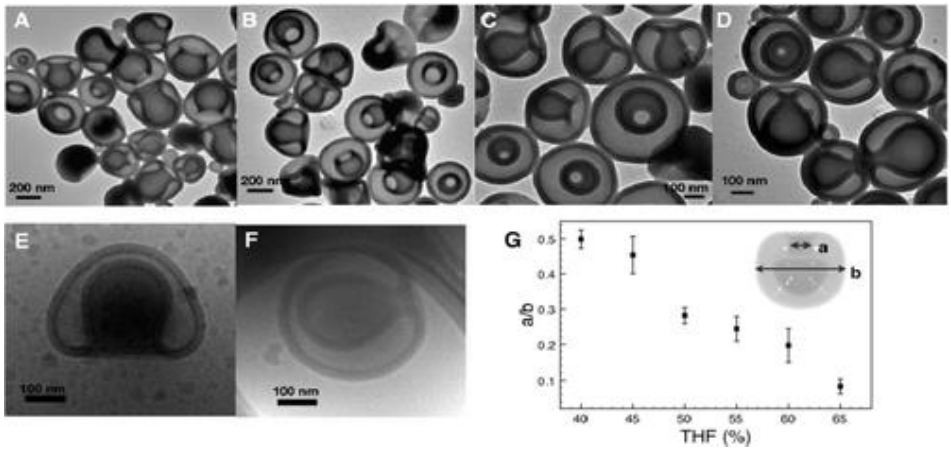

Figure 1.12. TEM images of polymersome stomatocytes obtained from dioxane-THF mixture as starting cosolvents, with THF ratio respectively at (A) 50%，(B) 55%，(C) 60% and (D) 65%. The Cryo-EM images of stomatocytes from cosolvents of THF ratio at (E) 50% and (F) 65%. (G) the plot of relationship between the size of stomatocyte opening and THF ratio of the starting cosolvent.

1.2.3.2 Permeability of polymersomes

As mentioned in above, polymersomes have relatively large membrane thickness (10−30 nm). Molecular dynamics simulation experiments show that the film thickness of the vesicles is positively correlated with the MW of the hydrophobic segment of the amphiphile. The bilayer film thickness $d \sim MW_{phob}^{b}$, for the amphiphilic block copolymer, the coefficient b is about 0.55 (Figure 1.13a).[56, 57] In the Fick's diffusion model driven by concentration gradient, the release rate of the encapsulated content from a vesicle is $\tau^{-1} = 3P/(2dR_V)$, where P is the permeability coefficient and R_V the vesicle radius.[2] Therefore, Polymersomes composed of high-MW copolymers are supposed to have rather low permeability (Fig. 1.13b).

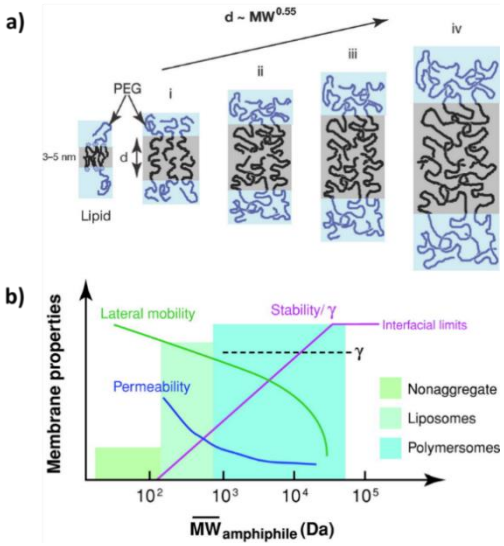

Figure 1.13. (a) The schematic illustration on the relationship between the thickness of vesicle bilayer and the MW of hydrophobic segment of the composing amphiphiles; (b) curves of membrane properties including permeability, mobility and stability, in function of the MW of amphiphiles.[57]

Besides molecular weight, the permeability is also closely related to the state of membrane. The team of Eisenberg conducted in-depth studies on vesicles composed of PS-based block copolymers. By the addition of dioxane to the PS-*b*-PAA vesicle system, the release rate of doxorubicin (DOX) and the proton diffusion rate of vesicles are significantly increases along with the proportion of dioxane.[58, 59] Dioxane acts as a plasticizer which swells the PS region of the vesicle membrane and loosens its structure, thereby increasing the permeability. In the vesicle system from the self-assembly of PEG-*b*-PS-*b*-poly(2-(*N*,*N*-diethylamino)ethyl acrylate) (PEG-*b*-PS-*b*-PDEA) triblock copolymer, the hydrophobic region of the vesicle membrane consists of PDEA as the middle layer and PS on both sides.[60] In basic environment, membrane structure is compact and the permeability of the polymersome keeps low. As pH decreases, the PDEA layer gets protonated and swollen, increasing the membrane thickness and vesicle size. When the pH drops below 6, defects and breakages appear in the membrane (Figure 1.14). The change is clearly fed back on permeability, allowing the significantly increased penetration to water and protons.

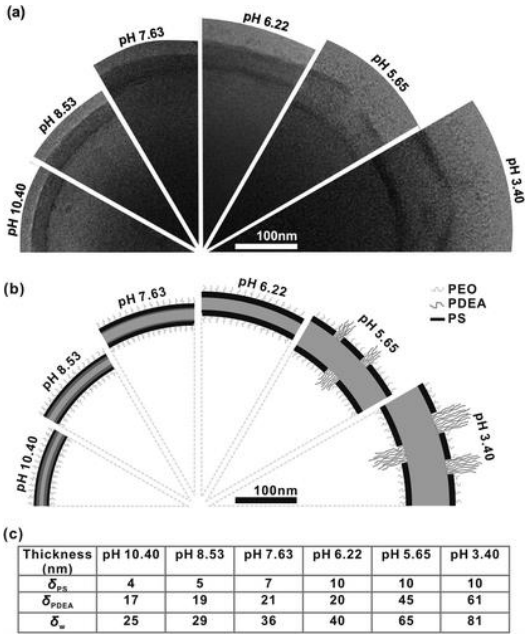

(c)

Thickness (nm)	pH 10.40	pH 8.53	pH 7.63	pH 6.22	pH 5.65	pH 3.40
δ_{PS}	4	5	7	10	10	10
δ_{PDEA}	17	19	21	20	45	61
δ_{w}	25	29	36	40	65	81

Figure 1.14. (a) Cryo-EM images of PEG-*b*-PS-*b*-PDEA vesicle membrane at different pH; (b) schematic membrane structure corresponding to (a); (c) thickness of PS region, PDEA region and vesicle membrane at different pH.[60]

Another way to alter the permeability is to embed functional substances in the vesicle membrane. Based on polymersomes from the self-assembly of poly(2-methyloxazoline)-*b*-polydimethylsiloxane-*b*-poly(2-methyloxazoline) (PMOXA-*b*-PDMS-*b*-PMOXA), Meier and coworkers insert channel protein (porin) into the vesicle membrane, to regulate the exchange of certain molecules.[61-63] Enzymes with specific functions are encapsulated inside the vesicle. The enzyme catalyzes reactions on consuming substrates inside the vesicles, while porin channel let substrate and product circulate along the vesicle membrane. Then, the polymersome is turned into a nanoreactor with highly catalytic function. Encapsulation inside the vesicles allows to protect the enzyme from the surrounding environment and to improve its work efficiency. Meier *et al.* reported in 2013 another way to change the membrane permeability, by using 2-hydroxy-4'-(2-hydroxyethoxy)-2-methylpropiophenone (PP-OH) under UV light.[64] UV-irradiation causes PP-OH to form two primary radicals (ketyl and alcohol), which leads to chemical modification of vesicle membrane with

PP-OH. The attachment of the hydrophilic PP-OH increases the ability of vesicle membrane to allow hydrophilic molecules to penetrate. This reaction is applicable to a variety of vesicles, and does not change their size and structure. The enzyme-entrapped polymersome can also be beneficial, to achieve the nanoreactor function in a simpler way.

1.3 Polymersomes in ROS-related applications

The high stability and low permeability give polymersomes advantages in applications as drug carriers. With the robust membrane, polymersomes protect the encapsulated drug from the surrounding environment and minimize the loss of early release before the target. In the other view, the most direct and effective way to achieve stimuli-responsive release is to break the stability of membrane, causing the change in permeability or structural disintegration of vesicle under specific stimuli. pH variation and redox reactions have been reported to trigger the controlled release of polymersome.[65, 66] The stimulation may cause the composing copolymers to change the solubility,[67, 68] to have degradation[69] or special cleavage of bond linking hydrophilic and hydrophobic blocks,[70] leading to the increase of permeability or the bursting release of polymersome. Some pathological bases such as the tissue of inflammation and tumor offer chemical environment differing from that of normal ones, and have specific accumulation of certain active substances. These active substances can be used as stimuli in the targeted sites.

Reactive oxygen species (ROS) refer to a class of byproducts from the process of oxygen-involving metabolism, including peroxide, superoxide, hydroxyl radical, singlet oxygen and alpha-oxygen, which have high oxidative activity.[71] The high oxidative property enables ROS to damage DNA and cell membrane structure, which can be used to destroy tumor cells in cancer therapy. On the one hand, for most of the radiotherapy and chemotherapy in cancer treatment, including the emerging photodynamic therapy (PDT), their mechanisms are based on or include the increase of

ROS concentration at target site.[72-75] On the other hand, significantly higher ROS concentrations found in some tumor and inflammatory tissues than in normal cells provide a means of targeted and ROS-responsive drug delivery.[54, 71, 76, 77]

1.3.1 Polymersomes as ROS generators or carriers

The commonly used anticancer drug, DOX, is considered in relation with the promotion of ROS production. [78] Lecommandox *et al.* reported that the intracellular introduction of DOX-containing vesicles of poly(γ-benzyl L-glutamate)-*block*-hyaluronic acid (PGlu(OBn)-*b*-HYA) can results in the obvious increase of ROS concentration.[79] Enzyme-catalyzed oxidation is one main source of ROS *in vivo*. Meier and Bruns reported the encapsulation of a commonly used oxidase, laccase, inside the vesicle of poly(*N*-vinylpyrrolidone)-*block*-polydimethylsiloxane-*block*-poly(*N*-vinylpyrrolidone) (PNVP-*b*-PDMS-*b*-PNVP).[80] PNVP-*b*-PDMS-*b*-PNVP vesicles have high permeability for oxygen and ROS, but low permeability for laccase. Therefore the entrapped laccase is well protected by vesicle, and meanwhile can efficiently turn oxygen into ROS. The laccase-loading polymersomes work as a ROS-generating nanoreactor.

In the working mechanism of PDT, photosensitizer is activated by light stimulation, and turns oxygen-containing substrates into ROS, for example singlet oxygen ($^1O_2$) from ground state oxygen.[73] In the combination of PDT and polymersome, photosensitizer is loaded on the membrane or inside the vesicle, for the generation and delivery of ROS. Chen and coworkers reported the use of polyion complex vesicle (PICsome) from PEG-*block*-poly(aspartic acid) (PEG-*b*-PAsp) and poly(5-aminopentyl asparagine) (P(Asp-AP)), as the carrier of photosensitizer Al(III) phthalocyanine chloride disulfonic acid (AlPcS2a).[81] AlPcS2a-loaded PICsomes are successfully delivered into the cells via endocytosis. Under the activation of light, AlPcS2a generates $^1O_2$ and oxygen-containing free radicals, which in turn damage the membrane of PICsome and lysosome. PICsomes and AlPcS2a enter the cytoplasm,

achieving photochemical internalization. The results of cellular uptake and viability test indicate that in comparison with the photosensitizer alone, PICsome-encapsulated AlPcS2a exhibits much higher degree of internalization, and stronger photocytotoxicity.

In another work reported recently by Chen, the photosensitizer boron dipyrromethene (Bodipy) is loaded in the vesicle membrane of 3-miktoarm star terpolymer, PEG-*star*-poly(*ε*-caprolactone)-*star*-poly(*N*-isopropylacrylamide) (PEG-*star*-PCL-*star*-PNIPAM).[82] Bodipy can form *J*-type and *H*-type aggregations in the membrane (Figure 1.15a), causing red-shifted excitation to near-infrared region and improved resistance to photobleaching. Under the irradiation of 660 nm laser, vesicles generate a large amount of $^1O_2$, which acts as PDT agent. Under the laser excitation at 785 nm, apart from $^1O_2$ generation, the excited state prefers to undergo non-radiative relaxation, leading to remarkable photothermal conversion efficiency, which works as PDT-synergized photothermal therapy (PTT), killing cancer cells by $^1O_2$-assisted hyperthermia. The Bodypy-loaded vesicles with wavelength-dependent photoconversion show great potential in photoinduced cancer therapy.

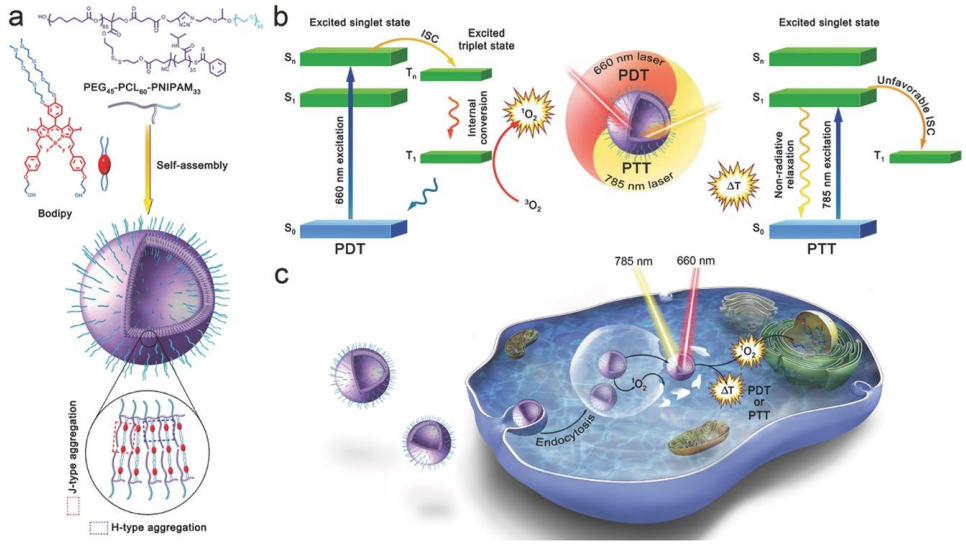

Figure 1.15. (a) Structure of PEG-*star*-PCL-*star*-PNIPAM, *J*-type and *H*-type aggregations; (b) electronic transitions respectively under the irradiation of 660 nm and

785 nm laser; (c) schematic illustration on the working mechanism of Bodypy-loaded vesicles in photoinduced cancer therapies.[82]

1.3.2 H_2O_2 gradient-sensitive targeting nanomotor

ROS accumulate at high level in tumor and inflammatory tissues, because of the increased metabolic activity, mitochondrial dysfunction and reduced ability to scavenge ROS, *etc*.[71, 83, 84] As a typical ROS, hydrogen peroxide (H_2O_2) is produced at a rate of 5 nmol per hour by ten thousand units of cancer cells.[85] Therefore concentration gradient of H_2O_2 is formed around the tumor tissue. Based on the H_2O_2 gradient, van Hest and Wilson developed a targeting nanomotor from the above-discussed polymersome stomatocyte.[54] Before the dialysis step, PNVP-modified platinum nanoparticles (PtNPs) are added to the system, so that PtNPs can be entrapped inside the one-way opening inner cavity during the shaping of a stomatocyte. When the PtNPs-loaded stomatocytes are placed with H_2O_2 around, under the catalysis of PtNPs, H_2O_2 decomposes into oxygen, which is released from the one-way opening, and drives the vesicle to move in the opposite direction (Figure 1.16). The nanomotor tends to move up the gradient towards the higher H_2O_2 concentration. Similar results are obtained from the experiment with neutrophils as the H_2O_2 source. This can be explained as follows. At the position of higher H_2O_2 concentration, more oxygen is produced, nanomotors move longer distances; while along with the direction of decreasing H_2O_2 concentration, the H_2O_2 "fuel" is exhausted, making the nanomotors slowing down. As the result, more and more vesicles accumulate around the H_2O_2 source. In the following studies, other substances such as glucose oxidase (GOx)[86, 87] and nickel nanoparticles (NiNPs)[88] were reported to be incorporated inside the cavity, respectively for further glucose-driven and magnetic field-driven functions. To achieve effective release at the targeted site, the nanomotors were upgraded by the incorporation of reduction-responsive disulfide,[55] or the hybrid of biodegradable PEG-*b*-PCL.[89]

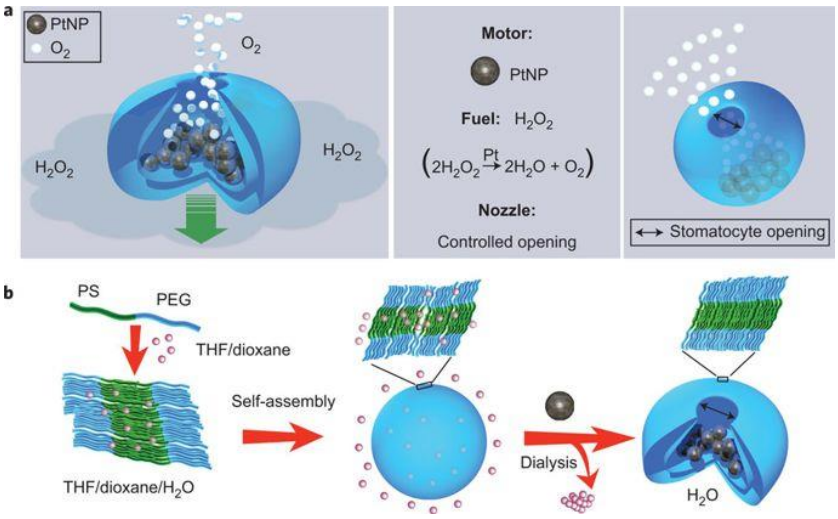

Figure 1.16. (a) Mechanism of the H2O2-driven nanomotor; (b) preparation of the nanomotor from the encapsulation of PtNPs by polymersome stomatocytes.[54]

1.3.3 ROS-responsive polymersomes

The accumulation of ROS in tumor and inflammatory tissues leads to another possible application: polymersomes responsive to ROS-stimulations.[90] It can be achieved by introduction of ROS-responsive linkages and groups.

1.3.3.1 ROS-responsive polymersomes based on thioether

As a sulfur-containing structure, the hydrophobic thioether can be transferred to hydrophilic sulfoxide and sulfone upon oxidation. The hydrophobic-to-hydrophilic transformation leads to structural changes or even direct dissolution of thioether-containing self-assemblies. The team of Hubell has published a series of works on the thioether-containing vesicles based on PEG-*block*-poly(propylene sulphide) (PEG-*b*-PPS) since 2004.[91] Film hydration of triblock PEG-*b*-PPS-*b*-PEG generates vesicles with a large diversity of sizes and shapes (Figure 1.17A). Under the treatment by H_2O_2, the morphological majority turns into worm-like micelles (Figure 1.17B). The turbidity decreases along with the time of H_2O_2 treatment, and approaches 0 after 10 hours (Figure 1.17C). The comparison of proton nuclear magnetic resonance spectra (^{1}H-NMR) of vesicle sample in deuterium oxide (D_2O), before (Figure 1.17D) and after

(Figure 1.17E) the H_2O_2 treatment, reveals the structural change of thiethers: the proton signals of methylene and methine groups (2.65–2.93 ppm) and methyl groups (1.41 ppm), which are adjacent to sulfur atom, shift downfield (respectively to 3.05–3.65 ppm and 1.53 ppm) because of the electron-pulling effect of sulfoxides and sulfones. With increased solubility in D_2O, the signals turn from weak and broad peaks to much sharper peaks.

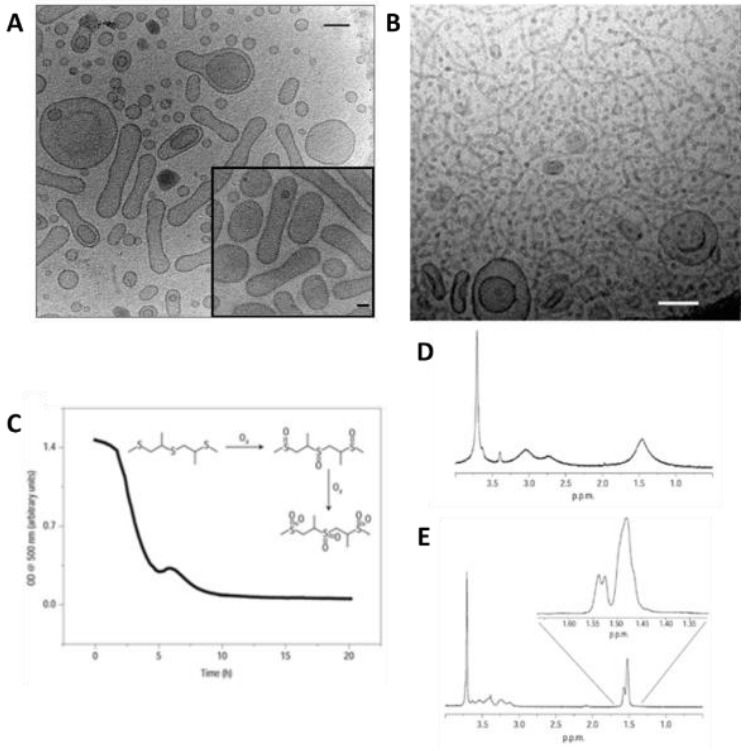

Figure 1.17. Cryo-EM images of self-assembly sample from film hydration of PEG_{16}-*b*-PPS_{50}-*b*-PEG_{16} (A)before and (B) after 150-min treatment of 3 vol% H_2O_2, scale bar = 100 nm; (C) The turbidity of vesicle sample in function of time in the treatment of 10 vol% H_2O_2; ^{1}H-NMR spectra of the vesicle sample in deuterium (D) before and (E) after the H_2O_2 treatment.[91]

Further, Hubell *et al*. encapsulated the enzyme glycose oxidase (GOx) inside the vesicles.[93] The suspension of GOx-loaded vesicles is placed in a dialysis bag, and inserted in a vial of glucose solution with air bubbling. H_2O_2 is generated from the GOx-catalyzed oxidation of the surrounding glucose which diffuses to the inside of

vesicles. The exposure to the *in-situ* generated H_2O_2 induces the disassembly of vesicles . In a work reported in 2012, the same group applied PEG-*b*-PPS polymersomes to get photochemical internalization through thioether oxidation.[94] The vesicles loaded with photosensitizer ethyl eosin in the membrane and with peptide antigens, in the inner cavity enter the cell by endocytosis. Under light stimulation, eosin converts dissolved oxygen to $^1O_2$, which further oxidizes the thioether, and causes the vesicle rupture. Consequently, the encapsulated antigens are released inside the cell.

PPS contains thioethers in the backbone, while copolymers reported by Boyer *et al.*,[76] contain thioethers in side chains..[76] Using tetraphenylporphyrin zinc (TPP-Zn) as the photocatalyst, photoinduced electron energy transfer - reversible addition-fragmentation chain transfer (PET-RAFT) polymerization of 2-(methylthio)ethyl methacrylate (MTEMA) is initiated by red light (635 nm) illumination. Using poly(oligo(ethylene glycol) methyl ether methacrylate) (POEGMA) as the macromolecular chain transfer agent (macro-CTA), MTEMA can be polymerized in aqueous phase to achieve polymerization induced self-assembling (PISA). Vesicles are obtained as the final self-assembly structure, with TPP-Zn embedded in the membrane. TPP-Zn can also act as a photosentisizer, which generates $^1O_2$ upon the stimulation of 560 nm light, and leads to the disassembly of POEGMA-*b*-PMTEMA vesicles.

1.3.3.2 ROS-responsive polymersomes based on arylboronate

Arylboronate ester is another oxidation-responsive structure. Taking pinacol phenylboronate as an example, the oxidation can convert the phenylboronate ester into phenol. Phenol is unstable in oxidative environment, and tends to undergo a quinone methide rearrangement, leading to the cleavage of aryl groups. For polymers with arylboronate ester on the side chains, the oxidation-induced cleavage of large compound groups can result in remarkable changes of properties.[95] In the work reported by Liu and coworkers,[96] phenylboronate (PB) and naphthylboronate (NB) esters are used as the capping moieties, which are connected to poly(2-aminoethyl methacrylate)

by carbamate bonds (in some of polymers, a *p*-aminobenzyl carbamate linker is added), forming the hydrophobic blocks of amphiphilic block copolymers PEG-*b*-PPBMA, PEG-*b*-PNBMA, PEG-*b*-PPBCMA and PEG-*b*-PNBCMA. Some of them can self-assemble into vesicles. For the polymersomes exposed to oxidation stimuli, the oxidation-triggered removal of PB and NB ester capping moieties leads to spontaneous self-immolative cleavage and exposure of primary amino groups. The revealed amino groups can initiate intra- and intermolecular amidation reactions, turning the vesicle membrane into a crosslinked structure with hydrophilic channels (Figure 1.18). The permeability is remarkably changed, while the vesicular structure is well maintained. Employed as theranostic nanocarriers, the constructed polymersomes can achieve targeted drug delivery and sustained release of payloads, which is modulated by oxidative stress of cellular ROS.

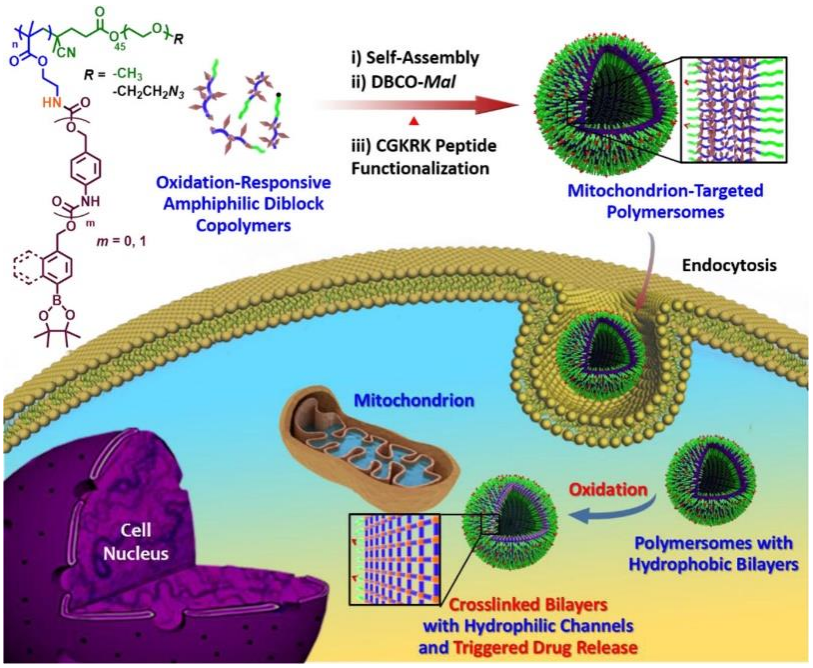

Figure 1.18. Fabrication and working mechanism of the oxidation-responsive vesicles based on arylboronate esters.[96]

1.4 Polymersomes based on polypeptides

As a class of polymers composed of amino acid repeating units, polypeptides have unique advantages due to the diversified side chain structures from natural amino acids and the composition similar to natural proteins and peptides.[97] Being biocompatible and biodegradable, the polypeptide-based self-assemblies are of great interest for the applications in biomedical fields. We review here examples of stimuli-responsive polymersomes based on polypeptides.

1.4.1 Redox-responsive polypeptide vesicles

In recent years, emerging work has been reported on the functionalization of polypeptides to achieve oxidation-responsibility, especially sulfur-containing polypeptides such as alkylated polycysteine (PCys) and polyhomocysteine (PHCys). In these polypeptides, oxidation-responsibility comes from the formed thioether group.[98-100] The oxidation of thioether not only changes the solubility, but also affects the chain conformation and secondary structure. In 2013, Deming *et al.* reported the self-assembly behavior of amphiphilic block copolypeptides, where the hydrophilic segment is glycol-modified polylysine with amide linkages (P(Gal-Lys)) or glycol-modified polycysteine with oxidized thioether bonds (P(Gal-Cys^{O})), and the hydrophobic block is polyleucine (PLeu).[101] With similar MWs and hydrophilic/hydrophobic ratios, P(Gal-Lys)$_{65}$-*b*-PLeu$_{20}$ can only form lamellae in water, while P(Gal-Cys^{O})$_{65}$-*b*-PLeu$_{20}$ is able to assemble into vesicles. The chain structure is considered to be the major reason: P(Gal-Lys) still has a secondary structure of α-helix in water, while P(Gal-Cys^{O}) forms random coil because of the oxidized thioether bonds.

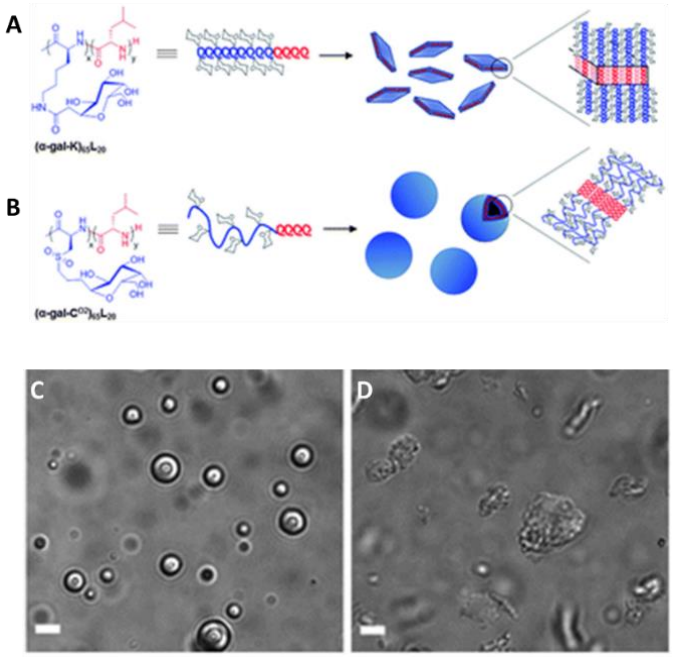

Figure 1.19. Schematic chain structures and assembly structures of the two amphiphilic block copolypeptides (A) P(Gal-Lys)-*b*-Leu and (B) P(Gal-Cys^{O})-*b*-PLeu; differential interference contrast (DIC) microscopic images of (C) vesicles formed by P(Gal-Cys^{O})$_{65}$-*b*-PLeu$_{20}$ and (D) lamellae from P(Gal-Lys)$_{65}$-*b*-Leu$_{20}$. Scale bar = 5 μm.[101]

Gu and coworkers also carried out very promising works on oxidation-responsive polypeptide vesicles. Firstly, nitroimidazole (NI) groups are attached, via thioether bonds, to polyserine (PSer) in an block copolymer to get PEG-*b*-P(Ser-S-NI).[102] PEG-*b*-P(Ser-S-NI) vesicles are prepared with GOx and insulin encapsulated inside the aqueous cavity. When glucose is introduced to the system, H_2O_2 is generated from the GOx-catalyzed glucose oxidation process, which oxidizes the thioether and turns P(Ser-S-NI) more water-soluble. At the same time, dissolved oxygen is consumed during the procedure, leading to hypoxia. NI group is thus reduced to aminoimidazoles, further increasing the hydrophilicity of the copolymers. Consequently, vesicles are disassembled, releasing the encapsulated insulin for the therapeutic function (Figure 1.20). The suspension of glucose-responsive vesicles are packaged inside a microneedle-array patch, which can be employed to modulate the blood glucose level in patients with diabetes or hyperglycemia. The thioether bonds not only act as

responsive, but also can consume excess H_2O_2, to avoid the interference with the function of GOx and the inflammation of skin tissues caused by H_2O_2. In the other work, pinacol phenylboronate is introduced to polyserine in copolymer synthesis. The obtained vesicles can also release insulin as the H_2O_2-mediated glucose-responsibility, and achieve the glycemic regulation.[103]

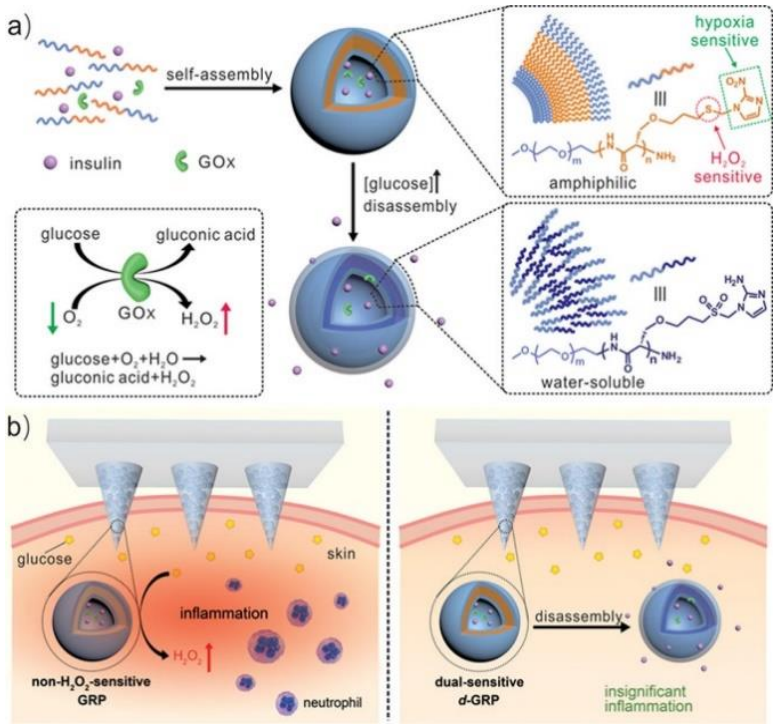

Figure 1.20. (a) Composition and working mechanism of the glucose-responsive vesicles based on thioether bonds and nitroimidazoles. (b) Microneedle array patches with insulin-encapsulated vesicles packaged inside. Inflammation of skin tissue is caused by excessive H_2O_2 from the patch of vesicles without H_2O_2-responsibility (left); while the presence of thioether bonds can consume excess H_2O_2, avoiding damages to skin tissue in the long-term therapy (right).[102]

Methionine is a natural amino acid with a 2-(methylthio)ethyl carbon-substituted (*C*-R) group. The thioether-bearing side chain endows the polypeptide of methionine, polymethionine (PMet), with broad prospect in applications.[104-105] Like other thioether-bearing polymers, PMet has a hydrophobic-hydrophilic transition based on the structural transformation of thioether groups under oxidation stimuli. The

transition is reversible, as the sulfone and sulfoxide structures can be converted back to thioethers under reductive conditions. Deming *et al.* reported in 2013 the polymersome formed by the block copolypeptide with the oxidized polymethionine ($PMet^{O}$), of which the thioethers are oxidized to sufoxides, as the hydrophilic segment, and the random copolymer of leucine and phenylalanine (P(Leu-*r*-Phe)) as the hydrophobic one.[106] $PMet^{O}$ can be reduced to PMet by the combination of dithiothreitol (DTT) and methionine sulfoxide reductase (MSR enzyme), which causes the collapse of vesicles and thus achieves reduction-responsive drug release (Figure 1.21). In the following study, PHArg is introduced to the system, thus obtaining the triblock copolypeptide PHArg-*b*-$PMet^{O}$-*b*-P(Leu-*r*-Phe), which can be blended with $PMet^{O}$-*b*-P(Leu-*r*-Phe), and constitutes vesicles with the cellular membrane-penetrating ability.[107]

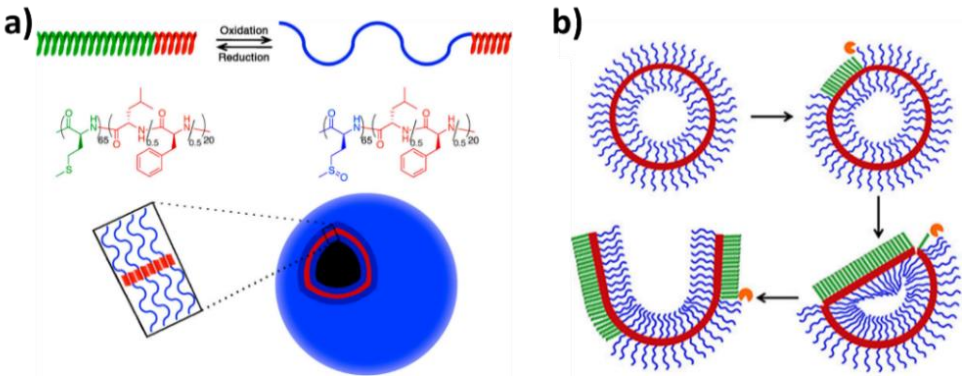

Figure 1.21. (a) The reversible structural transformation between PMet-*b*-P(Leu-*r*-Phe) and $PMet^{O}$-*b*-P(Leu-*r*-Phe) under redox conditions, and the vesicle formed by $PMet^{O}$-*b*-P(Leu-*r*-Phe); (b) The responsive collapse of a $PMet^{O}$-*b*-P(Leu-*r*-Phe) vesicle under the combined reductive stimuli of DTT and MSR enzymes.[106]

Besides the redox-responsibility, another property of thioether has also caught the attention of scientists. The sulfur atom in thioether has nucleophilicity, and based on it, PMet can undergo alkylation reactions with substances including halides, triflates and epoxides.[104, 108] As the result, the side chains of PMet are alkylated with functional groups,[109] and simultaneously, sulfoniums are obtained with positive charges. Such reactions not only serve as functionalization with “click” features, but also generate

polyelectrolytes with positive charges and water-solubility, which could be employed for DNA complexation.[110] As reported by Deming *et al.*, the alkylation of PMet-*b*-P(Leu-*r*-Phe) results in the methylated and carboxymethylated PMet blocks with sulfoniums on the side chains (respectively $PMet^{M}$ and $PMet^{C}$), which serves as the hydrophilic blocks in amphiphilic copolypeptides, and form vesicles in water.[111] $PMet^{M}$ is found to have low cytotoxicity and work excellently as a component of cell-penetrating peptides. The polypeptide vesicles based on alkylated methionine has the potential for further applications.[112]

1.4.2 pH-responsive polypeptide vesicles

The pH-responsive polypeptide vesicles are majorly based on the polar charged groups of amino acids, including positively charged lysine, ornithine, arginine, histidine, and negatively charged glutamic acid, aspartic acid. Polypeptides composed of these amino acids are uncharged and hydrophobic in certain pH range, and possess secondary structure. Once being charged, the polypeptides turn hydrophilic and adopt the conformation of random coil due to the mutual exclusion of the same charges.[113] Based on the fundamental work on polypeptide synthesis, the team of Deming has conducted systematic and in-depth studies on the self-assembly of charged polypeptides.[92, 114-116] As early as 2004, they reported a pH-responsive polypeptide vesicle composed of di(ethylene glycol)-modified polylysine (PDEGLys) as hydrophilic segment and the random copolymer of lysine and leucine (P(Lys-*r*-Leu)) as hydrophobic one.[92] At pH = 10.6, the copolypeptides assemble into vesicles, with hydrophilic fluorophores entrapped inside the cavity. As pH decreases to 3.0, the lysine units get protonated, leading to the destabilization of vesicles and the release of payloads. Lecommandoux *et al.* reported polypeptide vesicles with reversible inside-outside leaflet's transformation triggered by pH variation.[117] Their vesicles are made from poly(glutamic acid) and polylysine (PGlu-*b*-PLys). Under the acidic condition of pH < 4, PLys is protonated as the hydrophilic segment, while PGlu is embedded as a

hydrophobic segment inside the vesicle membrane. In the neutral condition of 5 < pH < 9, PLys and PGlu and both partially protonated, causing the disassembly of vesicles. When the pH is raised over 10 in a basic condition, PLys is totally deprotonated and turns into the hydrophobic segment, while PGlu plays as the hydrophilic block with the negatively charged carboxylates. The copolymers with a flipped structure re-assemble into vesicles (Figure 1.22).

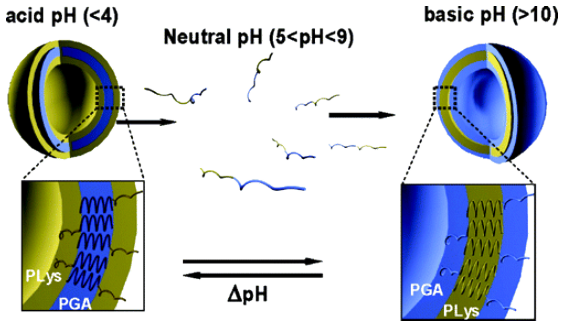

Figure 1.22. Schematic representation of the reversible inside-out transformation of $PGlu_{15}$-*b*-$PLys_{15}$ vesicles under the modulation of pH.

The team of Kataoka reported the preparation of PICsome from PEG-*b*-PAsp and PEG-*b*-P(Asp-AP),[118] where the inner layer of the vesicle membrane is stabilized by the electrostatic interaction of PAsp and P(Asp-AP). Because of the water-soluble ion pairs, PICsome has higher permeability compared with common polymersomes. The electrostatic interaction can be regulated by pH, which in turn can modulate the permeability of PICsomes.[119]

1.5 Polymersomes based on polypeptoids

Polypeptide vesicles have enormously high value to be developed as biocompatible multifunctional drug carriers. However, the researches on polypeptide-containing vesicles, especially the systematic study on polymersomes assembled entirely from copolypeptides is still few. It is related to the inherent structures and properties of polypeptides. Inter- and intramolecular hydrogen bonds are formed by amide bonds on the backbone of the polypeptide, which leads to the tightly packed

secondary structures such as α-helix and β-sheet.[120] On the one hand, the uniformly packed polypeptides are hard to be dissolved by most organic solvents, especially the ones with relatively low polarity. On the other hand, the excessively formed hydrogen bonds make polypeptides difficult to be thermally processed, and they are often thermally degraded before reaching the melting point.[121, 122] In many cases, the conventional conditions for copolymer self-assembly and polymersome preparation are unsuitable for polypeptides.

Nevertheless, polypeptoids, a type of polymers with the backbone composed of polyglycine and the side chain substituting the hydrogen at the nitrogen atom of amides (*N*-R), show promising properties. On the one hand, polypeptoid has a backbone structure very similar to that of polypeptide, thus maintains good biocompatibility.[123] On the other hand, due to the *N*-substitution, inter- and intramolecular hydrogen bonds along the backbone are missing. Polypeptoids are soluble in common organic solvent,[124] and can be thermally processed like other thermoplastic polymers.[125, 126] Various *N*-R side groups can be utilized to tailor the physicochemical properties of polypeptoids.[122, 123] Studies have shown that polypeptoids exhibit better resistance to proteolytic hydrolysis than polypeptides,[127] but can be oxidatively degraded under the conditions mimicking inflammation.[128] These advantages lead to increasing interest in the design, synthesis and self-assembly study of amphiphilic block copolymers based on polypeptoids.[129-131] Synthesis and self-assembly (especially polymersomes) of polypeptoid-containing block copolymers will be reviewed in the following.

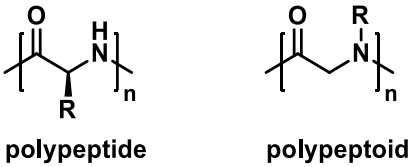

polypeptide polypeptoid

Scheme 1.1. The representative structures of polypeptide and polypeptoid

1.5.1 Synthesis of polypeptoid-containing block copolymers

1.5.1.1 Solid phase synthesis

Polypeptoid can be synthesized using solid-phase submonomer synthesis (SPSS).[132] SPSS is developed from solid-phase peptide synthesis (SPPS),[133] but is much simpler than SPPS that requires repeated "amidation−deprotection" cycles. In SPSS, the amino groups on solid supports are firstly amidated by haloacetic acid, which is then reacted by primary amines bearing desired groups. Polypeptoids are obtained from several cycles (Scheme 1.2). Copolypeptoids with highly accurate sequential structure can be achieved from SPSS, only by regulating the type of introduced amines. Zuckermann *et al.* designed a robot which can realize fully automated SPSS for polypeptoids.[134] However, the yield is still limited in SPSS, and it takes a large number of substrates and time for high MW polypeptoids. It is more suitable for the synthesis of oligopeptoids (DP < 30).

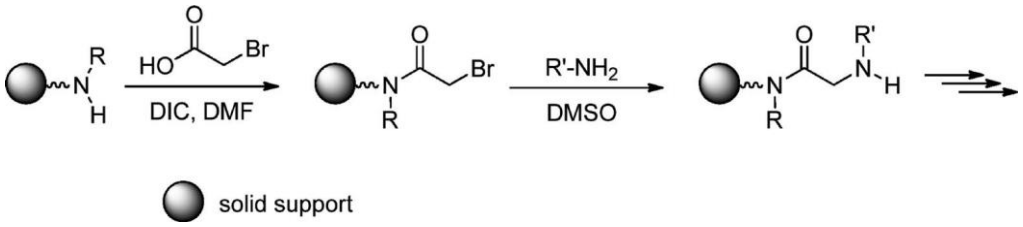

Scheme 1.2. The representative procedure of SPSS.

1.5.1.2 Ring-opening polymerization of NNCAs

Ring-opening polymerization (ROP) of N-substituted amino acid N-carboxyanhydride (NNCA) is currently the most widely reported method for the synthesis of polypeptoids, with advantages including high yield, controllable MWs and short production cycle. The ROP of NNCA is achieved through normal amine mechanism (NAM), where a nucleophile such as primary amine acts as the initiator to do nucleophilic attack on 5-CO of NNCA to form an unstable aminomethanoic acid intermediate, which tends to decompose via the removal of carbon dioxide (CO_2),

exposing a secondary amino end group and continue to attack other NNCAs for chain propagation (Scheme 1.3).

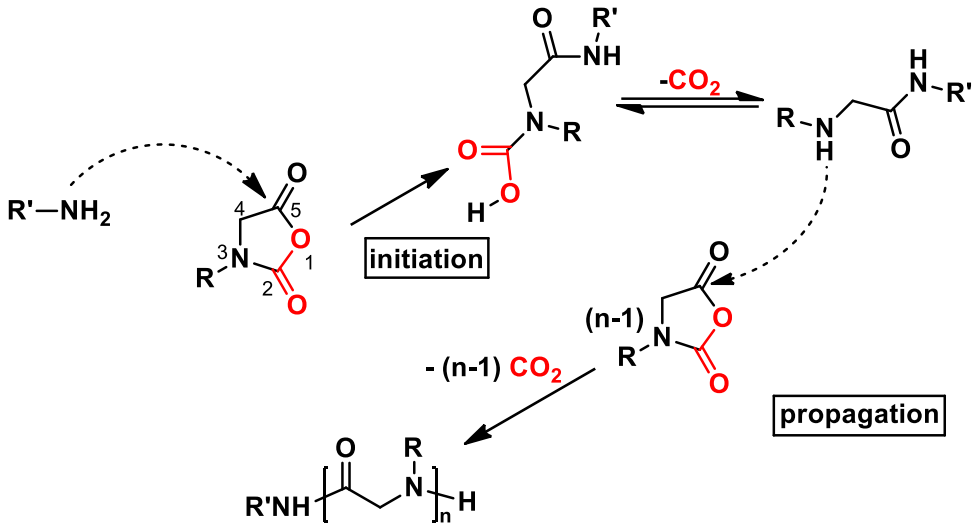

Scheme 1.3. ROP of NNCAs through NAM, for polypeptoid synthesis.

Luxenhofer *et al.* reported in 2011 a series of ROP of NNCAs, using benzylamine as the initiator, and polypeptoids with various *N*-substituent side chains are obtained, with controlled MWs and narrow distribution. The reactions exhibit living polymerization characteristics.[135] Based on it, sequential monomer feedings are performed, to obtain amphiphilic block copolypeptoids with poly(*N*-methyl glycine), that is polysarcosine (PSar) as the hydrophilic segment, and respectively poly(*N*-n-propyl glycine) (PNPG), poly(*N*-n-butyl glycine) (PNBG) and poly(*N*-isobutyl glycine) (PNIBG) as the hydrophobic segments (Scheme 1.4). Resin spheres and silicon wafers were also reported as the initiator, with amino groups on the surface, to initiate ROP of NNCA. Surface modification is achieved with grafting block copolypeptoids.[135, 136]

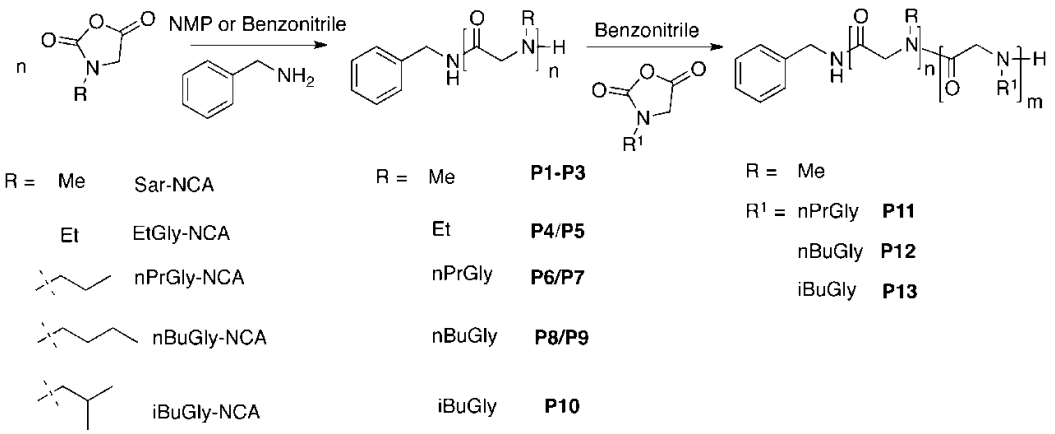

Scheme 1.4. ROP of NNCAs with benzylamine as the initiator, for the synthesis of a series of polypeptoid homopolymers and block copolymers.[135]

In most cases for the preparation of polypeptoid segment in block copolymers, ROP of NNCAs is the first choice, with primary amines as initiators.[137-150] What should be noted is the work reported by Zhang and coworkers, on the ring-expansion polymerization of NNCAs, initiated by *N*-heterocyclic carbene (NHC).[151, 152] In this reaction, NHC nucleophilically attacks a NNCA, forming a zwitterion with positive charge at one end and negative charge at the other end. The negatively charged end of the zwitterion attacks further NNCA or other zwitterions to achieve chain propagation. In low-polar solvent such as THF, the chain can be maintained in the form of a ring during the propagation (Scheme 1.5), because of the strong electrostatic interaction between the two ends. The electrostatic interaction of the positively charged NHC end can reduce the basicity and nucleophilicity of the aminocarboxylate anion at the other end, effectively inhibiting side reactions, thereby ensuring high efficiency and good control over MW and distribution, showing characteristics of living polymerization. In this way, cyclic and linear polypeptoids can be controllably obtained as desired.[153] By sequential feeding of monomers, they successfully prepared cyclic block copolypeptoids, including PSar-*b*-PNBG and PSar-*block*-poly(*N*-decyl glycine) (PSar-*b*-PNDG).[130, 151, 153]

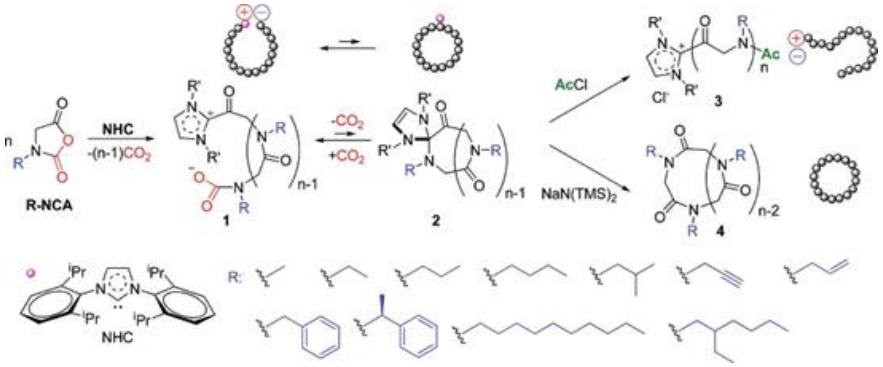

Scheme 1.5. Routes and mechanism of NHC-initiated zwitterionic ring-expansion polymerization of NNCAs, for cyclic and linear polypeptoids.[152]

1.5.1.3 Ring-opening polymerization of NNTAs

The high reactivity of *N*-carboxyanhydrides (NCAs) is a double-blade sword. On the one hand, ROP of NCAs stands out with high efficiency, but on the other hand, NCAs are also very susceptible to the external environment, in particular very sensitive to moisture and heat. The synthesis and purification of NCA often needs to be carried out under strict anhydrous conditions, and the obtained monomer cannot be stored for long time. It is often necessary to re-purify the monomer before use.[154] *N*-thiocarboxyanhydride (NTA), as the thio-analogue of NCA, has higher stability than NCA. The synthesis and purification of NTAs can be carried out directly in open air, and can be stored for long time without isomerization.[155] Under the action of initiator or catalyst, the polypeptoid can also be obtained from the ROP of *N*-substituted amino acid NTA (NNTAs), with the emission of carboyl sulfide (COS). In 2008, Kricheldorf used primary amines as the initiators to re-exploit the ROP of NTAs, but found that most of the NTA monomers have low polymerization activity.[156] The *N*-methyl substituted sarcosine NTA (Sar-NTA) is also included in the report. The maximum degree of polymerization (DP) of the synthesized PSar is only about 30.

The group of Jun Ling (our collaborators) has conducted since 2012 a systematic and in-depth study on the ROP of NNTAs. Their results revealed that polypeptoids from ROP of NNTAs can also get considerable MWs through the optimization of

polymerization conditions.[157, 158] In the solution of acetonitrile at 60 ℃, Sar-NTA can be polymerized to the DP of about 262 with the initiation of benzylamine, and the DP can even exceed 390 under the catalysis of yttrium borohydride ($Y(BH_4)_3(THF)_3$). In the solution of THF and initiated by benzylamine at 60 ℃, *N*-ethyl glycine NTA (NEG-NTA) is able to polymerize into poly(*N*-ethylgl ycine) (PNEG) with DP at 287. In the above-mentioned polymerizations, MWs are well controlled by the monomer-to-initiator/catalyst ratios. Moreover, under the condition of using primary amines as the initiators, the ROP of Sar-NTA and NEG-NTA can tolerate the initiating dose of other nucleophilic groups including hydroxyl and thiol, and the MWs of obtained polypeptoids are still proportionally controlled by monomer-to-amine ratios.[159, 160]

In one of their work, Tao *et al.* employed PEG amine ($PEG\text{-}NH_2$) as the macromolecular initiator, to achieve controlled ROP of Sar-NTA in THF, and prepared a double hydrophilic block copolymer (DHBC) PEG-*b*-PSar.[161] PSar is originally insoluble in THF, but the presence of PEG promotes the solubilization of the block copolymers, and enables the successful performance of the reaction. The sequential feeding of Sar-NTA and NEG-NTA with benzylamine as the initiator yields another DHBC PSar-*b*-PNEG.[158] With cysteamine as the initiator, both Sar-NTA and NEG-NTA can undergo ROP through NAM, without being affected by thiol groups. The obtained PSar and PNEG have the structure of one thiol end group and the other secondary amino end group. The thiol end group can initiate the addition of styrene via a free radical mechanism in excessive azobisisobutyronitrile (AIBN), and form a segment of oligopolystyrene (OS). Thus the block copolymers are obtained as OS-*b*-PSar and OS-*b*-PNEG.[160]

1.5.2 Self-assembly of PSar-containing amphiphilic block copolymers

Sarcosine is a natural amino acid. In human body it serves as an intermediate in the metabolism of choline to glycine. PSar, which is composed of sarcosine repeating unit, is a neutral water-soluble polypeptoid. It has been reported that PSar shows

biocompatibility[123] and antifouling of proteins,[162] and is degradable under simulated *in vivo* oxidative stress.[128] With these outstanding properties, PSar is considered to be an alternative to replace PEG in many domains.[163] Increasing numbers of work have been reported on PSar-containing amphiphilic block copolymers.

1.5.2.1 Self-assembly of polypeptide-*block*-PSar

Early in 1998, Kimura *et al.* reported the synthesis of the block copolymer polyalanine-*block*-PSar (PAla-*b*-PSar) by ROP of NCA, and self-assembly is prepared via a "film hydration−extrusion" procedure, from copolymers of three different Ala/Sar ratios (41/22, 34/22 and 34/27).[137] They found that the copolymer with larger Ala/Sar ratio can form self-assemblies with larger size, which are able to load higher amount of the fluorescent probe 8-anilinonaphthalene-1-sulfonic acid (ANS). $PAla_{34}$-*b*-$PSar_{27}$ forms micelles with a core-shell structure, sized about 30 nm, while the self-assemblies of $PAla_{34}$-*b*-$PSar_{22}$ and $PAla_{41}$-*b*-$PSar_{22}$ are over 80-90 nm, which are considered to be structures with multiple dimensions. In another work, they reported self-assemblies of PSar-containing copolymers, including PAla-*b*-PSar, poly(γ-methyl L-glutamate)-*block*-PSar (PGlu(OMe)-*b*-PSar) and poly(N_ε-benzyloxycarbonyl-L-lysine)-*block*-PSar (PLys(Z)-*b*-PSar) prepared by the W/O/W double emulsion method.[138, 164-166] After the evaporation of the organic solvent (*e. g.* chloroform), microcapsules are formed with a porous inner structure. pH-responsibility can be achieved in microcapsules of PGlu(OMe)-*b*-PSar after partial deprotection, and of PLys(Z)-*b*-PSar microcapsules after partial deprotection and subsequent grafting of PGlu.[165]

The team of Kimura focused on the synthesis and self-assembly of polypeptide-*block*-PSar of which the hydrophobic segments are helical short-chain peptides. The peptides are majorly composed of the amide of leucine and 2-aminoisobutyric acid (Leu-Aib) as the repeating unit, wherein the presence of 2-aminoisobutyric acid (Aib) allows the short-chain peptide to form uniformly helical structure. The copolymer PSar-*b*-P(Leu-Aib) is obtained from P(Leu-Aib)-initiated ROP of Sar-NCA. Through a

solvent replacement method similar to nanoprecipitation, the stereotactic PSar-*b*-P(L-Leu-Aib) with right-handed helix, and PSar-*b*-P(D-Leu-Aib) with left-handed helix, can both form sheet-shaped structures. The sheets curves into nanotubes after the heating treatment at 90 ℃.[167] The length can be adjusted by the time of heating, and other structures such as three-way nanotubes can be obtained by the blends of copolymers with the same helix but different chain lengths. The introduction of a histidine unit with imidazole side group between the hydrophilic and hydrophobic segments can result in pH-responsive nanotubes.[168, 169] The equimolar racemic mixture of $PSar_{25}$-*b*-P(L-Leu-Aib)$_6$ and $PSar_{25}$-*b*-P(D-Leu-Aib)$_6$ turns nanotubes back to sheets, and then transforms to vesicles after being heated at 90 ℃ (Figure. 1.23).[170] The size of vesicles can be controlled by heating time, as the larger vesicles are formed from inter-vesicular fusion.[171] When the mixed left-handed and right-handed components are not equal, say 20:80 or 80:20, the heated self-assemblies undergo phase separation, forming racemic domain and one-component domain. The racemic domain forms a vesicular part, while the one-component domain forms a tubular part, which are spliced together to form a flask-like structure.[172] Through other approaches including alternating chain structure (such as changing the AB copolymer into a A_3B type), introducing other amino acids (such as alanine, proline, histidine, *etc.*), more structures are obtained with their own specificities.[168, 173, 174] Moreover, the splicing of different structures can be further achieved, increasing the morphological diversity.[175] Note that the spliced structures are only part of the obtained self-assembly result, which in total is a nonergodic mixture of multiple morphologies.

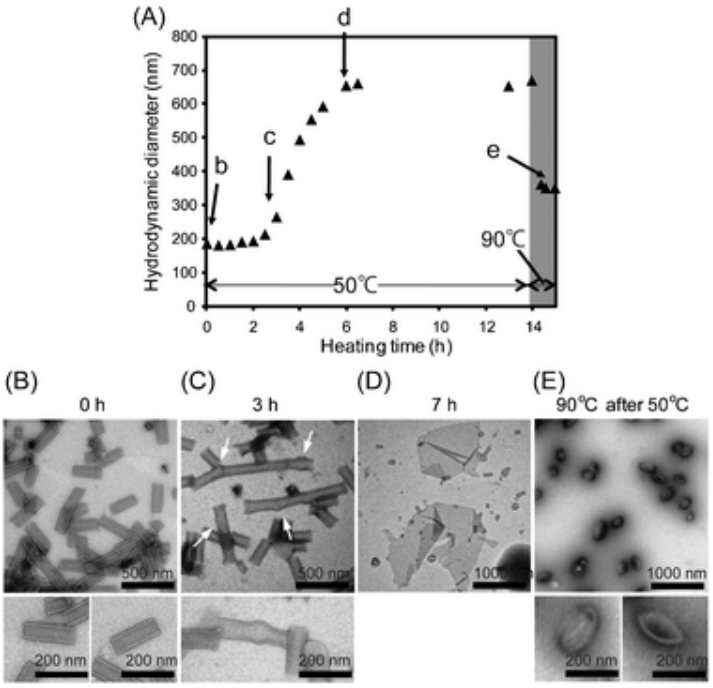

Figure 1.23. (A) Variation of hydrodynamic diameter in function of time, determined by DLS, and (B−E) TEM images of structures at different stages, during the procedure of equimolar mixing of PSar$_{25}$-*b*-P(L-Leu-Aib)$_6$ and PSar$_{25}$-*b*-P(D-Leu-Aib)$_6$ at 50 ℃ and following heating treatment at 90 ℃.[170]

The team of Barz obtained a series of PGlu(OBn)-*b*-PSar and PLys(Z)-*b*-PSar block copolymers by sequential feeding of NCA monomers.[140] In these two PSar-containing copolymers, the DPs of PSar segments are in the range 100−400, and the copolymers can respectively form spherical micelles. Among them the micelles of PGlu(OBn)$_{25}$-*b*-PSar$_{200}$ is used as the inhibitor of adenylate cyclase. The copolymers are also employed as macromolecular surfactants to stabilize microemulsions, for the preparation of polystyrene and polylactide microspheres. For the copolymer PGlu(OBn)$_{46}$-*b*-PSar$_{111}$, due to its relatively low hydrophilic ratio (44 wt%) among the obtained copolymers, it can form vesicles with the diameter at about 70 nm. The polymersomes are studied for the development towards a versatile platform for vaccination.[143] PLys(Z)-*b*-PSar and poly(N_ε-trifluoroacetyl-L-lysine)-*block*-PSar (PLys(TFA)-*b*-PSar) are deprotected to PLys-*b*-PSar, which is applied in the complexation with DNA.[141] In other two work, disulfide bonds are respectively

introduced to poly(γ-tert-butyl L-glutamate)-*block*-PSar (PGlu(OtBu)-*b*-PSar) and star-shaped poly(N_ε-tert-butoxycarbonyl-L-lysine)-*block*-PSar (PLys(Boc)-*b*-PSar), to prepare reduction-responsive micelles.[142, 176]

1.5.2.2 Self-assembly of polyester-*block*-PSar

The team of Kimura is also the pioneer in the study of polyester-*block*-PSar. They prepared a series of PSar-*block*-polylactide (PSar-*b*-PLA) copolymers, and named the self-assemblies of PSar-*b*-PLA as "Lactosome".[139, 177-179] Copolymers with different chain structures are prepared, including AB-, A_2B- and A_3B-types. The different chain structures result in differences in self-assembly, including morphologies and hydrodynamic diameters.[177] Simultaneously, the properties of micelles related to medical applications, such as blood clearance time, were studied. Their blood clearance time is shown to be affected by the chain structure of copolymers,[179] and the chirality and stereoregularity of the PLA segments.[178]

Guo *et al.* employed PSar directly as a macromolecular initiator for the ROP of ε-caprolactone (CL) and lactide along with catalysts, and successfully synthesized block copolymers PSar-*b*-PCL[144, 147] and PSar-*b*-PLA.[146] The obtained copolymers are applied in self-assembly to form micelles and nanoparticles.

1.5.2.3 Self-assembly of PSar-containing double hydrophilic block copolymers (DHBC)

DHBC composed of two hydrophilic polymers can still undergo phase separation in water due to structural differences between the two segments and their difference in solubility, which as the result forms self-assembly structures. Tao *et al.* explored the self-assembly behavior of PEG-*b*-PSar obtained from ROP of Sar-NTA,[161] and found unstable nanoparticles in water. In these nanoparticles, the PEG segments are wrapped inside, while the PSar segments serve as the corona. PEG-*b*-PSar can also act as a macromolecular surfactant to stabilize the O/W emulsion, where

dichloromethane (DCM) is dispersed in water. Likewise, the PEG segments are mainly distributed in DCM phase, while the PSar segments are arranged on the emulsion surface. The size of emulsion droplets can be adjusted by PEG/PSar ratios. Schlaad *et al.* reported a DHBC dextran-*block*-PSar (Dex-*b*-PSar), and prepared nano- and micrometer-scale vesicles based on the structural difference and phase separation of Dex and PSar segments.[180] The obtained vesicles have highly water-permeable membrane. With the similar property to cellular membrane, this type of vesicles is expected for further applications in biomedical fields.

1.5.3 Self-assembly of amphiphilic block copolypeptoids

The research on self-assemblies of amphiphilic block copolypeptoids entirely composed of polypeptoid blocks, including polypeptoid vesicles, is still at their begining. Zuckermann *et al.* reported lamellar, helical and tubular aggregates by short-chain amphiphilic copolypeptoids obtained by SPSS.[181, 182] In a work reported by Gaitzsch and Battaglia in 2015, short-chain amphiphilic copolypeptoids are prepared with oligo(*N*-hydroxyethyl glycine) (ONHEG) or oligo(*N*-methoxyethyl glycine) (ONMeOEG) as the hydrophilic segment, and oligo(*N*-n-pentyl glycine) (ONPG) as the hydrophobic segment. Vesicles are generated from these copolypeptoids by film hydration method.[183]

The team of Schlaad studied the thermo-responsive self-assembly and crystallization behavior of PSar-*b*-PNPG with relatively high MWs in water.[149, 150] PNPG has a lowest critical solution temperature (LCST) in water, below which the polymers are well dissolved in water, and once the temperature rises above LCST, phase separation occurs, turning the homogeneous solution to cloudy suspension (therefore the critical temperature is also called as cloud point (T_{cp})). In addition, PNPG is a crystallizable polypeptoid. As the result, PSar-*b*-PNPG copolymers aggregate in water above T_{cp}. During the following heating and annealing, the PNPG segments crystallize in the core, and affect the size and morphology of the obtained aggregates.

Zhang *et al*. reported the self-assemblies of PSar-*b*-PNDG driven by crystallization in methanol.[130] The copolymers first form spherical micelles, which are converted into cylindrical micelles driven by the crystallization of PNDG. Through the advancement of the crystallization, all the spherical micelles are consumed and the cylinders grow longer and longer, and eventually a large number of nano-fibers are obtained.

The team of Luxenhofer, studied a series of copolypolypeptoids in which PSar serves as a hydrophilic block, and the polypeptoids with different length of *N*-substituent groups (from ethyl to pentyl) as the second block.[131] As revealed by the determination of critical micellar concentration (CMC), the copolypeptoid with longer *N*-substituent groups has lower CMC, and is more likely to aggregate in water. For the same type of copolymers, the higher the proportion of hydrophobic segment, the larger the hydrodynamic diameter of resulted self-assemblies. They also compared the size and structure of various copolypeptoids prepared by nanoprecipitation and film hydration methods.[184] According to the DLS and TEM results, most of the copolypeptoids form nonergodic self-assemblies, including spherical micelles, worm-like micelles, vesicles and lamellae, with wide distributions in morphologies and sizes.

1.6 Conclusion

With robust cell-mimicking bilayer structure, polymersome has high stability and drug-loading capability, and has been considered as a promising drug delivery vehicle for biomedical applications. The high MW and low mobility of the composing copolymers cause the nonergodicity of polymeric self-assemblies. Therefore, the morphologies of self-assemlies including polymersomes depend largly on the preparation methods and conditions. Using stimuli-responsive polymersomes, smart drug delivery can be achieved by changing the membrane permeability, creating defects in the membrane or prompting structural disruption of polymersomes under the action of various stimuli. Among these stimuli, ROS, highly oxidative substances, have a variety of sources and also accumulate at relatively higher level in tumor and

inflammatory tissues. Therefore, ROS play an active role in cancer treatment. The research on polymersomes including ROS-function is emerging in both fundamental and applied fields.

For biomedical applications, the biocompatibility of polymersomes and their composing copolymers, is a key point to be considered. Polypeptoids, the derivatives of polypeptides bearing substituting group on the nitrogen atom of amides, show good biocompatibility and biodegradability as polypeptides. Moreover, because of the absence of of intra- and intermolecular hydrogen bonds polypeptoids have much better solubility in common organic solvent than polypeptides. The synthesis and self-assembly of polypeptoid-containing block copolymers harvest more and more attentions. Polypeptoid vesicle system is a new fertile land waiting for deep investigation and exploitation.

This PhD thesis aims to synthesize novel polypeptoid-containing amphiphilic block copolymers, to prepare polypeptoid vesicles through controlled self-assembly, and to develop stimuli-responsive, especially oxidation-responsive polypeptoid vesicles.

In the following texts, the Chapter 2 is focused on the preparation of polypeptoid-containing amphiphilic block copolymers through ROP of NNTAs. The syntheses of copolymers PCL-*b*-PSar, PSar-*b*-PCL-*b*-PSar, PEG-*block*-poly(*N*-3-(methylthio)propyl glycine) (PEG-*b*-PMeSPG) and PMeSPG-*b*-PSar are described. The Chapter 3 presents the self-assemblies of triblock copolymers PSar-*b*-PCL-*b*-PSar. Thermo-induced morphological transformation of self-assemblies towards vesicle formation is highlighted. The Chapter 4 discusses the self-assemblies of PEG-*b*-PMeSPG and PMeSPG-*b*-PSar with different compositions, MWs, hydrophilic/hydrophobic ratios, using different methods like nanoprecipitation, fil; hydration and double emulsion. Finally, in the last Chapter 5, we present the oxidation-

responsive and photo-responsive polymersomes based on PMeSPG-*b*-PSar where PMeSPG contains thioether side groups.

References

1. Hyde, S. T., Curvature and the global structure of interfaces in surfactant-water systems. *J. Phys.* **1990,** *51* (23), 7209-7228.

2. Antonietti, M.; Forster, S., Vesicles and liposomes: A self-assembly principle beyond lipids. *Adv. Mater.* **2003,** *15* (16), 1323-1333.

3. Blanazs, A.; Armes, S. P.; Ryan, A. J., Self-Assembled Block Copolymer Aggregates: From Micelles to Vesicles and their Biological Applications. *Macromol. Rapid Commun.* **2009,** *30* (4-5), 267-277.

4. Denkova, A. G.; Mendes, E.; Coppens, M.-O., Non-equilibrium dynamics of block copolymer micelles in solution: recent insights and open questions. *Soft matter* **2010,** *6* (11), 2351-2357.

5. Jain, S.; Bates, F. S., Consequences of nonergodicity in aqueous binary PEO-PB micellar dispersions. *Macromolecules* **2004,** *37* (4), 1511-1523.

6. Shen, H. W.; Eisenberg, A., Block length dependence of morphological phase diagrams of the ternary system of PS-b-PAA/dioxane/H2O. *Macromolecules* **2000,** *33* (7), 2561-2572.

7. Jia, L.; Levy, D.; Durand, D.; Imperor-Clerc, M.; Cao, A.; Li, M.-H., Smectic polymer micellar aggregates with temperature-controlled morphologies. *Soft matter* **2011,** *7* (16), 7395-7403.

8. McKenzie, B. E.; de Visser, J. F.; Friedrich, H.; Wirix, M. J. M.; Bomans, P. H. H.; de With, G.; Holder, S. J.; Sommerdijk, N. A. J. M., Bicontinuous Nanospheres from Simple Amorphous Amphiphilic Diblock Copolymers. *Macromolecules* **2013,** *46* (24), 9845-9848.

9. Rizis, G.; van de Ven, T. G. M.; Eisenberg, A., "Raft" Formation by Two‐Dimensional Self‐Assembly of Block Copolymer Rod Micelles in Aqueous Solution. *Angew. Chem. Int. Ed. Engl.* **2014,** *126* (34), 9146-9149.

10. Ku, K. H.; Shin, J. M.; Klinger, D.; Jang, S. G.; Hayward, R. C.; Hawker, C. J.; Kim, B. J., Particles with Tunable Porosity and Morphology by Controlling Interfacial Instability in Block Copolymer Emulsions. *ACS Nano* **2016,** *10* (5), 5243-5251.

11. Wang, X. Y.; Feng, X. Y.; Ma, G. P.; Zhang, D.; Chai, Y. H.; Ge, M. F.; Yao, L., Dual-Phase Separation in a Semiconfined System: Monodispersed Heterogeneous Block-Copolymer Membranes for Cell Encoding and Patterning. *Adv. Mater.* **2017,** *29* (19), e1605932.

12. Battaglia, G.; Ryan, A. J., Pathways of polymeric vesicle formation. *J. Phys. Chem. B* **2006,** *110* (21), 10272-10279.

13. Deng, R.; Li, H.; Zhu, J.; Li, B.; Liang, F.; Jia, F.; Qu, X.; Yang, Z., Janus Nanoparticles of Block Copolymers by Emulsion Solvent Evaporation Induced Assembly. *Macromolecules* **2016,** *49* (4), 1362-1368.

14. Cui, H.; Chen, Z.; Wooley, K. L.; Pochan, D. J., Origins of toroidal micelle formation through charged triblock copolymer self-assembly. *Soft matter* **2009,** *5* (6), 1269-1278.

15. Cui, H.; Chen, Z.; Zhong, S.; Wooley, K. L.; Pochan, D. J., Block copolymer assembly via kinetic control. *Science* **2007,** *317* (5838), 647-650.

16. Zhong, S.; Cui, H.; Chen, Z.; Wooley, K. L.; Pochan, D. J., Helix self-assembly through the coiling of cylindrical micelles. *Soft matter* **2008,** *4* (1), 90-93.

17. Jain, S.; Bates, F. S., On the origins of morphological complexity in block copolymer surfactants. *Science* **2003,** *300* (5618), 460-464.

18. Battaglia, G.; Tomas, S.; Ryan, A. J., Lamellarsomes: metastable polymeric multilamellar aggregates. *Soft matter* **2007,** *3* (4), 470-475.

19. Xu, B.; Pinol, R.; Nono-Djamen, M.; Pensec, S.; Keller, P.; Albouy, P. A.; Levy, D.; Li, M. H., Self-assembly of liquid crystal block copolymer PEG-b-smectic polymer in pure state and in dilute aqueous solution. *Faraday Discuss.* **2009,** *143*, 235-250.

20. Jia, L.; Cao, A.; Levy, D.; Xu, B.; Albouy, P. A.; Xing, X. J.; Bowick, M. J.; Li, M. H., Smectic polymer vesicles. *Soft matter* **2009,** *5* (18), 3446-3451.

21. Discher, B. M.; Won, Y. Y.; Ege, D. S.; Lee, J. C. M.; Bates, F. S.; Discher, D. E.; Hammer, D. A., Polymersomes: Tough vesicles made from diblock copolymers. *Science* **1999,** *284* (5417), 1143-1146.

22. Discher, D. E.; Eisenberg, A., Polymer vesicles. *Science* **2002,** *297* (5583), 967-973.

23. Uneyama, T., Density functional simulation of spontaneous formation of vesicle in block copolymer solutions. *J. Chem. Phys.* **2007,** *126* (11), 114902.

24. He, X. H.; Schmid, F., Dynamics of spontaneous vesicle formation in dilute solutions of amphiphilic diblock copolymers. *Macromolecules* **2006,** *39* (7), 2654-2662.

25. Adams, D. J.; Adams, S.; Atkins, D.; Butler, M. F.; Furzeland, S., Impact of mechanism of formation on encapsulation in block copolymer vesicles. *J. Control. Release* **2008,** *128* (2), 165-170.

26. Yu, K.; Eisenberg, A., Bilayer morphologies of self-assembled crew-cut aggregates of amphiphilic PS-b-PEO diblock copolymers in solution. *Macromolecules* **1998,** *31* (11), 3509-3518.

27. Blanazs, A.; Madsen, J.; Battaglia, G.; Ryan, A. J.; Armes, S. P., Mechanistic Insights for Block Copolymer Morphologies: How Do Worms Form Vesicles? *J. Am. Chem. Soc.* **2011,** *133* (41), 16581-16587.

28. Yu, Y. S.; Eisenberg, A., Control of morphology through polymer-solvent interactions in crew-cut aggregates of amphiphilic block copolymers. *J. Am. Chem. Soc.* **1997,** *119* (35), 8383-8384.

29. Yu, Y. S.; Zhang, L. F.; Eisenberg, A., Morphogenic effect of solvent on crew-cut aggregates of apmphiphilic diblock copolymers. *Macromolecules* **1998,** *31* (4), 1144-1154.

30. Menger, F. M.; Angelova, M. I., Giant vesicles: Imitating the cytological processes of cell membranes. *Acc. Chem. Res.* **1998,** *31* (12), 789-797.

31. Battaglia, G.; Ryan, A. J., Effect of amphiphile size on the transformation from a lyotropic gel to a vesicular dispersion. *Macromolecules* **2006,** *39* (2), 798-805.

32. Battaglia, G.; Ryan, A. J., The evolution of vesicles from bulk lamellar gels. *Nat. Mater.* **2005,** *4* (11), 869-876.

33. Battaglia, G.; Ryan, A. J., Neuron-like tubular membranes made of diblock copolymer amphiphiles. *Angew. Chem. Int. Ed. Engl.* **2006,** *45* (13), 2052-2056.

34. Photos, P. J.; Bacakova, L.; Discher, B.; Bates, F. S.; Discher, D. E., Polymer vesicles in vivo: correlations with PEG molecular weight. *J. Control. Release* **2003,** *90* (3), 323-334.

35. Ghoroghchian, P. P.; Li, G. Z.; Levine, D. H.; Davis, K. P.; Bates, F. S.; Hammer, D. A.; Therien, M. J., Bioresorbable vesicles formed through spontaneous self-assembly of amphiphilic poly(ethylene oxide)-block-polycaprolactone. *Macromolecules* **2006,** *39* (5), 1673-1675.

36. Howse, J. R.; Jones, R. A. L.; Battaglia, G.; Ducker, R. E.; Leggett, G. J.; Ryan, A. J., Templated formation of giant polymer vesicles with controlled size distributions. *Nat. Mater.* **2009,** *8* (6), 507-511.

37. Odonnell, P. B.; McGinity, J. W., Preparation of microspheres by the solvent evaporation technique. *Adv. Drug. Deliv. Rev.* **1997,** *28* (1), 25-42.

38. Wang, W.; Qi, H.; Zhou, T.; Mei, S.; Han, L.; Higuchi, T.; Jinnai, H.; Li, C. Y., Highly robust crystalsome via directed polymer crystallization at curved liquid/liquid interface. *Nat. Comm.* **2016,** *7*, 10599.

39. Wang, W.; Staub, M. C.; Zhou, T.; Smith, D. M.; Qi, H.; Laird, E. D.; Cheng, S.; Li, C. Y., Polyethylene nano crystalsomes formed at a curved liquid/liquid interface. *Nanoscale* **2017,** *10* (1), 268-276.

40. Wyman, I.; Njikang, G.; Liu, G., When emulsification meets self-assembly: The role of emulsification in directing block copolymer assembly. *Prog. Polym. Sci.* **2011,** *36* (9), 1152-1183.

41. Bae, J.; Russell, T. P.; Hayward, R. C., Osmotically driven formation of double emulsions stabilized by amphiphilic block copolymers. *Angew. Chem. Int. Ed. Engl.* **2014,** *53* (31), 8240-8245.

42. Park, M.-K.; Jun, S.; Kim, I.; Jin, S.-M.; Kim, J.-G.; Shin, T. J.; Lee, E., Stepwise Drug-Release Behavior of Onion-Like Vesicles Generated from Emulsification-Induced Assembly of Semicrystalline Polymer Amphiphiles. *Adv. Funct. Mater.* **2015,** *25* (29), 4570-4579.

43. Lorenceau, E.; Utada, A. S.; Link, D. R.; Cristobal, G.; Joanicot, M.; Weitz, D. A., Generation of polymerosomes from double-emulsions. *Langmuir* **2005,** *21* (20), 9183-9186.

44. Shum, H. C.; Kim, J.-W.; Weitz, D. A., Microfluidic fabrication of monodisperse biocompatible and biodegradable polymersomes with controlled permeability. *J. Am. Chem. Soc.* **2008,** *130* (29), 9543-9549.

45. Shum, H. C.; Zhao, Y.-j.; Kim, S.-H.; Weitz, D. A., Multicompartment Polymersomes from Double Emulsions. *Angew. Chem. Int. Ed. Engl.* **2011,** *50* (7), 1648-1651.

46. Lee, J. C. M.; Bermudez, H.; Discher, B. M.; Sheehan, M. A.; Won, Y. Y.; Bates, F. S.; Discher, D. E., Preparation, stability, and in vitro performance of vesicles made with diblock copolymers. *Biotechnol. Bioeng.* **2001,** *73* (2), 135-145.

47. Mui, B. L. S.; Dobereiner, H. G.; Madden, T. D.; Cullis, P. R., Influence of transbilayer area asymmetry on the morphology of large unilamellar vesicles. *Biophys. J.* **1995,** *69* (3), 930-941.

48. Lipowsky, R., The conformation of membranes. *Nature* **1991,** *349* (6309), 475-481.

49. Julicher, F.; Seifert, U.; Lipowsky, R., Phase-diagrams and shape transformations of toroidal vesicles. *J. Phys. II* **1993,** *3* (11), 1681-1705.

50. Kim, K. T.; Zhu, J.; Meeuwissen, S. A.; Cornelissen, J. J. L. M.; Pochan, D. J.; Nolte, R. J. M.; van Hest, J. C. M., Polymersome Stomatocytes: Controlled Shape Transformation in Polymer Vesicles. *J. Am. Chem. Soc.* **2010,** *132* (36), 12522-12524.

51. Meeuwissen, S. A.; Kim, K. T.; Chen, Y.; Pochan, D. J.; van Hest, J. C. M., Controlled Shape Transformation of Polymersome Stomatocytes. *Angew. Chem. Int. Ed. Engl.* **2011,** *50* (31), 7070-7073.

52. Rikken, R. S. M.; Engelkamp, H.; Nolte, R. J. M.; Maan, J. C.; van Hest, J. C. M.; Wilson, D. A.; Christianen, P. C. M., Shaping polymersomes into predictable morphologies via out-of-equilibrium self-assembly. *Nat. Comm.* **2016,** *7*, 12606.

53. Men, Y.; Li, W.; Janssen, G.-J.; Rikken, R. S. M.; Wilson, D. A., Stomatocyte in Stomatocyte: A New Shape of Polymersome Induced via Chemical-Addition Methodology. *Nano Lett.* **2018,** *18* (3), 2081-2085.

54. Wilson, D. A.; Nolte, R. J.; van Hest, J. C., Autonomous movement of platinum-loaded stomatocytes. *Nat. Chem.* **2012,** *4* (4), 268-274.

55. Tu, Y.; Peng, F.; White, P. B.; Wilson, D. A., Redox-Sensitive Stomatocyte Nanomotors: Destruction and Drug Release in the Presence of Glutathione. *Angew. Chem. Int. Ed. Engl.* **2017,** *56* (26), 7620-7624.

56. Srinivas, G.; Discher, D. E.; Klein, M. L., Self-assembly and properties of diblock copolymers by coarse-grain molecular dynamics. *Nat. Mater.* **2004,** *3* (9), 638-644.

57. Discher, D. E.; Ahmed, F., Polymersomes. In *Annu. Rev. Biomed. Eng.*, 2006; Vol. 8, pp 323-341.

58. Choucair, A.; Soo, P. L.; Eisenberg, A., Active loading and tunable release of doxorubicin from block copolymer vesicles. *Langmuir* **2005,** *21* (20), 9308-9313.

59. Wu, J.; Eisenberg, A., Proton diffusion across membranes of vesicles of poly(styrene-b-acrylic acid) diblock copolymers. *J. Am. Chem. Soc.* **2006,** *128* (9), 2880-2884.

60. Yu, S.; Azzam, T.; Rouiller, I.; Eisenberg, A., "Breathing" Vesicles. *J. Am. Chem. Soc.* **2009,** *131* (30), 10557-10566.

61. Nardin, C.; Thoeni, S.; Widmer, J.; Winterhalter, M.; Meier, W., Nanoreactors based on (polymerized) ABA-triblock copolymer vesicles. *Chem. Commun.* **2000,** (15), 1433-1434.

62. Ranquin, A.; Versees, W.; Meier, W.; Steyaert, J.; Van Gelder, P., Therapeutic nanoreactors: Combining chemistry and biology in a novel triblock copolymer drug delivery system. *Nano Lett.* **2005,** *5* (11), 2220-2224.

63. Kumar, M.; Grzelakowski, M.; Zilles, J.; Clark, M.; Meier, W., Highly permeable polymeric membranes based on the incorporation of the functional water channel protein Aquaporin Z. *Proc. Natl. Acad. Sci. USA* **2007,** *104* (52), 20719-20724.

64. Spulber, M.; Najer, A.; Winkelbach, K.; Glaied, O.; Waser, M.; Pieles, U.; Meier, W.; Bruns, N., Photoreaction of a Hydroxyalkyphenone with the Membrane of Polymersomes: A Versatile Method To Generate Semipermeable Nanoreactors. *J. Am. Chem. Soc.* **2013,** *135* (24), 9204-9212.

65. Meng, F. H.; Zhong, Z. Y.; Feijen, J., Stimuli-Responsive Polymersomes for Programmed Drug Delivery. *Biomacromolecules* **2009,** *10* (2), 197-209.

66. Du, J. Z.; O'Reilly, R. K., Advances and challenges in smart and functional polymer vesicles. *Soft matter* **2009,** *5* (19), 3544-3561.

67. Grafe, D.; Gaitzsch, J.; Appelhans, D.; Voit, B., Cross-linked polymersomes as nanoreactors for controlled and stabilized single and cascade enzymatic reactions. *Nanoscale* **2014,** *6* (18), 10752-10761.

68. Yassin, M. A.; Appelhans, D.; Wiedemuth, R.; Formanek, P.; Boye, S.; Lederer, A.; Temme, A.; Voit, B., Overcoming Concealment Effects of Targeting Moieties in the PEG Corona: Controlled Permeable Polymersomes Decorated with Folate-Antennae for Selective Targeting of Tumor Cells. *Small* **2015,** *11* (13), 1580-1591.

69. Dan, K.; Ghosh, S., One-Pot Synthesis of an Acid-Labile Amphiphilic Triblock Copolymer and its pH-Responsive Vesicular Assembly. *Angew. Chem. Int. Ed. Engl.* **2013,** *52* (28), 7300-7305.

70. Jia, L.; Cui, D.; Bignon, J.; Di Cicco, A.; Wdzieczak-Bakala, J.; Liu, J.; Li, M. H., Reduction-responsive cholesterol-based block copolymer vesicles for drug delivery. *Biomacromolecules* **2014,** *15* (6), 2206-2217.

71. Liou, G.-Y.; Storz, P., Reactive oxygen species in cancer. *Free Radical Res.* **2010,** *44* (5), 479-496.

72. Renschler, M. F., The emerging role of reactive oxygen species in cancer therapy. *European Journal of Cancer* **2004,** *40* (13), 1934-1940.

73. Dolmans, D.; Fukumura, D.; Jain, R. K., Photodynamic therapy for cancer. *Nat. Rev. Cancer* **2003,** *3* (5), 380-387.

74. Zhou, Z.; Song, J.; Nie, L.; Chen, X., Reactive oxygen species generating systems meeting challenges of photodynamic cancer therapy. *Chem. Soc. Rev.* **2016,** *45* (23), 6597-6626.

75. Yuan, Z.; Yu, S.; Cao, F.; Mao, Z.; Gao, C.; Ling, J., Near-infrared light triggered photothermal and photodynamic therapy with an oxygen-shuttle endoperoxide of anthracene against tumor hypoxia. *Polym. Chem.* **2018,** *9* (16), 2124-2133.

76. Xu, S.; Ng, G.; Xu, J.; Kuchel, R. P.; Yeow, J.; Boyer, C., 2-(Methylthio)ethyl Methacrylate: A Versatile Monomer for Stimuli Responsiveness and Polymerization-Induced Self-Assembly in the Presence of Air. *ACS Macro Lett.* **2017,** *6* (11), 1237-1244.

77. Yan, B.; Zhang, Y.; Wei, C.; Xu, Y., Facile synthesis of ROS-responsive biodegradable main chain poly(carbonate-thioether) copolymers. *Polym. Chem.* **2018,** *9* (7), 904-911.

78. Kim, S.-Y.; Kim, S.-J.; Kim, B.-J.; Rah, S.-Y.; Chung, S. M.; Im, M.-J.; Kim, U.-H., Doxorubicin-induced reactive oxygen species generation and intracellular Ca2+ increase are reciprocally modulated in rat cardiomyocytes. *Exp. Mol. Med.* **2006,** *38* (5), 535-545.

79. Upadhyay, K. K.; Bhatt, A. N.; Mishra, A. K.; Dwarakanath, B. S.; Jain, S.; Schatz, C.; Le Meins, J.-F.; Farooque, A.; Chandraiah, G.; Jain, A. K.; Misra, A.; Lecommandoux, S., The intracellular drug delivery and anti tumor activity of doxorubicin loaded poly(γ-benzyl l-glutamate)-b-hyaluronan polymersomes. *Biomaterials* **2010,** *31* (10), 2882-2892.

80. Spulber, M.; Baumann, P.; Saxer, S. S.; Pieles, U.; Meier, W.; Bruns, N., Poly(N-vinylpyrrolidone)-Poly(dimethylsiloxane)-Based Polymersome Nanoreactors for Laccase-Catalyzed Biotransformations. *Biomacromolecules* **2014,** *15* (4), 1469-1475.

81. Chen, H.; Xiao, L.; Anraku, Y.; Mi, P.; Liu, X.; Cabral, H.; Inoue, A.; Nomoto, T.; Kishimura, A.; Nishiyama, N.; Kataoka, K., Polyion Complex Vesicles for Photoinduced Intracellular Delivery of Amphiphilic Photosensitizer. *J. Am. Chem. Soc.* **2014,** *136* (1), 157-163.

82. He, H.; Ji, S.; He, Y.; Zhu, A.; Zou, Y.; Deng, Y.; Ke, H.; Yang, H.; Zhao, Y.; Guo, Z.; Chen, H., Photoconversion-Tunable Fluorophore Vesicles for Wavelength-Dependent Photoinduced Cancer Therapy. *Adv. Mater.* **2017,** *29* (19), e1606690.

83. Doskey, C. M.; Buranasudja, V.; Wagner, B. A.; Wilkes, J. G.; Du, J.; Cullen, J. J.; Buettner, G. R., Tumor cells have decreased ability to metabolize H2O2: Implications for pharmacological ascorbate in cancer therapy. *Redox Bio.* **2016,** *10*, 274-284.

84. Ohshima, H.; Tatemichi, M.; Sawa, T., Chemical basis of inflammation-induced carcinogenesis. *Arch. Biochem. Biophys.* **2003,** *417* (1), 3-11.

85. Szatrowski, T. P.; Nathan, C. F., Production of large amounts of hydrogen-peroxide by human tumor-cells. *Cancer Res.* **1991,** *51* (3), 794-798.

86. Abdelmohsen, L. K. E. A.; Nijemeisland, M.; Pawar, G. M.; Janssen, G.-J. A.; Nolte, R. J. M.; van Hest, J. C. M.; Wilson, D. A., Dynamic Loading and Unloading of Proteins in Polymeric Stomatocytes: Formation of an Enzyme-Loaded Supramolecular Nanomotor. *ACS Nano* **2016,** *10* (2), 2652-2660.

87. Nijemeisland, M.; Abdelmohsen, L. K. E. A.; Huck, W. T. S.; Wilson, D. A.; van Hest, J. C. M., A Compartmentalized Out-of-Equilibrium Enzymatic Reaction Network for Sustained Autonomous Movement. *ACS Central Sci.* **2016,** *2* (11), 843-849.

88. Fei, P.; Yingfeng, T.; Yongjun, M.; M., v. H. J. C.; A., W. D., Supramolecular Adaptive Nanomotors with Magnetotaxis Behavior. *Adv. Mater.* **2017,** *29* (6), 1604996.

89. Tu, Y.; Peng, F.; Andre, A. A. M.; Men, Y.; Srinivas, M.; Wilson, D. A., Biodegradable Hybrid Stomatocyte Nanomotors for Drug Delivery. *ACS Nano* **2017,** *11* (2), 1957-1963.

90. Deng, Z.; Hu, J.; Liu, S., Reactive Oxygen, Nitrogen, and Sulfur Species (RONSS)-Responsive Polymersomes for Triggered Drug Release. *Macromol. Rapid Commun.* **2017,** *38* (11), e1600685.

91. Napoli, A.; Valentini, M.; Tirelli, N.; Muller, M.; Hubbell, J. A., Oxidation-responsive polymeric vesicles. *Nat. Mater.* **2004,** *3* (3), 183-189.

92. Bellomo, E. G.; Wyrsta, M. D.; Pakstis, L.; Pochan, D. J.; Deming, T. J., Stimuli-responsive polypeptide vesicles by conformation-specific assembly. *Nat. Mater.* **2004,** *3* (4), 244-248.

93. Napoli, A.; Boerakker, M. J.; Tirelli, N.; Nolte, R. J. M.; Sommerdijk, N.; Hubbell, J. A., Glucose-oxidase based self-destructing polymeric vesicles. *Langmuir* **2004,** *20* (9), 3487-3491.

94. Vasdekis, A. E.; Scott, E. A.; O'Neil, C. P.; Psaltis, D.; Hubbell, J. A., Precision Intracellular Delivery Based on Optofluidic Polymersome Rupture. *ACS Nano* **2012,** *6* (9), 7850-7857.

95. Broaders, K. E.; Grandhe, S.; Fréchet, J. M. J., A Biocompatible Oxidation-Triggered Carrier Polymer with Potential in Therapeutics. *J. Am. Chem. Soc.* **2011,** *133* (4), 756-758.

96. Deng, Z.; Qian, Y.; Yu, Y.; Liu, G.; Hu, J.; Zhang, G.; Liu, S., Engineering Intracellular Delivery Nanocarriers and Nanoreactors from Oxidation-Responsive Polymersomes via

Synchronized Bilayer Cross-Linking and Permeabilizing Inside Live Cells. *J. Am. Chem. Soc.* **2016,** *138* (33), 10452-10466.

97. Deming, T. J., Synthesis of Side-Chain Modified Polypeptides. *Chem. Rev.* **2016,** *116* (3), 786-808.

98. Kramer, J. R.; Deming, T. J., Glycopolypeptides with a Redox-Triggered Helix-to-Coil Transition. *J. Am. Chem. Soc.* **2012,** *134* (9), 4112-4115.

99. Fu, X.; Ma, Y.; Shen, Y.; Fu, W.; Li, Z., Oxidation-responsive OEGylated poly-L-cysteine and solution properties studies. *Biomacromolecules* **2014,** *15* (3), 1055-1061.

100. Kramer, J. R.; Deming, T. J., Multimodal switching of conformation and solubility in homocysteine derived polypeptides. *J. Am. Chem. Soc.* **2014,** *136* (15), 5547-5550.

101. Kramer, J. R.; Rodriguez, A. R.; Choe, U.-J.; Kamei, D. T.; Deming, T. J., Glycopolypeptide conformations in bioactive block copolymer assemblies influence their nanoscale morphology. *Soft matter* **2013,** *9* (12), 3389-3395.

102. Yu, J.; Qian, C.; Zhang, Y.; Cui, Z.; Zhu, Y.; Shen, Q.; Ligler, F. S.; Buse, J. B.; Gu, Z., Hypoxia and H2O2 Dual-Sensitive Vesicles for Enhanced Glucose-Responsive Insulin Delivery. *Nano Lett.* **2017,** *17* (2), 733-739.

103. Hu, X.; Yu, J.; Qian, C.; Lu, Y.; Kahkoska, A. R.; Xie, Z.; Jing, X.; Buse, J. B.; Gu, Z., H2O2-Responsive Vesicles Integrated with Transcutaneous Patches for Glucose-Mediated Insulin Delivery. *ACS Nano* **2017,** *11* (1), 613-620.

104. Kramer, J. R.; Deming, T. J., Preparation of Multifunctional and Multireactive Polypeptides via Methionine Alkylation. *Biomacromolecules* **2012,** *13* (6), 1719-1723.

105. Yamada, S.; Ikkyu, K.; Iso, K.; Goto, M.; Endo, T., Facile synthesis of polymethionine oxides through polycondensation of activated urethane derivative of alpha-amino acid and their application to antifouling polymer against proteins and cells. *Polym. Chem.* **2015,** *6* (10), 1838-1845.

106. Rodriguez, A. R.; Kramer, J. R.; Deming, T. J., Enzyme-Triggered Cargo Release from Methionine Sulfoxide Containing Copolypeptide Vesicles. *Biomacromolecules* **2013,** *14* (10), 3610-3614.

107. Rodriguez, A. R.; Choe, U.-J.; Kamei, D. T.; Deming, T. J., Blending of Diblock and Triblock Copolypeptide Amphiphiles Yields Cell Penetrating Vesicles with Low Toxicity. *Macromol. Biosci.* **2015,** *15* (1), 90-97.

108. Gharakhanian, E. G.; Deming, T. J., Versatile Synthesis of Stable, Functional Polypeptides via Reaction with Epoxides. *Biomacromolecules* **2015,** *16* (6), 1802-1806.

109. Deming, T. J., Functional Modification of Thioether Groups in Peptides, Polypeptides, and Proteins. *Bioconjugate Chem.* **2017,** *28* (3), 691-700.

110. Jana, S.; Biswas, Y.; Mandal, T. K., Methionine-based cationic polypeptide/polypeptide block copolymer with triple-stimuli responsiveness: DNA polyplexation and phototriggered release. *Polym. Chem.* **2018,** *9* (14), 1869-1884.

111. Rodriguez, A. R.; Choe, U.-J.; Kamei, D. T.; Deming, T. J., Use of Methionine Alkylation to Prepare Cationic and Zwitterionic Block Copolypeptide Vesicles. *Isr. J. Chem.* **2016,** *56* (8), 607-613.

112. Kramer, J. R.; Schmidt, N. W.; Mayle, K. M.; Kamei, D. T.; Wong, G. C. L.; Deming, T. J., Reinventing Cell Penetrating Peptides Using Glycosylated Methionine Sulfonium Ion Sequences. *ACS Central Sci.* **2015,** *1* (2), 83-88.

113. Deming, T. J., Synthetic polypeptides for biomedical applications. *Prog. Polym. Sci.* **2007,** *32* (8-9), 858-875.

114. Holowka, E. P.; Pochan, D. J.; Deming, T. J., Charged polypeptide vesicles with controllable diameter. *J. Am. Chem. Soc.* **2005,** *127* (35), 12423-12428.

115. P., H. E.; J., D. T., Synthesis and Crosslinking of L-DOPA Containing Polypeptide Vesicles. *Macromol. Biosci.* **2010,** *10* (5), 496-502.

116. Yaroslavov, A. A.; Zaborova, O. V.; Sybachin, A. V.; Kalashnikova, I. V.; Kesselman, E.; Schmidt, J.; Talmon, Y.; Rodriguez, A. R.; Deming, T. J., Biodegradable containers composed of anionic liposomes and cationic polypeptide vesicles. *RSC Adv.* **2015,** *5* (119), 98687-98691.

117. Rodr ́guez-Hern ́andez, J.; Lecommandoux, S., Reversible Inside−Out Micellization of pH-responsive and Water-Soluble Vesicles Based on Polypeptide Diblock Copolymers. *J. Am. Chem. Soc.* **2005,** *127* (7), 2026-2027.

118. Koide, A.; Kishimura, A.; Osada, K.; Jang, W. D.; Yamasaki, Y.; Kataoka, K., Semipermeable polymer vesicle (PICsome) self-assembled in aqueous medium from a pair of oppositely charged block copolymers: Physiologically stable micro-/nanocontainers of water-soluble macromolecules. *J. Am. Chem. Soc.* **2006,** *128* (18), 5988-5989.

119. Kishimura, A.; Liamsuwan, S.; Matsuda, H.; Dong, W.-F.; Osada, K.; Yamasaki, Y.; Kataoka, K., pH-dependent permeability change and reversible structural transition of PEGylated polyion complex vesicles (PICsomes) in aqueous media. *Soft matter* **2009,** *5* (3), 529-532.

120. Song, Z.; Han, Z.; Lv, S.; Chen, C.; Chen, L.; Yin, L.; Cheng, J., Synthetic polypeptides: from polymer design to supramolecular assembly and biomedical application. *Chem. Soc. Rev.* **2017,** *46* (21), 6570-6599.

121. Bonduelle, C., Secondary structures of synthetic polypeptide polymers. *Polym. Chem.* **2018,** *9* (13), 1517-1529.

122. Chan, B. A.; Xuan, S.; Li, A.; Simpson, J. M.; Sternhagen, G. L.; Yu, T.; Darvish, O. A.; Jiang, N.; Zhang, D., Polypeptoid polymers: Synthesis, characterization, and properties. *Biopolymers* **2018,** *109* (1), e23070.

123. Secker, C.; Brosnan, S. M.; Luxenhofer, R.; Schlaad, H., Poly(alpha-Peptoid)s Revisited: Synthesis, Properties, and Use as Biomaterial. *Macromol. Biosci.* **2015,** *15* (7), 881-891.

124. Fetsch, C.; Grossmann, A.; Holz, L.; Nawroth, J. F.; Luxenhofer, R., Polypeptoids from N-Substituted Glycine N-Carboxyanhydrides: Hydrophilic, Hydrophobic, and Amphiphilic Polymers with Poisson Distribution. *Macromolecules* **2011,** *44* (17), 6746-6758.

125. Lee, C.-U.; Li, A.; Ghale, K.; Zhang, D., Crystallization and Melting Behaviors of Cyclic and Linear Polypeptoids with Alkyl Side Chains. *Macromolecules* **2013,** *46* (20), 8213-8223.

126. Fetsch, C.; Luxenhofer, R., Thermal Properties of Aliphatic Polypeptoids. *Polymers* **2013,** *5* (1), 112-127.

127. Miller, S. M.; Simon, R. J.; Ng, S.; Zuckermann, R. N.; Kerr, J. M.; Moos, W. H., Proteolytic studies of homologous peptide and N-substituted glycine peptoid oligomers. *Bioorg. Med. Chem. Lett.* **1994,** *4* (22), 2657-2662.

128. Ulbricht, J.; Jordan, R.; Luxenhofer, R., On the biodegradability of polyethylene glycol, polypeptoids and poly(2-oxazoline)s. *Biomaterials* **2014,** *35* (17), 4848-4861.

129. Sun, J.; Zuckermann, R. N., Peptoid Polymers: A Highly Designable Bioinspired Material. *ACS Nano* **2013,** *7* (6), 4715-4732.

130. Lee, C.-U.; Smart, T. P.; Guo, L.; Epps, T. H., III; Zhang, D., Synthesis and Characterization of Amphiphilic Cyclic Diblock Copolypeptoids from N-Heterocyclic Carbene-Mediated Zwitterionic Polymerization of N-Substituted N-Carboxyanhydride. *Macromolecules* **2011,** *44* (24), 9574-9585.

131. Fetsch, C.; Flecks, S.; Gieseler, D.; Marschelke, C.; Ulbricht, J.; van Pee, K. H.; Luxenhofer, R., Self-Assembly of Amphiphilic Block Copolypeptoids with C-2-C-5 Side Chains in Aqueous Solution. *Macromol. Chem. Phys.* **2015,** *216* (5), 547-560.

132. Zuckermann, R. N.; Kerr, J. M.; Kent, S. B. H.; Moos, W. H., Efficient method for the preparation of peptoids oligo(N-substituted glycines) by submonomer solid-phase synthesis. *J. Am. Chem. Soc.* **1992,** *114* (26), 10646-10647.

133. Simon, R. J.; Kania, R. S.; Zuckermann, R. N.; Huebner, V. D.; Jewell, D. A.; Banville, S.; Ng, S.; Wang, L.; Rosenberg, S.; Marlowe, C. K.; Spellmeyer, D. C.; Tan, R. Y.; Frankel, A. D.; Santi, D. V.; Cohen, F. E.; Bartlett, P. A., PEPTOIDS - A MODULAR APPROACH TO DRUG DISCOVERY. *Proc. Natl. Acad. Sci. USA* **1992,** *89* (20), 9367-9371.

134. Zuckermann, R. N., Peptoid Origins. *Biopolymers* **2011,** *96* (5), 545-555.

135. Gangloff, N.; Fetsch, C.; Luxenhofer, R., Polypeptoids by Living Ring-Opening Polymerization of N-Substituted N-Carboxyanhydrides from Solid Supports. *Macromol. Rapid Commun.* **2013,** *34* (12), 997-1001.

136. Schneider, M.; Fetsch, C.; Amin, I.; Jordan, R.; Luxenhofer, R., Polypeptoid Brushes by Surface-Initiated Polymerization of N-Substituted Glycine N-Carboxyanhydrides. *Langmuir* **2013,** *29* (23), 6983-6988.

137. Kidchob, T.; Kimura, S.; Imanishi, Y., Thermoresponsive release from poly(Glu(OMe))-block-poly(Sar) microcapsules with surface-grafting of poly(N-isopropylacrylamide). *J. Control. Release* **1998,** *50* (1-3), 205-214.

138. Kidchob, T.; Kimura, S.; Imanishi, Y., Amphiphilic poly(Ala)-b-poly(Sar) microspheres loaded with hydrophobic drug. *J. Control. Release* **1998,** *51* (2-3), 241-248.

139. Makino, A.; Yamahara, R.; Ozeki, E.; Kimura, S., Preparation of novel polymer assemblies, "lactosome", composed of Poly(L-lactic acid) and poly(sarcosine). *Chem. Lett.* **2007,** *36* (10), 1220-1221.

140. Birke, A.; Huesmann, D.; Kelsch, A.; Weilbacher, M.; Xie, J.; Bros, M.; Bopp, T.; Becker, C.; Landfester, K.; Barz, M., Polypeptoid-block-polypeptide Copolymers: Synthesis, Characterization, and Application of Amphiphilic Block Copolypept(o)ides in Drug Formulations and Miniemulsion Techniques. *Biomacromolecules* **2014,** *15* (2), 548-557.

141. Heller, P.; Birke, A.; Huesmann, D.; Weber, B.; Fischer, K.; Reske-Kunz, A.; Bros, M.; Barz, M., Introducing PeptoPlexes: Polylysine-block-Polysarcosine Based Polyplexes for Transfection of HEK 293T Cells. *Macromol. Biosci.* **2014,** *14* (10), 1380-1395.

142. Holm, R.; Weber, B.; Heller, P.; Klinker, K.; Westmeier, D.; Docter, D.; Stauber, R. H.; Barz, M., Synthesis and Characterization of Stimuli-Responsive Star-Like Polypept(o) ides: Introducing Biodegradable PeptoStars. *Macromol. Biosci.* **2017,** *17* (6), 1600514.

143. Weber, B.; Kappel, C.; Scherer, M.; Helm, M.; Bros, M.; Grabbe, S.; Barz, M., PeptoSomes for Vaccination: Combining Antigen and Adjuvant in Polypept(o)ide-Based Polymersomes. *Macromol. Biosci.* **2017,** *17* (10), 1700061.

144. Cui, S.; Wang, X.; Li, Z.; Zhang, Q.; Wu, W.; Liu, J.; Wu, H.; Chen, C.; Guo, K., One-Pot Glovebox-Free Synthesis, Characterization, and Self-Assembly of Novel Amphiphilic Poly(Sarcosine-b-Caprolactone) Diblock Copolymers. *Macromol. Rapid Commun.* **2014,** *35* (22), 1954-1959.

145. Wu, W.; Cui, S.; Li, Z.; Liu, J.; Wang, H.; Wang, X.; Zhang, Q.; Wu, H.; Guo, K., Mild Bronsted acid initiated controlled polymerizations of 2-oxazoline towards one-pot synthesis of novel double-hydrophilic poly(2-ethyl-2-oxazoline)-block-poly(sarcosine). *Polym. Chem.* **2015,** *6* (15), 2970-2976.

146. Chen, S.; Liu, Y.; Li, Z.; Wang, X.; Dong, H.; Sun, H.; Yang, K.; Gebru, H.; Guo, K., H-bonding binary organocatalysis promoted amine-initiated ring-opening polymerizations of lactide from polysarcosine to diblock copolymers. *Eur. Polym. J.* **2017,** *97*, 389-396.

147. Cui, S.; Pan, X.; Gebru, H.; Wang, X.; Liu, J.; Liu, J.; Li, Z.; Guo, K., Amphiphilic star-shaped poly(sarcosine)-block-poly(epsilon-caprolactone) diblock copolymers: one-pot synthesis, characterization, and solution properties. *J. Mater. Chem. B* **2017,** *5* (4), 679-690.

148. Pan, X.; Liu, Y.; Li, Z.; Cui, S.; Gebru, H.; Xu, J.; Xu, S.; Liu, J.; Guo, K., Amphiphilic Polyoxazoline-block-Polypeptoid Copolymers by Sequential One-Pot Ring-Opening Polymerizations. *Macromol. Chem. Phys.* **2017,** *218* (6), 1600483.

149. Secker, C.; Voelkel, A.; Tiersch, B.; Koetz, J.; Schlaad, H., Thermo-Induced Aggregation and Crystallization of Block Copolypeptoids in Water. *Macromolecules* **2016,** *49* (3), 979-985.

150. Bogomolova, A.; Secker, C.; Koetz, J.; Schlaad, H., Thermo-induced multistep assembly of double-hydrophilic block copolypeptoids in water. *Colloid. Polym. Sci.* **2017,** *295* (8), 1305-1312.

151. Guo, L.; Zhang, D., Cyclic Poly(alpha-peptoid)s and Their Block Copolymers from N-Heterocyclic Carbene-Mediated Ring-Opening Polymerizations of N-Substituted N-Carboxylanhydrides. *J. Am. Chem. Soc.* **2009,** *131* (50), 18072-18074.

152. Zhang, D.; Lahasky, S. H.; Guo, L.; Lee, C.-U.; Lavan, M., Polypeptoid Materials: Current Status and Future Perspectives. *Macromolecules* **2012,** *45* (15), 5833-5841.

153. Guo, L.; Lahasky, S. H.; Ghale, K.; Zhang, D., N-Heterocyclic Carbene-Mediated Zwitterionic Polymerization of N-Substituted N-Carboxyanhydrides toward Poly(alpha-peptoid)s: Kinetic, Mechanism, and Architectural Control. *J. Am. Chem. Soc.* **2012,** *134* (22), 9163-9171.

154. Kramer, J. R.; Deming, T. J., General Method for Purification of alpha-Amino acid-N-carboxyanhydrides Using Flash Chromatography. *Biomacromolecules* **2010,** *11* (12), 3668-3672.

155. Dewey, R. S.; Schoenewaldt, E. F.; Joshua, H.; Paleveda, W. J.; Schwam, H.; Barkemeyer, H.; Arison, B. H.; Veber, D. F.; Denkewalter, R. G.; Hirschmann, R., Synthesis of peptides in aqueous medium. V. Preparation and use of 2,5-thiazolidinediones (NTA's). Use of the 13C-H nuclear magnetic resonance signal as internal standard for quantitative studies. *J. Am. Chem. Soc.* **1968,** *90* (12), 3254-3255.

156. Kricheldorf, H. R.; Sell, M.; Schwarz, G., Primary amine-initiated polymerizations of alpha-amino acid N-thiocarbonic acid anhydrosulfide. *J. Macromol. Sci., Pure Appl. Chem.* **2008,** *45* (6), 425-430.

157. Tao, X.; Deng, Y.; Shen, Z.; Ling, J., Controlled Polymerization of N-Substituted Glycine N-Thiocarboxyanhydrides Initiated by Rare Earth Borohydrides toward Hydrophilic and Hydrophobic Polypeptoids. *Macromolecules* **2014,** *47* (18), 6173-6180.

158. Tao, X.; Zheng, B.; Kricheldorf, H. R.; Ling, J., Are N-Substituted Glycine N-Thiocarboxyanhydride Monomers Really Hard to Polymerize? *J. Polym. Sci., Part A: Polym. Chem.* **2017,** *55* (3), 404-410.

159. Tao, X.; Zheng, B.; Bai, T.; Zhu, B.; Ling, J., Hydroxyl Group Tolerated Polymerization of N-Substituted Glycine N-Thiocarboxyanhydride Mediated by Aminoalcohols: A Simple Way to alpha-Hydroxyl-omega-aminotelechelic Polypeptoids. *Macromolecules* **2017,** *50* (8), 3066-3077.

160. Tao, X.; Zheng, B.; Bai, T.; Li, M.-H.; Ling, J., Polymerization of N-Substituted Glycine N-Thiocarboxyanhydride through Regioselective Initiation of Cysteamine: A Direct Way toward Thiol-Capped Polypeptoids. *Macromolecules* **2018**.

161. Tao, X.; Deng, C.; Ling, J., PEG-amine-initiated polymerization of sarcosine N-thiocarboxyanhydrides toward novel double-hydrophilic PEG-b-polysarcosine diblock copolymers. *Macromol. Rapid Commun.* **2014,** *35* (9), 875-881.

162. Ostuni, E.; Chapman, R. G.; Holmlin, R. E.; Takayama, S.; Whitesides, G. M., A survey of structure-property relationships of surfaces that resist the adsorption of protein. *Langmuir* **2001,** *17* (18), 5605-5620.

163. Birke, A.; Ling, J.; Barz, M., Polysarcosine-containing copolymers: Synthesis, characterization, self-assembly, and applications. *Prog. Polym. Sci.* **2018,** *81*, 163-208.

164. Kidchob, T.; Kimura, S.; Imanishi, Y., Preparation, structure and release profile of polypeptide microcapsules. *J. Control. Release* **1996,** *40* (3), 285-291.

165. T., K.; S., K.; Y., I., pH-responsive release from polypeptide microcapsules. *J. Appl. Polym. Sci.* **1997,** *63* (4), 453-458.

166. Shunsaku, K.; Tongjit, K.; Yukio, I., Controlled release from amphiphilic polymer aggregates. *Polym. Adv. Technol.* **2001,** *12* (1‐2), 85-95.

167. Tatsuya, K.; Yoshiki, H.; Akira, M.; Junji, S.; Shunsaku, K., Nanotube and Three-Way Nanotube Formation with Nonionic Amphiphilic Block Peptides. *Macromol. Biosci.* **2008,** *8* (11), 1026-1033.

168. Uesaka, A.; Ueda, M.; Makino, A.; Imai, T.; Sugiyama, J.; Kimura, S., Self-Assemblies of Triskelion A2B-Type Amphiphilic Polypeptide Showing pH-Responsive Morphology Transformation. *Langmuir* **2012,** *28* (14), 6006-6012.

169. Uesaka, A.; Ueda, M.; Makino, A.; Imai, T.; Sugiyama, J.; Kimura, S., Morphology Control between Twisted Ribbon, Helical Ribbon, and Nanotube Self-Assemblies with His-Containing Helical Peptides in Response to pH Change. *Langmuir* **2014,** *30* (4), 1022-1028.

170. Ueda, M.; Makino, A.; Imai, T.; Sugiyama, J.; Kimura, S., Transformation of peptide nanotubes into a vesicle via fusion driven by stereo-complex formation. *Chem. Commun.* **2011,** *47* (11), 3204-3206.

171. Ueda, M.; Makino, A.; Imai, T.; Sugiyama, J.; Kimura, S., Temperature-Triggered Fusion of Vesicles Composed of Right-Handed and Left-Handed Amphiphilic Helical Peptides. *Langmuir* **2011,** *27* (8), 4300-4304.

172. Ueda, M.; Makino, A.; Imai, T.; Sugiyama, J.; Kimura, S., Tubulation on peptide vesicles by phase-separation of a binary mixture of amphiphilic right-handed and left-handed helical peptides. *Soft matter* **2011,** *7* (9), 4143-4146.

173. Uesaka, A.; Ueda, M.; Imai, T.; Sugiyama, J.; Kimura, S., Facile and Precise Formation of Unsymmetric Vesicles Using the Helix Dipole, Stereocomplex, and Steric Effects of Peptides. *Langmuir* **2014,** *30* (15), 4273-4279.

174. Kim, C. J.; Ueda, M.; Imai, T.; Sugiyama, J.; Kimura, S., Tuning the Viscoelasticity of Peptide Vesicles by Adjusting Hydrophobic Helical Blocks Comprising Amphiphilic Polypeptides. *Langmuir* **2017,** *33* (22), 5423-5429.

175. Ueda, M.; Makino, A.; Imai, T.; Sugiyama, J.; Kimura, S., Versatile peptide rafts for conjugate morphologies by self-assembling amphiphilic helical peptides. *Polym. J.* **2013,** *45*, 509-515.

176. Regina, H.; Kristina, K.; Benjamin, W.; Matthias, B., Synthesis of Amphiphilic Block Copolypept(o)ides by Bifunctional Initiators: Making PeptoMicelles Redox Sensitive. *Macromol. Rapid Commun.* **2015,** *36* (23), 2083-2091.

177. Makino, A.; Hara, E.; Hara, I.; Ozeki, E.; Kimura, S., Size Control of Core–Shell-type Polymeric Micelle with a Nanometer Precision. *Langmuir* **2014,** *30* (2), 669-674.

178. Hara, E.; Ueda, M.; Makino, A.; Hara, I.; Ozeki, E.; Kimura, S., Factors Influencing in Vivo Disposition of Polymeric Micelles on Multiple Administrations. *ACS Med. Chem. Lett.* **2014,** *5* (8), 873-877.

179. Makino, A.; Hara, E.; Hara, I.; Yamahara, R.; Kurihara, K.; Ozeki, E.; Yamamoto, F.; Kimura, S., Control of in vivo blood clearance time of polymeric micelle by stereochemistry of amphiphilic polydepsipeptides. *J. Control. Release* **2012,** *161* (3), 821-825.

180. Brosnan, S. M.; Schlaad, H.; Antonietti, M., Aqueous Self-Assembly of Purely Hydrophilic Block Copolymers into Giant Vesicles. *Angew. Chem. Int. Ed. Engl.* **2015,** *54* (33), 9715-9718.

181. Murnen, H. K.; Rosales, A. M.; Jaworski, J. N.; Segalman, R. A.; Zuckermann, R. N., Hierarchical Self-Assembly of a Biomimetic Diblock Copolypeptoid into Homochiral Superhelices. *J. Am. Chem. Soc.* **2010,** *132* (45), 16112-16119.

182. Sun, J.; Jiang, X.; Lund, R.; Downing, K. H.; Balsara, N. P.; Zuckermann, R. N., Self-assembly of crystalline nanotubes from monodisperse amphiphilic diblock copolypeptoid tiles. *Proc. Natl. Acad. Sci. USA* **2016,** *113* (15), 3954-3959.

183. Gaitzsch, J.; Karu, K.; Battaglia, G., Peptoidosomes as nanoparticles from amphiphilic block alpha-peptoids using solid-phase-synthesis. *Eur. Polym. J.* **2015,** *73*, 447-454.

184. Fetsch, C.; Gaitzsch, J.; Messager, L.; Battaglia, G.; Luxenhofer, R., Self-Assembly of Amphiphilic Block Copolypeptoids - Micelles, Worms and Polymersomes. *Sci. Rep.* **2016,** *6*, 33491.

Chapter 2. Synthesis of Polypeptoid-Containing Amphiphilic Block Copolymers

2.1 Introduction

To develop polypeptoid materials for further applications, their syntheses are the first step. The ring-opening polymerization (ROP) of amino acid NCA is the most widely-used method for polypeptide and polypeptoid syntheses.[1, 2] However, the application of NCA is seriously limited because of their high sensibility to moisture and heat and their instability upon storage.[3] In contrast, amino acid NTA, the thio-analog of amino acid NCA, is much more robust. But its relatively low reactivity restricted for a long time its use to stepwise synthesis.[4, 5] Kricheldorf reported in 2008 the ROP of Leu-NTA, Phe-NTA and Sar-NTA initiated by primary amine and prepared poly(amino acids) with well-defined structures.[6] Based on the interfacial ROP of NTAs in hexanes or heptane suspension, Zhang and coworkers achieved the synthesis of polypeptides with controlled MWs and narrow MW distributions.[7] The group of Ling made systematic researches on the solution ROP of NTAs, and through the initiation of primary amines or rare earth catalysis, in optimized conditions (at 60 ℃, in the solution of THF or acetonitrile), the controlled polymerizations of Sar-NTA, NBG-NTA, NEG-NTA and DOPA-NTA are successfully realized.[8-13]

To obtain new polypeptoid-containing amphiphilic block copolymers, we employed the ROP of NTAs in this chapter, ether by the initiation of macromolecular initiators, or sequential feeding of different NTA monomers. Three kinds of polypeptoid-containing amphiphilic block copolymers have been elaborated. The first one contains PSar and PCL blocks; the second one contains PEG and PMeSPG blocks; the third one contains PSar and PMeSPG blocks.

For the block copolymers composed of PSar and PCL blocks, Mitsunobu reaction is first applied to synthesize oxyamino-ended PCLs, which act as the

macromolecular initiators for ROP of Sar-NTA to produce diblock copolymers PCL-*b*-PSar and triblock copolymers PSar-*b*-PCL-*b*-PSar. For the block copolymers contained PMeSPG, a thioether-bearing *N*-substituted glycine, *N*-3-(methylthio)propyl glycine (MeSPG) is first synthesized from methionine through a "decarboxylation−*N*-carboxymethylation" procedure followed by a cylization to monomer MeSPG-NTA. Then, amphiphilic block copolymers PEG-*b*-PMeSPG is obtained from the ROP of MeSPG-NTA initiated by amino-ended PEG (PEG-NH_2), while amphiphilic block copolymers PMeSPG-*b*-PSar is prepared by the ROP initiated by benzylamine with the sequential monomer feeding of MeSPG-NTA and Sar-NTA.

2.2 Experimental section

2.2.1 Materials

Sarcosine (98%, Sigma Aldrich), carbon disulfide (99%, Alfa Aesar), sodium chloroacetate (98%, Alfa Aesar), phosphorus tribromide (99%, Sigma Aldrich), diphenyl phosphate (DPP, 99%, Acros Organics), *N*-hydroxyphthalimide (NHP, 99%, Adamas Reagent), triphenyl phosphine (PPh_3, 99%, Adamas Reagent), diisopropyl azodicarboxylate (DIAD, 98%, J&K Chemical), D,L-Methionine (98%, Sigma Aldrich), PEG-NH_2 (MW = 2000 Da, Polymer Source), sodium hydroxide (NaOH, 99%, VWR), magnesium sulfate ($MgSO_4$, dry, 98%, VWR), glyoxylic acid (50 wt% aqueous solution, Alfa Aesar), R-(−)-carvone (98%, Alfa Aesar), 1-octanol (99%, Acros), methanol (99%, VWR), diethyl ether (99%, VWR), DCM (99%, VWR), chloroform (99%, VWR), hydrochloric acid (HCl, 37 wt% aqueous solution, VWR), ethyl acetate (99%, VWR), petroleum ether (boiling point 40−60 ℃, VWR) and hydrazine (Sinopharm Chemical Reagent) were used as received. THF and toluene were refluxed before use over sodium/benzophenone ketyl and potassium/benzophenone ketyl, respectively. CL, benzyl alcohol (BO), 1,4-butanediol (BDO), benzylamine (BA) and acetonitrile (CH_3CN) were stirred over CaH_2 (95%, Sigma Aldrich) and distilled.

2.2.2 Synthesis of Sar-NTA

Typically *S*-ethoxythiocarbonylmercaptoacetic acid (XAA) was firstly prepared through the reaction of NaOH, ethanol, carbon disulfide and the following addition of sodium chloroacetate (molar ratio = 1:1.5:1.5:1), and then extracted by chloroform after acidification. Equivalent amounts of sarcosine and XAA were dissolved in basic aqueous solution to obtain *N*-ethoxythiocarbonylsarcosine (Sar-XAA). PBr_3 (1.2 times of Sar-XAA) was utilized to catalyze the cyclization of Sar-XAA, and eventually Sar-NTA was obtained after column chromatographic purification (ethyl acetate : petroleum ether = 1 : 3). ^{1}H-NMR ($CDCl_3$/TMS) δ: 3.11 ppm (s, 3H), 4.21 ppm (s, 2H).

2.2.3 Synthesis of oxyamino-ended PCLs

All the polymerizations were performed using Schlenk technique, and all the polymerization tubes were predried and purged with argon. A typical synthesis procedure is described as follows. CL (15.0 mL, 140 mmol), DPP (0.528 g, 2.11 mmol) and BO (0.31 mL, 2.84 mmol) were dissolved in toluene (39 mL) with stirring for 7 h at 25 °C. The polymer was isolated by precipitation from cold methanol and dried under vacuum (15.347 g, 91.0%). The obtained hydroxyl-ended PCL (PCL-OH) was then dissolved in DCM with NHP (0.548 g, 4.18 mmol) and PPh_3 (0.904 g, 4.18 mmol). DIAD (0.6 mL, 3.88 mmol) was then added to the mixture cooled with ice-water bath. The reaction lasted for 18 h with stirring and afterwards precipitated by cold methanol. The reaction was repeated twice to fulfill the conversion, and thus PCL-O-NHP was obtained (14.721 g). Hydrazine (0.11 mL, 3.41 mmol) was added dropwise to the DCM solution of PCL-O-NHP and reacted for 30 min. Some wax-like precipitates appeared in the solution and were removed by filtration. The purified polymer was isolated by dropping the filtrate in cold methanol. After being dried in vacuum, the oxyamino-ended PCL (PCL-ONH_2) was obtained (10.654 g, 69.2%). When the synthesis started with BDO as the initiator, the double oxyamino-ended PCL (H_2NO-PCL-ONH_2) could be obtained.

2.2.4 Synthesis of PCL/PSar block copolymers

The ROP of Sar-NTA initiated by PCL-ONH_2 and H_2NO-PCL-ONH_2 were conducted with Schlenk line. As a typical synthetic procedure, H_2NO-PCL_{40}-ONH_2 (0.645 g, 0.138 mmol) was firstly added to a Schlenk tube, which was connected to Schlenk line. The PCL was dried at 70 ℃ under vacuum for 4 h, followed by the refill of argon. Anhydrous THF (8.8 mL) was added to dissolve the PCL initiator, then Sar-NTA (0.429 g, 3.27 mmol) was added with stirring at 60 ℃. The polymerization was quenched after 24 h and precipitated from diethyl ether. After being dried in vacuum, the triblock copolymer PSar-*b*-PCL-*b*-PSar was obtained (0.466 g, 54.8%).

2.2.5 Synthesis of MeSPG-NTA

MeSPG hydrochloride was firstly synthesized in basis of methionine. As a typical reaction, methionine (20.1 g, 0.134 mol) was dissolved in 100 mL 1-octanol, followed by the addition of R-(−)-carvone (40.3 g, 0.268 mol). The suspension was stirred in reflux at 195 ℃, and turned into homogeneous solution after 30 min. 100 mL 2 M HCl was then added to the system and keep reflux for 10 min. Methionine was decarboxylated to 3-(methylthio)propyl amine (MeSPA) at this acidic high-temperature situation.[14] After the solution was cooled down, glyoxylic acid aqueous solution (50 wt%, 39.7 g, 0.268 mol) was added with 50 mL 2 M HCl and the system was refluxed again at 120 ℃ for 12 h. During this step MeSPA was carboxymethylated to *N*-substituted glycine.[15] The solvent was removed by evaporation and solid was precipitated from the addition of acetone. After twice of crystallization by acetone, MeSPG hydrochloride was obtained (20.7 g, yield = 77.3%). MeSPG-NTA was synthesized by the same procedure of Sar-NTA from MeSPG hydrochloride and XAA. The crude product was purified by column chromatography (ethyl acetate : petroleum ether = 1 : 5). Yellow oil was obtained (10.3 g, yield 37.4%) and stored under an argon atmosphere. ^{1}H-NMR ($CDCl_3$/TMS) δ 1.94 ppm (m, 2H), 2.12 ppm (s, 3H), 2.55 ppm (t, 2H), 3.64 ppm (t, 2H), 4.22 ppm (s, 2H). ^{13}C-NMR ($CDCl_3$/TMS) δ 15.63 ppm (-

$CH_2CH_2CH_2SCH_3$), 26.74 ppm (-$CH_2CH_2CH_2SCH_3$), 31.20 ppm (-$CH_2CH_2CH_2SCH_3$), 43.35 ppm (-$CH_2CH_2CH_2SCH_3$), 60.16 ppm (-NCH_2CO-), 165.02 ppm (-NCOSCO-), 193.77 ppm (-NCOSCO-).

2.2.6 Polymerization of MeSPG-NTA

All the ROP reactions of MeSPG-NTA were conducted with Schlenk line. In a typical reaction, MeSPG-NTA (0.305 g, 1.48 mmol) was dissolved in 3.0 mL of dry THF, followed by 0.26 mL THF solution of BA (0.0768 M). The tube was sealed and placed in a 60 ℃ oil bath for 48 h. The polymer was isolated by precipitation from diethyl ether and dried in a vacuum (0.186 g, 86.6%).

2.2.7 Synthesis of PEG-*b*-PMeSPG

As a typical synthetic procedure, PEG-NH_2 (0.161 g, 0.080 mmol) was firstly added to a Schlenk tube, which was connected to Schlenk line. The PEG was dried at 60 ℃ under vacuum for 4 h, followed by the refill of argon. Anhydrous THF (6.4 mL) was added to dissolve the PEG-NH_2, then MeSPG-NTA (0.645 g, 3.14 mmol) was added with stirring at 60 ℃. The polymerization was quenched after 48 h and precipitated from diethyl ether. After being dried in vacuum, the block copolymer PEG-*b*-PMeSPG was obtained (0.513 g, 83.2%).

2.2.8 Synthesis of PMeSPG-*b*-PSar

The syntheses of PMeSPG-*b*-PSar copolymers were conducted through the sequential feeding of MeSPG-NTA and Sar-NTA. As a typical block copolymerization, MeSPG-NTA (0.416 g, 2.03 mmol) was dissolved in 4.0 mL dry THF, followed by 0.38 mL THF solution of BA (0.1059 M). The tube was sealed and placed in a 60 ℃ oil bath. After 36 h, a small amount of solution was extracted from the reaction mixture for the analytical investigations of the first block. Then Sar-NTA (0.279 g, 2.13 mmol) was added to the system. The mixture was stirred for additional 24 h. The polymer was isolated by precipitation from diethyl ether and dried in vacuum (0.354 g, 95.3%).

2.2.9 Characterizations

MWs and polydispersity indices (*Đ*) were determined by gel-permeation chromatography (GPC) which was consisted of a Waters 1515 isocratic high performance liquid chromatograph pump, two columns of PL gel 5 μm MIXED-C and a refractive index (RI) detector. DMF containing 0.01 M LiBr (or 0.05 M) was used as the eluent with a flow rate of 1.0 mL/min at 60 ℃. Commercial monodispersed PS, PEG and poly(methyl methacrylate) (PMMA) were used as the calibration standards.

NMR spectra were recorded on a Bruker Avance DMX 500 or Bruker Avance DMX 400 spectrometer with deuterium oxide (D_2O), DMSO-d_6 or $CDCl_3$ as solvent.

Matrix-assisted laser desorption/ionization time-of-flight mass spectrometer (MALDI-ToF MS) was measured on a Bruker UltraFLEX MALDI-ToF mass spectrometer. The nitrogen laser wavelength was set at 337 nm with a pulse interval of 3 ns. The acceleration voltage was set at 20 kV in reflection mode. 2,5-dihydroxybenzoic acid (DHB) is used as the substrate.

2.3 Results and discussion

2.3.1 PCL-*b*-PSar and PSar-*b*-PCL-*b*-PSar

We employed a totally metal-free protocol to prepare the amphiphilic di- and triblock polyester/polypeptoid copolymers. The synthesis is conducted in a sequential approach, through a three-step procedure of "ROP of CL−end group transition−ROP of Sar-NTA" (Scheme 2.1). Firstly we synthesize PCLs with different MWs by ROP of CL with DPP as catalyst.[16] BO and BDO are chosen as the initiators respectively for PCLs with one (PCL-OH) or two terminal hydroxyl group(s) (HO-PCL-OH). The transformation from hydroxyl to oxyamino group is achieved based on Mitsunobu reaction.[17] Three PCL-ONH_2 and three NH_2O-PCL-ONH_2 are synthesized with controlled DPs, narrow MW distributions and high yields (Table 2.1, PCL1 to PCL6). ROP of Sar-NTA is then initiated by these PCL oxyamines on Schlenk line. Di- and

triblock copolymers, PSar-*b*-PCL and PSar-*b*-PCL-*b*-PSar, with different MWs and hydrophilic/hydrophobic ratios are obtained (see Table 2.1, CS1 to CS13). Figure 2.1 reveals the ^{1}H-NMR spectra of HO-PCL$_{40}$-OH, the intermediate NHP-O-PCL$_{40}$-O-NHP and the oxyamino-ended H_2NO-PCL$_{40}$-ONH_2, that is PCL5 in Table 2.1, and confirms the complete transition of the end groups. ^{1}H-NMR spectrum of CS10 (Figure 2.2) shows legible signals from both PCL and PSar blocks, while GPC traces of CS10 together with that of its initiator PCL5 (Figure 2.3) show clearly a MW increase from 9.0 kDa for PCL5 to 14.5 kDa for CS10 without distribution broadening (*Đ* from 1.25 to 1.24). These results indicate the successful polymerization of Sar-NTAs initiated by oxyamino-ended PCL5, generating CS10 with explicit block copolymer structure. In addition, the ABA triblock structure of PSar-*b*-PCL-*b*-PSar is reported for the first time, and its synthetic route through direct oxyamine-initiated ROP is much easier compared to PEG-*b*-PCL-*b*-PEG copolymers, which need additional coupling reactions between PCL and PEG.[18]

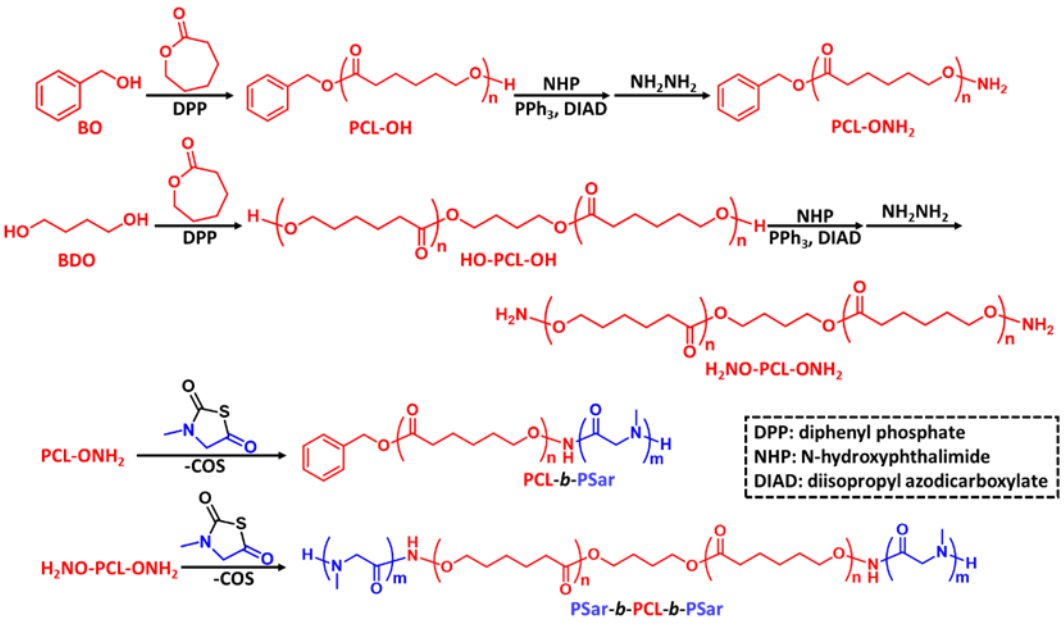

Scheme 2.1. Preparation of diblock and triblock copolymers PCL-*b*-PSar and PSar-*b*-PCL-*b*-PSar.

Table 2.1. Syntheses of oxyamino-ended PCL macro-initiators and block copolymers PCL-*b*-PSar and PSar-*b*-PCL-*b*-PSar.

Sample	Initiator	T (℃)	[M]/[I]	Composition [a]	$f_{PSar,wt}$ [a]	$M_{n\ NMR}$ (kDa) [a]	$M_{n\ GPC}$ (kDa) [b]	$Đ$ [b]	Yield (%)
PCL1	BO	50	20	PCL_{20}-ONH_2	-	2.3	3.9	1.12	92.5
PCL2	BO	50	35	PCL_{35}-ONH_2	-	4.1	6.4	1.12	69.2
PCL3	BO	50	70	PCL_{80}-ONH_2	-	9.2	14.1	1.36	74.3
PCL4	BDO	50	28	H_2NO-PCL_{28}-ONH_2	-	3.2	5.5	1.17	81.6
PCL5	BDO	50	35	H_2NO-PCL_{40}-ONH_2	-	4.7	9.0	1.25	65.4
PCL6	BDO	50	70	H_2NO-PCL_{70}-ONH_2	-	8.1	14.8	1.30	78.9
CS1	PCL1	60	23	PCL_{20}-*b*-$PSar_8$	20%	2.9	5.0	1.16	50.8
CS2	PCL1	60	19	PCL_{20}-*b*-$PSar_{24}$	43%	4.0	6.2	1.24	61.6
CS3	PCL1	60	38	PCL_{20}-*b*-$PSar_{48}$	60%	5.7	9.2	1.24	73.9
CS4	PCL2	60	30	PCL_{35}-*b*-$PSar_5$	10%	4.5	7.0	1.18	58.6
CS5	PCL3	60	70	PCL_{80}-*b*-$PSar_{70}$	35%	14.2	21.5	1.35	82.1
CS6	PCL4	60	11	$PSar_4$-*b*-PCL_{28}-*b*-$PSar_4$	15%	3.8	6.8	1.35	> 99
CS7	PCL4	60	21	$PSar_8$-*b*-PCL_{28}-*b*-$PSar_8$	25%	4.3	7.9	1.37	95.6
CS8	PCL4	60	20	$PSar_{13}$-*b*-PCL_{28}-*b*-$PSar_{13}$	36%	6.3	8.4	1.30	91.3
CS9	PCL4	60	48	$PSar_{22}$-*b*-PCL_{28}-*b*-$PSar_{22}$	48%	6.3	10.7	1.41	92.4
CS10	PCL5	60	22	$PSar_{16}$-*b*-PCL_{40}-*b*-$PSar_{16}$	34%	7.0	14.5	1.24	54.8
CS11	PCL6	60	38	$PSar_{10}$-*b*-PCL_{70}-*b*-$PSar_{10}$	14%	9.6	18.9	1.37	82.3
CS12	PCL6	60	62	$PSar_{19}$-*b*-PCL_{70}-*b*-$PSar_{19}$	26%	10.8	22.8	1.36	68.5
CS13	PCL6	60	48	$PSar_{23}$-*b*-PCL_{70}-*b*-$PSar_{23}$	29%	11.4	21.8	1.35	83.9

[a] Calculated from the integrals in ^{1}H-NMR spectra; [b] Determined by GPC in 0.05 M LiBr/DMF, with rate at 1 mL/min, PMMA as standard.

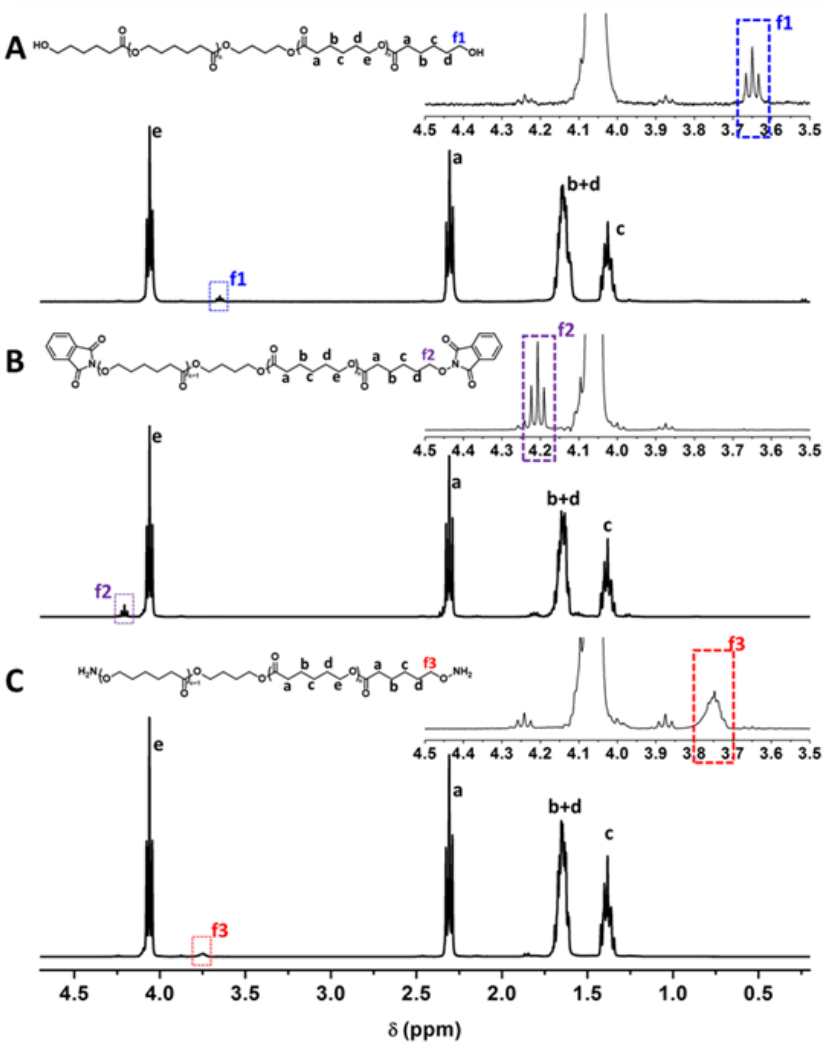

Figure 2.1. ^{1}H-NMR spectra of HO-PCL$_{40}$-OH, NHP-O-PCL$_{40}$-O-NHP and H_2NO-PCL$_{40}$-ONH_2 (PCL5) in $CDCl_3$.

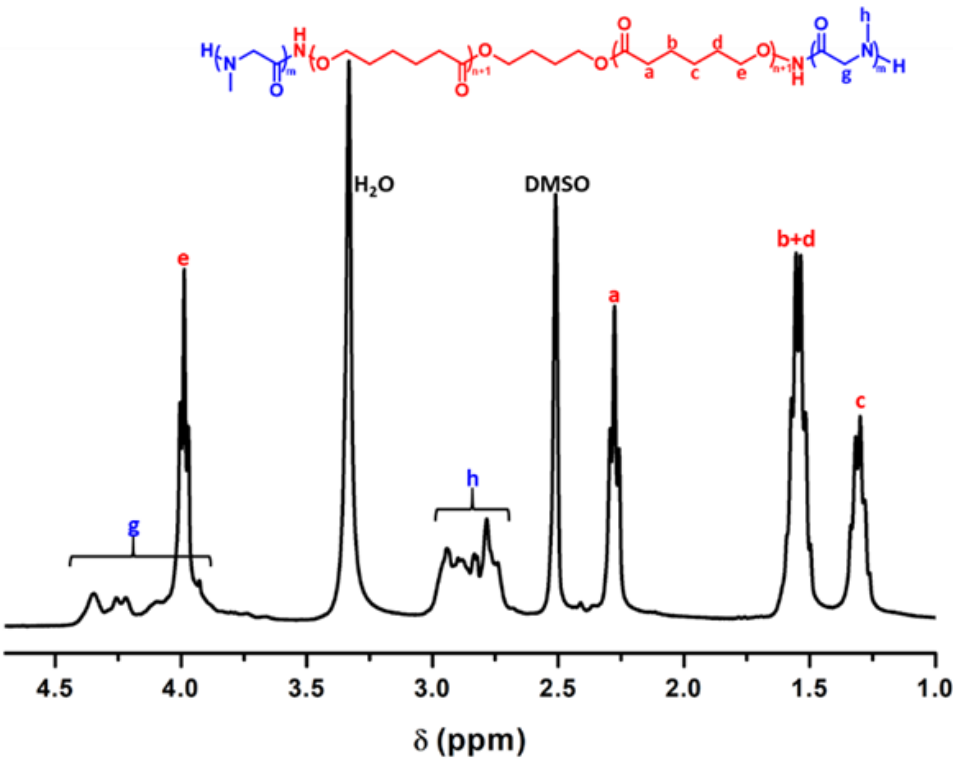

Figure 2.2. ^{1}H-NMR spectrum of CS10 (PSar$_{16}$-*b*-PCL$_{40}$-*b*-PSar$_{16}$) in DMSO-*d*$_6$.

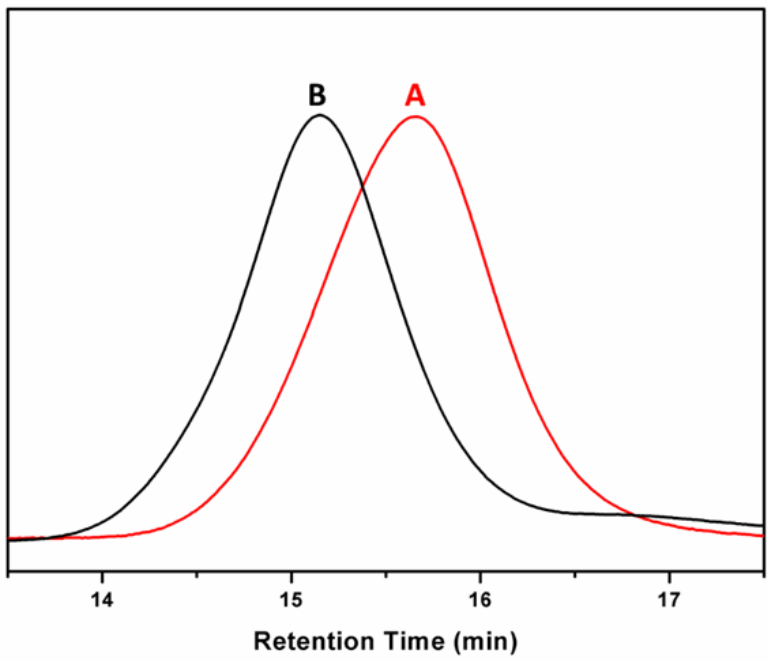

Figure 2.3. GPC traces (0.05 M LiBr/DMF as eluent) of (A) PCL5 (H_2NO-PCL$_{40}$-ONH_2) and (B) CS10 (PSar$_{16}$-*b*-PCL$_{40}$-*b*-PSar$_{16}$).

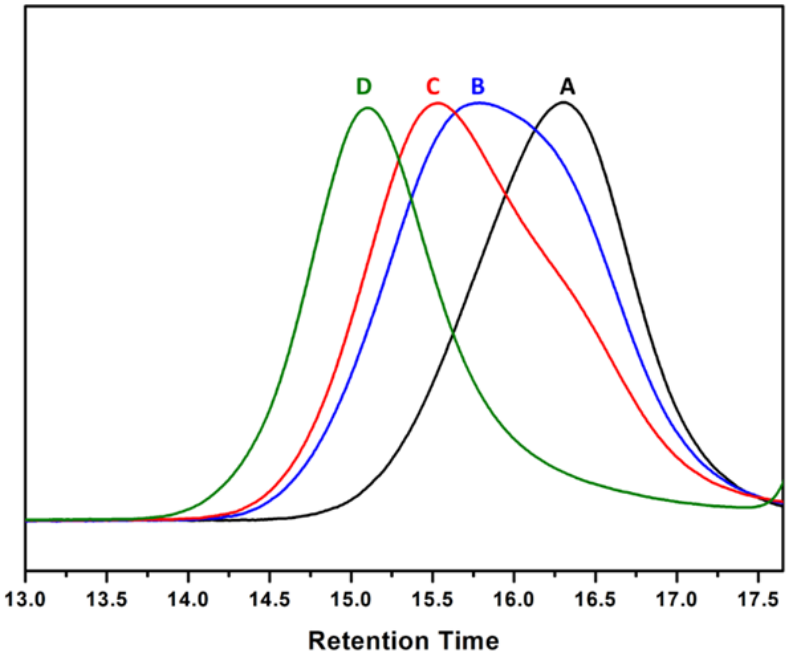

Figure 2.4. GPC traces (0.05 M LiBr/DMF as eluent) of (A) PCL4, (B) CS6, (C) CS7 and (D) CS8.

Nevertheless, DPs of PSar blocks could not be accurately controlled by feeding ratio. As listed in Table 2.1, *Đ* of copolymers are not always below 1.2. Tails and shoulders are often recorded in the GPC traces of some copolymer samples (Figure 2.4). These observations can be explained by two factors. On one hand the oxyamino group is less nucleophilic than alkylamino group and has a relatively low initiation activity. Thus the initiation reaction is slow, which may results in relatively high *Đ*. On the other hand the relatively low reactivity of NTA makes it necessary to have relatively long reaction time (up to 48 h) and high reaction temperature (60 ℃). Consequently the possibility of side reactions increases, *e.g.*, the nucleophilic attack of amino end groups on ester linkages of PCL block that makes chain scission and forms chains of low MWs detected as shoulders and tails in GPC traces.

2.3.2 PMeSPG and PEG-*b*-PMeSPG

The *N*-substituted thioether-bearing amino acid, MeSPG, is firstly synthesized from the natural amino acid methionine, through a sequential one-pot

"decarboxylation−*N*-carboxymethylation" procedure (Scheme 2.2). We implemented this method, for the first time, to transfer the substituent group R of amino acid from *C*-substituted position (*C*-R) to *N*-substituted position (*N*-R). Potentially, a number of *N*-R glycines can be readily synthesized from natural amino acids using this approach. MeSPG-NTA is obtained from the following cyclization reaction, as a new NNTA monomer with thioether-containing *N*-substituent side chain (Figure 2.5 shows the ^{1}H-NMR and ^{13}C-NMR results of MeSPG-NTA). PMeSPG is synthesized through ROP of MeSPG-NTA (Scheme 2.3) initiated by benzylamine, with different DPs depending on the monomer/initiator ([M]/[I]) feeding ratios (Table 2.2). Polymer with MW over 27000 Da is obtained, while *Đ* is maintained within 1.22. As shown in Figure 2.6, all the PMeSPG samples have relatively narrow and symmetric unimodal GPC traces, and are in an order from right to left, as the MW increases. The MALDI-ToF result of P1 (Figure 2.7) confirms the BA-initiated and secondary amino-ended structure. These results indicate good controllability of the polymerization.

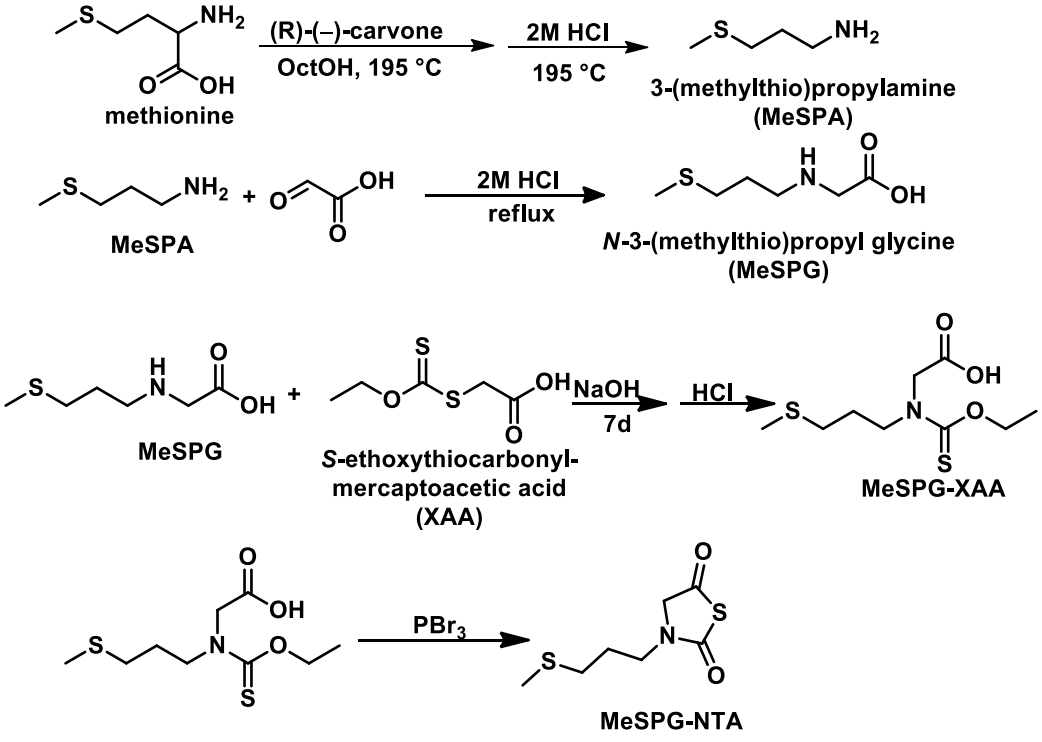

Scheme 2.2. Synthetic route of MeSPG and MeSPG-NTA

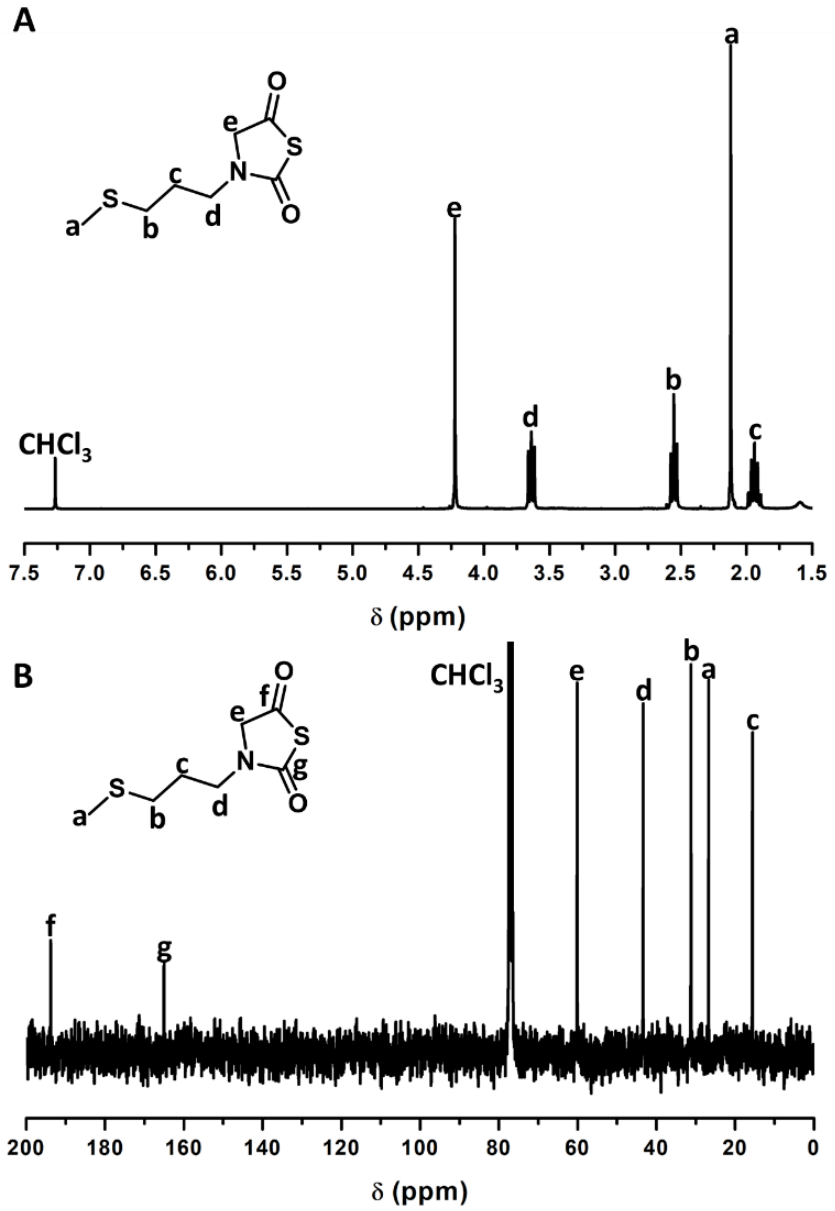

Figure 2.5. (A) ^{1}H-NMR and (B) ^{13}C-NMR spectra of MeSPG-NTA

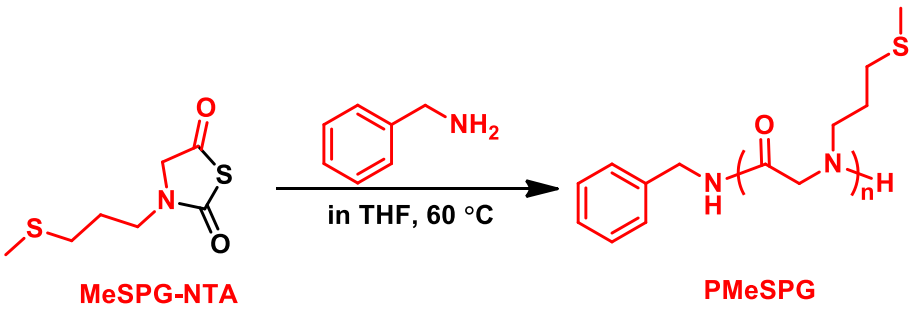

Scheme 2.3. Synthesis of PMeSPG through ROP of MeSPG-NTA

Table 2.2. Syntheses of PMeSPG homopolymers.

Sample	[M]/[I]	Solvent	Time	Yield	DP [a]	$M_{n,\ NMR}$ [a]	$M_{n,\ GPC}$ [b]	Đ [b]
P1	46	CH_3CN	24 h	89.6%	40	5800	6700	1.11
P2	79	THF	40 h	72.6%	65	9400	11200	1.11
P3	75	THF	48 h	82.6%	75	10900	14200	1.15
P4	100	THF	48 h	64.2%	84	12200	17800	1.14
P5	200	THF	64 h	77.5%	186	27000	25000	1.22

[a] Calculated from the integrals in ^{1}H-NMR spectra; [b] Determined by GPC in 0.01 M LiBr/DMF, with rate at 1 mL/min, PS as standard.

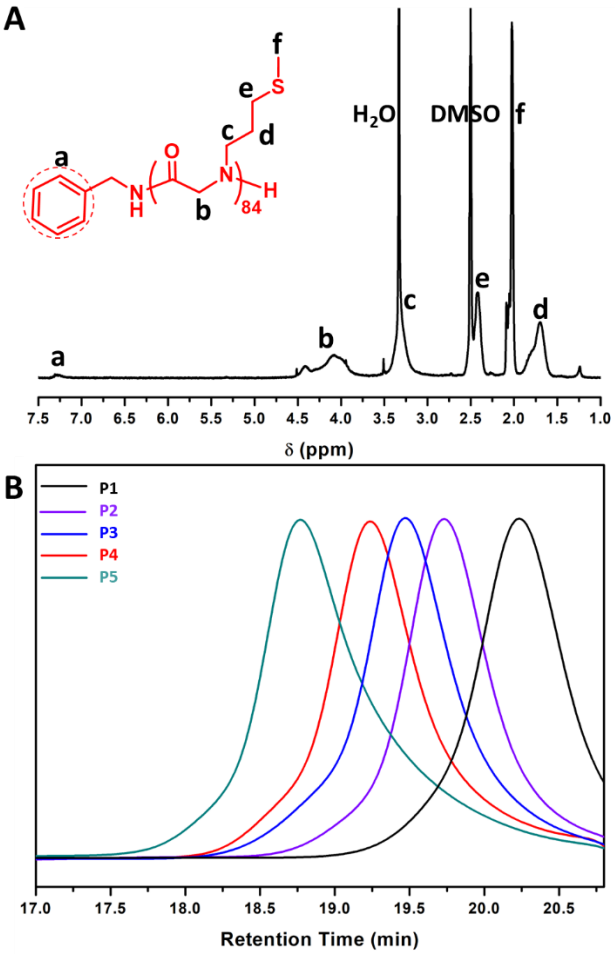

Figure 2.6. (A) ^{1}H-NMR spectrum of P4 ($PMeSPG_{84}$), in DMSO-d_6; (B) GPC traces of PMeSPG homopolymers P1−P5, 0.01 M LiBr/DMF as eluent.

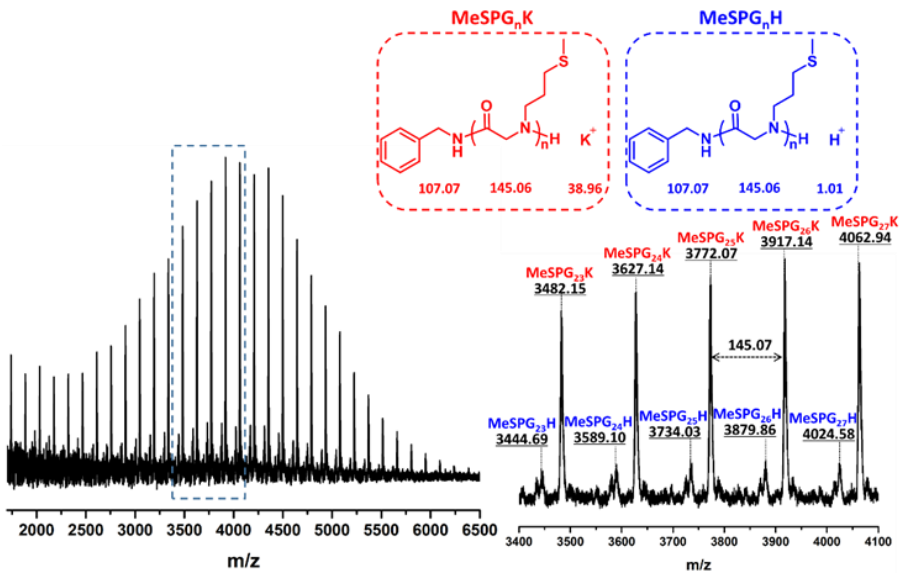

Figure 2.7. MALDI-ToF of P1 (PMeSPG$_{40}$), with potassium trifluoroacetate as ionizer and DHB as substrate.

Encouraged by the successful syntheses of PMeSPG homopolymers, the block copolymers PEG-*b*-PMeSPG were developed as a further step, with amino-ended PEG of MW = 2000 Da (PEG$_{45}$-NH$_2$) as the macromolecular initiator (Scheme 2.4). As listed in Table 2.3, by controlling the feeding ratio, three PEG-*b*-PMeSPG amphiphilic block copolymers are synthesized of different MWs and hydrophilic/hydrophobic ratios: EM1 (PEG$_{45}$-*b*-PMeSPG$_{17}$), EM2 (PEG$_{45}$-*b*-PMeSPG$_{40}$) and EM3 (PEG$_{45}$-*b*-PMeSPG$_{71}$). The MW distribution of the copolymers can be controlled within 1.2. Figure 2.8 shows the ^{1}H-NMR spectrum of EM3 and GPC traces of the three copolymers, revealing the clear structure and controllable MWs.

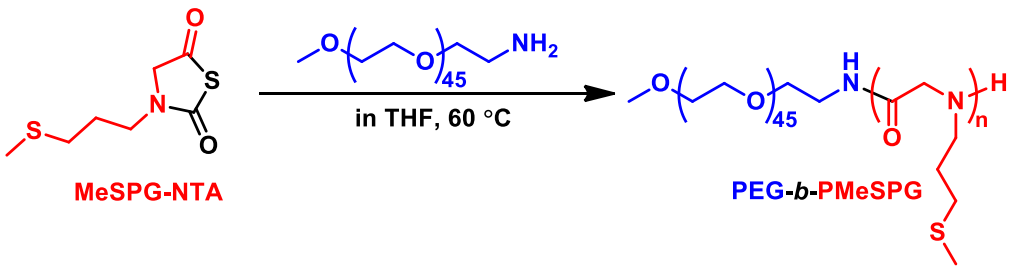

Scheme 2.4. Synthesis of PEG-*b*-PMeSPG through ROP of MeSPG-NTA initiated by PEG$_{45}$-NH$_2$.

Table 2.3. Syntheses of PEG-*b*-PMeSPG copolymers.

Sample	[M]/[I]	Yield	DP_{MeSPG}/DP_{EG} [a]	$f_{PEG,wt}$ [a]	$M_{n,\ NMR}$ [a]	$M_{n,\ GPC}$ [b]	Đ [b]
EM1	14	91.1%	17/45	45%	4400	3600	1.14
EM2	39	83.2%	40/45	26%	7700	4900	1.19
EM3	82	82.5%	71/45	16%	12300	7700	1.15

[a] DPs, MWs and PEG weight ratios ($f_{PEG,wt}$) are calculated from the integrals in ^{1}H-NMR spectra; [b] Determined by GPC in 0.01 M LiBr/DMF, with rate at 1 mL/min, PEG as standard.

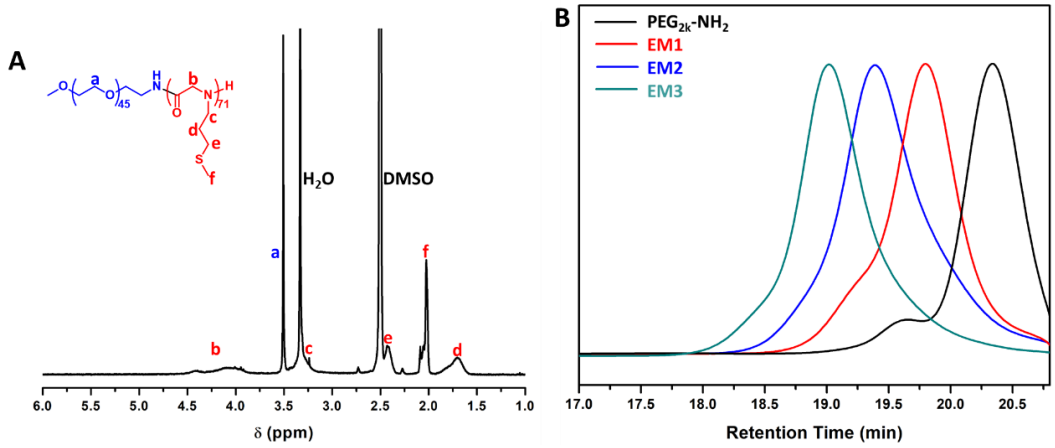

Figure 2.8. (A) ^{1}H-NMR spectrum of EM3 (PEG_{45}-*b*-$PMeSPG_{71}$); (B) GPC traces of PEG-*b*-PMeSPG copolymers EM1−EM3, 0.01 M LiBr/DMF as eluent.

2.3.3 Amphiphilic block copolypeptoid PMeSPG-*b*-PSar

Block copolypeptoids can be synthesized through sequential feeding of different NNTA monomers.[9] After confirming the amino-ended structure of PMeSPG by MALDI-ToF (Figure 2.7), the amphiphilic block copolypeptoid PMeSPG-*b*-PSar is designed and synthesized, by sequential monomer feeding of MeSPG-NTA and Sar-NTA (Scheme 2.5). As the results, copolypeptoids MS1 ($PMeSPG_{45}$-*b*-$PSar_{65}$), MS2 ($PMeSPG_{60}$-*b*-$PSar_{50}$) and MS3 ($PMeSPG_{75}$-*b*-$PSar_{25}$) are obtained with different hydrophilic/hydrophobic ratios and similar MWs. The ^{1}H-NMR spectra (Figure

2.9A−C) show legible signals from both PMeSPG and PSar blocks, while The GPC results (Figure 2.9D−E) reveal a shift of monomodal traces towards shorter retention time, from the first block to the terminated copolymer. The block structure of the copolypeptoids is well confirmed.

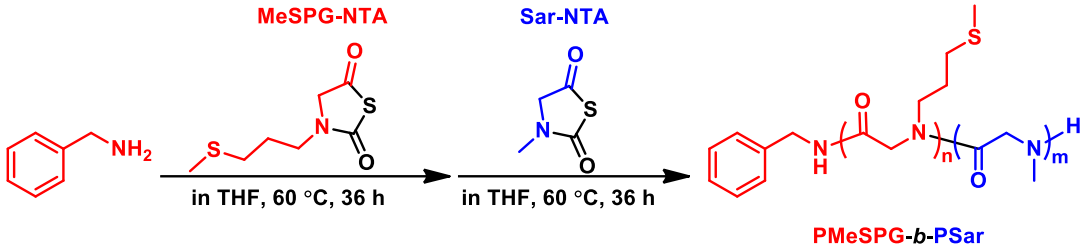

Scheme 2.5. Synthesis of PMeSPG-*b*-PSar through sequential monomer feeding and ROP of MeSPG-NTA and Sar-NTA.

Table 2.4. Syntheses of PMeSPG-*b*-PSar copolypeptoids.

Sample	[MeSPG] : [Sar] : [I]	Yield	DP_{MeSPG}/DP_{Sar} [a]	$f_{PSar, wt}$ [a]	$M_{n, NMR}$ [a]	$M_{n, GPC}$ [b]	$Đ$ [b]
MS1	50 : 70 : 1	95.3%	45/65	41%	11200	15400	1.20
MS2	70 : 55 : 1	85.6%	60/50	29%	12300	15100	1.21
MS3	97 : 44 : 1	71.4%	75/25	14%	12700	17600	1.20

[a] DPs, MWs and PSar weight ratios ($f_{PSar,wt}$) are calculated from the integrals in ^{1}H-NMR spectra; [b] Determined by GPC in 0.01 M LiBr/DMF, with rate at 1 mL/min, PS as standard.

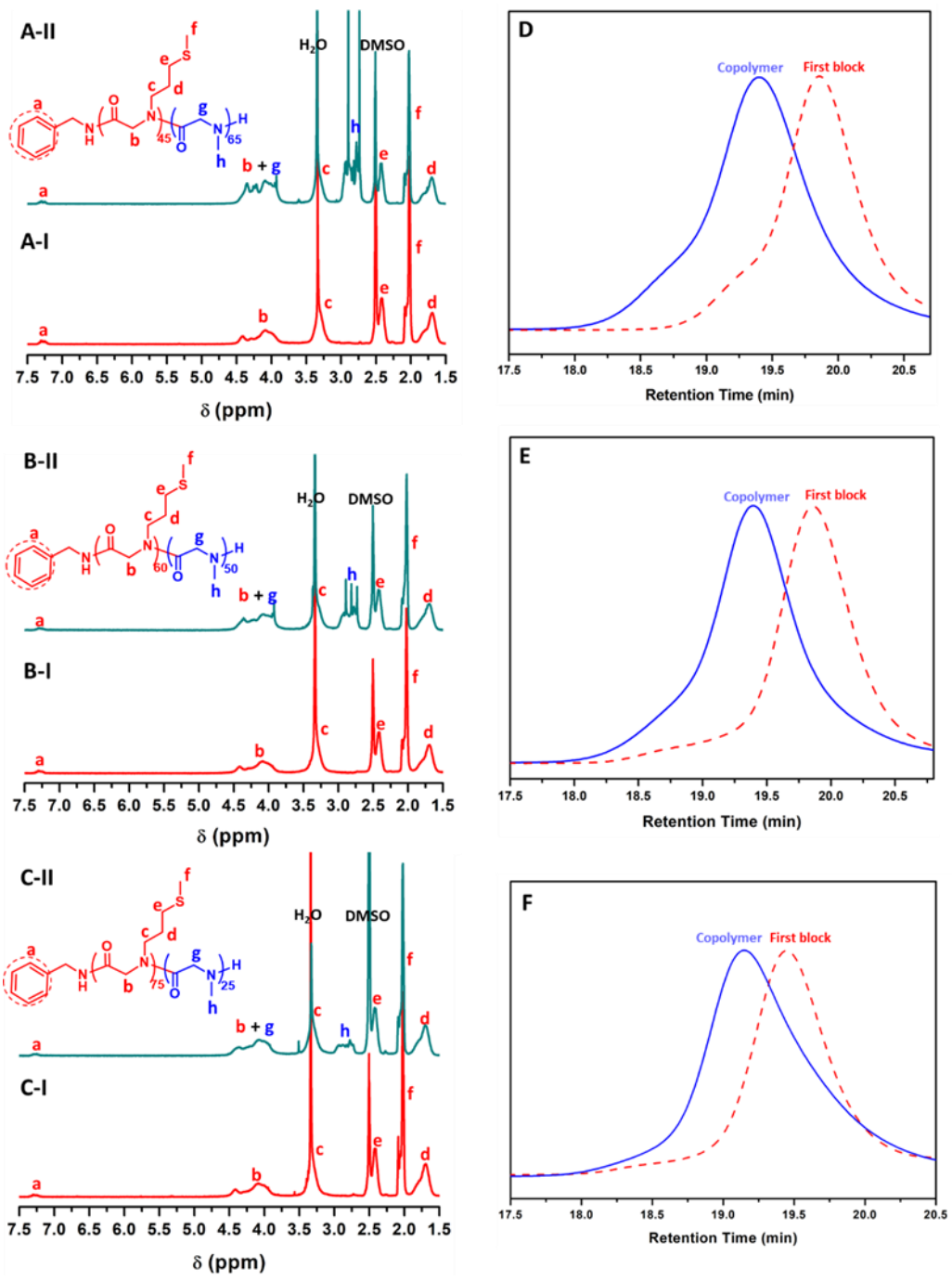

Figure 2.9. ^{1}H-NMR spectra of (A) MS1, (B) MS2 and (C) MS3 revealing structures of the first blocks (I) and the terminated copolymers (II); GPC traces of (D) MS1, (E) MS2 and (F) MS3 revealing MWs of the first blocks (dash red) and the terminated copolymers (solid blue).

2.4 Conclusion

We synthesized three kinds of polypeptoid-containing amphiphilic block copolymers: di- and triblock copolymers PCL-*b*-PSar and PSar-*b*-PCL-*b*-PSar, PMeSPG-containing copolymers PEG-*b*-PMeSPG and PMeSPG-*b*-PSar. The diblock PCL-*b*-PSar and triblock PSar-*b*-PCL-*b*-PSar are obtained from ROP of Sar-NTA, initiated by oxyamino-ended PCL-ONH_2 and H_2NO-PCL-ONH_2, respectively. Among them PSar-*b*-PCL-*b*-PSar has a scarcely reported ABA structure with PCL in the middle, and PSar blocks at both sides. The thioether-bearing polypeptoid PMeSPG is synthesized from controlled ROP of a new NNTA monomer, MeSPG-NTA, developed for the first time by us. MeSPG-NTA is obtained from methionine using a "decarboxylation−*N*-carboxymethylation" procedure followed by a cyclization reaction. The ROP of MeSPG-NTA initiated by PEG_{45}-NH_2 results in PEG-*b*-PMeSPG amphiphilic block copolymers with different MWs and hydrophilic/hydrophobic ratios, *i. e.*, EM1 (PEG_{45}-*b*-$PMeSPG_{17}$), EM2 (PEG_{45}-*b*-$PMeSPG_{40}$) and EM3 (PEG_{45}-*b*-$PMeSPG_{71}$). The amphiphilic block copolypeptoid PMeSPG-*b*-PSar is synthesized from the sequential monomer feeding of MeSPG-NTA and Sar-NTA in the amine-initiated ROP. The reaction is well controlled and gives copolypeptoids including MS1 ($PMeSPG_{45}$-*b*-$PSar_{65}$), MS2 ($PMeSPG_{60}$-*b*-$PSar_{50}$) and MS3 ($PMeSPG_{75}$-*b*-$PSar_{25}$). The chain structures of all these block copolymers are confirmed by NMR, GPC and MALDI-ToF.

References

1. Kricheldorf, H. R., Polypeptides and 100 Years of Chemistry of α-Amino Acid N-Carboxyanhydrides. *Angew. Chem. Int. Ed.* **2006,** *45* (35), 5752-5784.

2. Deming, T. J., Polypeptide and polypeptide hybrid copolymer synthesis via NCA polymerization. In *Peptide Hybrid Polymers*, Klok, H. A.; Schlaad, H., Eds. 2006; Vol. 202, pp 1-18.

3. Kramer, J. R.; Deming, T. J., General Method for Purification of alpha-Amino acid-N-carboxyanhydrides Using Flash Chromatography. *Biomacromolecules* **2010,** *11* (12), 3668-3672.

4. Kato, H.; Higashim.T; Okamura, S., Condensation polymerization of N-dithiocarbonyl alkoxycarbonyl amino acids .V. Studies on reaction mechanism. *Makromol Chem* **1967,** *109* (Nov), 9-21.

5. Dewey, R. S.; Schoenew.Ef; Joshua, H.; Paleveda, W. J.; Schwam, H.; Barkemey.H; Arison, B. H.; Veber, D. F.; Denkewal.Rg; Hirschma.R, Synthesis of peptides in aqueous medium .V. Preparation and use of 2,5-thiazolidinediones (NTAs) . Use of 13C-H nuclear magnetic resonance signal as internal standard for quantitative studies. *J Am Chem Soc* **1968,** *90* (12), 3254-3255.

6. Kricheldorf, H. R.; Sell, M.; Schwarz, G., Primary amine-initiated polymerizations of alpha-amino acid N-thiocarbonic acid anhydrosulfide. *J. Macromol. Sci., Pure Appl. Chem.* **2008,** *45* (6), 425-430.

7. Cao, J.; Siefker, D.; Chan, B. A.; Yu, T.; Lu, L.; Saputra, M. A.; Fronczek, F. R.; Xie, W.; Zhang, D., Interfacial Ring-Opening Polymerization of Amino-Acid-Derived N-Thiocarboxyanhydrides Toward Well-Defined Polypeptides. *ACS Macro Lett.* **2017,** *6* (8), 836-840.

8. Tao, X.; Deng, Y.; Shen, Z.; Ling, J., Controlled Polymerization of N-Substituted Glycine N-Thiocarboxyanhydrides Initiated by Rare Earth Borohydrides toward Hydrophilic and Hydrophobic Polypeptoids. *Macromolecules* **2014,** *47* (18), 6173-6180.

9. Tao, X.; Zheng, B.; Kricheldorf, H. R.; Ling, J., Are N-Substituted Glycine N-Thiocarboxyanhydride Monomers Really Hard to Polymerize? *J. Polym. Sci., Part A: Polym. Chem.* **2017,** *55* (3), 404-410.

10. Tao, X.; Zheng, B.; Bai, T.; Zhu, B.; Ling, J., Hydroxyl Group Tolerated Polymerization of N-Substituted Glycine N-Thiocarboxyanhydride Mediated by Aminoalcohols: A Simple Way to alpha-Hydroxyl-omega-aminotelechelic Polypeptoids. *Macromolecules* **2017,** *50* (8), 3066-3077.

11. Tao, X.; Zheng, B.; Bai, T.; Li, M.-H.; Ling, J., Polymerization of N-Substituted Glycine N-Thiocarboxyanhydride through Regioselective Initiation of Cysteamine: A Direct Way toward Thiol-Capped Polypeptoids. *Macromolecules* **2018**.

12. Tao, X.; Deng, C.; Ling, J., PEG-amine-initiated polymerization of sarcosine N-thiocarboxyanhydrides toward novel double-hydrophilic PEG-b-polysarcosine diblock copolymers. *Macromol. Rapid Commun.* **2014,** *35* (9), 875-881.

13. Miao, Y.; Xie, F.; Cen, J.; Zhou, F.; Tao, X.; Luo, J.; Han, G.; Kong, X.; Yang, X.; Sun, J.; Ling, J., Fe3+@polyDOPA-b-polysarcosine, a T1-Weighted MRI Contrast Agent via Controlled NTA Polymerization. *ACS Macro Lett.* **2018,** *7* (6), 693-698.

14. Jackson, D. M.; Ashley, R. L.; Brownfield, C. B.; Morrison, D. R.; Morrison, R. W., Rapid Conventional and Microwave-Assisted Decarboxylation of L-Histidine and Other Amino Acids via Organocatalysis with R-Carvone Under Superheated Conditions. *Synth. Commun.* **2015,** *45* (23), 2691-2700.

15. Gibbs, T. J. K.; Boomhoff, M.; Tomkinson, N. C. O., A mild and efficient method for the one-pot monocarboxymethylation of primary amines. *Synlett* **2007,** (10), 1573-1576.

16. Makiguchi, K.; Satoh, T.; Kakuchi, T., Diphenyl Phosphate as an Efficient Cationic Organocatalyst for Controlled/Living Ring-Opening Polymerization of delta-Valerolactone and epsilon-Caprolactone. *Macromolecules* **2011,** *44* (7), 1999-2005.

17. Schlick, T. L.; Ding, Z. B.; Kovacs, E. W.; Francis, M. B., Dual-surface modification of the tobacco mosaic virus. *J. Am. Chem. Soc.* **2005,** *127* (11), 3718-3723.

18. Zhou, Y. Y.; Li, L.; Chen, W.; Li, D. A.; Zhou, N. C.; He, J. L.; Ni, P. H.; Zhang, Z. B.; Zhu, X. L., A twin-tailed tadpole-shaped amphiphilic copolymer of poly(ethylene glycol) and cyclic poly(epsilon-caprolactone): synthesis, self-assembly and biomedical applications. *Polym. Chem.* **2018,** *9* (33), 4343-4353.

Chapter 3. Thermo-Responsive Self-Assembly of PSar-*b*-PCL-*b*-PSar

3.1 Introduction

Drug delivery for smart diagnosis and treatment is a major approach where polymeric self-assemblies have huge potential to be applied.[1] The suitable properties for biomedical applications, including stealthiness, biocompatibility and biodegradability, majorly depend on the employed amphiphilic block copolymers. PEG-*b*-PCL is of great interest for preparation of self-assemblies, including polymersomes, for biomedical uses, because both PEG and PCL have been applied in polymeric drug-carrier formations which have entered clinical trials, and some drugs containing them have been approved by FDA.[2, 3] PCL is a biocompatible and biodegradable hydrophobic polymer which shows slow erosion kinetics and a certain stability against degradation under neutral pH environments.[4] PEG is a water-soluble macromolecule with anti-fouling property.[2] Nano- and giant vesicles prepared from PEG-*b*-PCL by different methods have been intensively investigated,[5-8] with discussion on their formation mechanism[6] and on their biomedical applications.[9]

The synthetic polymer PEG has often been considered as a relatively benign and immunologically safe material, and has been a common choice for the hydrophilic block of copolymers. However, recent works have revealed that PEGs show oxidative activity in physiological cellular environment[10] and that PEGs can generate complement activation products in human serum on a time scale of minutes.[11, 12] As a water-soluble polypeptoid composed of natural amino acid sarcosine, PSar is comparable with or even better than PEG in properties including biocompatibility, biodegradability and anti-fouling ability.[13]

In Chapter 2 we demonstrated the synthesis of PSar-*b*-PCL-*b*-PSar triblock copolymers based in ROP of Sar-NTA with H_2NO-PCL-ONH_2 as macromolecular

initiator. In this chapter, we study the self-assembly of this kind of triblock copolymers, via vesicle preparation methods including nanoprecipitation and film hydration. Based on the crystallization of PCL blocks, the thermo-responsive morphological transitions are studied with the help of heating treatment.

3.2 Experimental section

3.2.1 Materials

DMF (99%, VWR), chloroform (99%, VWR), Nile Red (Sigma Aldrich). The copolymers CS7 ($PSar_8$-*b*-PCL_{28}-*b*-$PSar_8$) and CS10 ($PSar_{16}$-*b*-PCL_{40}-*b*-$PSar_{16}$) were prepared with the method described in Chapter 2.

3.2.2 Nanoprecipitation

Typically the copolymer was dissolved in 1 mL of DMF (at 0.5 or 0.1 wt%). 1 mL of deionized milli-Q water was injected slowly to the organic solution under mild shaking (2−3 μL of water per minute to 1mL of polymer solution). The process of nanoprecipitation was carried out at 25 ℃. The turbid mixtures were then dialyzed against water for 3 days (water was changed every 12 h) to remove DMF using a Spectra/Por regenerated cellulose membrane with a molecular weight cutoff (MWCO) of 3500.

3.2.3 Film hydration

The copolymer was dissolved in chloroform (1 wt%) with 0.01 wt% Nile Red, and deposited on the surface of roughened Teflon. The polymer films were then dried for > 4 h under vacuum and rehydrated in a 250 mmol/L sucrose aqueous solution. The samples were subsequently sealed and heated at 65 ℃ for 24 to 48 h. Each aqueous sample was then diluted in 250 mmol/L glucose aqueous solution at the ratio 30:70 for the following microscopic observation.

3.2.4 Characterizations

Differential scanning calorimetry (DSC) analyses were performed on a TA Q200 instrument. The synthesized copolymers were heated from 0 to 130 ℃ at a rate of 10 ℃/min under a nitrogen purge.

Turbidity measurements were performed using a UV-2550 UV-Vis spectrophotometer (Shimadzu) equipped with a TCC-240A temperature controlled cell holder (Shimadzu). UV-Vis optical density (O.D.) of the samples was recorded at a wavelength of 600 nm with a slit width of 2 nm.

Cryo-EM experiments were conducted in INSERM U1196, Institut Curie, in collaboration with Sylvain Trepout. A total of 5 μL of samples were deposited onto a 200 mesh holey copper grid (Ted Pella Inc., U.S.A.) and flash-frozen in liquid ethane cooled down at liquid nitrogen temperature. The images were acquired on a JEOL 2200FS energy-filtered (20eV) field emission gun electron microscope operating at 200 kV using a Gatan ssCCD 2048 × 2048 pixels. Energy-filtered (Zero-loss) cryo-electron tomography images were collected at 12000x (corresponding pixel size 0.8 nm) from -64 °up to 64 °using a Saxton scheme (1 °at high tilts and 2 °at low tilts). Energy-filtered (Zero-loss) cryo-electron tomography images were collected at 12000x (corresponding pixel size 0.8 nm) from -64 °up to 64 °using a Saxton scheme (1 °at high tilts and 2 °at low tilts). Alignment of the tilt-series and reconstruction of the final 3D volume were computed using TomoJ v2.28.

CLSM images were obtained on a Nikon confocal laser-scanning microscope A1R, with the laser of HeNe 543 nm.

The hydrodynamic diameters of the nanoparticles were measured by DLS, using a particle size analyzer (Zetasizer Nano Series, Malvern Instruments) at 25 ℃. The measurements were made at a fixed angle at 90 °and a wavelength of 657 nm.

Cytotoxicity test was conducted in collaboration with Vincent Semetey. The experiment was carried out with a sample of the self-assemblies of CS10 prepared by nanoprecipitation. In a 6-well culture plate (Nunc/ThermoScientific, Roskilde, Denmark), 5000 cells/150 μL of cell suspension (L929 cell line) were used to seed each well. The cells were incubated overnight to allow for cell attachment, recovery and growth. CS10 suspensions were then added to the wells in order to obtain 6.9, 34.5, 69, 345, 690 μg/mL as final concentration of CS10, respectively. Cells were incubated with CS10 samples for 4 hours at 37 ℃. The medium was then removed and replaced by 1.8 mL of fresh culture medium, and 200 μL of a 5 mg/mL solution of the 3-(4,5-dimethylthiazol-2-yl)-2,5-diphenyltetrazolium bromide (MTT) in PBS (Sigma-Aldrich, Saint-Quentin-Fallavier, France) was added to each well. Cells were incubated further at 37 ℃ for 2 h. The resulting violet formazan precipitate was solubilized by the addition of 500 μL DMSO and was allowed to incubate at 37 ℃ for additional 10 min. The samples were then analyzed on UV/Vis spectrophotometer (Lambda 800, Perkin Elmer) at 540 nm to determine the absorbance. Experiments were performed in triplicate. Relative cell viability was defined as the ratio of the absorbance of cells incubated with CS10 self-assemblies over the absorbance of cells incubated only with growth medium.

3.3 Results and discussion

Vesicular morphologies are generally considered to be generated from the block copolymers possessing a hydrophilic weight fraction in the range of 35 ± 10 wt%.[14] Hence CS7 ($PSar_8$-*b*-PCL_{28}-*b*-$PSar_8$, $f_{PSar,\ wt}$ = 25%) and CS10 ($PSar_{16}$-*b*-PCL_{40}-*b*-$PSar_{16}$, $f_{PSar,\ wt}$ = 34%) are chosen for systematic studies of self-assembly in order to obtain polymersomes.

3.3.1 Thermodynamic behaviors of PSar-*b*-PCL-*b*-PSar

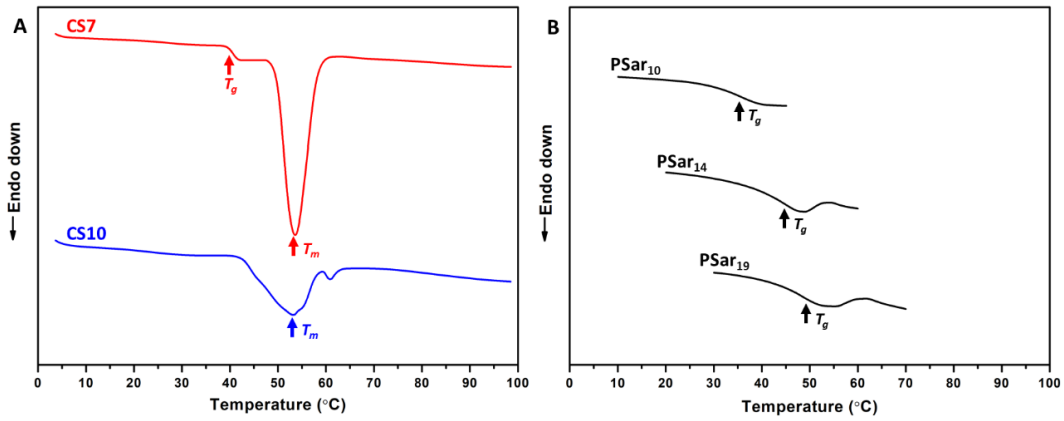

Figure 3.1. DSC thermograms of the first heating scan recorded at 10 ℃/min: (A) the triblock copolymers CS7 ($PSar_8$-*b*-PCL_{28}-*b*-$PSar_8$) and CS10 ($PSar_{16}$-*b*-PCL_{40}-*b*-$PSar_{16}$); (B) three homopolymerized PSar with DPs respectively at 10, 14 and 19. T_m is the melting temperature of PCL block and T_g the glass transition of PSar block. PSar samples are synthesized from BA-initiated ROP of Sar-NTA, and the DPs are calculated from ^{1}H-NMR results.

Before self-assemby studies, the two triblock copolymers are firstly analyzed by DSC. Figure 3.1A shows typical DSC thermograms of CS7 and CS10 at the first heating scan at 10 ℃/min. CS7 exhibits a typical melting peak with peak value T_m = 54 ℃ and melting enthalpy ΔH_m = 46.1 J/g, while CS10 has a peak of relatively wide and asymmetric shape, with T_m = 53 ℃ and ΔH_m = 27.5 J/g. Both melting peaks are attributed to PCL melting. When weighted by the weight ratio of PCL part, the melting enthalpy equals to 61.5 J/g for CS7 (75% PCL) and 41.7 J/g for CS10 (66% PCL). These values are smaller than 136 J/g, which is taken as the value of ΔH_m of PCL homopolymer with 100% crystallinity.[15] It suggests the PCL blocks are semi-crystalline in the block copolymers. Higher is PSar/PCL ratio, lower is the PCL crystallinity. A detectable glass transition temperature (T_g) for PSar block is recorded at 40 ℃ for CS7. For CS10, we attempt to assign the signal around 62 ℃ as the glass transition of PSar block, which is overlapping with the PCL melting peak. Comparing to T_g of the

homopolymers $PSar_{10}$ (T_g = 36 ℃), $PSar_{14}$ (T_g = 47 ℃) and $PSar_{19}$ (T_g = 59 ℃) (Figure 3.1B) measured in the same conditions, the T_g values found here for CS7 and CS10 are reasonable. However, the T_g is not observable either in the first cooling scan or in the second heating scan. It is possibly because the PSar ratios ($f_{PSar, wt}$) are relatively low in these two copolymers (25% for CS7 and 34% for CS10). For the copolymer samples before the first scan, of which the polymer chains are "frozen" in non-equilibrium state as obtained from the instant precipitation by diethyl ether, chain relaxation enthalpy is detected from the first scan of DSC, in the form of a endothermic peak,[16] and makes the T_g signal more obvious. The heating in the first scan eliminates the thermal history, and also makes the PSar domains more dispersed. As the result, T_g becomes hard to be detected in the following scans.

3.3.2 Self-assembly from nanoprecipitation

In self-assembly preparation through nanoprecipitation, water is dropped into a copolymer solution in DMF, and PCL blocks tended to assemble together by hydrophobic interaction as water content increased. Turbidity measurement is conducted during water addition until water content reaches 50% (Figure 3.2). For both copolymers the turbidity of solutions increased sharply at water content around 5%, revealing the appearance of nanoparticles. The turbid mixtures are then dialyzed against water for 3 days to remove DMF. After dialysis, the mixtures remained turbid and visible precipitates appeared at bottom of flask after hours of standing. DLS is used to try to measure the hydrodynamic diameters of nanoparticles. As the result, multi-modal distributions are detected (Figure 3.3).

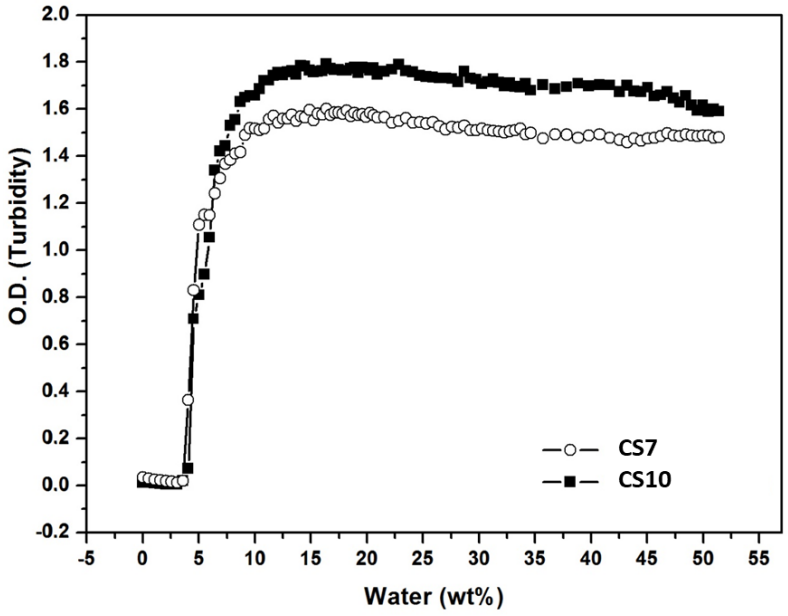

Figure 3.2. Turbidity versus water content measured at wavelength of 600 nm for CS7 (○) and CS10 (■) at 25 °C. Water was added dropwise to a solution of polymer in DMF at an initial concentration of 0.5 wt%.

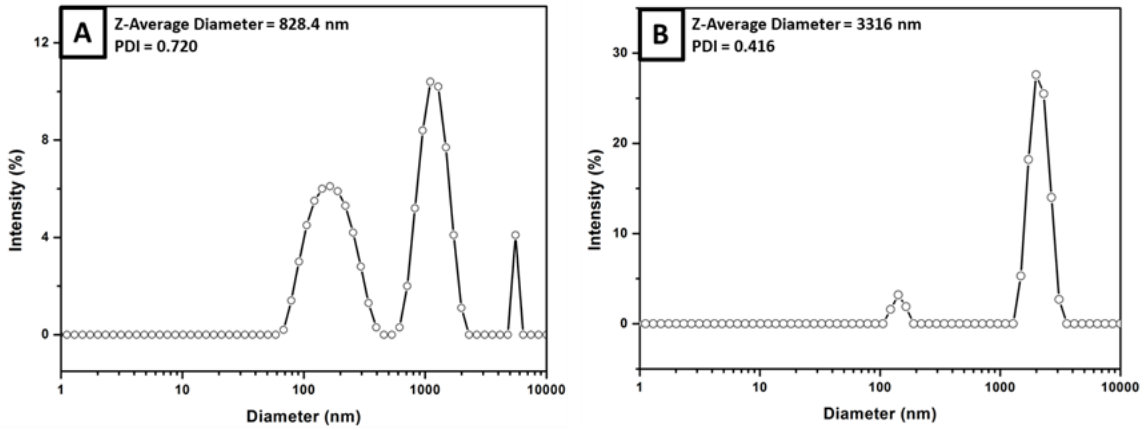

Figure 3.3. DLS results of the nanoprecipitated samples of (A) CS7 and (B) CS10.

Cryo-EM is then utilized to visualize the morphologies. Large lamellar structures are observed for self-assemblies of CS7 (Figure 3.4A−D), while lamellae together with long nanofibers are observed for CS10 (Figure 3.4E−H). The membrane thickness can be measured in the place where the sheet folds up. It is 8−9 nm for CS7 and 9−10 nm for CS10, and the diameter of nanofibers of CS10 is of 9−10 nm. As only hydrophobic part is measured in cryo-EM, the size 8−9 nm and 9−10 nm corresponding

to the PCL thickness of the unilamellar organization of triblock copolymers, is in good agreement with the value reported for vesicles of PEG_{23}-*b*-PCL_{40} where a bilayer of PCL_{40} is measured to be around 15 nm in the unilamellar organization of the diblock copolymer.[6] The interdigitation and entanglement of the polymer chains cause partially blending of hydrophobic layers of diblock copolymers,[17] while triblock copolymers are considered to have a mixed conformation of the bent U-shape and the stretched I-shape in the self-assembled membrane, with less difussivities.[18] That is the reason why the bilayer thickness of PEG_{23}-*b*-PCL_{40} is slightly smaller than the twice of that of $PSar_{16}$-*b*-PCL_{40}-*b*-$PSar_{16}$.

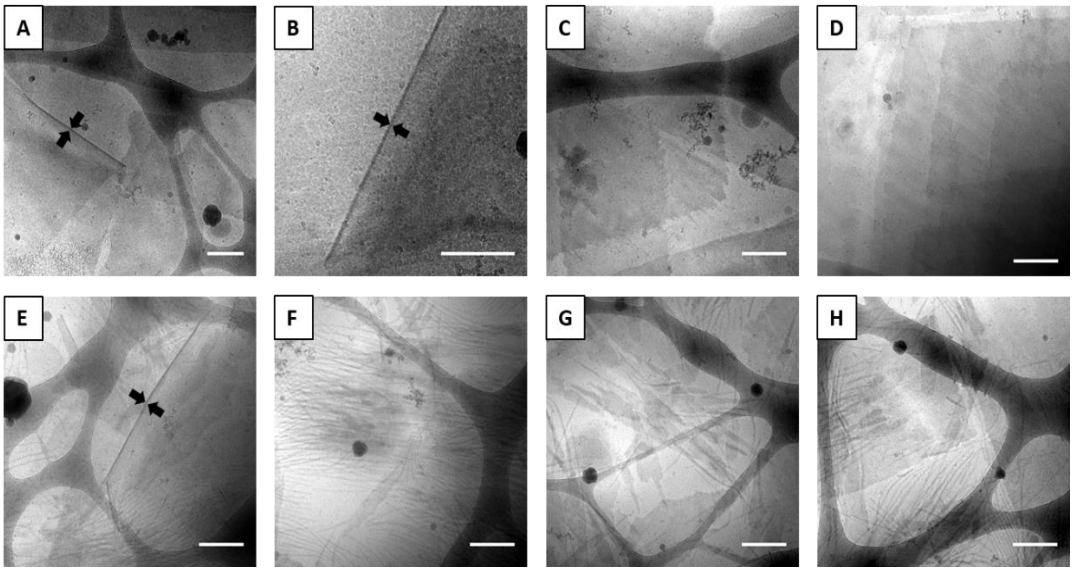

Figure 3.4. Cryo-EM images of nanoprecipitated samples of (A−D) CS7 and (E−H) CS10. Scale bar = 300 nm.

3.3.3 Morphological transformation upon heating treatment

The lamellar structure is a good indication of the possibility of vesicle formation. As discussed in Chapter 1, the Mechanism I of vesicle formation concludes with the wrapping-up of lamellar sheets to form the final vesicles, by minimizing the sum of curvature energy and interfacial energy.[19] Antonietti *et al.* discussed the formation and stability of bilayer lamellar structures.[20] The interfacial energy of hydrophilic/hydrophobic interfaces, and the entropy loss of forcing polymer chains into

confined micro-domains, are the two major contributions to the free energy in self-assembly procedure. When the entropy loss is small and the interfacial energy is large, the latter dominates the minimization of free energy, consequently copolymers in water will assemble as much as possible into structures with the least interfacial area, based on their own properties (packing parameter). The interfacial area per unit volume can be present as $A_V = d\varphi/l$, where φ and l are respectively the volume fraction of the hydrophobic domain and chain length of the hydrophobic blocks, while d is the dimensionality, representing the orientations copolymers can take in the self-assemblies. For bilayer lamellae $d = 1$, which is smaller than that of spherical ($d = 3$) and cylindrical ($d = 2$) structures. Therefore the copolymers with low conformational entropy, including rod-like polymers, mesogen-bearing polymers and crystallizable polymers, have the tendency to form lamellar structures with pronounced stability. For PSar-*b*-PCL-*b*-PSar in water, the crystallization of PCL blocks promotes the spontaneous formation of lamellae, where the spontaneous curvature = 0 because of the 3D positional order of polymer chains in crystalline domains. In addition the high bending modulus of crystalline domains also hinders the wrapping-up of lamellar sheets, which as the result, makes it difficult for PSar-*b*-PCL-*b*-PSar copolymers to form vesicles spontaneously. In order to break through the confinement by the crystallization of PCL, heating treatments are introduced to PSar-*b*-PCL-*b*-PSar self-assemblies, to promote further morphological evolution.

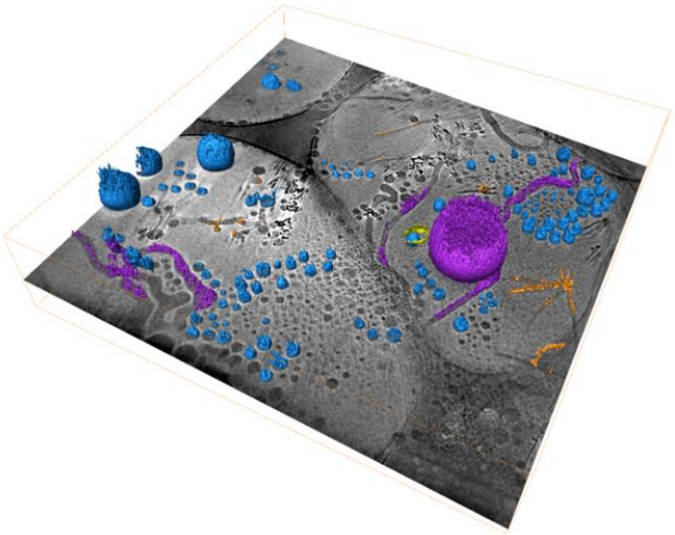

Figure 3.5. Diversity of CS7 polymer nanoparticles obtained after heating treatment at 65 ℃, unveiled by cryo-electron tomography. Solid spheres of various diameters in blue; cylindrical structures in purple; nanofibers in orange; a vesicle in yellow.

The aqueous suspensions of CS7 and CS10 nanoparticles are first heated at 65 ℃ for 30 min followed by a slow cooling to room temperature at about 0.2 ℃/min. The temperature of 65 ℃ is chosen since it is higher than both the T_m of PCL block and the T_g of PSar block (Figure 3.1). Major changes are indeed observed by cryo-EM in the samples after the heating treatment. Spheres with diameters ranging from 30 to 100 nm, together with worm-like cylinders having similar diameters and a few nanofibers are generated in CS7 (Figure 3.5 and Figure 3.6A**)**. The solid spherical nature rather than disk-like one for the observed round-particles is proved by cryo-tomography made on CS7 sample in Figure 3.5. Different morphologies are represented in different colors: full spheres in blue, worm-like cylinders in violet, thin nanofibers in orange; we even observed one vesicle with empty core near the center of image (in yellow). More vesicles are observed in CS10 after heating at 65 ℃ (Figure 3.6B), even though the majority of morphologies remain spheres and worm-like cylinders (Figure 3.6B and Figure 3.7A−C). In these results, solid spheres seem to bud from the tip of cylinders (Figure 3.6A&B, Figure 3.7A−C).

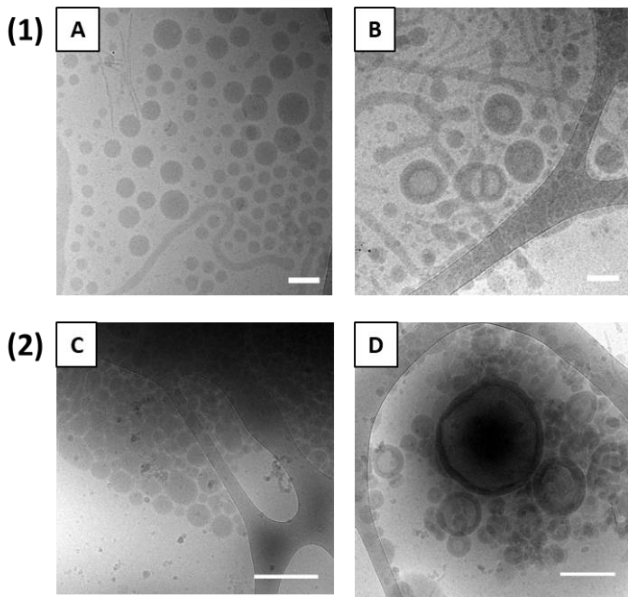

Figure 3.6. Cryo-EM images of nanoprecipitated samples of: (1) CS7 (A) and CS10 (B) after 30-min heating at 65 ℃; (2) CS7 (C) and CS10 (D) after 24-h heating at 90 ℃. Scale bar = 100 nm in A and B. Scale bar = 300 nm in C and D.

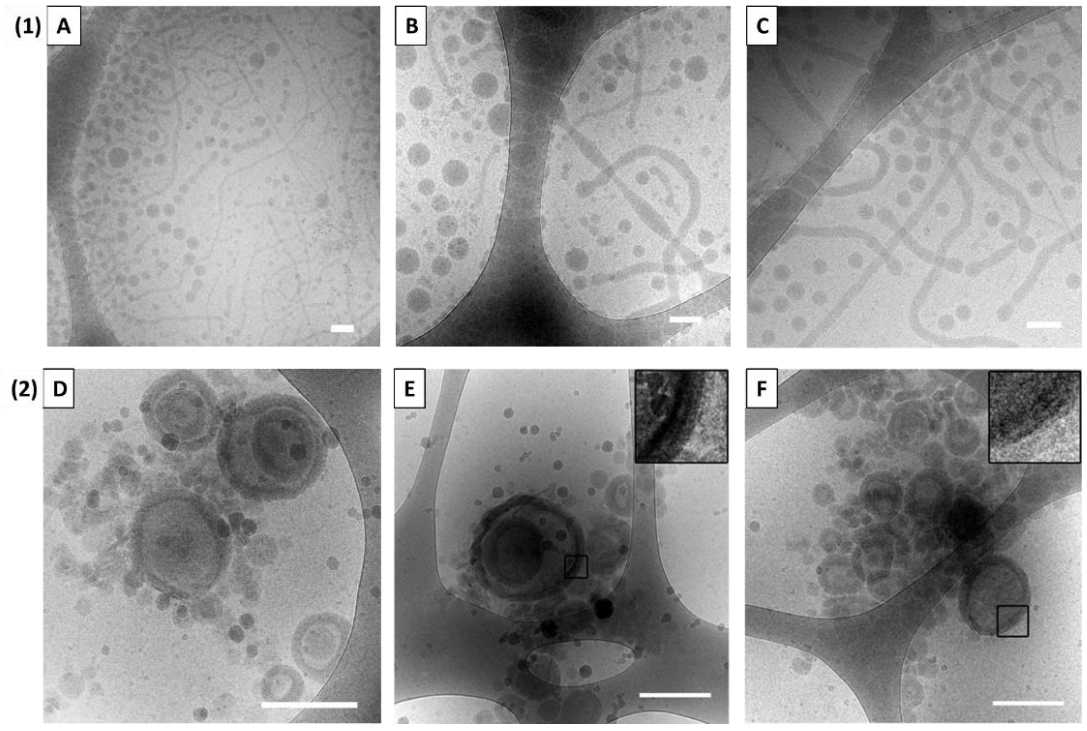

Figure 3.7. Cryo-EM images of CS10 nanoprecipitation samples: (1) after 30-min heating at 65 ℃ (A−C); (2) after 24-h heating at 90 ℃ (D−F). Scale bar = 100 nm in A−C. Scale bar = 300 nm in D−F.

In order to achieve complete morphological transformation, a reinforced thermal treatment is then carried out for both samples by heating at 90 ℃ for 24 h. In the case of CS7, only increases in size and in amount of the spheres occurred accompanied by the disappearance of worm-like cylinders (Figure 3.6C). However, abundant vesicular structures with diameters ranging mainly from 100 to 500 nm and with membrane thickness from 20−50 nm are indeed generated in CS10 sample (Figure 3.6D and Figure 3.7D−F), with the coexistence of small solid spheres. Some vesicles-in-vesicles structures, onion-like vesicles and small spheres (diameter typically smaller than 50 nm) are also recorded (Figure 3.7D&E). The hydrodynamic diameter measurement by DLS on the post-heating samples (Figure 3.8) is in good agreement with the observation of cryo-EM, nearly monomodal size distribution below 1000 nm being detected.

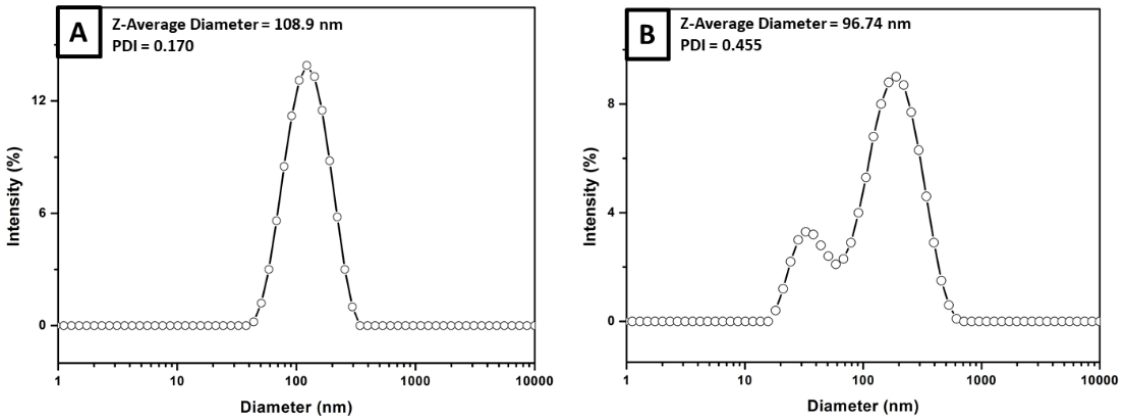

Figure 3.8. DLS results of the nanoprecipitated samples of (A) CS7 and (B) CS10 after 24-h heating at 90 ℃.

To illustrate the mechanism of the morphological transformation, dynamic turbidity measurements are performed during the thermal treatment of the nanoprecipitated CS7 and CS10 suspensions at a rate of 1 ℃/min. Figure 3.9 shows the optical densities of the samples recorded as a function of temperature. Dramatic declines of turbidities happen around 50−55 ℃ for both samples, corresponding to the size decrease of the particles in the suspensions from larges sheets (width > 1000 nm)

and long nanofibers to smaller spheres, worm-like cylinders and vesicles (diameter < 1000 nm). This temperature range around 50−55 ℃ falls into the melting peak of PCL block recorded in DSC analysis (Figure 3.1). Therefore, these dynamic turbidity measurements suggest that the chain mobility improvement upon melting is responsible for the morphological change. Direct observation shows the turbid suspensions transformed to translucent ones when heating from 25 to 80 ℃. The transformation is kept unchanged as sample cooling back to room temperature, and stable even for months of conservation at room temperature. This morphological preservation suggests that the transitions are irreversible and the resulted morphologies are probably frozen by PCL partial crystallization.

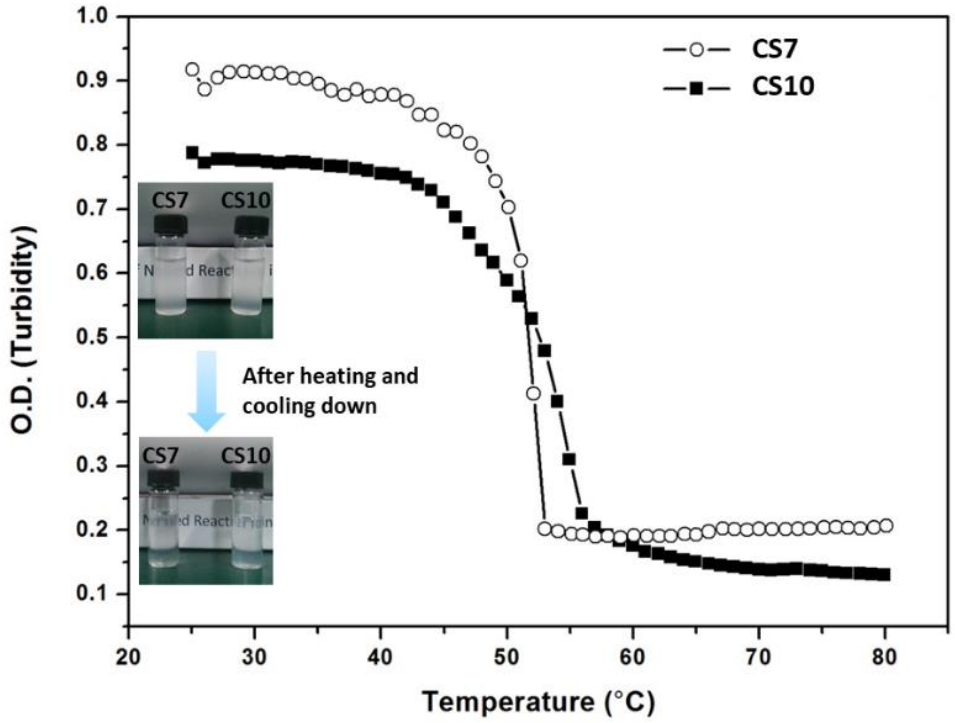

Figure 3.9. Turbidity evolution as a function of temperature for aqueous dispersions of self-assemblies of CS7 (○) and CS10 (■) prepared by nanoprecipitation, measured at wavelength of 600 nm with temperature interval of 1 ℃ at the rate of 1 ℃/min from 25 to 80 ℃. The photographs at left side directly reveal the turbidity change of CS7 and CS10 nanoprecipitated samples after the heating treatment.

The morphological transformation starts from lamellae, however, the formation of vesicles seems different from Mechanism I, where lamellae close up into vesicles. A detailed analysis of polymersomes of the sample CS10 ($PSar_{16}$-*b*-PCL_{40}-*b*-$PSar_{16}$) reveals that the vesicles are not unilamellar but multilamellar. The unilamellar thickness of CS10 at room temperature is measured as 9−10 nm (Figure 3.4E), while the vesicles detected after annealing at 90 ℃ have membrane thickness ranging from 20−50 nm, and the multilayers are visible in the cryo-EM images (Figure 3.7E&F). Moreover, the self-assemblies treated at 65 ℃ are mainly spheres, worm-like cylinders with a few of vesicles, but without any lamellar sheets remaining. After heating at 90 ℃, vesicles are observed only for CS10, while CS7 ($PSar_8$-*b*-PCL_{28}-*b*-$PSar_8$) concluded with spheres. Therefore, we propose a different scenario for the vesicle formation here. Upon heating from room temperature to 65 ℃, lamellar sheets reorganize into cylindrical and spherical polymer nanoparticles; upon further heating to 90 ℃, cylindrical structures are transformed completely into spheres (by budding) and water diffused then into the spherical structures. In the case of CS10, multilamellar vesicles are eventually formed. As for CS7 the final morphology is mainly spherical polymer nanoparticles. The difference between CS7 and CS10 self-assembling behavior is unable to explain for now, which needs a systematic study on the self-assemblies of copolymers with extended composition ranges. The scenario of vesicle formation for the CS10 proposed in this work corresponds to the Mechanism II rather than the Mechanism I of polymersome formation, even though the pathway to achieve the bigger and complex micelles (called here spherical particles) is different from that described theoretically.

3.3.4 Self-assembly from film hydration

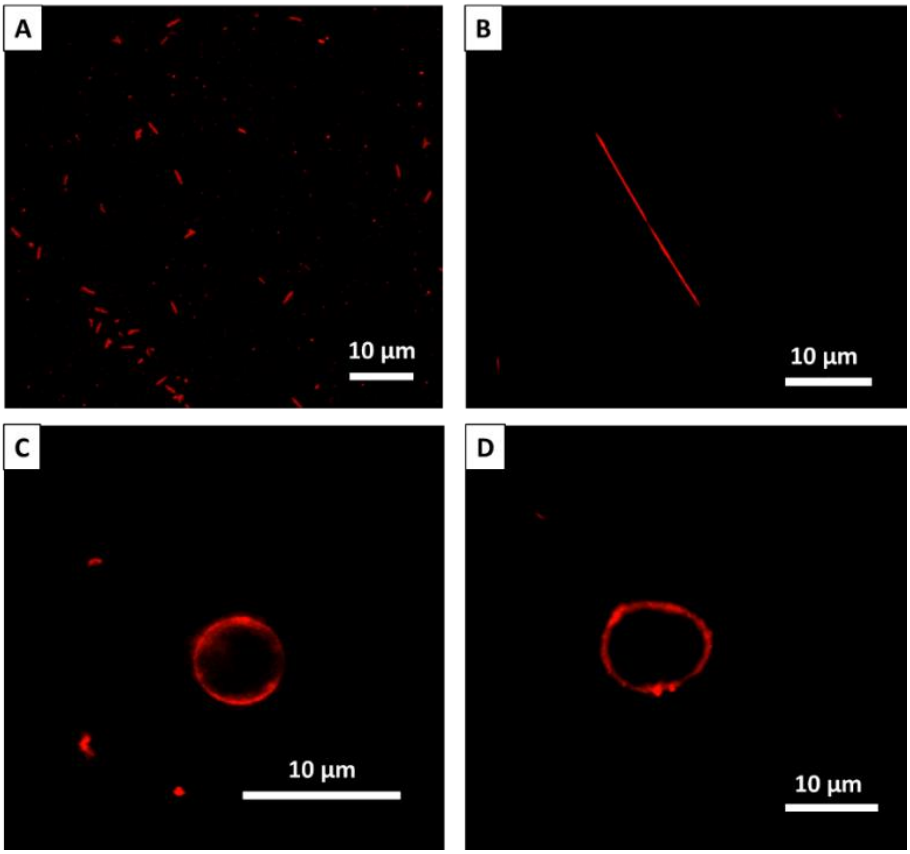

Figure 3.10. CLSM images of self-assemblies obtained from CS7 (A, C) and CS10 (B, D). Nile Red was added in the preparation at a weight ratio of 1:100 (Nile Red to copolymer) for observation. Rods and giant vesicles are observed. Scale bar = 10 µm.

Another self-assembly method, film hydration, which also includes a heating treatment during the hydration step, is carried out on the two copolymers, in order to obtain micrometer-sized vesicles. Polymer thin films are prepared with mixtures of copolymers and Nile Red (100:1 in weight) as described in the experimental section, followed by hydration at 65 ℃ for 24 h. The temperature of 65 ℃ is higher than the T_m of PCL and T_g of PSar. Therefore the chain mobility is increased, and promotes the destabilization of the polymeric film, enabling the formation of self-assemblies including polymersomes. As revealed by CLSM, micrometer-sized rods (Figures 3.10A&B) and a few vesicles (Figures 3.10C&D) are observed for both copolymers CS7 and CS10.

3.3.5 Cell viability test

To assess the biocompatibility, the dialyzed aqueous solution of CS10 from nanoprecipitation is employed in cell viability test with MTT as the indicator. The histogram presented in Figure 3.11 declares that the relative viability of the tested cells sustain to be over 80% even with the self-assemblies of CS10 in a concentration of 0.69 mg/mL, which confirms reliable biocompatibility of PCL/PSar copolymers and their self-assembly structures.

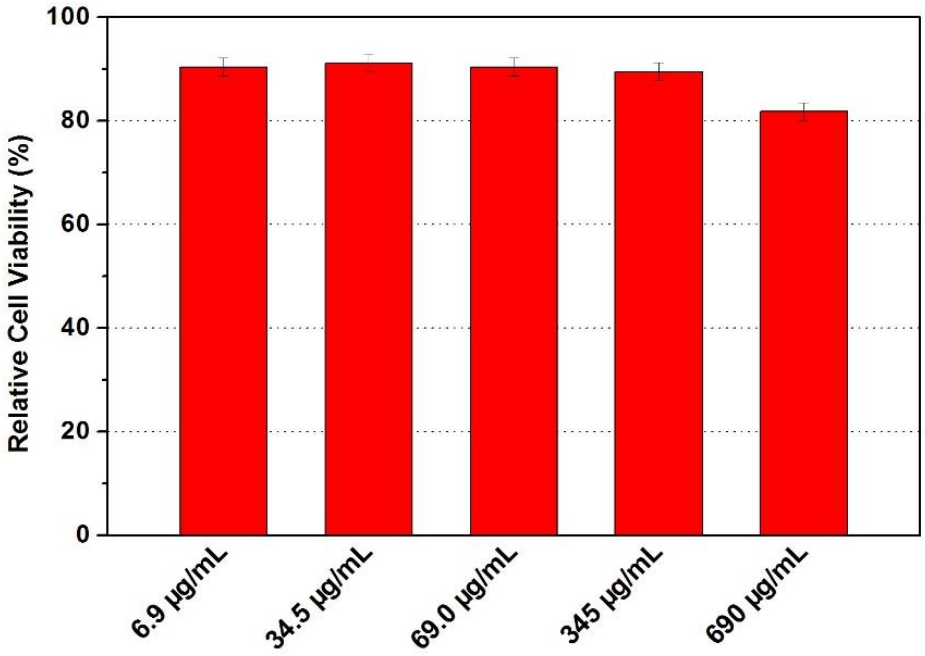

Figure 3.11. Relative cell viability of CS10 for L929 cells after 4 h incubation at 37 ℃ and at concentration of 6.9, 34.5, 69.0, 345 and 690 μg/mL.

3.4 Conclusion

The self-assembly behaviors of two triblock PCL/PSar copolymers CS7 ($PSar_8$-*b*-PCL_{28}-*b*-$PSar_8$) and CS10 ($PSar_{16}$-*b*-PCL_{40}-*b*-$PSar_{16}$) in water are studied in detail using nanoprecipitation and film hydration methods. Large unilamellar sheets and nanofibers (of 8−10 nm in thickness and diameters) are formed by nanoprecipitation at room temperature using DMF/water as co-solvents. A thermal treatment by heating the aqueous suspensions to 65 ℃ transforms the lamellae and fibrous structures into worm-

like cylinders and spheres (of 30−100 nm in diameter). Heating the initial aqueous suspension of nanoprecipitation to 90 ℃ leads multilamellar polymersomes (of 100−500 nm in diameter and 20−50 nm in thickness) coexisting with a few polymer spheres for CS10, while only polymer spheres are obtained for CS7 after heating to 90 ℃. The turbidity measurement as a function of temperature reveals that the morphological transformation starts around the melting point of PCL blocks, suggesting a close connection with the crystalline behavior of PCL and its mobility. A pathway close to Mechanism II of polymersome formation is then proposed, where multilamellar polymersomes are formed by water diffusion into polymer spheres (*i.e.*, bigger and complex micelles) upon thermal treatment. By film hydration method, where a heating treatment at 65 ℃ is performed during the hydration procedure, rod-like particles and a few of giant polymersomes are obtained. The cell viability test on the self-assemblies of CS10 confirms that the PCL/PSar copolymer and self-assembly systems developed in this work are not cytotoxic and suitable for possible applications in biomedical fields.

References

1. Talelli, M.; Barz, M.; Rijcken, C. J. F.; Kiessling, F.; Hennink, W. E.; Lammers, T., Core-crosslinked polymeric micelles: Principles, preparation, biomedical applications and clinical translation. *Nano Today* **2015,** *10* (1), 93-117.

2. Khutoryanskiy, V. V., Beyond PEGylation: Alternative surface-modification of nanoparticles with mucus-inert biomaterials. *Adv. Drug. Deliv. Rev.* **2018,** *124*, 140-149.

3. Malikmammadov, E.; Tanir, T. E.; Kiziltay, A.; Hasirci, V.; Hasirci, N., PCL and PCL-based materials in biomedical applications. *J. Biomat. Sci.-Polym. E.* **2018,** *29* (7-9), 863-893.

4. Sinha, V. R.; Bansal, K.; Kaushik, R.; Kumria, R.; Trehan, A., Poly-epsilon-caprolactone microspheres and nanospheres: an overview. *Int. J. Pharm.* **2004,** *278* (1), 1-23.

5. Ghoroghchian, P. P.; Li, G. Z.; Levine, D. H.; Davis, K. P.; Bates, F. S.; Hammer, D. A.; Therien, M. J., Bioresorbable vesicles formed through spontaneous self-assembly of amphiphilic poly(ethylene oxide)-block-polycaprolactone. *Macromolecules* **2006,** *39* (5), 1673-1675.

6. Adams, D. J.; Kitchen, C.; Adams, S.; Furzeland, S.; Atkins, D.; Schuetz, P.; Fernyhough, C. M.; Tzokova, N.; Ryan, A. J.; Butler, M. F., On the mechanism of formation of vesicles from poly(ethylene oxide)-block-poly(caprolactone) copolymers. *Soft matter* **2009,** *5* (16), 3086-3096.

7. Qi, W.; Ghoroghchian, P. P.; Li, G.; Hammer, D. A.; Therien, M. J., Aqueous self-assembly of poly(ethylene oxide)-block-poly(epsilon-caprolactone) (PEO-b-PCL) copolymers: disparate diblock copolymer compositions give rise to nano- and meso-scale bilayered vesicles. *Nanoscale* **2013,** *5* (22), 10908-10915.

8. Sui, X.; Kujala, P.; Janssen, G.-J.; de Jong, E.; Zuhorn, I. S.; van Hest, J. C. M., Robust formation of biodegradable polymersomes by direct hydration. *Polym. Chem.* **2015,** *6* (5), 691-696.

9. Lee, J. S.; Feijen, J., Biodegradable polymersomes as efficient nanocarriers for controlled paclitaxel delivery. *J. Control. Release* **2010,** *148* (1), E15-E16.

10. Meng, F. H.; Zhong, Z. Y.; Feijen, J., Stimuli-Responsive Polymersomes for Programmed Drug Delivery. *Biomacromolecules* **2009,** *10* (2), 197-209.

11. Hamada, I.; Hunter, A. C.; Szebeni, J.; Moghimi, S. M., Poly(ethylene glycol)s generate complement activation products in human serum through increased alternative pathway turnover and a MASP-2-dependent process. *Molecular Immunology* **2008,** *46* (2), 225-232.

12. Sung, H. J.; Luk, A.; Murthy, N. S.; Liu, E.; Jois, M.; Joy, A.; Bushman, J.; Moghe, P. V.; Kohn, J., Poly(ethylene glycol) as a sensitive regulator of cell survival fate on polymeric biomaterials: the interplay of cell adhesion and pro-oxidant signaling mechanisms. *Soft matter* **2010,** *6* (20), 5196-5205.

13. Birke, A.; Ling, J.; Barz, M., Polysarcosine-containing copolymers: Synthesis, characterization, self-assembly, and applications. *Prog. Polym. Sci.* **2018,** *81*, 163-208.

14. Discher, D. E.; Eisenberg, A., Polymer vesicles. *Science* **2002,** *297* (5583), 967-973.

15. Perez, R. A.; Cordova, M. E.; Lopez, J. V.; Hoskins, J. N.; Zhang, B.; Grayson, S. M.; Mueller, A. J., Nucleation, crystallization, self-nucleation and thermal fractionation of cyclic and linear poly(epsilon-caprolactone)s. *React. Funct. Polym.* **2014,** *80*, 71-82.

16. Groenewoud, W. M., Chapter 1 - Differential scanning calorimetry. In *Characterisation of Polymers by Thermal Analysis*, Groenewoud, W. M., Ed. Elsevier Science B.V.: Amsterdam, 2001; pp 10-60.

17. Battaglia, G.; Ryan, A. J., Bilayers and interdigitation in block copolymer vesicles. *J. Am. Chem. Soc.* **2005,** *127* (24), 8757-8764.

18. Itel, F.; Chami, M.; Najer, A.; Lörcher, S.; Wu, D.; Dinu, I. A.; Meier, W., Molecular Organization and Dynamics in Polymersome Membranes: A Lateral Diffusion Study. *Macromolecules* **2014,** *47* (21), 7588-7596.

19. Uneyama, T., Density functional simulation of spontaneous formation of vesicle in block copolymer solutions. *J. Chem. Phys.* **2007,** *126* (11), 114902.

20. Antonietti, M.; Forster, S., Vesicles and liposomes: A self-assembly principle beyond lipids. *Adv. Mater.* **2003,** *15* (16), 1323-1333.

Chapter 4. Self-Assembly of PMeSPG-Containing Amphiphilic Block Copolymers

4.1 Introduction

With the *N*-substituted structure, the formation of intra- and intermolecular hydrogen bonds can be avoided in polypeptoid chains. Consequently polypeptoids have good solubility in common organic solvents, and thermodynamic behavior close to conventional thermoplastic polymers.[1] These properties give polypeptoids much potential serving as manageable materials for biomedical uses, which is a major advantage of polypeptoids over polypeptides.

For example, in Chapter 1 we introduced the polypeptide vesicles based on polymethionine (PMet). Due to the thioether-containing side chains, PMet stands out with reversible redox responsiveness[2, 3] and capability of functionalization.[4] However, like many other polypeptides, PMet is hard to dissolve in most organic solvents, except for strongly polar solvents like hexafluoroisopropanol and acetic acid. It limits the controllable synthesis of PMet and self-assembly of PMet-containing amphiphilic block copolymers. Most of the current studies on PMet-based polypeptide vesicles are reported by the team of Deming. In their work, $PMet^{O}$ of which the thioethers are oxidized to sulfoxides,[3, 5] and $PMet^{M}$ of which the thioethers are alkylated to a sulfonium ions,[6] are serving as the hydrophilic blocks for vesicle preparation. Only a few reports directly employ PMet as hydrophobic segments in self-assembly for oxidation-responsive applications.[7]

Vesicle preparation methods commonly used, including nanoprecipitation, double emulsion and film hydration, require the copolymers either to be well soluble in organic solvent or to have low T_g and a certain wettability. Thus, amphiphilic block copolymers containing polypeptoids can be self-assembled readily into vesicles if their amphiphilic characters are well balanced. However, only a few works in the literature

described the vesicle preparation of amphiphilic block copolymers containing polypeptoids.[8, 9] In this thesis, we have explored all these techniques, nanoprecipitation, film hydration and double emulsion, to study the self-assemblies of peptoid-containing amphiphilic block copolymers. This chapter describe the self-assembly of poly(*N*-3-(methylthio)propyl glycine) (PMeSPG)-containing amphiphilic block copolymers, including PEG-*b*-PMeSPG and the copolypeptoid PMeSPG-*b*-PSar. Copolymers with different MWs and hydrophilic/hydrophobic ratios are used studied. Cryo-EM, CLSM and optical microscope are employed to characterize the self-assembly structures. Various morphologies including spheres, cylinders, lamellae, vesicles and bicontinuous structures, are observed, which depend on the inherent properties of copolymers and external self-assembly conditions. The mechanism of the self-assembly will be discussed in detail.

4.2 Experimental sections

4.2.1 Materials

DMF (99%, VWR), chloroform (99%, VWR), Nile Red (Sigma Aldrich). The copolymers PEG-*b*-PMeSPG and PMeSPG-*b*-PSar were prepared with the method described in Chapter 2.

4.2.2 Nanoprecipitation

Typically, the copolymer was dissolved in 1 mL of DMF (at 0.5 wt%). A total of 2 mL of deionized milli-Q water was injected slowly to the organic solution under mild shaking (0.2 mL of water per hour to 1 mL of polymer solution). The process of nanoprecipitation was carried out at 25 ℃. The turbid mixtures were then dialyzed against water for 3 days to remove DMF using a Spectra/Por regenerated cellulose membrane with a molecular weight cutoff (MWCO) of 3500.

4.2.3 Film hydration

The copolymers were dissolved in chloroform at 1 wt% concentration (0.01 wt % fluorescent dye was added in some cases, for CLSM observation), and deposited on the surface of roughened Teflon. The polymer films were then dried for > 4 h under vacuum and rehydrated in 20 mL water. The samples were subsequently sealed and heated at 70 ℃ for 48 h.

In electroformation method, 20 μL chloroform solution of copolymer at 0.5 wt% was deposited on the conductive side of an ITO slide. The solution was averagely spread and the solvent was removed by vacuum pump for 1 h, thus a thin film was formed. A rubbery ring was put around the formed layer and 750 μL water was added inside the ring. The second ITO slide was put on the ring with the conductive side downsides. An alternating electric field with amplitude at 6 V, frequency at 10 Hz was applied on the chamber, and the temperature was set at 50 ℃.

4.2.4 Double emulsion

In a typical self-assembly preparation through double emulsion, 1 mL copolymer solution was prepared at 0.5 wt% concentration, and followed by addition of 10 μL water, then mixed by the homogenizer ULTRA-TURRAX T25, at the rate of 20000 rpm for 5 min, to prepare W/O inverse emulsion. 300 μL W/O emulsion was transferred to 3 mL water, and dispersed by the homogenizer at 5000 rpm, for 1 h. The obtained W/O/W double emulsion was heated at 50 ℃ with stirring (around 500 rpm) for 36 h, to remove chloroform by evaporation, leading to the formation of self-assemblies.

4.2.5 Characterizations

Differential scanning calorimetry (DSC) analyses were performed on a TA Q200 instrument. The synthesized polymers were heated from 0 to 170 ℃ at a rate of 20 ℃/min under a nitrogen purge.

Cryo-EM experiments were conducted in INSERM U1196, Institut Curie, in collaboration with Sylvain Trepout. A total of 5 μL of samples were deposited onto a 200 mesh holey copper grid (Ted Pella Inc., U.S.A.) and flash-frozen in liquid ethane cooled down at liquid nitrogen temperature. The images were acquired on a JEOL 2200FS energy-filtered (20eV) field emission gun electron microscope operating at 200 kV using a Gatan ssCCD 2048 × 2048 pixels. Energy-filtered (Zero-loss) cryo-electron tomography images were collected at 12000x (corresponding pixel size 0.8 nm) from -64 ° up to 64 ° using a Saxton scheme (1 ° at high tilts and 2 ° at low tilts).

Optical microscopic images were obtained from a Motic PM1820 microscope with widefield eyepieces WF10 ×/18mm and achromatic objectives EA 10 × and 40 ×.

CLSM images were obtained with Leica TCS SP5 confocal scanning system equipped with the HeNe 543 nm laser and 63 × oil immersion objective.

The hydrodynamic diameters of the nanoparticles were measured by DLS, using a particle size analyzer (Zetasizer Nano Series, Malvern Instruments) at 25 ℃. The measurements were made at a fixed angle at 90 ° and a wavelength of 657 nm.

Small angle neutron scattering (SANS) experiments were conducted at Orphée reactor in Léon Brillouin Laboratory (CEA Saclay) in collaboration with Annie Brûlet. Small angle neutron scattering monitors were conducted on PAXY and PACE, two devices giving access to monochromatic neutron beams. The neutrons were produced from uranium fission. The polymer sample was dissolved in deuterium oxide (D_2O). The neutron beam was emitted through the sample, and after the diffusion, neutrons are detected by a 2D detector filled with BF_3 gas. The detector has an area of 64 × 64 cm^2, consisting of 15500 5 × 5 mm^2 cells. This gives access to the neutron scattering intensity as a function of the scattering angle θ, and scattering vector Q ($Q = 4\pi sin\theta/\lambda$). The obtained values of I and Q are fitted with the Correlation Length Model (SasView.org) to give the fitting curves.

4.3 Results and discussion

4.3.1 Self-assembly of PEG-*b*-PMeSPG by nanoprecipitation

As obtained from ROP of MeSPG-NTA initiated by PEG_{2k}-NH_2, the copolymers EM1 (PEG_{45}-*b*-$PMeSPG_{17}$), EM2 (PEG_{45}-*b*-$PMeSPG_{40}$) and EM3 (PEG_{45}-*b*-$PMeSPG_{71}$) with different MWs and hydrophilic/hydrophobic ratios (Table 4.1) are applied in nanoprecipitation, where water is added dropwise into the copolymer/DMF solution. Cryo-EM is utilized to visualize the self-assembly structures from the samples after dialysis, and the results are present in Figure 4.1. Spheres with diameters around 20−90 nm are majorly obtained from EM1 (Figure 4.1A−C). Along with the spheres, a few unilamellar vesicles are also obtained (as pointed in Figure 4.1A−C), with diameters around 50−130 nm, and membrane thickness around 9 nm. EM2 forms densely dispersed micelles, with spherical and worm-like shapes, and diameters around 18−22 nm (Figure 4.1D−F). EM3 has the largest MW (12300 Da) and lowest hydrophilic ratio (16%) in these three copolymers, and in its self-assembly result, polymersomes are found with broad size distribution (diameters: 50−550 nm) and membrane thickness around 12−14 nm (Figure 4.1G−I). Simultaneously, lamellae are formed along with vesicles, and many of them are in a disk-like shape. Lamellae also have a diversity of size, with diameters in the range of 250−2000 nm. Through the measurement in the folded place of a lamella (Figure 4.1I), the thickness is found to be around 12 nm, close to that of membrane thickness of the vesicles. Figure 4.2 shows the DLS results of EM1−EM3. The hydrodynamic diameters and size distributions revealed by DLS correspond well with the visualized self-assembly structures in cryo-EM.

According to the self-assembly morphologies, the packing parameter (p) can be estimated of the three copolymers. EM1 has $p \leq 1/3$, since spherical nanoparticles are majorly formed; for EM2 it is supposed to be $1/3 \leq p \leq 1/2$, with the formation of ubiquitous cylindrical and worm-like micelles; while EM3 has $1/2 \leq p \leq 1$, as vesicles

and lamellae being the majorities. In Figure 4.1I four vesicles with irregular shapes are found inside a folded lamella, seeming like "embryonic" vesicles being generated from the enclosure of lamellae. Combing with the similarity in bilayer thickness between vesicles and lamellae, the vesicles formed by EM3 are considered to be formed through the Mechanism I, where lamellae close up into vesicles. While for the small number of vesicles from EM1, no lamella is found in the self-assembly structures, therefore it is very possible that the vesicles are formed in a close way to Mechanism II, where water diffuses into polymeric spheres, leading to the formation of vesicles with a aqueous cavity.

Table 4.1. Molecular information of the copolymers EM1−EM3.

Sample	Structure [a]	$f_{PEG,wt}$ [a]	$M_{n,\ NMR}$ [a]	$M_{n,\ GPC}$ [b]	$Đ$ [b]
EM1	PEG_{45}-*b*-$PMeSPG_{17}$	45%	4400	3600	1.14
EM2	PEG_{45}-*b*-$PMeSPG_{40}$	26%	7700	4900	1.19
EM3	PEG_{45}-*b*-$PMeSPG_{71}$	16%	12300	7700	1.15

[a] DPs, MWs and PEG weight ratios ($f_{PEG,wt}$) are calculated from the integrals in ^{1}H-NMR spectra; [b] Determined by GPC in 0.01 M LiBr/DMF, with rate at 1 mL/min, PEG as standard.

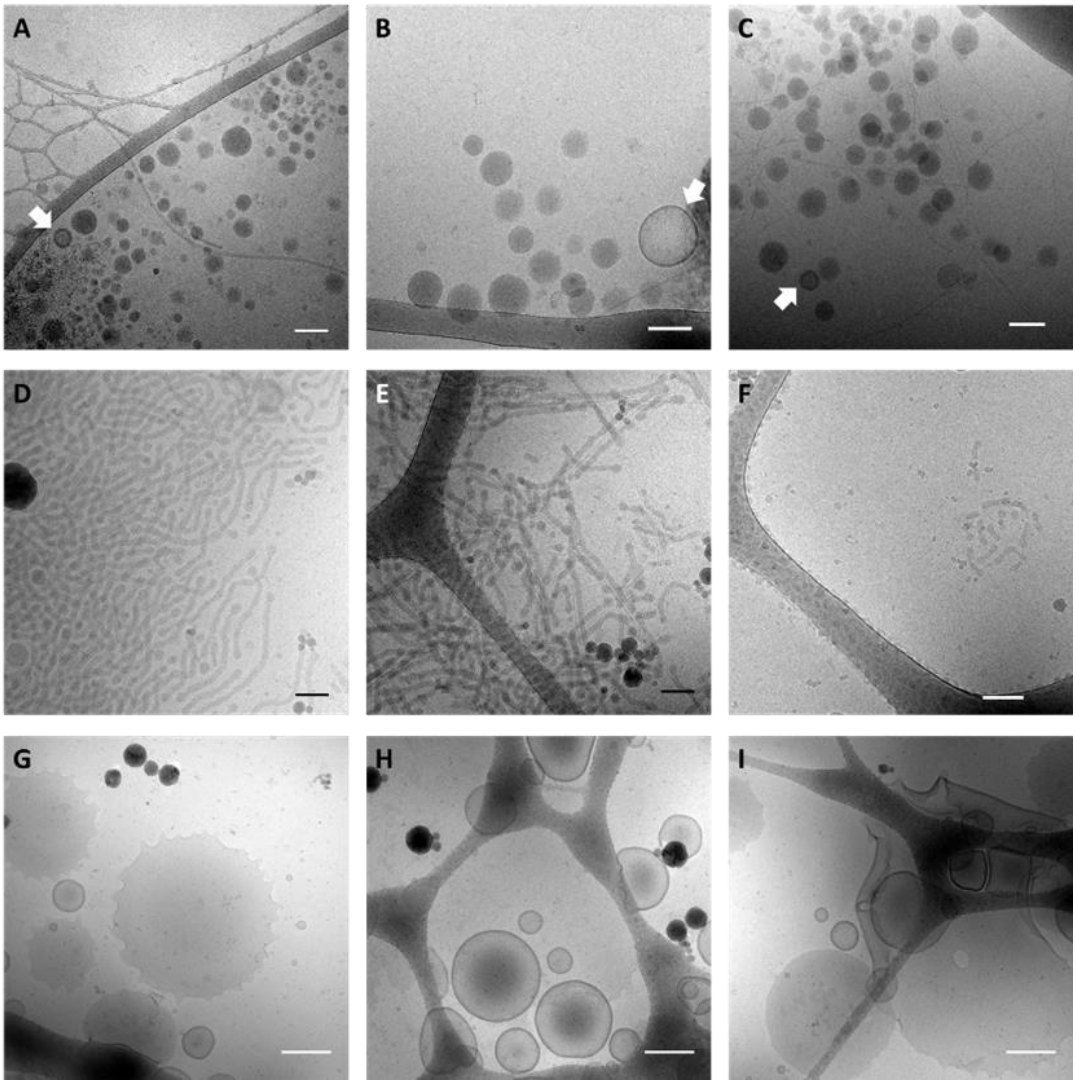

Figure 4.1. Cryo-EM images of self-assemblies of (A−C) EM1, (D−F) EM2 and (G−I) EM3 through nanoprecipitation. Scale bar = 100 nm for A−F; scale bar = 300 nm for G−I.

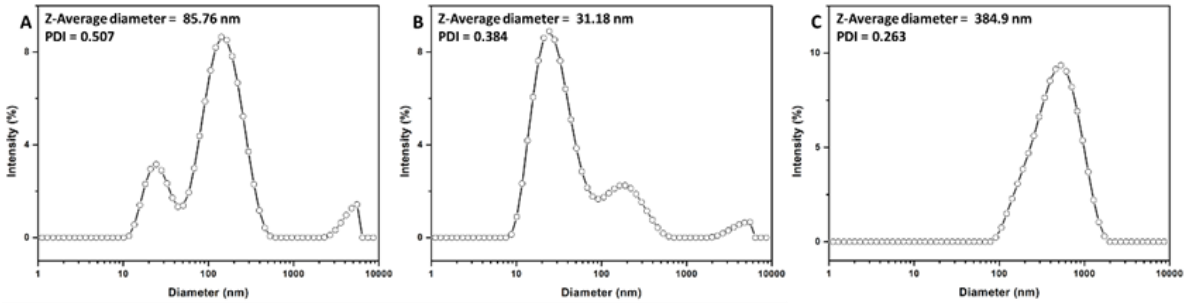

Figure 4.2. DLS results of (A) EM1, (B) EM2 and (C) EM3.

4.3.2 Self-assembly of PMeSPG-*b*-PSar by nanoprecipitation

Table 4.2. Molecular information of PMeSPG-*b*-PSar copolymers.

Sample	Structure [a]	$f_{PSar,\ wt}$ [a]	$M_{n,\ NMR}$ [a]	$M_{n,\ GPC}$ [b]	$Đ$ [b]
MS1	$PMeSPG_{45}$-*b*-$PSar_{65}$	41%	11200	15400	1.20
MS2	$PMeSPG_{60}$-*b*-$PSar_{50}$	29%	12300	15100	1.21
MS3	$PMeSPG_{75}$-*b*-$PSar_{25}$	14%	12700	17600	1.20

[a] DPs, MWs and PSar weight ratios ($f_{PSar,wt}$) are calculated from the integrals in ^{1}H-NMR spectra; [b] Determined by GPC in 0.01 M LiBr/DMF, with rate at 1 mL/min, PEG as standard.

With the same conditions conducted on EM copolymers, nanoprecipitation is also performed on the PMeSPG-*b*-PSar copolymers MS1 ($PMeSPG_{45}$-*b*-$PSar_{65}$), MS2 ($PMeSPG_{60}$-*b*-$PSar_{50}$) and MS3 ($PMeSPG_{75}$-*b*-$PSar_{25}$), with different hydrophilic/hydrophobic ratios (Table 4.2). Cryo-EM is also employed to analyze the self-assembly samples. As revealed in Figure 4.3, polymersomes are generated from all the three copolymers.

With a relatively high weight percentage of PSar (41.4%), MS1 is found to form a quantity of little spheres sized around 10 nm and a number of disk-like lamellae ranging from 200 nm to 1 μm (Figure 4.3A). Vesicles are recorded neighboring lamellae, and majorly around 100−250 nm in diameter, with membrane thickness around 11−14 nm (Figure 4.3B&C). However, besides spherical vesicles, some membrane structures with irregular shapes are worth being noted. As dashcircled in Figure 4.3B, an unclosed octopus-like structure is clearly captured. Worm-like micelles are formed at the open edge, like the “arms” of the “octopus”. The “octopus” has a membrane thickness around 14 nm, close to that of vesicles, which implies an intermediate structure during the procedure where lamella encloses to form vesicle, as

described in the Mechanism I. Moreover, two vesicles pointed in Figure 4.3C are found to form a stomatocyte-like structure, in which the membrane is budding inversely.

Diverse morphologies are also observed in MS2 (Figure 4.3D−F). Along with spherical micelles around 10 nm, most of vesicles are found with diameters around 300−900 nm, membrane thickness around 11−13 nm. Compared with MS1, the vesicles formed by MS2 have not only bigger size, but also more irregular shape. The vesicles are basically non-spherical. For instance, Figure 4.3E shows a vesicle with a twisted tube-like structure, and more interestingly, a crescent-like vesicle is recorded in Figure 4.3F, with a curved shape and two end-points.

What is more striking is the self-assembly formed by MS3 (Figure 4.3G−I), which has a very low PSar weight ratio around 14%. Aggregates sized 200−1000 nm take the majority, which are a mixture of spheres, vesicles, lamellae and inverted bicontinuous structures. Vesicles have a membrane thickness of 16−18 nm, and like MS1, are often captured in company with lamellae (Figure 4.3G&H). However, different from disk-like lamellae observed in MS1, the lamellar structure of MS3 are more complicated. They have wide coverage, and are often found to form a circle and surround a vesicle (Figure 4.3G). Porous and network-like structures are observed and suspected coming from lamellae (Figure 4.3H). Moreover, a large compound sponge-like structure is found with an inverted bicontinuous shape (Figure 4.3I). It has holes on the surface, while inside of the structure is a network-like labyrinth.

The nanoprecipitated self-assembly structures of MS1−MS3 exhibit nonergodic characteristics. In the self-assembly result of one sample, various structures including spherical micelles, lamellae, and vesicles are formed simultaneously, and the vesicles exhibit a diversity of shapes, rather than uniform spherical structure. According to the intermediate structure shown in Figure 4.3B, it is very possible that the vesicles are formed by the route of Mechanism I, where amphiphilic block copolymers firstly assemble into spherical micelles rapidly, which then slowly evolve into cylindrical

micelles and open lamellae by collision. To compensate the energy loss due to the interfacial tension effects (edge energy), the large lamella overcomes the bending energy and encloses like a pulled bag (Figure 4.3B). In the process of morphological evolvement towards vesicle formation, including the collision of micelles, the enclosure of lamella, and the shape adjustment of vesicles, all involve the rearrangement of copolymers. Due to the relatively high MWs and low mobility of copolymers, kinetic barriers lie in the way of self-assembly formation and evolution towards the global equilibrium state. As a certain case in nanoprecipitation procedure, the copolymers aggregate as the water content increases, while their mobility decreases at the same time. When the water content reaches a certain level, the mobility of copolymer can be insufficient to promote further transition to the global equilibrium state, but leaves the self-assemblies trapped midway, forming the coexistence of various metastable morphologies, including intermediate structures. It is also called as a “kinetically frozen” situation.

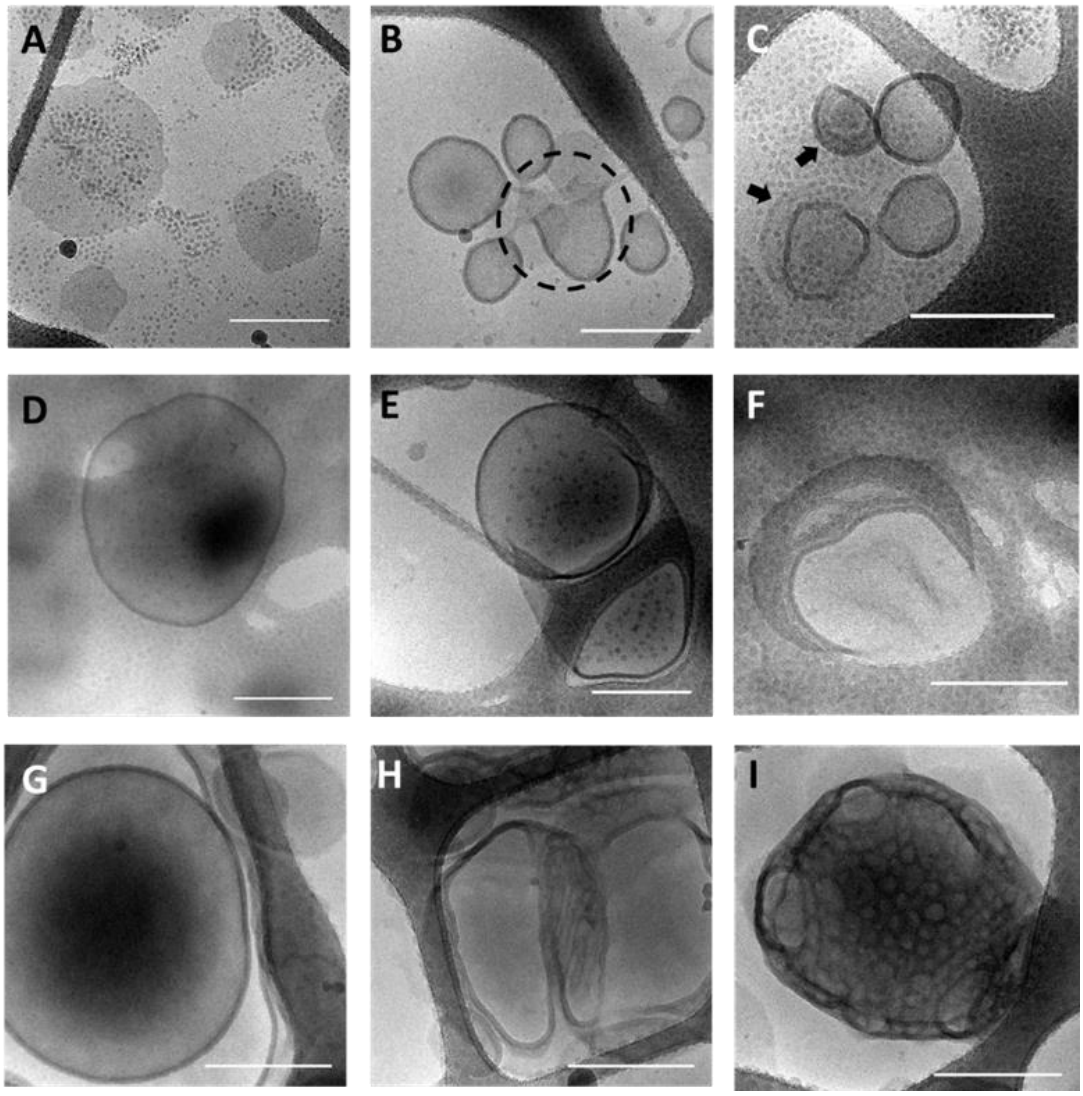

Figure 4.3. Cryo-EM images of self-assemblies of (A−C) MS1, (D−F) MS2 and (G−I) MS3 through nanoprecipitation. Scale bar = 300 nm.

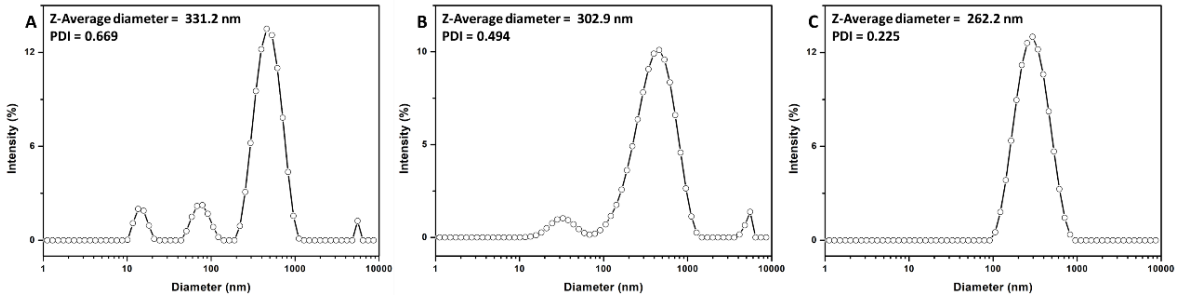

Figure 4.4. DLS results of (A) MS1, (B) MS2 and (C) MS3.

4.3.3 Behavior of PSar in water

The nanoprecipitated results differ significantly between PEG-*b*-PMeSPG and PMeSPG-*b*-PSar. Especially the copolymers EM3 (PEG_{45}-*b*-$PMeSPG_{71}$) and MS3 ($PMeSPG_{75}$-*b*-$PSar_{25}$), which have similar MWs and hydrophilic ratios, but obtain very different self-assembly results: EM3 forms vesicles and lamellae, which are majorly in spherical and disck-like shapes, respectively, while MS3 forms a mixture of large vesicles, lamellae, bicontinuous structures and intermediate structures. Obviously the difference lies between the hydrophilic segments PEG and PSar, which constitute the corona of self-assembly structures. The conformation and behavior of hydrophilic segments in water can influence the resulted morphology.

To study the chain conformation of PSar in water, small angle neutron scattering (SANS) is performed on the deuterium oxide (D_2O) solutions of PSar homopolymers, where a neutron beam is emitted through the solution, with the scattering intensity *I* and scattering vector *Q* (the momentum transferred from scattering angle θ, as $Q = 4\pi sin\theta/\lambda$) recorded. The analyzed PSar samples PSA1−4 are listed in Table 4.3, and the values of *I* obtained from different *Q* are plotted in Figure 4.5, which are obtained from the experiments on solutions with concentration at 10 g/L, respectively at 20 ℃ and 40 ℃.

Table 4.3. Molecular information of homopolymer PSar in SANS

Sample	Initiator	DP [a]	M_n [a]	$Đ$ [b]
PSA1	n-hexylamine	35	2500	1.13
PSA2	n-hexylamine	75	5400	1.15
PSA3	$Y(BH_4)_3$	171	12200	1.16
PSA4	$Y(BH_4)_3$	389	27700	1.22

[a] DPs and MWs are calculated from the integrals in ^{1}H-NMR spectra; [b] Determined by GPC in 0.05 M LiBr/DMF, with rate at 1 mL/min, PS as standard.

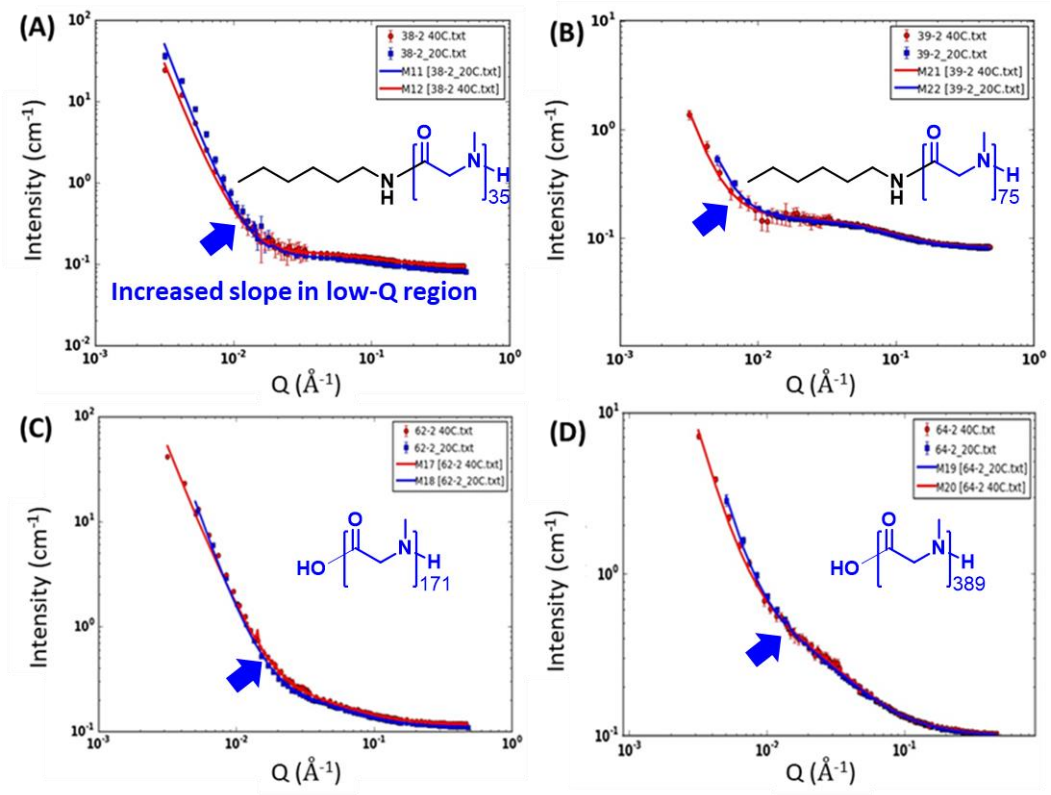

Figure 4.5. The plots and fitting curves of scattering intensity in function of scattering vectors (Q) of (A) PSA1, (B) PSA2, (C) PSA3 and (D) PSA4, obtained from SANS on polymer/D_2O solutions (10 g/L), respectively at 20 ℃ (blue) and 40 ℃ (red).

In SANS, the relation between I and Q can be termed as an empirical functional form below:

$$I(Q) = \frac{A}{Q^n} + \frac{C}{1 + (Q\xi)^m} + B$$

In this function, the first term describes Porod scattering from clusters (exponent = n), and the second term is a Lorentzian function describing scattering from polymer chains (exponent = m). The second term represents the polymer/solvent interactions and therefore the thermodynamics. The two multiplicative factors A and C, the incoherent background B and the two exponents n and m are used as fitting parameters. The final parameter ξ is a correlation length for the polymer chains. In the curve of $I(Q)$ *vs* Q, the high-Q region (> 0.01) characterizes the polymer chains, while the low-Q region (< 0.01) characterizes the size of clusters. The plots in Figure 4.5 are fitted with

function above, obtaining the corresponding curves. All the curves have an obvious ascent with increased slope, when entering the low-Q region. The ascent in low-Q region implies the formation of clusters. As obtained from the fitting curves, the fitting parameters are listed in Table 4.4. In the range of test, temperature has very few impacts on the parameters, and the results obtained from 20 ℃ and 40 ℃ are very close. The coefficient m is around 2, and is as low as 1.7 for PSA4 with relatively high MW. The coefficient n which indicates clusters is close to 4 for PSA1 and decreases to 2.7 for PSA4. The multiplicative factors A increases as the MW increases. According to the parameters, we can conclude that aggregations are formed for all the samples, and PSar with higher MW forms cluster with bigger size, but lower compactness. The correlation length ξ is around 8.7 Å for PSA1, and increases along with MW, reaching around 36.6 Å for PSA4. The radius of gyration R_g is given by $R_g = \sqrt{2}\xi$. As the calculated results, R_g = 12.7 Å for PSA1 and R_g = 51.8 Å for PSA4. As the comparison, the R_g of PEG with MW at 1730 and 23800 are respectively 16 Å and 43 Å, which are obtained from SANS conducted on the PEG/D_2O solutions of 12 g/L.[10] PSar and PEG have comparable chain size, however, aggregations exist in PSar/D_2O solution, which is actually the major difference between PSar and PEG.

To further exploit the behavior of PSar in water, the aqueous solutions of the four samples are analyzed by DLS, to measure the hydrodynamic radii (R_h). The ratio $\rho = R_g/R_h$ can be used to estimate the state of polymer in a solution. When polymers form dispersed single-chain coils in a solution, R_g is often larger than R_h, and we have $\rho > 1$; when aggregates are formed in a solution, R_h is larger than R_g, and ρ is as smaller as more compact the aggregated particles are.[11] As revealed in Figure 4.6, the polymers PSA1−3 all show signal peaks with $R_h \sim 100$ nm. The R_h obtained from PSA4 is smaller, but is still around 10 nm, larger than the calculated R_g (5.18 nm). The existence of clusters is implied. As the comparison, three PEG samples with MWs respectively at 2000 Da, 3300 Da and 5000 Da are also dissolved in water and analyzed by DLS (Figure 4.7). The obtained R_h are respectively 1.3 nm, 0.9 nm and 0.9 nm, all in a

reasonable region (as theoretically predicted,[12] in a good solvent, $R_h = 0.64R_g$). The results of PEG are supported by reference,[13] where the R_h of PEG in water is reported to be measured by DLS, in the form of single-chain coil. According to the SANS and DLS results, the water-solubility of PSar need to be revisited. Generally, PSar is hydrophilic and can be used as the hydrophilic block in self-assembly studies,[14] however, in the molecular level, the polymer chains of PSar are not totally solvated by water, but form clusters instead, which might be caused by the polarity difference between PSar and water. The comparison among PSar samples reveals another aspect. For PSA1 and PSA2, which were synthesized by the initiation of n-hexylamine, have more tendency to aggregate than PSA3 and PSA4, which were obtained from rare-earth-catalyzed polymerization. PSA3 with DP at 171 showed more aggregation than PSA4 with DP at 389. PSA1 and PSA2 have a hydrophobic end-group, while PSA3 and PSA4 do not. It suggests that the behavior of PSar in water is very sensitive to the end-group structure, a small hydrophobic "tail" can induce the aggregation. For polymers without the "tail", aggregation can be weakened along with the increase of DP, and might be eventually avoided with enough chain length.

The water-solubility of PSar is a reason for the morphological differences between PEG-*b*-PMeSPG and PMeSPG-*b*-PSar self-assemblies, and is also probably responsible for the low mobility of copolymers in water, causing the obvious nonergodicity of PMeSPG-*b*-PSar self-assemblies.

Table 4.4. The parameters of fitting curves obtained from the SANS of PSA1−4.

Sample	M_n	Temperature (℃)	*A*	*m*	*C*	*ξ* (Å)	*n*	*B* (cm^{-1})
PSA1	3500	40	2.25E-08	3.6	0.0468	8.7	2.1	0.09240
		20	8.57E-09	3.8	0.0426	8.7	2.1	0.08078
PSA2	5400	40	9.07E-09	3.2	0.0725	12.8	2.1	0.08204
		20	2.60E-08	3.1	0.0691	12.8	2.1	0.08069

PSA3	12200	40	2.22E-06	2.9	0.0827	14.2	2.1	0.11639
		20	8.98E-07	3.1	0.0816	14.2	2.3	0.10965
PSA4	27700	40	1.39E-06	2.6	0.3429	36.6	1.8	0.10046
		20	1.27E-06	2.7	0.3272	36.6	1.7	0.09876

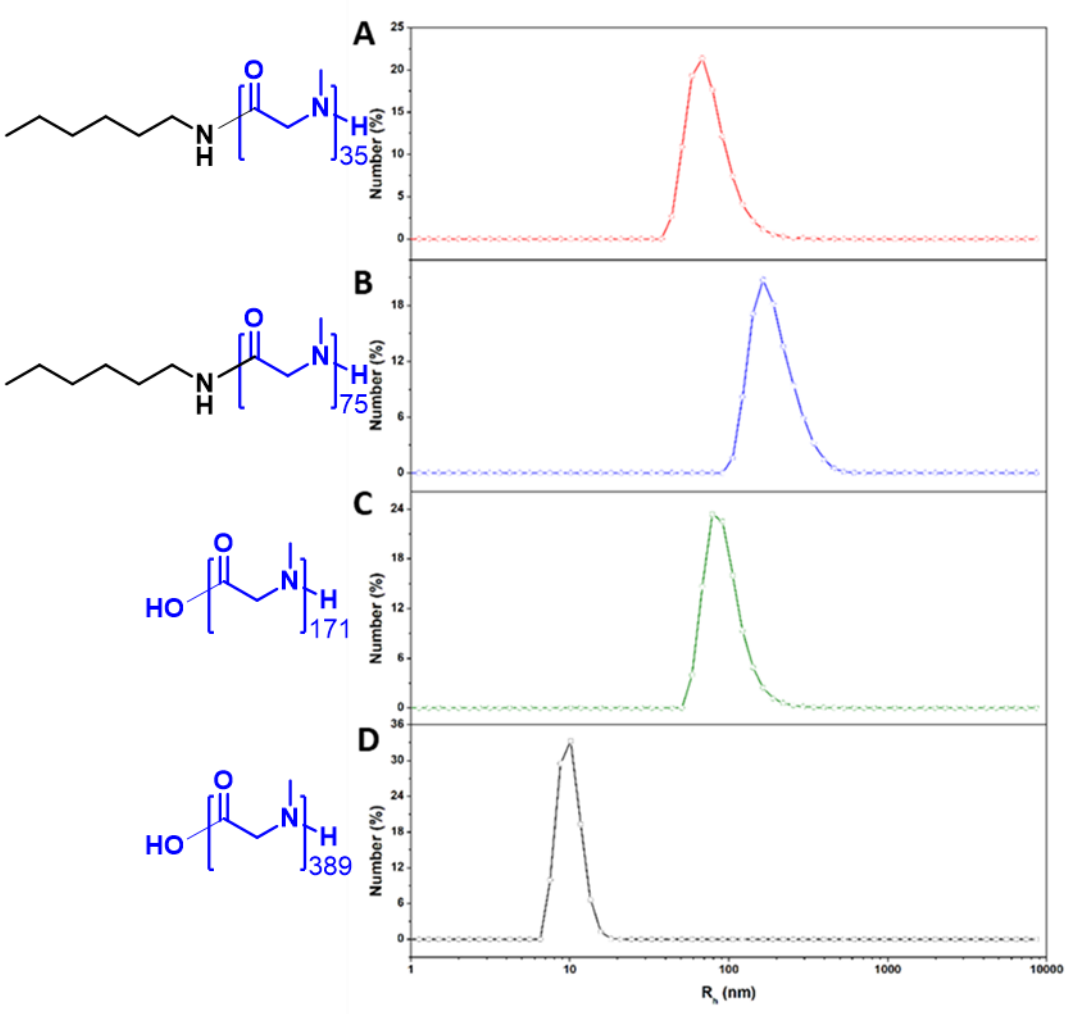

Figure 4.6. DLS results of PSar homopolymers (A) PSA1, (B) PSA2, (C) PSA3 and (D) PSA4 in water

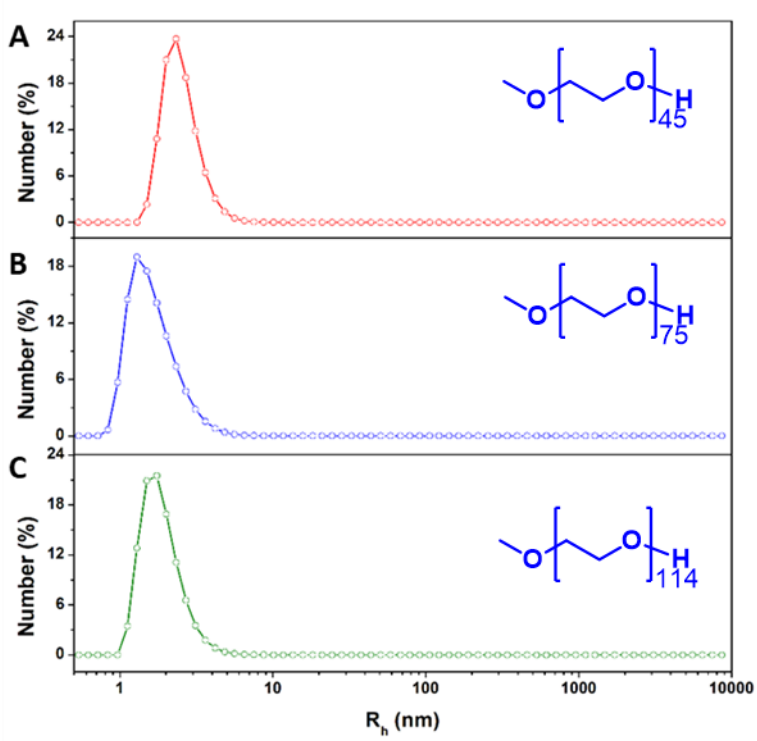

Figure 4.7. DLS results of PEG with MW at (A)2000, (B) 3300 and (C) 5000 in water.

4.3.4 Self-assembly of PMeSPG-*b*-PSar by film hydration.

As the hydrophobic part, PMeSPG is also investigated on its properties. The thermodynamic behavior of PMeSPG with different DPs is analyzed by DSC (Figure 4.8). During the first cycle of heating treatment at rate of 20 ℃/min, the PMeSPG polymers with DPs at 45, 58 and 85, are respectively found with a glass transition temperature (T_g), at 23.2 ℃, 26.8 ℃ and 27.0 ℃, and a melting temperature (T_m), at 132.1 ℃, 138.2 ℃ and 141.2 ℃. According to former studies,[15-17] T_g is attributed to the glass transition of the polypeptoid backbone, while T_m comes from the melting of incomplete crystals formed by the backbone. It could be concluded that with DP at 45−85, PMeSPG polymer is a semi-crystalline solid at room temperature, while the amorphous part is in glass transition state (15−35 °C). As an interesting consequence, PMeSPG polymer is generally at an intermediate state between glassy (*e. g.* polystyrene (PS)[18] with T_g > 95 ℃) and rubbery (*e. g.* polybutadiene (PBD)[19] with T_g < 0 ℃).

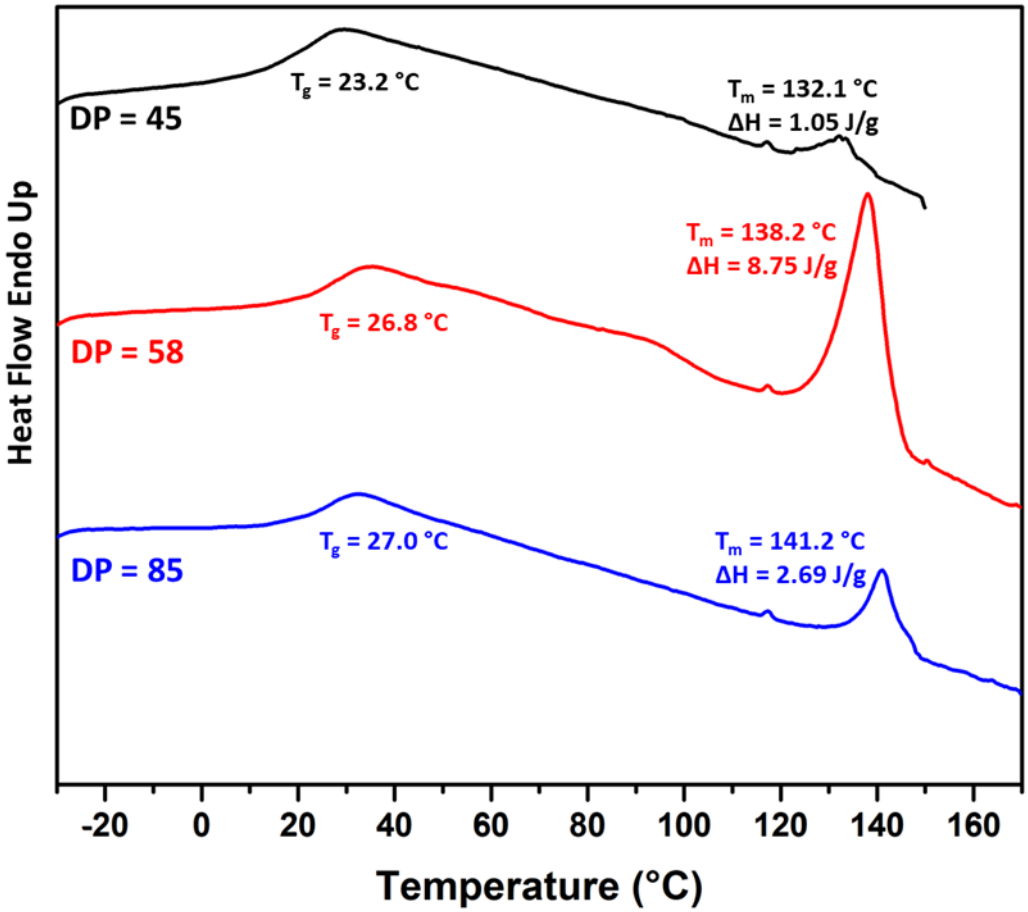

Figure 4.8. DSC thermograms of the first heating scan of PMeSPG samples with DPs at 45 (black), 58 (red) and 85 (blue), recorded at 20 ℃/min.

The thermodynamic properties of PMeSPG remind us the possibility in self-assembly methods involving heating treatment. The results from Chapter 3 suggest the effects of heating treatment with temperature above T_m and T_g, to improve mobility of copolymers, promoting the evolvement of self-assemblies towards the global equilibrium state. PMeSPG has a T_m above 100 ℃, however, it has a *N*-substituted polyglycine backbone, which is the same as that of PSar, and is water-soluble. Hence PMeSPG can be partially solvated in water, which as a result makes the crystallinity and T_m decline. Heating treatment could be employed to accelerate and control the self-assembly procedure of PMeSPG-*b*-PSar. As a commonly used method to direct the formation of micrometer-sized vesicles,[20-23] film hydration is used in self-assembly study. MS1−MS3 are applied with film hydration method, where the Teflon plate

deposed with film of 2 mg copolymer and 20 μg Nile Red are incubated in 20 mL water at 70 ℃ for 48 h. The temperature is higher than their T_g (15−35 °C) in bulk state.

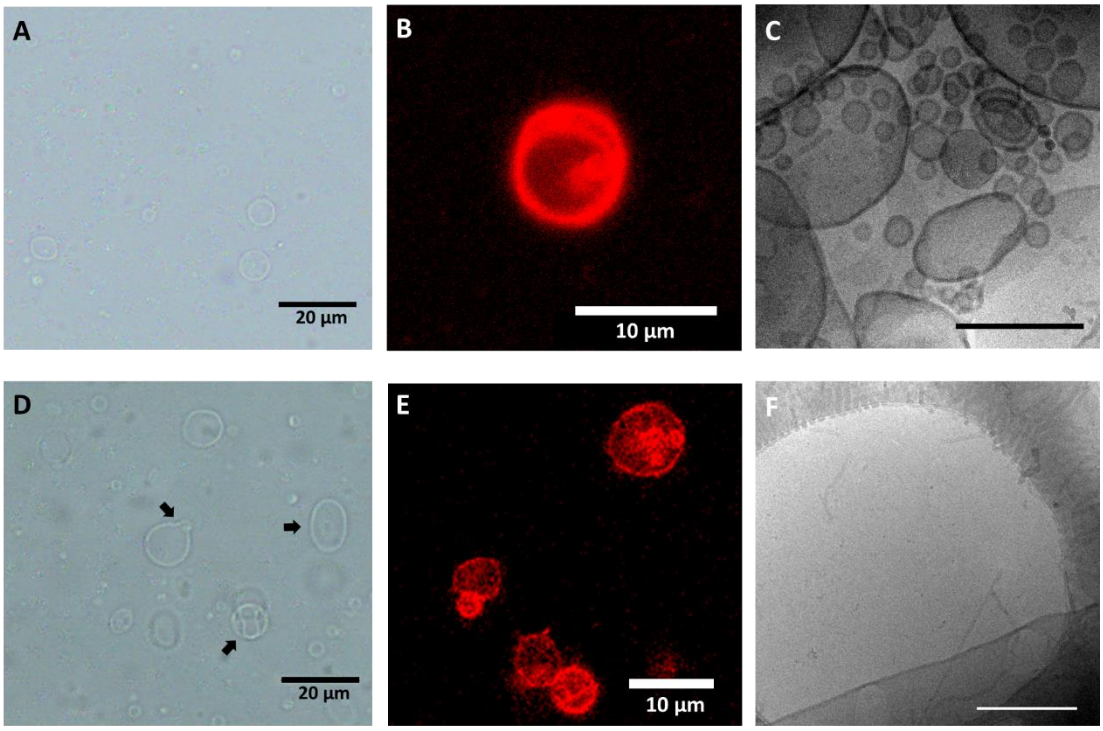

Figure 4.9. Bright-field optical microscopic (A, D), CLSM (B, E) and cryo-EM (C, F) images of self-assemblies from MS1 (A−C) and MS2 (D−F), by film hydration with 48-h heating treatment at 70 ℃. Scale bar = 300 nm for C and F.

After 48-hour heating, the incubated aqueous samples turned slightly turbid pink for MS1 and MS2. As observed under optical microscope and CLSM (Figure 8A, B, D and E), MS1 and MS2 are both found with micrometer-sized vesicles, but nothing is found for MS3. It is believed the film of MS3 is not rehydrated successfully, probably attributed to its relatively low hydrophilic ratio ($f_{PSar,\,wt}$ = 14%). The productive samples, MS1 and MS2, have some differences from each other and from the previous nanoprecipitated samples in morphology. Many spherical vesicles sized 2−8 μm are observed from MS1 under optical and confocal microscope (Figure 4.9A&B), while cryo-EM reveals the widely distributed vesicles ranging from 30 nm to 1 μm with membrane thickness 10−13 nm, along with some lamellae. No spherical micelle or unclosed intermediate is found. The small vesicles below 100 nm maintain a round

shape, while more ellipsoidal shapes are present from the large vesicles. MS2 vesicles shows more irregular shapes sized 2−10 μm, polymersomes with budding, inverse budding and ellipsoidal shapes are captured from optical and confocal microscope (Figure 4.9D&E, pointed in Figure 4.9D). While in nanoscale, nearly no vesicle under the size of 2 μm is found. Accompanied with giant vesicles (downright in Figure 4.9F, membrane thickness ~ 11 nm) are ubiquitous worm-like micelles with diameter at 11−13 nm, and some lamellae (Figure 4.9F).

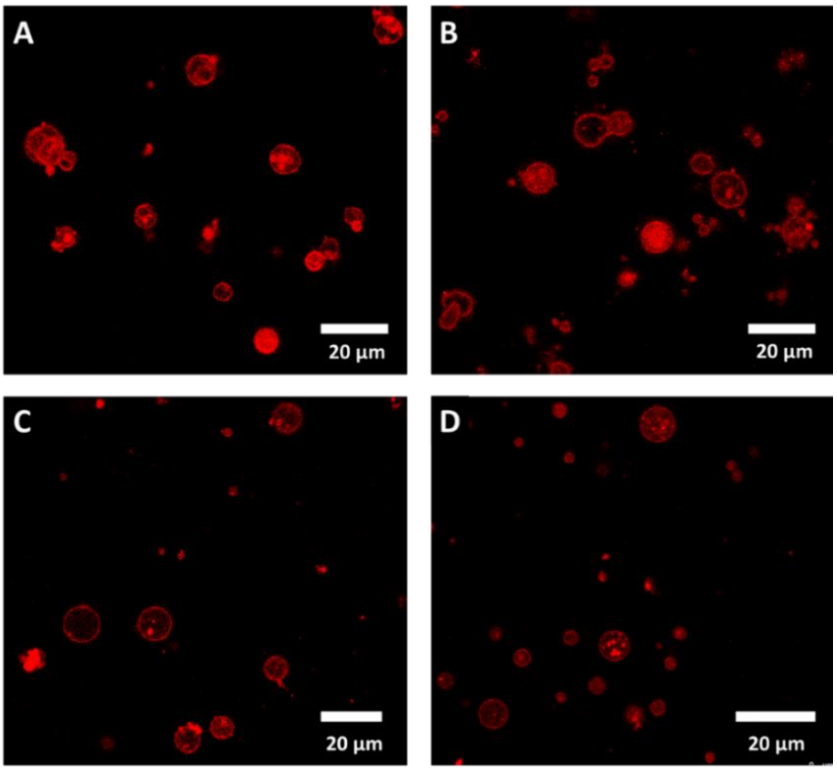

Figure 4.10. CLSM images of MS2 film hydration sample after (A) 48 h, (B) 72 h, (C) 144 h and (D) 168 h of heating treatment at 70 ℃.

Compared with the ubiquitous vesicles from MS1, the self-assembly results of MS2, including irregularly shaped vesicles and worm-like micelles, have obviously higher nonergodicity. On the one hand, self-assembly of block copolymers is a time-consuming procedure. The “frozen” intermediates and irregularly shaped vesicles are possibly still transforming but at a slow rate. On the other hand, the nonergodic morphologies imply that a wide range of structures could be formed by the same block

copolymer, and it is potentially controllable by the conditions of preparation.[24-26] To verify the morphological control in film hydration, the heating treatment is extended to a week for MS2, and the morphological changes are followed in the long term. As revealed in Figure 4.10, compared with the morphologies of samples after 48 h (Figure 4.10A) and 72 h (Figure 4.10B) of heating, the samples heated over 144 h (Figure 4.10C&D) have mostly spherical shapes, showing a tendency towards the equilibrium state, which is achieved by the extended heating treatment.

With close relation to conventional film hydration method, electroformation is another hydration approach to prepare vesicles, which is also developed from the fabrication of giant liposomes.[27, 28] Block copolymers such as PB-*b*-PEO and PMOXA-*b*-PDMS-*b*-PMOXA have been reported to form giant polymersomes via electroformation.[21, 29, 30] Herein the electroformation is employed in the self-assembly of MS1. A sealed chamber full of water is constituted by two ITO slides, with one side deposited with the thin film of copolymers on the conductive side. An AC field of 6 V and 10 Hz is applied to the chamber at 50 ℃. The aqueous sample from 120-min treatment of electroformation is characterized. Unfortunately no giant vesicle beyond 1 μm can be observed under optical microscope. While the further characterization with cryo-EM indeed find vesicles and other structures in nanoscale, including spherical micelles, worm-like micelles and lamellae (Figure 4.11). Showing a large diversity, vesicles with spherical, ellipsoidal, tube-like and vesicle-in-vesicle structures are observed, in Figure 4.11C we can even find a twisted vesicle with a snake-like shape. The electroformation sample demonstrates a primary state of the self-assembly structures from the swelling of films. According to the work of Battaglia and Ryan,[23] multilamellar tube-like “myelin” structures are firstly formed from the rehydrated film, and vesicles are generated from the destabilization of “myelin” structures. Compared with heating treatment, the conditions in electroformation are possibly not strong enough to push the “myelin”-mediated transition from film to vesicles in a complete way, resulting in the observed metastable structures with various morphologies.

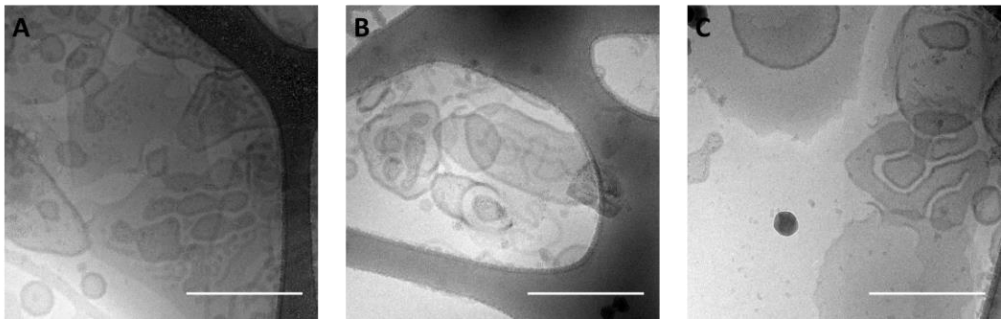

Figure 4.11. Cryo-EM images of MS1 self-assembly structures from 120-min treatment of electroformation, applied with an AC field of 6 V and 10 Hz, at 50 ℃. Scale bar = 300 nm.

4.3.5 Self-assembly of PMeSPG-*b*-PSar by double emulsion.

The film hydration method for polymersomes, however, can only yield a low concentration of self-assemblies (below 0.01 wt %, compared with 0.1 wt % for nanoprecipitated samples after dialysis), and is unable to work for copolymers which are hard to get swollen (MS3 for example). Microemulsion used to be majorly employed to form micrometer-sized spheres and cavities from crystallizable homopolymers, with the help of surfactants.[26, 31, 32] In recent years it has become a versatile approach to study the self-assembly of amphiphilic block copolymers.[25, 33-36] Here we apply water-in-oil-in-water (W/O/W) double emulsion to prepare vesicles from PMeSPG-*b*-PSar, to pursue higher universality and efficiency. Double emulsion is firstly prepared through a two-step emulsification of chloroform and water, with the help of homogenizer. The copolymers are packaged in chloroform and chloroform/water interface, serving as macromolecular surfactants to stabilize the emulsion. 50 ℃ heating is applied on the emulsion to remove chloroform by evaporation. Directed by emulsion structure and driven by solvent evaporation, self-assembly of PMeSPG-*b*-PSar is thus achieved towards vesicle formation (Scheme 4.1). As shown in Figure 4.12A, MS1-containing W/O/W emulsion droplets around 5−15 μm are formed and dispersed. Following the system by optical microscope during solvent evaporation, the shrinking of the emulsion droplets is recorded in function of

time, and after 12 h, some droplets are captured to generate vesicular structures (dashcircled in Figure 4.12B). Many vesicles sized 2−10 μm have been formed after 24 h, along with residual chloroform droplets (Figure 4.12C). Two bowling-like structures are captured (pointed in Figure 4.12C), which are speculated to be the incomplete vesicles, with residual chloroform droplets at the joints. No droplet is left after 40 h of heating, while the sizes of vesicles mostly decrease below 2 μm (Figure 11A and D). MS2 and MS3 are also explored with double emulsion method, and as revealed in Figure 4.13, vesicles are obtained for both copolymers after 40 h of chloroform evaporation. MS2 have ubiquitous giant vesicles sized 2−20 μm, with a uniformly spherical unilamellar shape. The vesicles of MS3 show a wide size distribution, from around 2 μm to over 20 μm, many of them have irregular shapes.

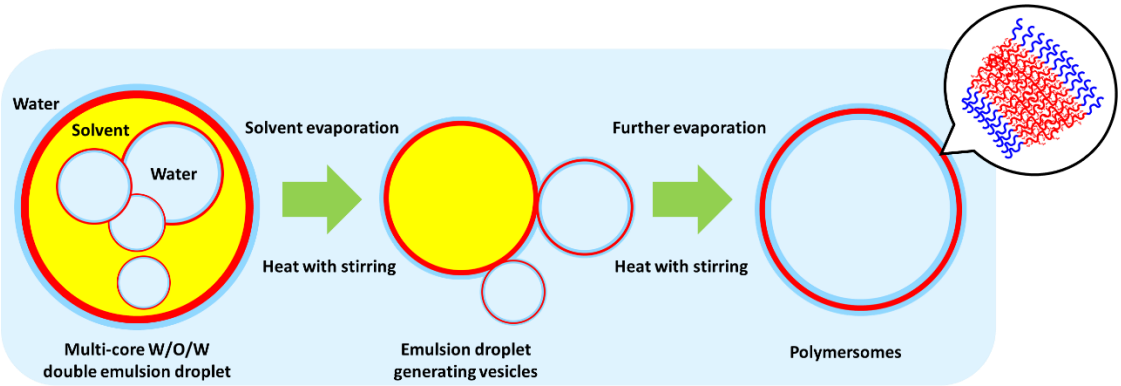

Scheme 4.1. Schematic illustration of the vesicle formation through solvent evaporation from W/O/W double emulsion.

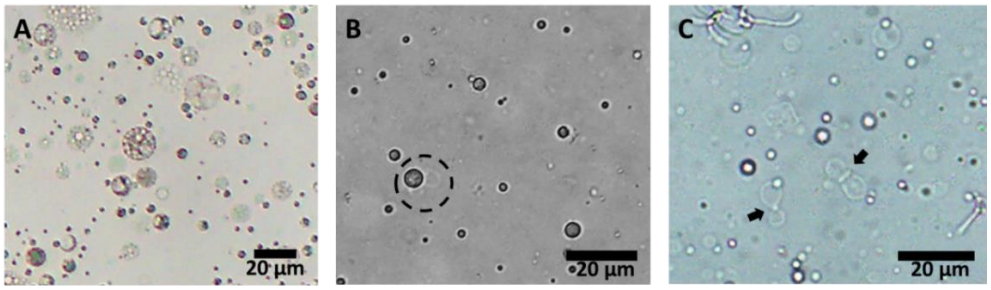

Figure 4.12. Bright-field optical microscopic images of the W/O/W double emulsion of MS1 (A) before chloroform evaporation; (B) after 12 h of chloroform evaporation; (C) after 24 h of chloroform evaporation.

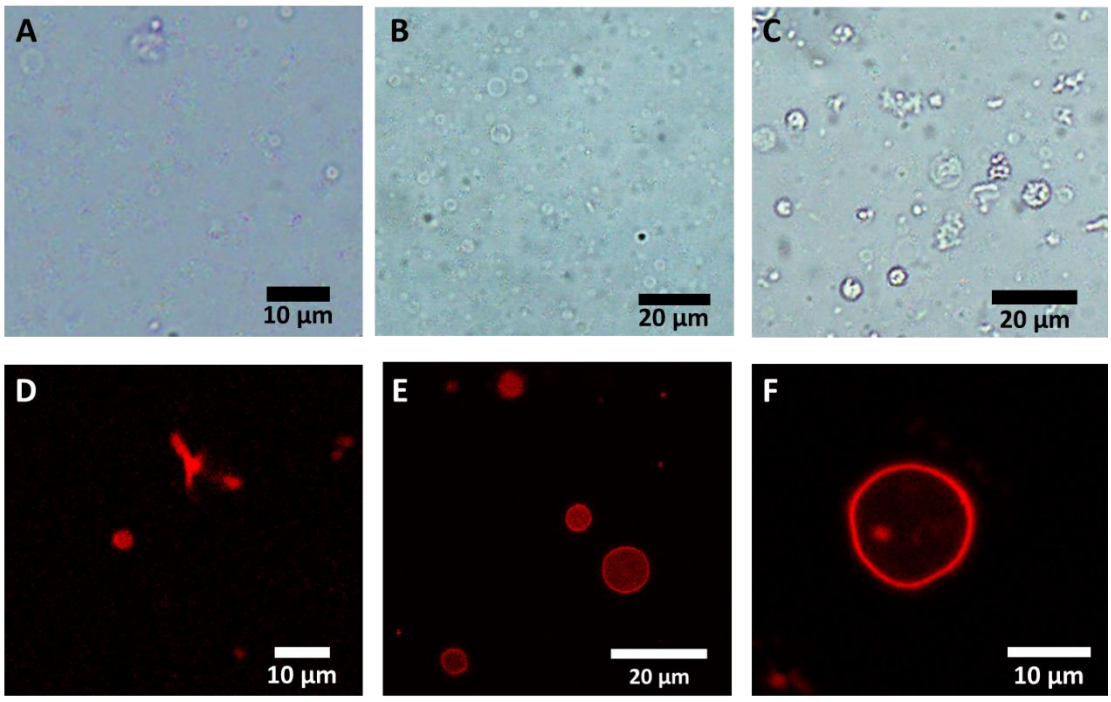

Figure 4.13. Bright-field optical microscopic (A−C) and CLSM (D−F) images of self-assemblies from MS1 (A, D), MS2 (B, E) and MS3 (C, F) by double emulsion, after 40 h of chloroform evaporation.

The nanoscale morphology of self-assemblies from double emulsion is further analyzed by cryo-EM. For MS1, the coexistence of spheres (10−20 nm in diameter), worms (12−15 nm in width), lamellae (600−800 nm in diameter) and vesicles is present in Figure 4.14A−C. Vesicles are dispersing around and sized from 30 to 300 nm, with the membrane at 8−12 nm in thickness. Some unclosed structures are observed (dashcircled in Figure 4.14A&C), while some of the vesicles are found to connect with a worm-like "tail" and form a tadpole-like shape (pointed in Figure 4.14C). Ubiquitous worm-like micelles (11−15 nm in width) are observed in nanoscale view of MS2 sample, decorated with micrometer-sized lamellae and vesicles measured 30−800 nm in size and 10−12 nm in membrane thickness (Figure 4.14D−F). The nanoscale self-assemblies of MS3 have an intriguing feature: many vesicles with size 30−300 nm and membrane thickness 14−16 nm, are found to stick together (Figure 4.14G) or interconnected via

branched worm-like micelles (Figure 4.14I). Dispersed vesicles, worm-like micelles (16−18 nm in width) and open lamellae (100−1000 nm) are also observed.

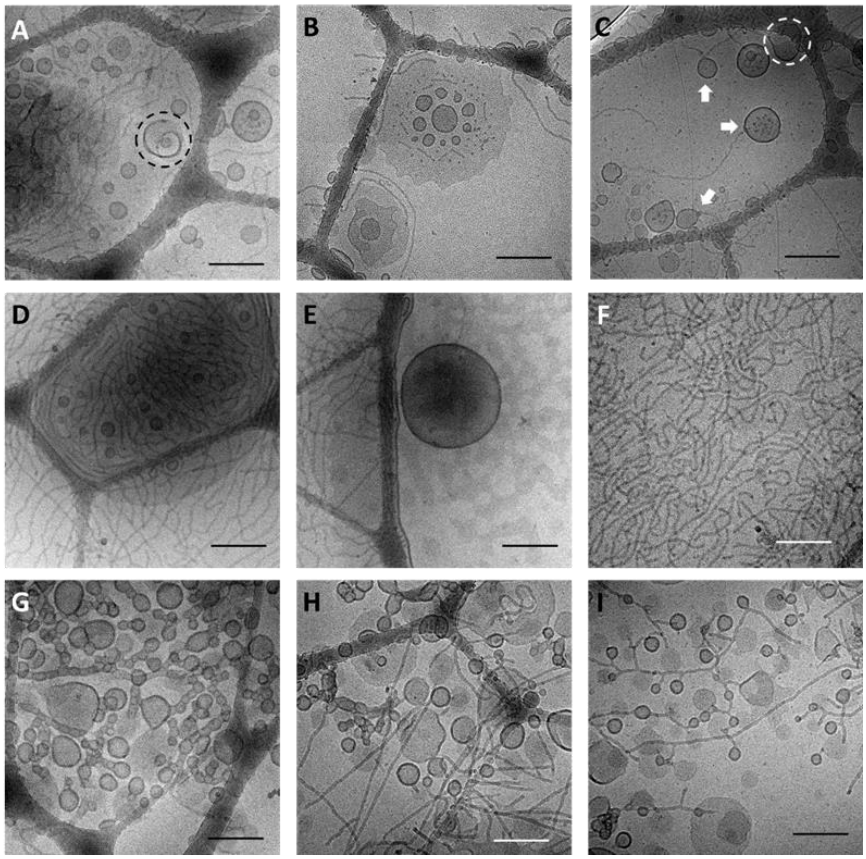

Figure 4.14. Cryo-EM images of self-assemblies formed by (A−C) MS1, (D−F) MS2 and (G−I) MS3, through double emulsion after 40 h of chloroform evaporation. Scale bar = 300 nm.

The nanoscale self-assembly structures may come from small (< 1 μm) O/W emulsion droplets. The self-assembly of copolymers in the small droplets during the chloroform evaporation process is not guided by the double emulsion template, thus forming highly nonergodic results, close to that of nanoprecipitation. As measured from cryo-EM images, the vesicles formed from double emulsion of the same copolymer have a smaller membrane thickness than the vesicles from nanoprecipitation. It can be attributed to the choosing of solvent and the way of removing solvent. Compared with the cosolvent DMF and its removal through dialysis in nanoprecipitation, using chloroform to dissolve copolymers and removing chloroform by evaporation at 50 ℃

in double emulsion method, may promote the formation of aggregates with higher compactness.

4.3.6 Bicontinuous structures and their formation mechanism

The self-assembly results of MS3 from nanoprecipitation and double emulsion often include some lamellar structures, which are not either spreaded like open lamellae, or closed like vesicles, but have higher degree of structural complexity (Figure 4.15). As a typical structure in Figure 4.15A, it has a porous surface, and a bicontinuous inner structure in the form of network-like labyrinth. These structures are collectively referred as "bicontinuous nanoparticles". Bicontinuous structures with interwoven lattices inside are often reported from block copolymers with packing parameter $p > 1$, where the hydrophobic block has a much larger volume than that of hydrophilic block.[37-39] In some circumstances, the internal periodic lattice could correspond to classic analogues inversely, such as cubic and hexagonal structures, therefore they are called respectively as "cubosomes"[39, 40] and "hexosomes"[39] in literatures. With extremely high surface area, which usually means high uptake effect, bicontinuous particles have been considered as potential nanocarriers for the use of highly efficient drug delivery and catalysis.[37]

The formation of bicontinuous nanoparticles is considered closely related to the dominant hydrophobic domain. Like spheres colliding with each other to form cylinders, the bilayers of lamellae and vesicles have the further trend to accumulate together, driven by hydrophobic interaction, therefore interlamellar fusion takes place.[41] As the mechanism proposed by Siegel *et al.* based on lipidic self-assembly (Scheme 4.2),[42] the interlamellar fusion starts with the formation of a stalk from the amphiphiles in the facing monolayers of the two bilayers; driven by the reduction of curvature energy of the exterior semitoroidal monolayer, the stalk expands and makes the distal monolayers meet, forming a trans-monolayer contact (TMC). Under the tension due to curvature and chain-packing stress, the diaphragm of TMC gets ruptured and a fusion pore is

formed as the result, which is also termed as interlamellar attachment (ILA). ILAs could be formed between any two approached bilayer structures as interconnecting tunnels, and could expand to ring-like open structures. If a large number of ILAs are formed in a stack of bilayers, for example a multilamellar vesicle, a sponge-like bicontinuous structure then will be obtained. ILA is proposed as the intermediate from lipidic bilayers to bicontinuous structures.[43-45] In the field of polymeric self-assembly, Lecommandoux *et al.* referred to the ILA pathway to illustrate the transition from stomatocyte-like vesicle to bilamellar nested vesicle.[46] Sommerdijk *et al.* reported the close relation between multi-lamellar polymersomes and bicontinuous nanoparticles, which are formed from the same copolymer via nanprecipitation, with different cosolvents[47-49]. But the detailed mechanism of polymeric bicontinuous nanoparticles involving interlamellar fusion has not yet been established. Bicontinuous nanoparticles are generated from MS3, which has a low hydrophilic ratio ($f_{PSar,\,wt}$ = 14%). Simultaneously, as a consequence of kinetically frozen effect, many self-assembly structures of MS3 are trapped in a metastable state, which can be used to explain how bicontinuous nanoparticles are formed. As a part of MS3 self-assemblies from nanoprecipitation, a network-like structure is present in Figure 4.15C, and as marked by dashcircle in the downright of the image, the network is found to be connected with an open lamella, which is supposed to be part of the original structure, evolving into the bicontinuous network through interlamellar fusion. Interconnected vesicles are frequently observed from the double emulsion self-assembly of MS3, as the result of interlamellar fusion (Figure 4.15 E&F). When the interconnected vesicles are accumulated intensively, the embryonic form of bicontinuous nanoparticles is generated (darshcircled in Figure 4.15E&F). The ILA tunnels and partial interlamellar fusion are respectively found in Figure 4.15D and Figure 4.15H. These are direct proofs to support the formation of polymeric bicontinuous nanoparticles, through the mechanism of interlamellar fusion.

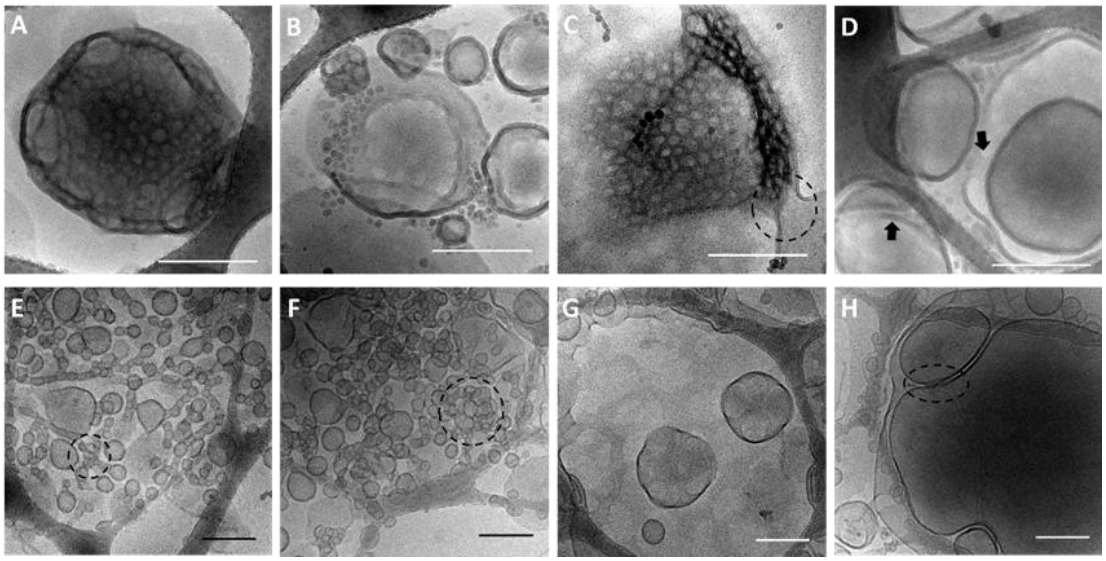

Figure 4.15. Cryo-EM images of Bicontinuous nanoparticles and intermediate structures formed by (A−D) nanoprecipitation and (E−H) double emulsion from MS3. Scale bar = 300 nm.

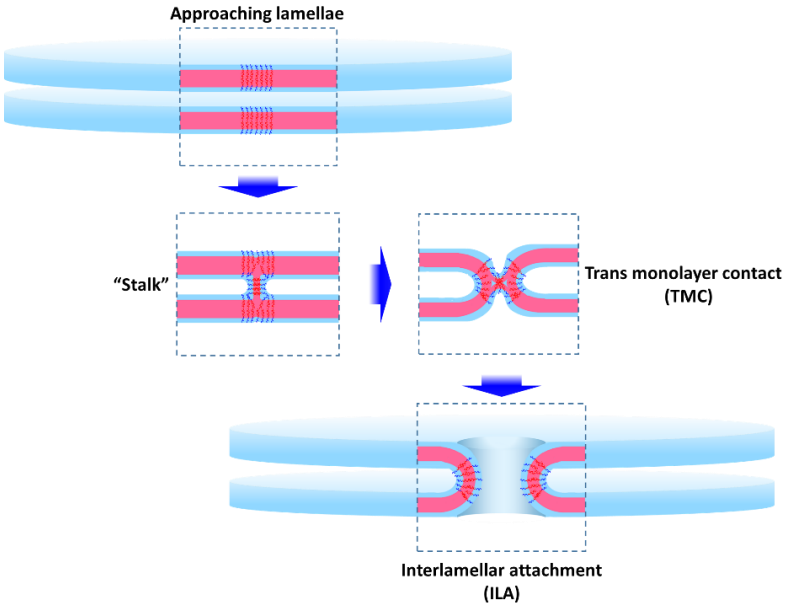

Scheme 4.2. The formation procedure of an interlamellar attachment (ILA) between two approached lamellae.

4.4 Conclusion

We present in this chapter the self-assembly of MeSPG-containing copolymers, PEG-*b*-PMeSPG and PMeSPG-*b*-PSar. In self-assembly study through

nanoprecipitation, three PEG-*b*-PMeSPG copolymers, EM1 (PEG_{45}-*b*-$PMeSPG_{17}$, $f_{PEG, wt}$ = 45%), EM2 (PEG_{45}-*b*-$PMeSPG_{40}$, $f_{PEG, wt}$ = 26%) and EM3 (PEG_{45}-*b*-$PMeSPG_{71}$, $f_{PEG, wt}$ = 16%), along with MW increasing and hydrophilic ratio declining, respectively form solid nanospheres, spherical and worm-like micelles, and lamellae and vesicles, as dominant structures. All the three PMeSPG-*b*-PSar copolypeptoids, MS1 ($PMeSPG_{45}$-*b*-$PSar_{65}$, $f_{PSar, wt}$ = 41%), MS2 ($PMeSPG_{60}$-*b*-$PSar_{50}$, $f_{PSar, wt}$ = 29%) and MS3 ($PMeSPG_{75}$-*b*-$PSar_{25}$, $f_{PSar, wt}$ = 14%), can form polymersomes from nanoprecipitation. The vesicular structure differs in morphologies and sizes due to the difference in hydrophilic ratios and MWs. At the same time, the self-assembly results of the three copolypeptoids are obviously nonergodic: metastable spherical micelles, lamellae, unclosed intermediates and irregularly shaped vesicles coexist in the result of the same copolymer. The behavior of PSar in water is analyzed by SANS and DLS, which reveal that PSar forms clusters in water, rather than purely single-chain coils like PEG. The difference of water-solubility between PSar and PEG is a major reason for self-assembly difference between PEG-*b*-PMeSPG and PMeSPG-*b*-PSar, and the insufficient water solubility of PSar is also possibly responsible for the nonergodicity of PMeSPG-*b*-PSar self-assemblies. Using the thermodynamic properties of PMeSPG, vesicles are obtained from MS1 and MS2 by film hydration involving heating treatment. The transition of MS2 vesicles from irregular shapes to uniform spherical shapes along with the heating time confirms the controllability of self-assembly morphology by preparation conditions. Micrometer-sized vesicles can be obtained from MS1−MS3 by double emulsion method, where vesicles are formed in guidance of W/O/W double emulsion droplets, during the evaporation of chloroform. MS3 forms nanoparticles with internal bicontinuous structure in self-assembly, due to the dominant hydrophobic ratio. Metastable intermediates are captured as a part of the nonergodicity of MS3 self-assemblies, and the morphological analysis on these intermediates can prove the formational mechanism of bicontinuous nanoparticles through interlamellar fusion.

As a class of manageable biocompatible polymers, polypeptoids have a huge value to be developed and promoted. By using the amphiphilic block copolypeptoid PMeSPG-*b*-PSar as a platform, we systematically studied its self-assembly behaviors and structures, and introduced external assisting approaches, such as heating treatment, alternating electric field and W/O/W double emulsion, to control the size and morphology of self-assembly structures. This work contribute certainly to the comprehension and the control of the self-assembly of polypeptoid-containing amphiphilic block copolymers.

References

1. Chan, B. A.; Xuan, S.; Li, A.; Simpson, J. M.; Sternhagen, G. L.; Yu, T.; Darvish, O. A.; Jiang, N.; Zhang, D., Polypeptoid polymers: Synthesis, characterization, and properties. *Biopolymers* **2018,** *109* (1), e23070.

2. Yamada, S.; Ikkyu, K.; Iso, K.; Goto, M.; Endo, T., Facile synthesis of polymethionine oxides through polycondensation of activated urethane derivative of alpha-amino acid and their application to antifouling polymer against proteins and cells. *Polym. Chem.* **2015,** *6* (10), 1838-1845.

3. Rodriguez, A. R.; Kramer, J. R.; Deming, T. J., Enzyme-Triggered Cargo Release from Methionine Sulfoxide Containing Copolypeptide Vesicles. *Biomacromolecules* **2013,** *14* (10), 3610-3614.

4. Kramer, J. R.; Deming, T. J., Preparation of Multifunctional and Multireactive Polypeptides via Methionine Alkylation. *Biomacromolecules* **2012,** *13* (6), 1719-1723.

5. Rodriguez, A. R.; Choe, U.-J.; Kamei, D. T.; Deming, T. J., Blending of Diblock and Triblock Copolypeptide Amphiphiles Yields Cell Penetrating Vesicles with Low Toxicity. *Macromol. Biosci.* **2015,** *15* (1), 90-97.

6. Rodriguez, A. R.; Choe, U.-J.; Kamei, D. T.; Deming, T. J., Use of Methionine Alkylation to Prepare Cationic and Zwitterionic Block Copolypeptide Vesicles. *Isr. J. Chem.* **2016,** *56* (8), 607-613.

7. Yu, S.; Wang, C.; Yu, J.; Wang, J.; Lu, Y.; Zhang, Y.; Zhang, X.; Hu, Q.; Sun, W.; He, C.; Chen, X.; Gu, Z., Injectable Bioresponsive Gel Depot for Enhanced Immune Checkpoint Blockade. *Adv. Mater.* **2018**, e1801527.

8. Gaitzsch, J.; Karu, K.; Battaglia, G., Peptoidosomes as nanoparticles from amphiphilic block alpha-peptoids using solid-phase-synthesis. *Eur. Polym. J.* **2015,** *73*, 447-454.

9. Fetsch, C.; Gaitzsch, J.; Messager, L.; Battaglia, G.; Luxenhofer, R., Self-Assembly of Amphiphilic Block Copolypeptoids - Micelles, Worms and Polymersomes. *Sci. Rep.* **2016,** *6*, 33491.

10. Alessi, M. L.; Norman, A. I.; Knowlton, S. E.; Ho, D. L.; Greer, S. C., Helical and coil conformations of poly(ethylene glycol) in isobutyric acid and water. *Macromolecules* **2005,** *38* (22), 9333-9340.

11. Mössmer, S.; Spatz, J. P.; Möller, M.; Aberle, T.; Schmidt, J.; Burchard, W., Solution Behavior of Poly(styrene)-block-poly(2-vinylpyridine) Micelles Containing Gold Nanoparticles. *Macromolecules* **2000,** *33* (13), 4791-4798.

12. Teraoka, I., Dynamics of Dilute Polymer Solutions. In *Polymer Solutions: An Introduction to Physical Properties*, 2002.

13. Linegar, K. L.; Adeniran, A. E.; Kostko, A. F.; Anisimov, M. A., Hydrodynamic radius of polyethylene glycol in solution obtained by dynamic light scattering. *Colloid J.* **2010,** *72* (2), 279-281.

14. Birke, A.; Ling, J.; Barz, M., Polysarcosine-containing copolymers: Synthesis, characterization, self-assembly, and applications. *Prog. Polym. Sci.* **2018,** *81*, 163-208.

15. Tao, X.; Deng, Y.; Shen, Z.; Ling, J., Controlled Polymerization of N-Substituted Glycine N-Thiocarboxyanhydrides Initiated by Rare Earth Borohydrides toward Hydrophilic and Hydrophobic Polypeptoids. *Macromolecules* **2014,** *47* (18), 6173-6180.

16. Fetsch, C.; Luxenhofer, R., Thermal Properties of Aliphatic Polypeptoids. *Polymers* **2013,** *5* (1), 112-127.

17. Lee, C.-U.; Li, A.; Ghale, K.; Zhang, D., Crystallization and Melting Behaviors of Cyclic and Linear Polypeptoids with Alkyl Side Chains. *Macromolecules* **2013,** *46* (20), 8213-8223.

18. Rieger, J., The glass transition temperature of polystyrene - Results of a round robin test. *J. Therm. Anal.* **1996,** *46* (3-4), 965-972.

19. Halasa, A. F.; Massie, J. M., Polybutadiene. In *Kirk‐Othmer Encyclopedia of Chemical Technology*, 2000.

20. Ghoroghchian, P. P.; Li, G. Z.; Levine, D. H.; Davis, K. P.; Bates, F. S.; Hammer, D. A.; Therien, M. J., Bioresorbable vesicles formed through spontaneous self-assembly of amphiphilic poly(ethylene oxide)-block-polycaprolactone. *Macromolecules* **2006,** *39* (5), 1673-1675.

21. Dionzou, M.; Morere, A.; Roux, C.; Lonetti, B.; Marty, J. D.; Mingotaud, C.; Joseph, P.; Goudouneche, D.; Payre, B.; Leonetti, M.; Mingotaud, A. F., Comparison of methods for the fabrication and the characterization of polymer self-assemblies: what are the important parameters? *Soft matter* **2016,** *12* (7), 2166-2176.

22. Battaglia, G.; Ryan, A. J., Pathways of polymeric vesicle formation. *J. Phys. Chem. B* **2006,** *110* (21), 10272-10279.

23. Battaglia, G.; Ryan, A. J., Neuron-like tubular membranes made of diblock copolymer amphiphiles. *Angew. Chem. Int. Ed. Engl.* **2006,** *45* (13), 2052-2056.

24. Hayward, R. C.; Pochan, D. J., Tailored Assemblies of Block Copolymers in Solution: It Is All about the Process. *Macromolecules* **2010,** *43* (8), 3577-3584.

25. Wang, X. Y.; Feng, X. Y.; Ma, G. P.; Zhang, D.; Chai, Y. H.; Ge, M. F.; Yao, L., Dual-Phase Separation in a Semiconfined System: Monodispersed Heterogeneous Block-Copolymer Membranes for Cell Encoding and Patterning. *Adv. Mater.* **2017,** *29* (19), e1605932.

26. Wang, W.; Qi, H.; Zhou, T.; Mei, S.; Han, L.; Higuchi, T.; Jinnai, H.; Li, C. Y., Highly robust crystalsome via directed polymer crystallization at curved liquid/liquid interface. *Nat. Comm.* **2016,** *7*, 10599.

27. Dimitrov, D. S.; Angelova, M. I., Electric-field mediated lipid swelling and liposome formation. *Studia Biophysica* **1987,** *119* (1-3), 61-65.

28. Dimitrov, D. S.; Angelova, M. I., Lipid swelling and liposome formation mediated by electric-fields. *Bioelectrochem. Bioenerg.* **1988,** *19* (2), 323-336.

29. Dimova, R.; Seifert, U.; Pouligny, B.; Förster, S.; Döbereiner, H.-G., Hyperviscous diblock copolymer vesicles. *The European Physical Journal E* **2002,** *7* (3), 241-250.

30. Ruysschaert, T.; Sonnen, A. F. P.; Haefele, T.; Meier, W.; Winterhaltert, M.; Fournier, D., Hybrid nanocapsules: Interactions of ABA block copolymers with liposomes. *J. Am. Chem. Soc.* **2005,** *127* (17), 6242-6247.

31. Wang, W.; Staub, M. C.; Zhou, T.; Smith, D. M.; Qi, H.; Laird, E. D.; Cheng, S.; Li, C. Y., Polyethylene nano crystalsomes formed at a curved liquid/liquid interface. *Nanoscale* **2017,** *10* (1), 268-276.

32. Schlegel, I.; Muñoz-Espí, R.; Renz, P.; Lieberwirth, I.; Floudas, G.; Suzuki, Y.; Crespy, D.; Landfester, K., Crystallinity Tunes Permeability of Polymer Nanocapsules. *Macromolecules* **2017,** *50* (12), 4725-4732.

33. Bae, J.; Russell, T. P.; Hayward, R. C., Osmotically driven formation of double emulsions stabilized by amphiphilic block copolymers. *Angew. Chem. Int. Ed. Engl.* **2014,** *53* (31), 8240-8245.

34. Kim, M. R.; Cheong, I. W., Stimuli-triggered Formation of Polymersomes from W/O/W Multiple Double Emulsion Droplets Containing Poly(styrene)-block-poly(N-isopropylacrylamide-co-spironaphthoxazine methacryloyl). *Langmuir* **2016,** *32* (36), 9223-9228.

35. Wyman, I.; Njikang, G.; Liu, G., When emulsification meets self-assembly: The role of emulsification in directing block copolymer assembly. *Prog. Polym. Sci.* **2011,** *36* (9), 1152-1183.

36. Park, M.-K.; Jun, S.; Kim, I.; Jin, S.-M.; Kim, J.-G.; Shin, T. J.; Lee, E., Stepwise Drug-Release Behavior of Onion-Like Vesicles Generated from Emulsification-Induced Assembly of Semicrystalline Polymer Amphiphiles. *Adv. Funct. Mater.* **2015,** *25* (29), 4570-4579.

37. Groeschel, A. H.; Walther, A., Block Copolymer Micelles with Inverted Morphologies. *Angew. Chem. Int. Ed. Engl.* **2017,** *56* (37), 10992-10994.

38. Holder, S. J.; Sommerdijk, N. A. J. M., New micellar morphologies from amphiphilic block copolymers: disks, toroids and bicontinuous micelles. *Polym. Chem.* **2011,** *2* (5), 1018-1028.

39. Barauskas, J.; Johnsson, M.; Tiberg, F., Self-assembled lipid superstructures: Beyond vesicles and liposomes. *Nano Lett.* **2005,** *5* (8), 1615-1619.

40. Park, C.; La, Y.; An, T. H.; Jeong, H. Y.; Kang, S.; Joo, S. H.; Ahn, H.; Shin, T. J.; Kim, K. T., Mesoporous monoliths of inverse bicontinuous cubic phases of block copolymer bilayers. *Nat. Comm.* **2015,** *6*, 6392.

41. Siegel, D. P., Inverted micellar intermediates and the transitions between lamellar, cubic, and inverted hexagonal amphiphile phases .3. Isotropic and inverted cubic state formation via intermediates in transitions between L-alpha and H-II phases. *Chem. Phys. Lipids* **1986,** *42* (4), 279-301.

42. Siegel, D. P., Energetics of intermediates in membrane-fusion - comparison of stalk and inverted micellar intermediate mechanisms. *Biophys. J.* **1993,** *65* (5), 2124-2140.

43. Siegel, D. P.; Epand, R. M., The mechanism of lamellar-to-inverted hexagonal phase transitions in phosphatidylethanolamine: Implications for membrane fusion mechanisms. *Biophys. J.* **1997,** *73* (6), 3089-3111.

44. Mulet, X.; Gong, X.; Waddington, L. J.; Drummond, C. J., Observing Self-Assembled Lipid Nanoparticles Building Order and Complexity through Low-Energy Transformation Processes. *ACS Nano* **2009,** *3* (9), 2789-2797.

45. Demurtas, D.; Guichard, P.; Martiel, I.; Mezzenga, R.; Hebert, C.; Sagalowicz, L., Direct visualization of dispersed lipid bicontinuous cubic phases by cryo-electron tomography. *Nat. Comm.* **2015,** *6*, 8915.

46. Salva, R.; Le Meins, J. F.; Sandre, O.; Brulet, A.; Schmutz, M.; Guenoun, P.; Lecommandoux, S., Polymersome Shape Transformation at the Nanoscale. *ACS Nano* **2013,** *7* (10), 9298-9311.

47. McKenzie, B. E.; de Visser, J. F.; Portale, G.; Hermida-Merino, D.; Friedrich, H.; Bomans, P. H.; Bras, W.; Monaghan, O. R.; Holder, S. J.; Sommerdijk, N. A., The evolution of bicontinuous polymeric nanospheres in aqueous solution. *Soft matter* **2016,** *12* (18), 4113-4122.

48. McKenzie, B. E.; de Visser, J. F.; Friedrich, H.; Wirix, M. J. M.; Bomans, P. H. H.; de With, G.; Holder, S. J.; Sommerdijk, N. A. J. M., Bicontinuous Nanospheres from Simple Amorphous Amphiphilic Diblock Copolymers. *Macromolecules* **2013,** *46* (24), 9845-9848.

49. Monaghan, O. R.; Bomans, P. H. H.; Sommerdijk, N. A. J. M.; Holder, S. J., Controlling the melting transition of semi-crystalline self-assembled block copolymer aggregates: controlling release rates of ibuprofen. *Polym. Chem.* **2017,** *8* (35), 5303-5316.

Chapter 5. Stimuli-Responsive Vesicles Based on PMeSPG-*b*-PSar

5.1 Introduction

In drug delivery applications, controlled release of therapeutic substances can be achieved through the use of copolymers that respond to the action of stimuli like redox reactions, pH changes, temperature variation, shear stress and light illumination.[1-5] Among these stimuli, the high levels of reactive oxygen species (ROS) in tumor and inflammatory tissues present special interests and have been used as important trigger to develop oxidation-responsive polymers in target-specific therapeutic delivery.[6, 7] Hydrogen peroxide (H_2O_2), singlet oxygen ($^1O_2$), superoxide and hydroxyl radicals are the most well studied ROS in cancer and inflammatory diseases.[8-11] These ROS can also be generated easily with spatiotemporal control by *in-situ* biochemical or photochemical reactions.[12, 13] For example, H_2O_2 can be produced by the glucose-oxidase(GOx)/glucose/oxygen system and induce destabilization of oxidation-sensitive polymersoms.[14] $^1O_2$ can be generated under light illumination through photosensitizers incorporated in polymersomes and eventually cause polymersome rupture and payload release.[13]

The most common oxidation-sensitive polymers include sulfur-containing aliphatic polymers (polythioethers), selenium/tellurium-based polymers, aryl oxalate-containing polymers and phenylboronic ester-containing polymers.[15-19] In recent years, there has been an emerging interest in both main-chain and side-chain types of polythioethers, such as main-chain poly(propylene sulfide) (PPS),[20] polypeptides with pendent thioethers (polymethionine (PMet) and *S*-substituted polycysteine (PCys))[21-25] and PEG with pendent thioethers.[26] Their main feature is that hydrophobic thioether groups can be transformed to more polar sulfoxide or sulfone groups under the oxidation by ROS, leading to significant increase of the water solubility of polymers.

This results in a change in the hydrophobic/hydrophilic balance of thioether-containing amphiphilic copolymers and leads to the dissolution or disassembly of their assemblies, such as polymersomes[20] and polymer micelles.[25, 27]

In this chapter, based on the thioether-to-sulfoxide transition in PMeSPG, the behavior and structural changes of PMeSPG-*b*-PSar vesicles in oxidative stimuli are accurately characterized, from the dynamic changes of vesicles to the signal transitions inside the molecules. The effect of H_2O_2 on the polymersome destruction is invesigated. In a further step, visible light is employed as remote and precise stimulus to generate *in-situ* $^1O_2$ in polymersomes incorporating a photosensitizer, tetraphenylporphyrin (TPP), and to lead to rupture of polymersomes. The PMeSPG-*b*-PSar vesicle system can be used in target-specific therapeutic delivery and in the combination of chemotherapy and photodynamic therapy (PDT),[28, 29] and show great potential in biomedical applications.

5.2 Experimental section

5.2.1 Oxidation reaction of PMeSPG

The oxidation of PMeSPG homopolymers was conducted at 0 ℃ for 90 min in the environment of 10 wt% H_2O_2, which was formed by slow addition of 0.5 mL 30 wt% H_2O_2 solution into the polymer suspension in water (10 mg polymer in 1 mL water) with stirring. The H_2O_2 was in large excess ([H_2O_2] : [MeSPG] = 64 : 1). The treatment was followed by addition of $Na_2S_2O_3$ to end the reaction and lyophilization to remove solvents. Finally, white powder was obtained for NMR analysis in DMSO-d_6. The proton peak of methyl adjacent to sulfoxide (c^O) is at around 2.5 ppm, overlapping the methyl peaks of dimethyl sulfoxide (DMSO), supporting the transition from thioether to sulfoxide as reported in Ref [30].

The treatment was repeated at room temperature, and it turned out that also only sulfoxide was formed. The H_2O_2 treatment on MS1 nanoprecipitation self-assembly

samples was conducted in a similar way at room temperature, with 30 wt% H_2O_2 solution slowly added to the copolymer suspension at volume ratio of 1 : 2, forming the environment of 10 wt% H_2O_2. Since the copolymer concentration turned to 1 g/L after dialysis, the excess of H_2O_2 was even larger ([H_2O_2] : [MeSPG] = 1086 : 1).

5.2.2 Surface modification of coverslips

The coverslips were firstly immersed in the mixture of 98% sulfuric acid and hydrogen peroxide (3 : 1) for 30 min, to modify the surface with hydroxyl groups. The hydroxyl-modified coverslips were cleaned and then treated with the ethanol solution of 3-aminopropyltriethoxysilane (APTES : EtOH = 1 : 15) for 2 h, to convert the hydroxyl to primary amino groups. Amino groups were converted to carboxyl groups by incubation in saturated ethanol solution of succinic anhydride (SA) overnight. The carboxyl-modified surface was reacted with a mixture of N-(3-dimethylaminopropyl)-N'-ethylcarbodiimide hydrochloride (EDC, 50 mg/mL) and N-hydroxysuccinimide (NHS, 5 mg/mL) in THF solution for 3 h. NHS-ester-modified coverslips were obtained as the result. The coverslips with NHS esters on the surface can trap PMeSPG-*b*-PSar vesicles, through the reaction between NHS esters and amino groups on the vesicle surface, as a result immobilize vesicles during microscopic analysis.

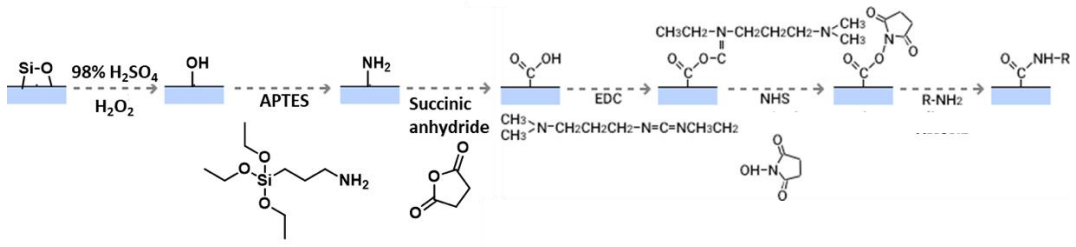

Scheme 5.1. NHS ester surface modified cover glass surface treatment reaction route.

5.2.3 Characterizations

NMR spectra were recorded on a Bruker Avance DMX 500 spectrometer (1H 500 MHz) with deuterium oxide (D_2O) or DMSO-d_6 as solvent.

The hydrodynamic diameters of the nanoparticles were measured by DLS using a particle size analyzer (Zetasizer Nano Series, Malvern Instruments) at 25 ℃. The measurements were made at a fixed angle at 90 °and a wavelength of 657 nm.

Cryo-EM experiments were conducted in INSERM U1196, Institut Curie, in collaboration with Sylvain Trepout. A total of 5 μL of samples were deposited onto a 200 mesh holey copper grid (Ted Pella Inc., U.S.A.) and flash-frozen in liquid ethane cooled down at liquid nitrogen temperature. The images were acquired on a JEOL 2200FS energy-filtered (20eV) field emission gun electron microscope operating at 200 kV using a Gatan ssCCD 2048 × 2048 pixels. Energy-filtered (Zero-loss) cryo-electron tomography images were collected at 12000x (corresponding pixel size 0.8 nm) from -64 °up to 64 °using a Saxton scheme (1 °at high tilts and 2 °at low tilts).

Optical microscopic images were obtained from a Motic PM1820 microscope with widefield eyepieces WF10×/18mm and achromatic objectives EA 10× and 40×.

CLSM images were obtained with Leica TCS SP5 confocal scanning system equipped with a 63× oil immersion objective. HeNe 543 nm laser (maximum working power at 1.5 mW) was employed to obtain the fluorescent images. A narrow chamber between a slide and a NHS-ester-modified coverslip was formed and separated by two parafilm strips. The vesicle samples were place inside the chamber through siphoning, for microscopic observation. In H_2O_2-sensitivity experiment, 10 μL 35 mM H_2O_2 aqueous solution was added to the chamber of 30 μL vesicle sample through siphoning, to form the environment of 8.8 mM H_2O_2 after mixing.

5.3 Results and discussion

5.3.1 H_2O_2-responsive PMeSPG-*b*-PSar nano-vesicles

H_2O_2 is a ubiquitous molecule in human body,[9] and is reported to accumulate at higher level in inflammatory cells and tumor tissues, because of the activated oxidant-generating enzymes and the decreased detoxifying ability.[10, 11] It has been reported on

the destabilization of thioether-containing polymersomes by H_2O_2.[14, 20] In this work, the homopolymer PMeSPG with DP at 84 (P4 in Chapter 2) is firstly treated by 10 wt% H_2O_2 (2.94 M) for 90 min. ^{1}H-NMR is conducted on the polymer before and after the treatment. According to the ^{1}H-NMR results (Figure 5.1B&C), the thioether groups of PMeSPG are all transferred to sulfoxides, in comparison with the spectra of PMet sulfoxides reported previously.[30]

After confirming the effect of H_2O_2 on PMeSPG, the treatment with 10 wt% of H_2O_2 is then applied to the polymersomes of MS1 ($PMeSPG_{45}$-*b*-$PSar_{60}$) from nanoprecipitation. As the result, no vesicle is found from the sample after 90-min H_2O_2 treatment in the observation of cryo-EM. Instead, only very few loose irregular clusters are visible with some disk-like cavities (Figure 5.2, disk-like cavities are pointed in Figure 5.2A&B). These objects are probably the residues left by the oxidized vesicles. DLS is employed in a parallel experiment, to measure the mean size of MS1 self-assemblies during the oxidation. The count rates measured by Zetasizer in kilo counts per second (kcps) represent the scattering intensity, and also indicate the evolution of particle size and/or concentration. Figure 5.3A shows that the count rates decreased exponentially upon the addition of H_2O_2 with a characteristic time τ = 20.2 min. The decline in count rates can be explained by the decrease in the size and/or concentration of the self-assemblies. After a 60-min or longer treatment, the count rates decreased to less than 100 kcps, which is the limit below which the size measurement becomes unreliable. The evolution of count rates confirmed the disruption of vesicles and other self-assemblies upon oxidation by H_2O_2.

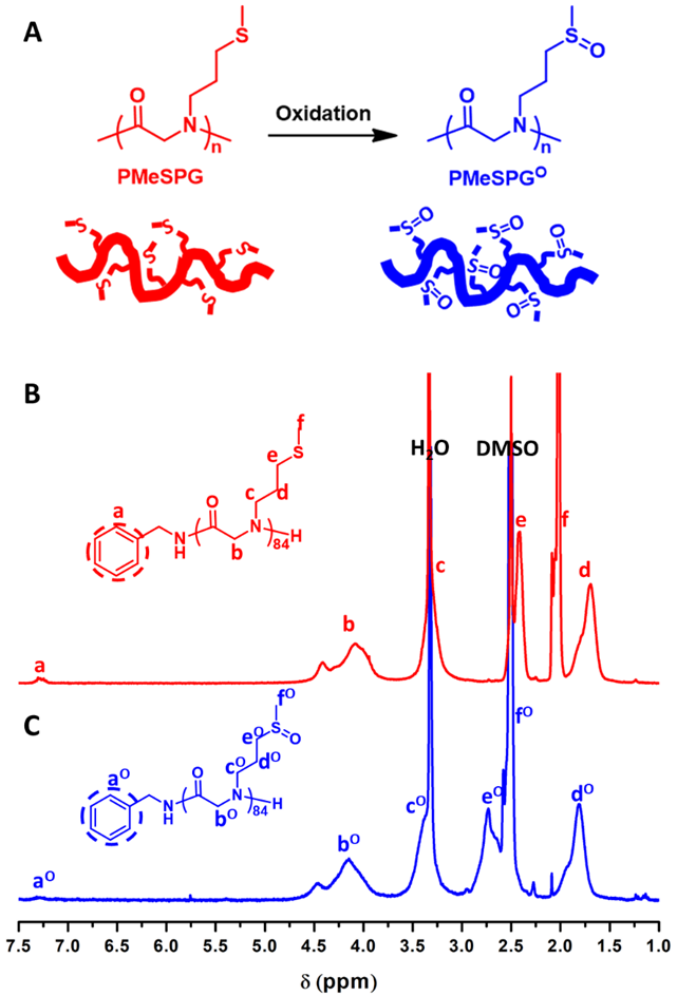

Figure 5.1. (A) Scheme of oxidation of the homopolymer PMeSPG with thioether to PMeSPG^{o} with sulfoxide. (B) PMeSPG and (C) PMeSPG^{o} traced by ^{1}H-NMR spectra (DMSO-d_6 as the solvent). The peaks of the protons adjacent to the sulfuric atom (d, e, f, red) shift downfield (d^{o}, e^{o}, f^{o}, blue), confirming the transition from thioether to sulfoxide.

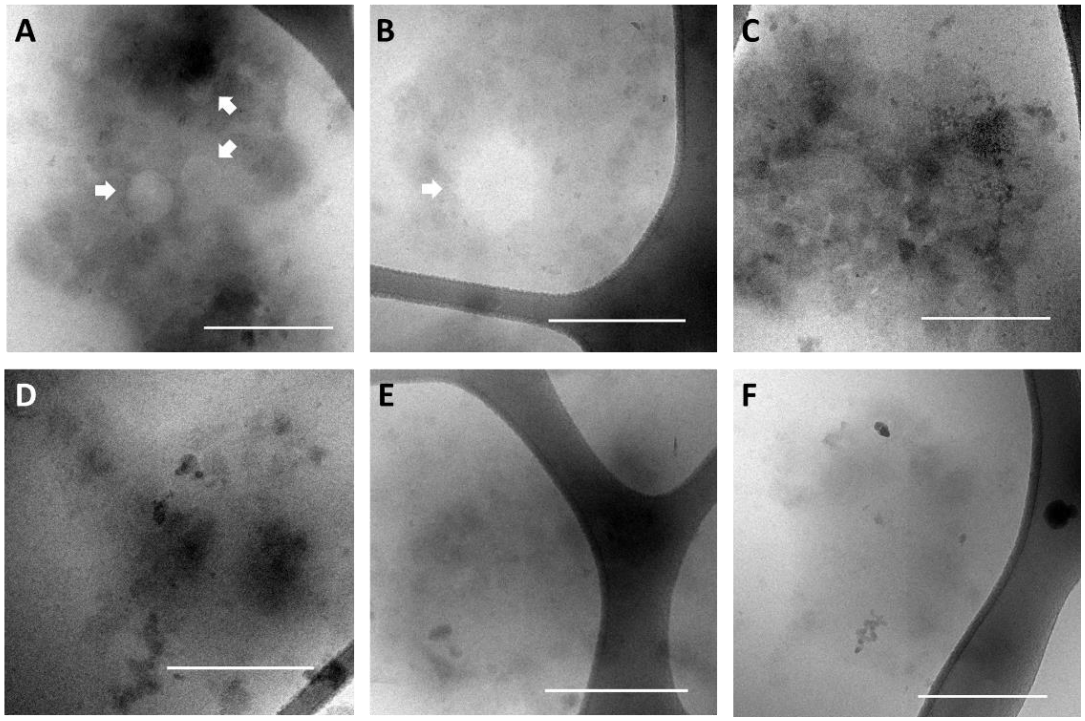

Figure 5.2. Cryo-EM images of the loose irregular clusters from the MS1 nanoprecipitated sample after 90 min treatment with 10 wt% H_2O_2.

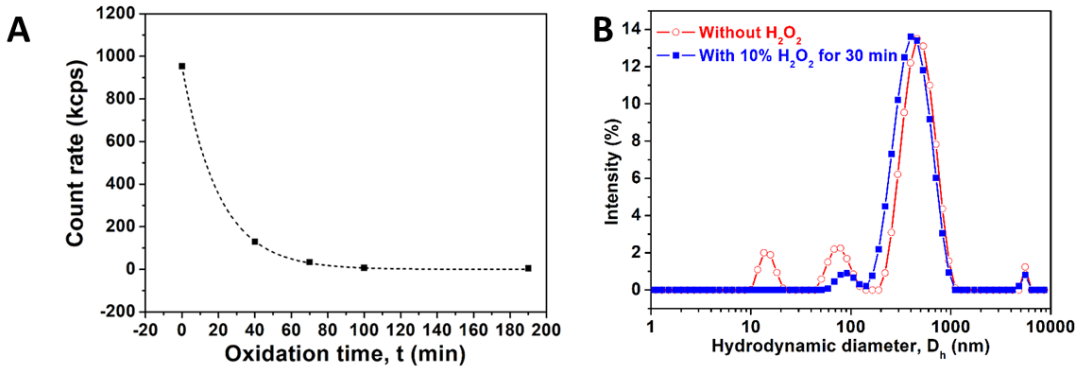

Figure 5.3. (A) The evolution of count rates of self-assemblies C1 measured by DLS as a function of the time of treatment with 2.9 M H_2O_2. The symbols are the experimental points. The dashed line is the fit with the exponential decay function $c = c_{max}e^{-t/\tau}$, where cmax is the maximum count rate at t = 0, and τ = 20.2 min is the characteristic time for c to decrease to 36.8% of c_{max}. (B) The size distribution of self-assemblies MS1 measured by DLS before any treatment and after 30-min treatment with 10 wt% H_2O_2.

5.3.2 H_2O_2-responsive PMeSPG-*b*-PSar giant vesicles

To address more in detail the oxidation-responsive transformation of the vesicular morphology, we recorded the behavior of micrometer-sized vesicles *in-situ* under the oxidation of H_2O_2 using CLSM. The giant vesicles of MS2 ($PMeSPG_{60}$-*b*-$PSar_{50}$) from double emulsion have an appropriate size distribution for the the observation (2−20 μm in diameter), and are therefore chosen as the major object in the following studies. The sample of giant polymersomes labelled with Nile Red (1 wt%) is placed between a slide and a surface-modified coverslip to observe the response of polymersomes to H_2O_2 oxidation under CLSM. The disruption of MS2 vesicles is initiated by the addition of H_2O_2: 10 μL of 35 mM H_2O_2 (0.12 wt%) is added into 30 μL of polymersome dispersion (60 wt% of copolymer), resulting in a final concentration of 8.8 mM for H_2O_2 and a molar ratio of $[H_2O_2]$: [MeSPG] = 3.62 : 1. We have observed two pathways in the vesicle disruption. Figure 5.4B present the pathway I^O (the superscript ^{O} indicate the trigger is H_2O_2) : the initial polymersome appears floppy with some slight membrane undulation; it turns to be well-rounded after 89 s of treatment; then the membrane fluctuates with more and more turbulence and many pores appear around the vesicle surface, which finally leads to the bursting of polymersome. The whole procedure takes 4 min. The pathway II^O (Figure 5.4C) starts also by transformation from floppy vesicle to well-rounded vesicle (achieved at around 282 s of H_2O_2 treatment), but followed by the slow shrinkage of the vesicle to smaller size and outward budding in the final stage. The pathway II^O takes longer time than that of the pathway I^O, over 13 min passing before the vesicle shrinking out of the focus. The change from undulated and floppy vesicle to well-rounded vesicle can be explained by the decrease of the membrane surface because of the first fraction of polymers changing from amphiphilic to water soluble upon the oxidation of thioether to sulfoxide. The difference between two pathways in time scale and disruption mode may be due to the concentration inhomogeneity in the mixture and the difference in the local molar ratio of $[H_2O_2]$: [MeSPG]. This ratio should be higher in pathway I^O than in pathway

II^O, leading rapid and drastic bursting of polymersome in pathway I^O. In contrast, in pathway II^O the oxidation is more progressive and the pores left by the solubilized $PMeSPG^O$-*b*-PSar may be healed promptly by reducing the vesicle surface area and whole size, avoiding thereby vesicle bursting.

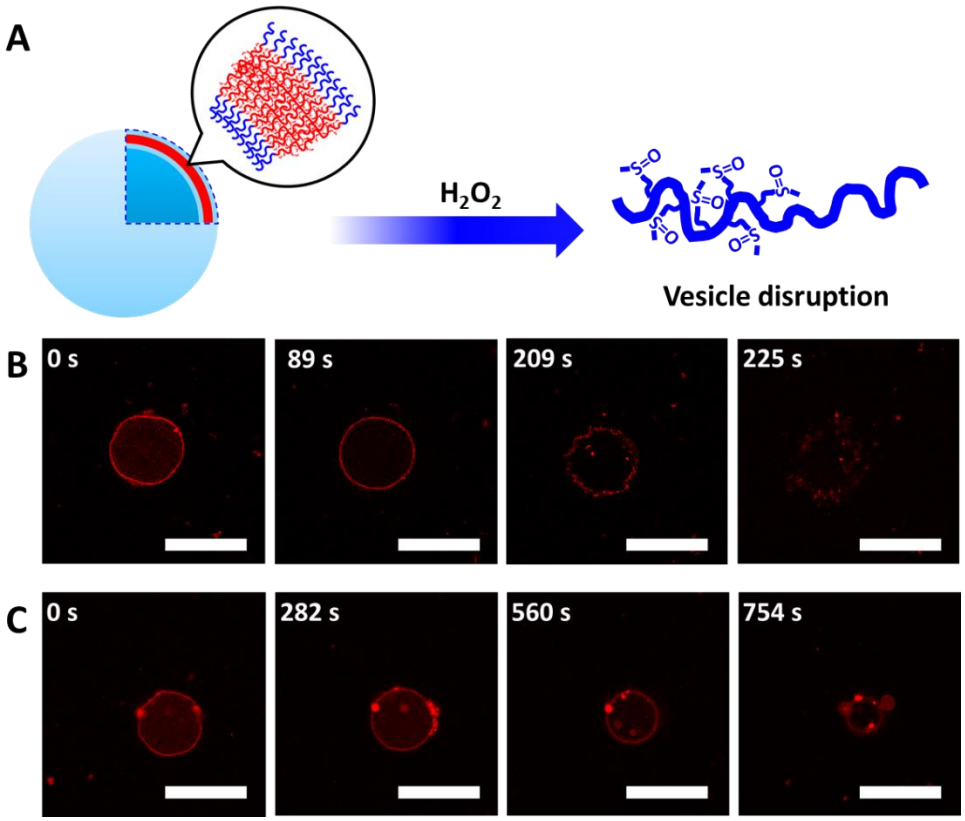

Figure 5.4. (A) Schematic illustration of the discruption of PMeSPG-*b*-PSar vesicle resulted from the thioether-to-sulfoxide transition in PMeSPG segments under H_2O_2 stimulation. CLSM records the vesicle disruption in two differenct pathways represented by (B) and (C), under the condition of 8.8 mM H_2O_2, with the molar ratio of [H_2O_2] : [MeSPG] = 3.62 : 1. (B) Pathway I^O: the vesicle turns first from undulated and floppy vesicle to well-rounded vesicle in the first 89 s, then the membrane starts to fluctuate more and more intensely and many pores appear around the vesicle surface (209 s) leading finally to vesicle bursting (225 s). (C) Pathway II^O: the vesicle changes first from undulated and floppy vesicle to well-rounded vesicle in the first 282 s, but followed by the slow shrinkage of the vesicle to smaller size (example at 560 s) and outward budding in the final stage (754 s). Scale bar = 25 μm.

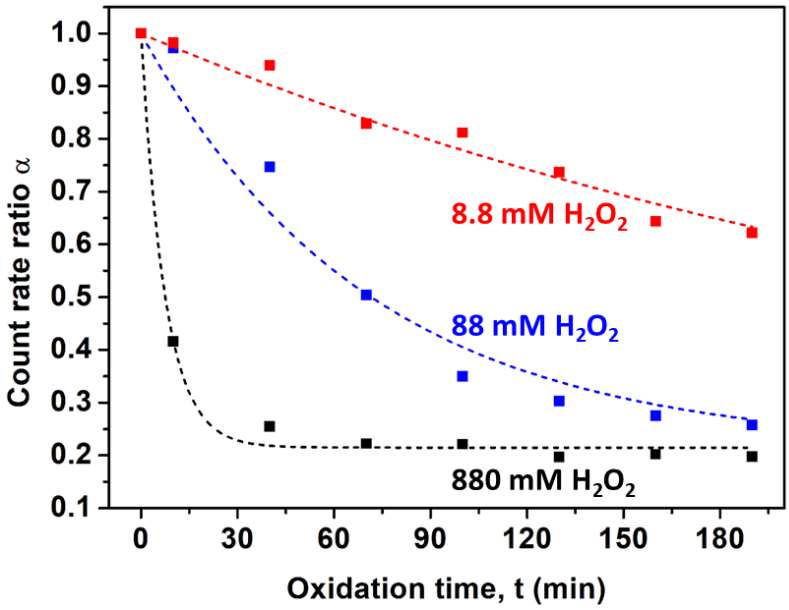

Figure 5.5. The ratio of count rates α (α = (count rates at the time t)/(count rate at t = 0 before H_2O_2 addition) as a function of oxidation time t, at different H_2O_2 concentrations (8.8 mM, 88 mM, and 880 mM). The symbols are the experimental points. The lines are the fits with the function $\alpha = (1 - \alpha_{min})e^{-t/\tau} + \alpha_{min}$, where $\alpha_{min} = 0.215$ is the minimum count rate ratio when the copolymers are totally oxidized, leaving a few aggregates of Nile Red molecules, and τ is the characteristic time when $(\alpha - \alpha_{min})$ declines to 36.8% of $(1 - \alpha_{min})$. τ is 302.6 min, 70.6 min, and 7.4 min for H_2O_2 concentration at 8.8 mM, 88 mM, and 880 mM, respectively.

To confirm the chemical oxidation of copolymers under the conditions of CLSM observation, we performed analyses by DLS for giant polymersomes C2 treated by 8.8 mM H_2O_2. The ratio of count rates α in Figure 5.5 represents the count rates at time t normalized with respect to count rates before H_2O_2 addition. The evolution of α as a function of time (Figure 5.5, red curve) supported the tendency of concentration/size of the self-assemblies to decrease through the oxidation. We also examined the cases with higher H_2O_2 concentrations (88 mM and 880 mM). As shown in Figure 5.5 (blue and black curves), the value of α decreased more rapidly when treated with higher H_2O_2 concentration. The decay of α under each condition was fitted

with an exponential function, giving the characteristic time τ of 302.6 min, 70.6 min, and 7.4 min for H_2O_2 concentration at 8.8 mM, 88 mM, and 880 mM, respectively.

We also traced the polymersome oxidation by ^{1}H-NMR. For this analysis the MS2 polymersomes are prepared by double emulsion using deuterium oxide (D_2O) instead of water. The mixture of MS2 polymersomes and H_2O_2 has a concentration of H_2O_2 at 176 mM, but with the molar ratio of [H_2O_2] : [copolymer] = 217 : 1, and of [H_2O_2] : [MeSPG] = 3.62 : 1 (the same molar ratio as used in CLSM experiment). The evolution of ^{1}H-NMR spectra as a function of oxidation time is shown in Figure 5.6 (only characteristic interval of chemical shift is chosen). In general, the intensities of a lot of signals tend to increase with time, either because of the rise of mobility of polymers in the polymer assemblies upon oxidation such as the signal c and low-field part (near 3.0 ppm) of signal d, or because of the appearance of oxidized signals such as a^O, b^O and c^O. The signals assigned to thioether disappear eventually after long enough oxidation time (here 12 h). The photographs of NMR sample tube beside the ^{1}H-NMR spectra show clearly the turbidity change of the polymersome dispersion. After 12 h of H_2O_2 treatment, the initial turbid dispersion becomes transparent, confirming the transformation from giant vesicles to solution of free polymers or of tiny aggregates.

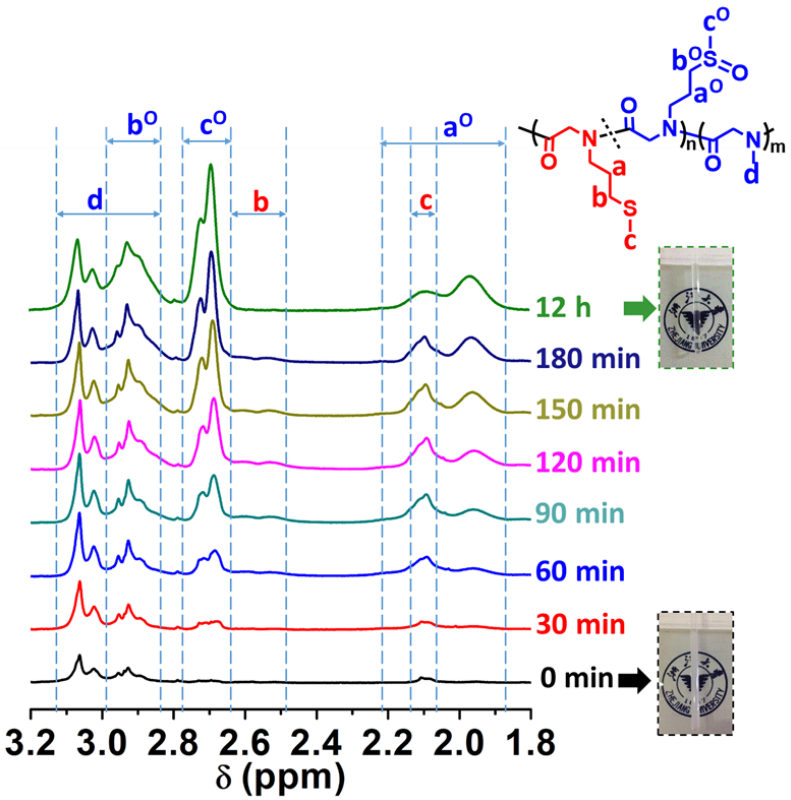

Figure 5.6. ^{1}H-NMR spectra of MS2 polymersomes obtained by double emulsion in D_2O in the presence of 176 mM H_2O_2 with the molar ratio of [H_2O_2] : [MeSPG] = 3.62 : 1. The photographs of NMR sample tube beside the ^{1}H-NMR spectra show clearly the turbidity change (from turbid to transparent) of the polymersome dispersion before and after oxidation.

5.3.3 Photo-responsive TPP-loaded polymersomes

After the use of H_2O_2 as oxidation trigger, we searched for more controllable method for vesicle destabilization. ROS can be produced by photosensitizers incorporated in polymersomes upon light exposure. The generation of ROS such as $^{1}O_2$ and free radicals can be triggered remotely and precisely by light. $^{1}O_2$ transformed from the ground state triplet oxygen ($^{3}O_2$) upon light illumination has been reported to disturb liposomes[31] and polymersomes[13, 32-34], one of which[18] proceeded by oxidation of thioether (in PPS) and was shown to be useful in precision intracellular delivery.

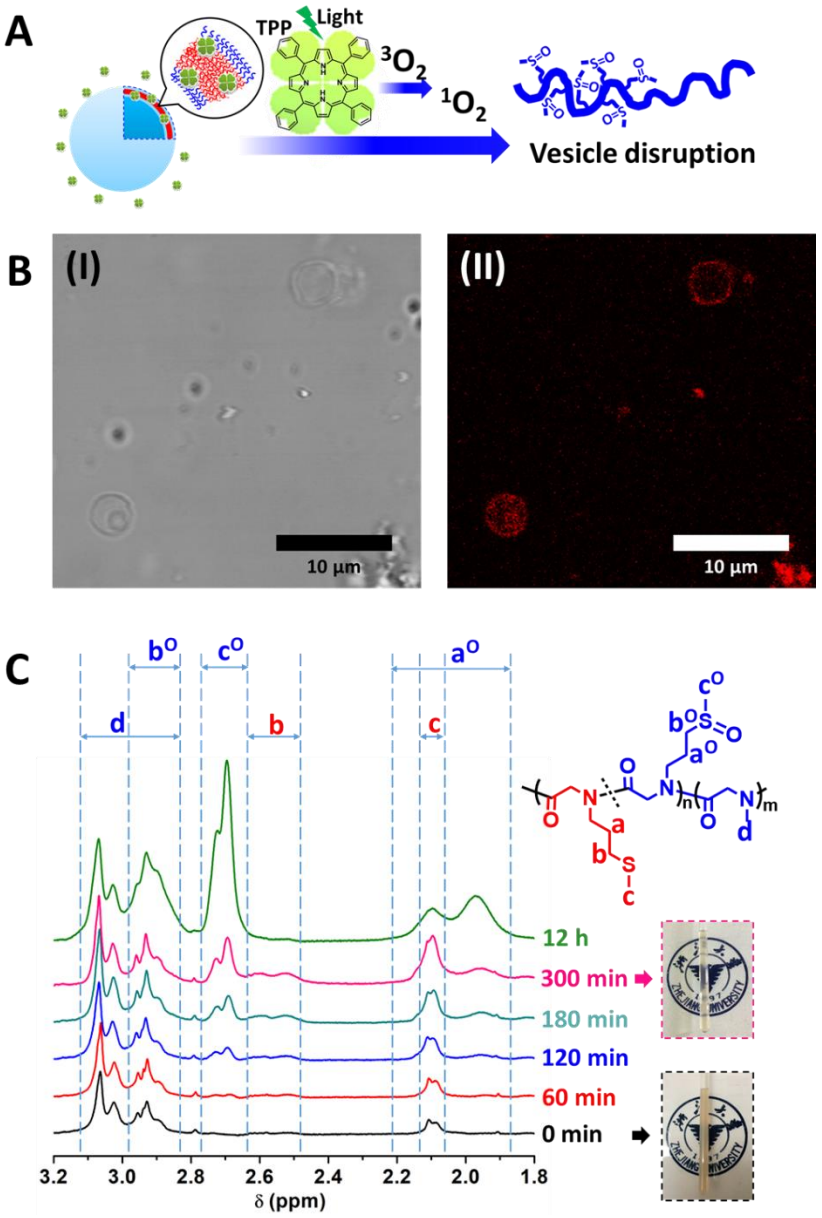

Figure 5.7. (A) The schematic illustration of the disruption process of MS2 polymersome by singlet oxygen generated from light-activated TPP. (B) Bright-field CLSM images (I) and fluorescence CLSM images (II) excited by laser of 543 nm, for MS2 polymersomes loaded with TPP (copolymer : TPP = 100 : 1 in weight). The fluorescence in (II) comes from TPP, which shows clearly that TPP molecules attach preferentially to the polymersome membrane, probably via hydrophobic interaction. (C) ^{1}H-NMR spectra of MS2 polymersome in D_2O and loaded with TPP under irradiation of 0.5 W/cm^2 white LED light. The concentration of MS2 polymersome is 10 g/L (1.63

mM), that of TPP is 1 g/L (3.26 mM), the molar ratio being [TPP] : [copolymer] = 2.00 : 1 and [TPP] : [MeSPG] = 1 : 30. The photographs at right show the turbidity change of the sample in NMR tube from turbid to transparent.

The MS2 giant polymersomes obtained by double emulsion method are blended with the photosensitizer, tetraphenylporphyrin (TPP).[34] TPP is a hydrophobic porphyrin, which shows red fluorescence under visible light excitation and can be activated to transfer the dissolved oxygen to $^1O_2$. We first check the loading ability of TPP by the polymersomes. The CLSM fluorescence image of the mixture of MS2 polymersomes and TPP shown in Figure 5.7B confirms that TPP molecules attach preferentially to the polymersome membrane via hydrophobic interaction (illustrated in Figure 5.7A). The evolution of ^{1}H-NMR spectra are followed of MS2 polymersomes in D_2O and loaded with TPP as a function of the illumination time under white LED light with irradiance of 500 mW/cm^2 (Figure 5.7C). The sample appearances in NMR tube before illumination and after 300 min of illumination are also shown in Figure 5.7C. Similar to the case of giant polymersomes triggered by H_2O_2, the transformation from thioether to sulfoxide, triggered here by light in the presence of photosensitizer TPP, also leads to the disassembly of giant polymersomes to free polymers or tiny aggregates.

For the *in situ* and real-time observation of the polymersome opening triggered by light under CLSM, we first prepared MS2 giant polymersomes labelled by Nile Red and then mixed with TPP solubilized in a tiny volume of THF (the final molar ratio is [TPP] : [MeSPG] = 1 : 30). Figure 5.8 shows the real-time evolution of vesicles until disruption provoked by the localized confocal laser (543 nm) of the microscope, with the maximum working power at 1.5 mW. The two vesicles in the view are disrupted through two different pathways, the upper vesicle by pathway I^L and the lower one by pathway II^L (the superscript L indicates the trigger is light, to distinguish from that of O with H_2O_2 trigger in the previous section). In the pathway I^L, the vesicle size decreases slightly in the first 37 s, then the membrane fluctuates (until 118 s) followed

by its opening at upper-right side with a micron-size pore and outward curling; the whole process of vesicle disassembling takes around 6 min. In contrast, in the pathway II^L the vesicle decreases its size continuously until its disappearance and the whole process lasts 14 min. The different ways of disruption could be explained by the different distribution of TPP in these vesicles. If the distribution of TPP molecules around a vesicle is not homogeneous and more concentrated in one place, a big pore localized in this place can be formed first by the attack of high concentration of $^1O_2$ generated by TPP. The vesicle bursts then rapidly: opening for release after only 118 s of illumination. This is the case of the pathway I^L. If the vesicle has TPP uniformly distributed at its surface, copolymers in the membrane are oxidized and withdrawn at a rather constant rate, leading to slow and progressive shrinking of the vesicle. This is the case of the pathway II^L that takes longer time (14 min).

If comparing the giant polymersomes triggered by H_2O_2 with those triggered by light in the presence of TPP, we can find some similarities between the pathways I^L and I^O as well as between the pathways II^L and II^O. They are all depending on local concentration of ROS, *i.e.*, H_2O_2 or $^1O_2$ generated by light and TPP. However, the polymersome bursting triggered by light can be controlled remotely, locally and timely. The disruption of polymersomes depends also on the total laser dose or the illumination duration. Figure 5.9 shows the CLSM images of a large area (I) before the observation and (II) after the observation of around 15 min with two focused spots marked by the circles (condition as described in Figure 5.8). The vesicles under the focus disappear, while those in other regions remain. During the photo capture and video recording, these two focused regions received more laser dose and produced more ROS leading to the vesicle disruption. This observation suggests that the PMeSPG-*b*-PSar vesicles can be opened or destroyed selectively in a controllable way through the manipulation of laser.

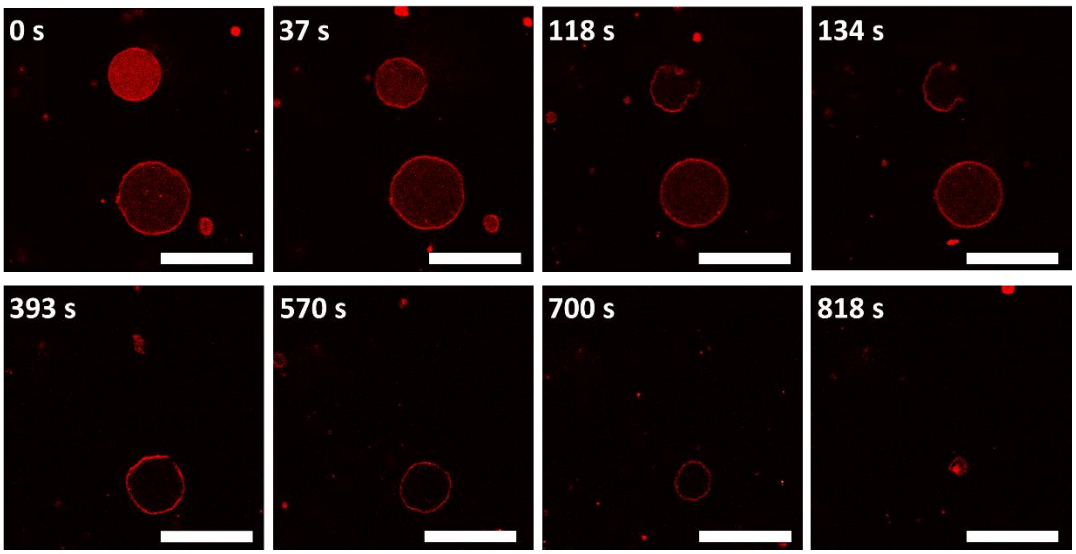

Figure 5.8. Snapshots of the sequence of evolution of two MS2 polymersomes labeled with Nile Red and loaded with TPP (the molar ratio of [TPP] : [MeSPG] = 1 : 30) under the illumination of the confocal laser (543 nm) of CLSM at the maximum working power of 1.5 mW. Two pathways are observed for the polymersome disruption. Scale bar = 25 nm.

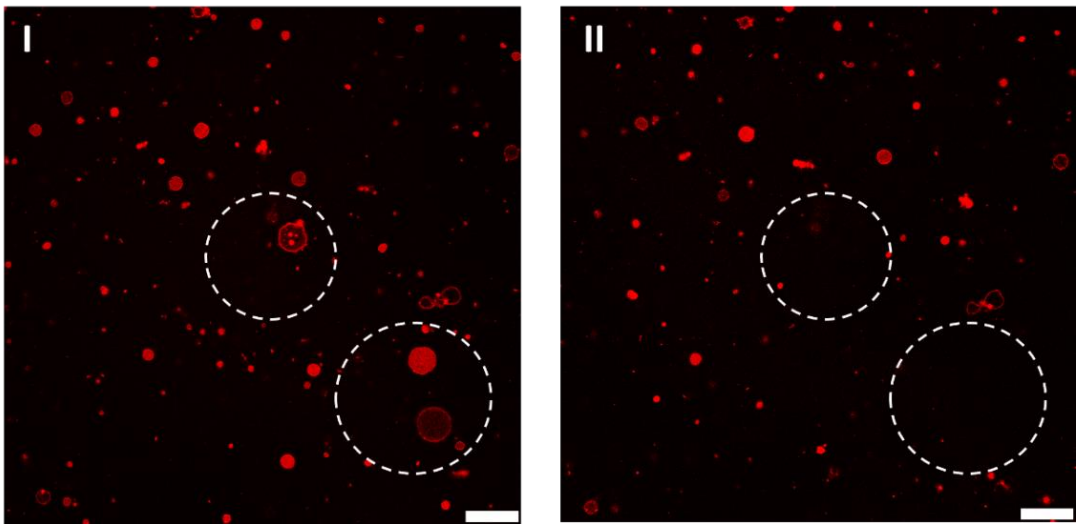

Figure 5.9. The CLSM images of a large area (I) before the observation and (II) after the observation of around 15 min with two focused spots marked by the circles as described in Figure 5.8. The vesicles under the focus disappear, while those in other regions remain. Scale bar = 25 nm.

5.4 Conclusion

In this chapter, we characterized and analyzed the stimuli-responsiveness of PMeSPG-*b*-PSar polymersomes, based on the thioether-to-sulfoxide transition of MeSPG under oxidative stimuli. The polymersomes and other self-assembly structures of MS1 ($PMeSPG_{45}$-*b*-$PSar_{60}$) from nanoprecipitation get disassembled after the treatment with 10 wt% (2.94 M) H_2O_2, only leaving very few loose irregular clusters with some disk-like cavities in the following cryo-EM observation. The detailed oxidation-responsive transformation is recorded by CLSM from the giant vesicles of MS2 ($PMeSPG_{60}$-*b*-$PSar_{50}$) from double emulsion, which have two pathways to distablize under the stimulation of 8.8 mM H_2O_2. DLS and NMR are employed to confirm the chemical oxidation of copolymers. In order to achieve responsiveness to remote and controllable stimulus, MS2 polymersomes are loaded with the photositisizer TPP, which can generate $^1O_2$ by the activation of light. In the real-time observation under CLSM, the destablization of TPP-loaded MS2 polymersomes is captured, which is initiated by the localized confocal laser (HeNe 543 nm with maximun working power at 1.5 mW) of CLSM. The light-stimulated vesicle destablization has similar pathways to that of H_2O_2-stimulated destablization, but can be achieved with much better controlability and efficiency. PMeSPG-*b*-PSar polymersomes are proved as smart vehicles with stimuli-responsiveness, based on the ROS or ROS-involving stimulations. It can be utilized for the precision intracellular delivery and for the conception of polymersome-based micro/nano-reactors to conduct sophisticated and cascade catalytic reactions.

References

1. Malikmammadov, E.; Tanir, T. E.; Kiziltay, A.; Hasirci, V.; Hasirci, N., PCL and PCL-based materials in biomedical applications. *J. Biomat. Sci.-Polym. E.* **2018,** *29* (7-9), 863-893.

2. Du, J. Z.; O'Reilly, R. K., Advances and challenges in smart and functional polymer vesicles. *Soft matter* **2009,** *5* (19), 3544-3561.

3. Meng, F. H.; Zhong, Z. Y.; Feijen, J., Stimuli-Responsive Polymersomes for Programmed Drug Delivery. *Biomacromolecules* **2009,** *10* (2), 197-209.

4. Kim, K. T.; Meeuwissen, S. A.; Nolte, R. J. M.; van Hest, J. C. M., Smart nanocontainers and nanoreactors. *Nanoscale* **2010,** *2* (6), 844-858.

5. Deng, Y.; Ling, J.; Li, M.-H., Physical stimuli-responsive liposomes and polymersomes as drug delivery vehicles based on phase transitions in the membrane. *Nanoscale* **2018,** *10*, 6781-6800.

6. Lux, C. d. G.; Joshi-Barr, S.; Trung, N.; Mahmoud, E.; Schopf, E.; Fomina, N.; Almutairi, A., Biocompatible Polymeric Nanoparticles Degrade and Release Cargo in Response to Biologically Relevant Levels of Hydrogen Peroxide. *J. Am. Chem. Soc.* **2012,** *134* (38), 15758-15764.

7. Shim, M. S.; Xia, Y., A Reactive Oxygen Species (ROS)-Responsive Polymer for Safe, Efficient, and Targeted Gene Delivery in Cancer Cells. *Angew. Chem. Int. Ed. Engl.* **2013,** *52* (27), 6926-6929.

8. Liou, G.-Y.; Storz, P., Reactive oxygen species in cancer. *Free Radical Res.* **2010,** *44* (5), 479-496.

9. Halliwell, B.; Clement, M. V.; Long, L. H., Hydrogen peroxide in the human body. *FEBS Lett.* **2000,** *486* (1), 10-13.

10. Ohshima, H.; Tatemichi, M.; Sawa, T., Chemical basis of inflammation-induced carcinogenesis. *Arch. Biochem. Biophys.* **2003,** *417* (1), 3-11.

11. Doskey, C. M.; Buranasudja, V.; Wagner, B. A.; Wilkes, J. G.; Du, J.; Cullen, J. J.; Buettner, G. R., Tumor cells have decreased ability to metabolize H2O2: Implications for pharmacological ascorbate in cancer therapy. *Redox Bio.* **2016,** *10*, 274-284.

12. Ikeda, M.; Tanida, T.; Yoshii, T.; Kurotani, K.; Onogi, S.; Urayama, K.; Hamachi, I., Installing logic-gate responses to a variety of biological substances in supramolecular hydrogel-enzyme hybrids. *Nat. Chem.* **2014,** *6* (6), 511-518.

13. Vasdekis, A. E.; Scott, E. A.; O'Neil, C. P.; Psaltis, D.; Hubbell, J. A., Precision Intracellular Delivery Based on Optofluidic Polymersome Rupture. *ACS Nano* **2012,** *6* (9), 7850-7857.

14. Napoli, A.; Boerakker, M. J.; Tirelli, N.; Nolte, R. J. M.; Sommerdijk, N.; Hubbell, J. A., Glucose-oxidase based self-destructing polymeric vesicles. *Langmuir* **2004,** *20* (9), 3487-3491.

15. Perez, R. A.; Cordova, M. E.; Lopez, J. V.; Hoskins, J. N.; Zhang, B.; Grayson, S. M.; Mueller, A. J., Nucleation, crystallization, self-nucleation and thermal fractionation of cyclic and linear poly(epsilon-caprolactone)s. *React. Funct. Polym.* **2014,** *80*, 71-82.

16. Ray, P. D.; Huang, B.-W.; Tsuji, Y., Reactive oxygen species (ROS) homeostasis and redox regulation in cellular signaling. *Cell. Signal.* **2012,** *24* (5), 981-990.

17. Su, Z.; Chen, M.; Xiao, Y.; Sun, M.; Zong, L.; Asghar, S.; Dong, M.; Li, H.; Ping, Q.; Zhang, C., ROS-triggered and regenerating anticancer nanosystem: an effective strategy to subdue tumor's multidrug resistance. *J. Control. Release* **2014,** *196*, 370-383.

18. Podual, K.; Doyle, F. J.; Peppas, N. A., Glucose-sensitivity of glucose oxidase-containing cationic copolymer hydrogels having poly(ethylene glycol) grafts. *J. Control. Release* **2000,** *67* (1), 9-17.

19. Song, C. C.; Du, F. S.; Li, Z. C., Oxidation-responsive polymers for biomedical applications. *J. Mater. Chem. B* **2014,** *2* (22), 3413-3426.

20. Napoli, A.; Valentini, M.; Tirelli, N.; Muller, M.; Hubbell, J. A., Oxidation-responsive polymeric vesicles. *Nat. Mater.* **2004,** *3* (3), 183-189.

21. Rodriguez, A. R.; Kramer, J. R.; Deming, T. J., Enzyme-Triggered Cargo Release from Methionine Sulfoxide Containing Copolypeptide Vesicles. *Biomacromolecules* **2013,** *14* (10), 3610-3614.

22. Kramer, J. R.; Deming, T. J., Reversible chemoselective tagging and functionalization of methionine containing peptides. *Chem. Commun.* **2013,** *49* (45), 5144-5146.

23. Yu, S.; Wang, C.; Yu, J.; Wang, J.; Lu, Y.; Zhang, Y.; Zhang, X.; Hu, Q.; Sun, W.; He, C.; Chen, X.; Gu, Z., Injectable Bioresponsive Gel Depot for Enhanced Immune Checkpoint Blockade. *Adv. Mater.* **2018**, e1801527.

24. Liu, H.; Wang, R.; Wei, J.; Cheng, C.; Zheng, Y.; Pan, Y.; He, X.; Ding, M.; Tan, H.; Fu, Q., Conformation-Directed Micelle-to-Vesicle Transition of Cholesterol-Decorated Polypeptide Triggered by Oxidation. *J. Am. Chem. Soc.* **2018,** *140* (21), 6604-6610.

25. Fu, X.; Ma, Y.; Shen, Y.; Fu, W.; Li, Z., Oxidation-responsive OEGylated poly-L-cysteine and solution properties studies. *Biomacromolecules* **2014,** *15* (3), 1055-1061.

26. Mitragotri, S.; Burke, P. A.; Langer, R., Overcoming the challenges in administering biopharmaceuticals: formulation and delivery strategies. *Nat. Rev. Drug. Discov.* **2014,** *13* (9), 655-672.

27. Yan, B.; Zhang, Y.; Wei, C.; Xu, Y., Facile synthesis of ROS-responsive biodegradable main chain poly(carbonate-thioether) copolymers. *Polym. Chem.* **2018,** *9* (7), 904-911.

28. Dolmans, D.; Fukumura, D.; Jain, R. K., Photodynamic therapy for cancer. *Nat. Rev. Cancer* **2003,** *3* (5), 380-387.

29. Zhou, Z.; Song, J.; Nie, L.; Chen, X., Reactive oxygen species generating systems meeting challenges of photodynamic cancer therapy. *Chem. Soc. Rev.* **2016,** *45* (23), 6597-6626.

30. Yamada, S.; Ikkyu, K.; Iso, K.; Goto, M.; Endo, T., Facile synthesis of polymethionine oxides through polycondensation of activated urethane derivative of alpha-amino acid and their application to antifouling polymer against proteins and cells. *Polym. Chem.* **2015,** *6* (10), 1838-1845.

31. Riske, K. A.; Sudbrack, T. P.; Archilha, N. L.; Uchoa, A. F.; Schroder, A. P.; Marques, C. M.; Baptista, M. S.; Itri, R., Giant Vesicles under Oxidative Stress Induced by a Membrane-Anchored Photosensitizer. *Biophys. J.* **2009,** *97* (5), 1362-1370.

32. Mabrouk, E.; Bonneau, S.; Jia, L.; Cuvelier, D.; Li, M.-H.; Nassoy, P., Photosensitization of polymer vesicles: a multistep chemical process deciphered by micropipette manipulation. *Soft matter* **2010,** *6* (19), 4863-4875.

33. Robbins, G. P.; Jimbo, M.; Swift, J.; Therien, M. J.; Hammer, D. A.; Dmochowski, I. J., Photoinitiated Destruction of Composite Porphyrin-Protein Polymersomes. *J. Am. Chem. Soc.* **2009,** *131* (11), 3872-3874.

34. Xu, S.; Ng, G.; Xu, J.; Kuchel, R. P.; Yeow, J.; Boyer, C., 2-(Methylthio)ethyl Methacrylate: A Versatile Monomer for Stimuli Responsiveness and Polymerization-Induced Self-Assembly in the Presence of Air. *ACS Macro Lett.* **2017,** *6* (11), 1237-1244.

General Conclusion and Perspectives

In this thesis work, we start from the synthesis of polypeptoid-containing amphiphilic block copolymers, then make in-depth studies on the self-assembly of these copolymers, and finally achieve the preparation of thermo-, oxidation- and photo-responsive polymersomes based on polypeptoids.

Di- and triblock copolymers PCL-*b*-PSar and PSar-*b*-PCL-*b*-PSar copolymers are synthesized through the ROP of Sar-NTA initiated by oxyamino-ended PCLs. Diblock copolymer PEG-*b*-PMeSPG is synthesized by PEG-amine-initiated ROP of MeSPG-NTA. The amphiphilic block copolypeptoid PMeSPG-*b*-PSar is synthesized by sequential ROP of MeSPG-NTA and Sar-NTA in amine-initiated system. Via a "decarboxylation−*N*-carboxymethylation" procedure on methionine followed by a cyclization, MeSPG-NTA, a new NNTA monomer with thioether-containing *N*-substituent side chain is prepared for the first time.

The self-assembling behaviors of two triblock PSar-*b*-PCL-*b*-PSar copolymers, CS7 ($PSar_8$-*b*-PCL_{28}-*b*-$PSar_8$) and CS10 ($PSar_{16}$-*b*-PCL_{40}-*b*-$PSar_{16}$) are studied in detail. Lamellar sheets and nanofibers are formed from the nanoprecipitation of these copolymers. The heating treatment at 65 ℃ transforms the lamellae and nanofibers to polymeric spheres and cylinders. Heating at 90 ℃ of nanoprecipitated samples results in densely dispersed spheres for CS7, while multilamellar vesicles for CS10. The lamellae and nanofibers come from the confinement of crystalline PCL blocks, and the heating which melts the crystals promotes the movement of copolymer chains and the evolution of self-assembly morphology. The multilamellar vesicles are formed by water diffusing into polymeric spheres, which is close to the Mechanism II for vesicular formation. The film hydration method involving 65 ℃ heating generates rods of micrometer-length and a few giant vesicles from both the copolymers. The cell-viability tests show the low cytotoxicity of PCL/PSar copolymers and of their self-assembly system.

Three PEG-*b*-PMeSPG copolymers, EM1 (PEG_{45}-*b*-$PMeSPG_{17}$), EM2 (PEG_{45}-*b*-$PMeSPG_{40}$) and EM3 (PEG_{45}-*b*-$PMeSPG_{71}$), with MW increasing and hydrophilic ratio decreasing from EM1 to EM3, form, respectively, polymer spheres (EM1), spherical and worm-like micelles (EM2) and vesicle and lamellae (EM3) by nanoprecipitation. Three PMeSPG-*b*-PSar copolypeptoids, MS1 ($PMeSPG_{45}$-*b*-$PSar_{65}$), MS2 ($PMeSPG_{60}$-*b*-$PSar_{50}$) and MS3 ($PMeSPG_{75}$-*b*-$PSar_{25}$), all form vesicles by nanoprecipitation, but with various metastable structures such as micelles, lamellae and non-closed vesicles coexisting in the self-assemblies. The nonergodicity possibly comes from the insufficient water-solubility of PSar and the low mobility of PMeSPG at room temperature. Film hydration is then applied to the copolypeptoids, where heating treatment and electric field are utilized to promote the destabilization of the polymer film in swelling process. The heating treatment leads to the number increase of spherical vesicles. W/O/W double emulsion is also used to prepare polymersomes of copolypeptoids, using chloroform as organic solvent. Giant vesicles are obtained with high efficiency by double emulsion. MS3, with the biggest hydrophobic ratio among the three copolypeptoids, can form many bicontinuous nanostructures by nanoprecipitation and double emulsion, probably through interlamellar fusion.

As the thioether side chain in PMeSPG block can undergo thioether-to-sulfoxide transformation in the presence of ROS such as H_2O_2 and $^1O_2$, amphiphilic block copolymer PMeSPG-*b*-PSar can be oxidized to entirely water soluble copolymers. Thus we have developed oxidation-responsive polypeptoid vesicles using H_2O_2 as stimulus, as well as photo-responsive polypeptoid vesicles using visible light as stimulus in the presence of photosensitizer TPP that generate $^1O_2$ under light activation. By treatment of 10 wt% H_2O_2, MS1 nano-vesicles obtained from nanoprecipitation disappear and only a few of irregular loose clusters remain. The destabilizations of MS2 giant vesicles in response to H_2O_2 and light stimuli are characterized by CLSM, with the confirmation of the chemical oxidation of copolypeptoids by NMR. Photo-responsive polymersomes

of MS2 loaded with TPP allow the destruction of vesicles with spatiotemporal control by laser manipulation.

This thesis work has opened perspectives in the research of stimuli-responsive polypeptoid vesicles. The ROS-responsive PMeSPG-*b*-PSar polymersomes can be further developed for the application in cancer treatment, since the preferable accumulation of ROS in tumor tissue. However, as the concentration of ROS in human body is variable and often lower than that necessary for polymersome destruction, other approaches such as the combination with PDT agents (photosensitizers) can be developed. Another example is PMeSPG-*b*-PSar polymersomes encapsulating glucose oxidase and insulin. These polyemersomes can disassemble in response to high glucose level and release insulin, which act as smart nanocarriers for the regulation of blood sugar.

Other than their oxidizable ability, the thioether groups in PMeSPG can also act as nucleophiles and react with substrates including alkyl halides, triflates and epoxides. This property can be employed to introduce new functions in PEG-*b*-PMeSPG and PMeSPG-*b*-PSar polymersomes. For example, the nucleophilic reactions yield sulfonium ions and lead to a positively charged surface. Suitable amount of charges can be used for DNA-loading and cell-penetration.

By introducing other functional groups in the *N*-substituent chains, a large number of functional polypeptoids and their amphiphilic block copolymers can be developed. Consequently, more functional and stimuli-responsive polypeptoid vesicles can be designed and prepared. We are confident that polypeptoid vesicles have good prospects in both fundamental research and application fields.

List of Publications and Conference Abstracts during the PhD Thesis

1. **Deng, Yangwei**; Ling, Jun; Li, Min-Hui, Physical stimuli-responsive liposomes and polymersomes as drug delivery vehicles based on phase transitions in the membrane. *Nanoscale* **2018,** *10*, 6781-6800.

2. **Deng, Yangwei**; Zou, Tao; Tao, Xinfeng; Semetey, Vincent; Trepout, Sylvain; Marco, Sergio; Ling, Jun; Li, Min-Hui, Poly(epsilon-caprolactone)-block-polysarcosine by ring-opening polymerization of sarcosine N-thiocarboxyanhydride: Synthesis and thermoresponsive self-assembly. *Biomacromolecules* **2015,** *16* (10), 3265-3274.

3. **Deng, Yangwei**; Chen, Hui; Tao, Xinfeng; Cao, Fangyi; Trepout, Sylvain; Ling, Jun; Li, Min-Hui, Oxidation-responsive polymersomes based on polypeptoids with thioether side-chain. In preparation.

4. **Deng, Yangwei**; Ling, Jun; Li, Min-Hui, Film hydration techniques for the formation of polypeptoid vesicles. In Preparation.

5. **Deng, Yangwei**; Zou, Tao; Tao, Xinfeng; Semetey, Vincent; Trepout, Sylvain; Marco, Sergio; Ling, Jun; Li, Min-Hui, Polymersomes of biodegradable polysarcosine-block-poly(epsilon-caprolactone). *J. Control. Release* **2015**, *213*, E130-E130. Conference abstract.

6. **Deng, Yangwei**; Trepout, Sylvain; Ling, Jun; Li, Min-Hui, Synthesis and self-assembly of amphiphilic block copolymers containing poly(N-methylthiopropyl glycine). *The 15th Pacific Polymer Conference*, Xiamen, China, December 10-14, 2017. Conference abstract.

RÉSUMÉ

Comme un nanoconteneur robuste formé d'une bicouche de polymères amphiphiles, vésicule polymère, aussi appelée polymersome, a été considérée comme un vecteur de médicament potentiel dans le domaine biomédical, grâce à sa structure imitant les cellules, sa grande stabilité et sa capacité à être fonctionnalisée. Pour l'utilisation pratique des polymeromes dans des applications biomédicales, la biocompatibilité des copolymères qui composent les vésicules devient un sujet important. Le polypeptoid est une classe de dérivés polypeptides dont les atomes d'azote des amides sont substitués. En évitant la formation de liaisons hydrogène inter- et intramoléculaires, les polypeptoids ont des solubilités bien meilleures que les polypeptides dans des solvants organiques usuels, tandis que la biocompatibilité est bien maintenue. Des travaux sur l'auto-assemblage de copolymères à blocs contenant polypeptoids émergent dans la littérature. Cependant, les travaux sur les vésicules polypeptoids sont encore rares. Dans cette thèse, deux familles de copolymères à blocs amphiphiles contenant les polypeptoids ont été synthétisées par la polymérisation par ouverture de cycle (ROP) de *N*-thiocarboxyanhydrides d'acides aminés *N*-substitués (NNTA). Différentes techniques telles que la nanoprécipitation, l'hydratation de film mince et la double émulsion ont été utilisées pour réaliser les auto-assemblages dans le but d'obtenir des vésicules polypeptoids. Les auto-assemblages ont été étudiés en détail par DLS, cryo-EM, microscope confocale à balayage laser (CLSM) et ^{1}H-RMN.

Dans la première famille de copolymères, la ROP de la sarcosine NTA (Sar-NTA) a été initiée par le poly(*ε*-caprolactone) (PCL) à terminaison -oxyamine, pour obtenir le copolymère dibloc PCL-*b*-PSar, et le copolymère tribloc PSar-*b*-PCL-*b*-PSar. Des feuilles et nanofibres unilamellaires ont été obtenues par nanoprécipitation des copolymères PSar-*b*-PCL-*b*-PSar à température ambiante. Ces lamelles et structures fibreuses peuvent être transformées en particules cylindriques et sphèriques après chauffage à 65 °C. Le chauffage à 90 °C conduit finalement à des polymeromes multilamellaires. La seconde famille de copolymères est basée sur un polypeptoid portant thioéthers, la poly(*N*-3-(méthylthio)propyl glycine) (PMeSPG). Le nouveau monomère, MeSPG-NTA, a été préparé par une procédure de « décarboxylation−*N*-carboxyméthylation » à partir de la méthionine, suivie d'une cyclisation. Les copolymères à blocs amphiphiles PEG-*b*-PMeSPG et PMeSPG-*b*-PSar ont été synthétisés avec de différentes masses moléculaires et de différents rapports de blocs hydrophile/hydrophobe. Les études d'auto-assemblage ont été menées sur ces copolymères pour la formation de vésicules polypeptoids. Des vésicules ont été obtenues avec de différentes méthodes, et le mécanisme de la formation des vésicules à travers diverses morphologies non-ergodiques a été discuté en détail.

Le polypeptoid portant thioéthers est conçu pour ses caractéristiques stiumulables en réponse à l'oxydation. En effet, le desassemblage des vésicules polypeptoids de PMeSPG-*b*-PSar sensible à l'oxydation a été obtenu en raison de la transition « thioéther−sulfoxyde » stimulée respectivement par le peroxyde d'hydrogène (H_2O_2) et par l'oxygène singulet ($^{1}O_2$) produit en presence de la lumière. Les vésicules polypeptoids oxydation-stimulable et photo-stimulable ainsi réalisés peuvent être des systèmes prometteurs dans des applications de relargages contrôlés des médicaments.

MOTS CLÉS

Auto-assemblage, polypeptoids, polymersome, oxydation-stimulable, photo-stimulable

ABSTRACT

As a robust nanocontainer with polymeric bilayer structure, polymer vesicle, also called polymersome, has been considered as potential drug carrier in biomedical field, because of its cell-mimicking structure, high stability and capability to be functionalized. For practical use of polymersomes in biomedical applications, the biocompatibility of the copolymers that compose the vesicles become an important issue. Polypeptoid is a class of polypeptide derivatives of which the nitrogen atoms of amides are substituted. By avoiding the formation of inter- and intramolecular hydrogen bonds, polypeptoids have much better solubility than polypeptides in common organic solvent, while the biocompatibility is well maintained. Reports on self-assemblies of polypeptoid-containing block copolymers start to appear in the literature. However, works on polypeptoid vesicles are still scarce. In the present study, two families of polypeptoid-containing amphiphilic block copolymers are synthesized through the ring-opening polymerization (ROP) of *N*-substituted amino acid *N*-thiocarboxyanhydrides (NNTAs). Various techniques like nanoprecipitation, film hydration and double emulsion are used to perform the self-assemblies with the objective to obtain polypeptoid vesicles. The self-assemblies are investigated in detail by DLS, cryo-EM, confocal laser scanning microscope (CLSM) and ^{1}H-NMR.

In the first family of copolymers, ROP of sarcosine NTA (Sar-NTA) is initiated by oxyamino-ended poly(ε-caprolactone) (PCL), to obtain diblock copolymer PCL-*b*-PSar and triblock copolymer PSar-*b*-PCL-*b*-PSar. Unilamellar sheets and nanofibers are obtained by nanoprecipitation of PSar-*b*-PCL-*b*-PSar copolymers at room temperature. These lamellae and fibrous structures are transformed into worm-like cylinders and spheres after heating to 65 °C. Heating at 90 °C leads eventually to multilamellar polymersomes. The second family of copolymers is based on a thioether-bearing polypeptoid, poly(*N*-3-(methylthio)propyl glycine) (PMeSPG). The new monomer, MeSPG-NTA is obtained from a "decarboxylation−*N*-carboxymethylation" procedure from methionine, followed by cyclization. The amphiphilic block copolymers PEG-*b*-PMeSPG and PMeSPG-*b*-PSar are synthesized with different molecular weights and hydrophilic/hydrophobic ratios. Vesicles have been achieved with different methods, and the mechanism of vesicle formation through diverse nonergodic morphologies are discussed in detail.

The thioether-bearing polypeptoid is designed because of its oxidation-responsive features. Effectively, oxidation-responsive disruption is achieved for the PMeSPG-*b*-PSar polypeptoid vesicles, based on the "thioether−sulfoxide" transition stimulated by hydrogen peroxide (H_2O_2) and light-induced singlet oxygen ($^{1}O_2$) respectively. The oxidation- responsive and photo-responsive polypeptoid vesicles can be used as promising vehicles for smart drug release applications.

KEYWORDS

Self-assembly, polypeptoids, polymersome, oxidation-responsive, photo-responsive